SEDIMENTARY FACIES EVOLUTION IN CONTINENTAL FAULT-BOUNDED BASINS FORMED BY CRUSTAL EXTENSION: THE CORINTH BASIN, GREECE

Richard E.Ll. COLLIER

October 1988

Submitted in accordance with the requirements for the degree of Doctor of Philosophy

Dept. of Earth Sciences
University of Leeds
LS2 9JT U.K.

1

Now Xenophanes holds that the earth is recurrently mingled with the sea and then as time passes is freed again of moisture. He puts forth such proofs as these: that shells are found far inland and on mountains; and that in the quarries of Syracuse imprints of a fish and of seaweed have been found, and in Paros the imprint of a small fry deep in the stone, and in Malta flat slabs [bearing the impressions] of all sorts of fish. He says that the imprint, made long ago when everything was covered with mud, then dried in the mud.

1: Xenophanes of Colophon (c.570-475 B.C.)

Hippolytus, Refutations of All Heresies I 14.5-6
(Diels, Fragmente der Vorsokratiker I 122)

ABSTRACT

Characteristic half-graben and graben geometries are generated by extensional tectonics. The sedimentary infill to such basins reflects their structural evolution. The actively extending basins of central Greece have provided an opportunity to study the mechanisms that control sediment distribution and the resultant facies patterns and geometries produced in such environments. The modern and precedent Neogene to Quaternary sediments studied, and their controlling processes, provide predictive templates for the analysis of controls acting upon ancient extensional basin fills.

On a basinwide scale, facies patterns are controlled by the geometry of major basin-controlling normal faults and by the structural level of the basin - determining alluvial, lacustrine or marine environments. Increments of movement on normal faults tilt and vertically displace the depositional surface, producing facies responses in terms of fluvial/submarine channel avulsion or preferential migration into topographic lows, lake or sea coastline advance or retreat across the depositional slope, and the progradation of clastic wedges off fault scarps and uplifted areas. The time-averaged product in the stratigraphic record is typically of clinoforms developed preferentially against basin margin faults and axial channel systems concentrated in the structurally constrained depocentre(s). Such gross morphologies are seen in the Lower Pliocene early rift history of the Corinth asymmetric graben; conglomerate-dominated fan deltas and alluvial fans prograded laterally into the basin. The progradation of an ophiolite-derived, fluvio-deltaic system along the basin axis illustrates the competition of sediment supply rates with tectonic subsidence rates in determining facies geometries.

A number of other controls on sediment distribution are variously important through time within extensional basins, in addition to structuration and sediment supply rates (itself a function of hinterland litho-type and structural evolution). These include eustatic and climatic variation and compactional subsidence rates. The Corinth Isthmus has been studied with the aim of establishing the interaction of concurrent tectonic and eustatic relative base-level changes. Computer-modelling of the migration of a coastline through theoretical stratigraphic sections illustrates the effects of varying rates of change of sea-level, tectonic subsidence (or uplift) and deposition with time. Incorporation of the global sea-level curve for the Late Quaternary into such models reasonably predicts observed facies geometries in the Late Pleistocene and Holocene of the Isthmus. U-series disequilibrium dating of corals from the Corinth Canal area has constrained transgressive beach sub-sequences as reflecting c. 100,000 year wavelength eustatic cycles. After subtraction of depositional levels constrained in time and space against the sea-level curve, an average net uplift rate is derived for the central Isthmus of more than 0.3m per 1000 years.

The areal distribution of Late Pleistocene marine facies in the southern Corinth Basin is principally controlled by the structural form and evolution at time of deposition. Subsequent tilt block faulting in an alluvial environment illustrates how intrabasinal fault block morphologies may generate axial and lateral sediment transport systems analagous to those on a basinwide scale.

The competition between process rates is emphasized. Three-dimensional sedimentary facies patterns within evolving syn-rift

basins are shown to be dependent upon the interaction of three principal factors: a) the rate of tectonic displacements through time, on both basinwide and local fault block scales, b) the rate of sea-level change through time (or lake-level change, whether determined by tectonic or climatic means), and c) the rate of deposition at any locality, itself a function of hinterland structure and lithology, climate and depositional geometries.

ACKNOWLEDGEMENTS

Thanks go to Dr Mike Leeder for offering this PhD project in the first place and for a starting point in the form of his paper with Dr Rob Gawthorpe (1987) on tectonic-induced facies patterns in extensional basins. Many discussions in the field, office or over a glass of vino have been vitally stimulating.

Grateful thanks to British Petroleum plc for sponsorship of this project. Thanks to Dr Tim Atkinson at the University of East Anglia for U-Th analytical work and constructive discussion on the results. To Dr John Athersuch at the BP Research Centre for micropalaeontological analyses and Dr Dave Rex here in Leeds for K-Ar dating.

Thanks to a whole bunch of people for geological discussions: Andy Simms, Alistair Welbon, Dr Rob Knipe, Dr Jan Alexander, and Pete Bentham, Chris Dart and others in Greece. In Greece, thanks are due to I.G.M.E. for permission to work there, and to friends in and around Corinth and the American School of Archaeology in Ancient Corinth for their hospitality.

Last but not least, love and thanks to my parents, and Jane McNicholas (hello Roseanne) and Amanda Harrison for continuing friendship and support . Ta.

CHAPTER 6 DISCUSSION - FACIES PATTERN CONTROLS AND EVOLUTION

LIST OF FIGURES

LIST OF TABLES

LIST OF PLATES

LIST OF ENCLOSURES

CHAPTER 1 GENERAL INTRODUCTION

1.1 AIMS OF RESEARCH

This research project was designed to investigate the evolution of sedimentary facies patterns through time and space within fault-bounded extensional basins. Two approaches are utilised. The first is to analyse the sedimentary rocks within a basin in order to establish their environment(s) of deposition and deduce the structural geometry and timing of structural activity within that basin's history. The second approach is to model the effects of certain controls acting on the basin/sedimentary system. In gaining an understanding of how individual controlling processes act upon the system, a better understanding can then be attained of how the various controls act in consort or in competition. The controls in question include:

a) Fault geometries and strain rates through time.

b) Eustatic sea-level variations and their rates of change.

c) Climatic variation, affecting rates of sub-aerial erosion and lake levels.

d) The lithology of footwalls and hinterland exposed to erosion, again influencing rates of erosion.

e) Sedimentary processes such as fluvial channel migration and flood or crevasse events redistributing locations of sedimentation.

f) Compaction and differential rates of compaction in the sedimentary pile locally influencing the topography of the sediment surface.

g) The lithology of exposed intrabasinal tilt blocks or topographic features.

Through a more complete understanding of the interaction and varying influence in four dimensions of these controls on the system, a more critical analysis and interpretation of extensional basin sediments may be achieved.

The major part of the research programme considers the Corinth Basin in central Greece, an actively extending asymmetric graben with a Neogene to Recent sedimentary fill. This basin therefore provides an opportunity to study sedimentary facies patterns within the syn-rift phase of basin evolution. Concepts and models derived from studies of this basin should be equally applicable to other continental extensional basins. Qualitative and quantitative approaches are described.

The seismic activity and structural form of the Corinth Basin have been investigated following the significant earthquakes near Corinth in 1981 (Jackson et al 1982a, Vita-Finzi & King 1985). This allowed the sedimentology of the exposed basin fill to be studied in the context of its structural framework.

Work has also been carried out on the distribution and controlling factors of sedimentation in the late Carboniferous (Westphalian) of the Northumberland Basin in northern Britain. This study was initiated to consider similar problems in relation to the sedimentary cover of a basin in its more mature thermal phase of basin evolution (after McKenzie 1978a). The history of the Northumberland Basin and modelling of that basin/sedimentary system contrast the relative importance of certain controlling processes between the syn-rift and thermal stages of basin development. The integration of the two conditions is, however, beyond the scope of this volume. The Northumberland studies are therefore not included in this thesis. Refer to Collier (in

press (a) and (b)).

The study of sedimentary facies and the factors controlling their distribution within a neotectonic environment such as the Corinth Basin has certain advantages. Principally, the processes which determined sediment style and distribution in the exposed basin fill are frequently still observable in action. The structural and environmental context of sedimentary facies may thus be inferred by fairly immediate uniformitarianism. Certain features such as the variability of strain rates are illustrated better than is possible in the geologically ancient record, where only discontinuities of (usually) indeterminate duration indicate variations in rates of strain or sedimentation. An opportunity also exists to consider which controls and processes may be determined and isolated in the sedimentary record. For example, the variation in eustatic base-level is relatively well constrained for the late Quaternary but not for earlier times.

Two primary methods of research have been followed. Firstly, field investigation and secondly, theoretical modelling. Little independent evidence exists in the form of seismic or borehole data against which to test models. Where appropriate, such additional methods are referred to in the text.

1.1.1 Key Themes

Three key themes are developed through the detailed studies undertaken:

1) The importance of timing structural activity is discussed. The sedimentary record provides evidence of active tectonic faulting through a variety of features such as non-sedimentary growth faulting, facies and thickness changes across active

structures. The deduced structural evolution of the basin may be quantifiable if chronostratigraphic data is available. Alternatively, a qualitative approach may be developed by establishing an event stratigraphy in relation to the 3-dimensional lithostratigraphy. This approach is analogous to the seismic stratigraphic framework of Hubbard et al (1985). Quantification of fault activity or vertical displacements through time combined with any available base-level reference datum enables tectonic strain rates to be isolated.

2) The second theme relates to scale, both in space and in time. Faulting occurs on structures of a range of scales. Faulting on any one structure may occur as a series of discrete seismic increments or as an aseismic continuum. The sedimentary response to each situation may be quite distinct.

3) The third, integrative theme is the significance of process rates and their interaction. This refers to the rates of change of each controlling process such as normal fault displacement, base-level change by eustacy or climate-determined lake level and sediment supply rates into the basin. Which controlling variable, if any, is the dominant one at any time will be a function of the rates of change of each variable at that time.

1.2 LOCATION OF FIELD AREA

The target of detailed research, the Corinth Basin, covers approximately 600 km^2 in central Greece (fig. 1.1). It forms one elongate ESE-WNW trending trough within the Gulf of Corinth extensional basin system (see section 2.3). Along the axis of the basin three "compartments" may be distinguished; the Gulf of Lechaios in the west, the Isthmus of Corinth and the Saronic

Figure 1.1

Geographic locations in and around the Corinth Basin. Inset locates the basin within central Greece and the Aegean province.
GC = Gulf of Corinth
LB = Livadostros Basin
MB = Megara Basin
Corinth Basin:
GL = Gulf of Lechaios
SG = Saronic Gulf
IC = Isthmus of Corinth
L = Loutraki
C = Corinth
AC = Ancient Corinth
K = Kechriae
I = Isthmia

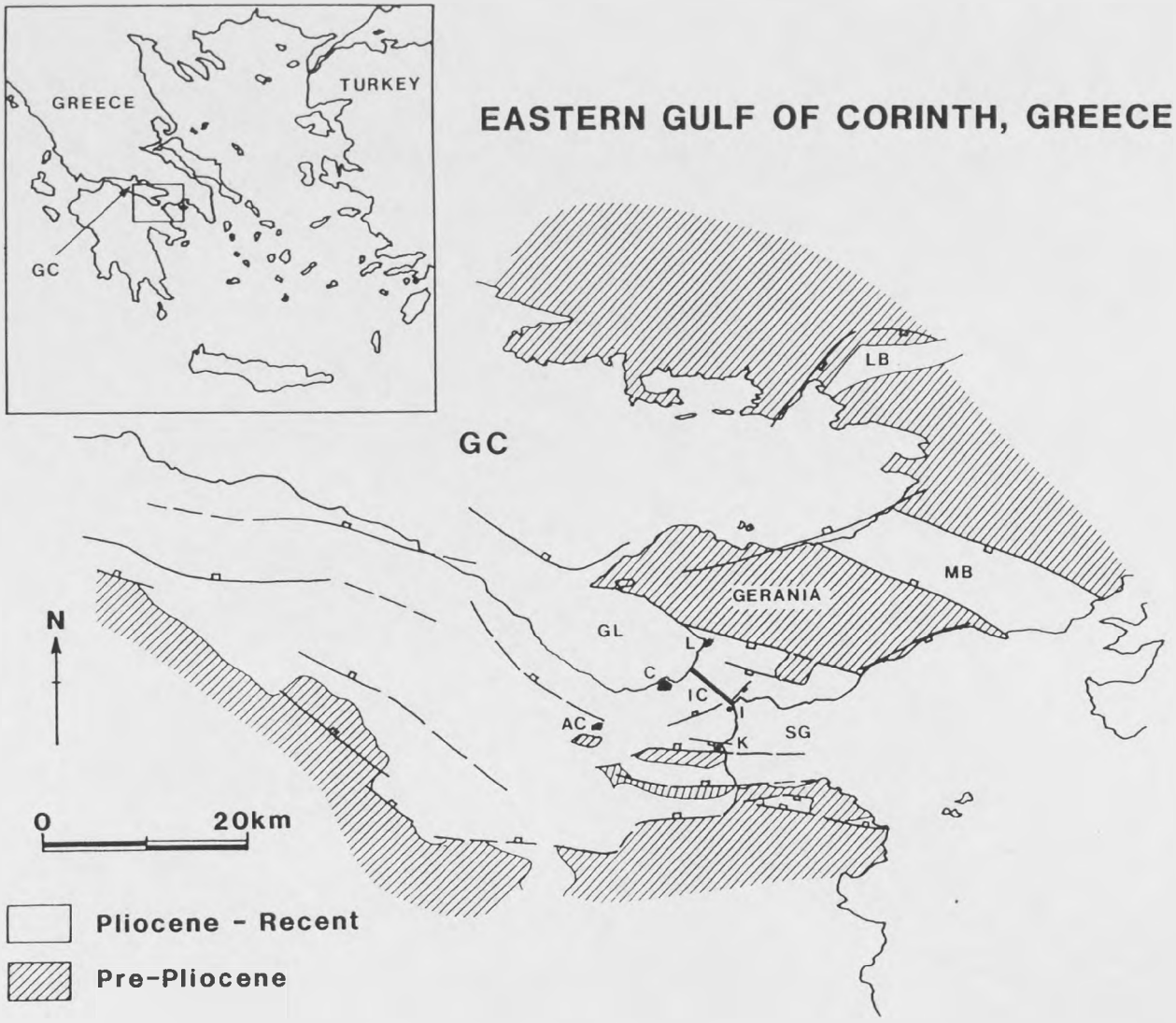
EASTERN GULF OF CORINTH, GREECE
GREECE
TURKEY
GC
GC
LB
GERANIA
MB
GL
L
C
IC
I
K
AC
SG
N
0
20km
Pliocene - Recent
Pre-Pliocene

Gulf. The basin is bounded to the north by the Gerania massif. To the west the Gulf of Lechaios opens into the Gulf of Corinth proper. To the east the Saronic Gulf opens into the Aegean Sea. The southern margin to the basin is more complex, but geographically bordered by the north Peloponnese hills to the east and east-north-east of Nemea.

Those areas described in detail within this thesis are outlined in figure 1.1. Other areas within central Greece and in western Turkey discussed in the text are located via the relevant passages.

1.3 FIELD WORK

As mentioned above, two areas of the Corinth Basin are currently underwater and therefore, obviously, inaccessible to a foot-based investigator. However, much of the southern and north-eastern areas of the basin have exposures of the sedimentary fill. The Isthmus of Corinth provides a land-link between these two more marginal areas and so provides a complete north-south cross-section through the topmost sediments in the Corinth Basin.

Topographic gradients are low in the central and southern parts of the basin where cultivation is extensive. Exposure thus tends to be limited to road-cuts, scarps of wave-cut and/or fault-scarp origin and ancient quarries. The Mediterranean climate, however, ensures that most outcrops are clean and free of vegetation. Calcretised, unvegetated sediment "pavements" also occur. Furthermore, the Corinth Canal offers a superb section through the sedimentary cover. The canal is 6km long with continuous cliff sections up to 90m high which are locally accessible by paths down the NE cliff-face and at the NW and SE

ends of the canal. This must be the finest cross-section through an intrabasinal tilt block train anywhere in Europe.

Basin-fill sediments are exposed extensively to the north and north-east of Kalamaki, to a height of 550m above present sea-level. Steep gradients and river-incised canyons provide good exposures here, with locally up to 80% outcrop.

Lithological logging, on appropriate scales, has been carried out on sediment sections across the basin, concentrating on areas of particular sedimentological interest or key sections for the interpretation of tectono-sedimentary relationships. Mapping was carried out as required. 1:50,000 geological and topographic maps were made available by the Institute of Geology and Mineral Exploration in Athens and by the Geographical Survey, Athens. Additional maps were supplied by the American School of Archaeology in Ancient Corinth.

Landsat imagery (black and white and colour composite) and aerial photography were employed to aid mapping and structural interpretation.

1.4 LABORATORY TECHNIQUES

Various laboratory techniques have been used to constrain the lithological character and chronology of field samples. Details of techniques appear in relevant text sections and appendices. Microscopy was generally limited to the use of transmitted light as no detailed diagenetic or mineralogic analyses were undertaken. Sections were half-stained with Alizarin Red-S and potassium ferricyanide if carbonate characterization was required. Scanning electron microscope (SEM) and x-ray

diffraction (XRD) examination of scleractinian coral samples was carried out to assess their suitability for uranium-series disequilibrium isotopic age determinations. Such U-Th analyses were carried out by Dr Tim Atkinson of the University of East Anglia. K-Ar dating of andesites from the northern Corinth Basin was carried out by Dr Dave Rex of the University of Leeds. Some 65 field samples were examined for micropalaeontological content by Dr John Athersuch of the BP Research Centre, Sunbury-on-Thames. Abbreviated results of his study are presented in appendix 1. Certain silt and mud specimens were collected with the intention of considering their suitability for C/S stable isotope analysis to determine depositional environments (Berner & Raiswell 1984). However, these samples contained levels of inorganic carbonate which precluded their analysis by this technique so this avenue was abandoned. All computer programming was written in Fortran 77 for use on the Leeds University Amdahl mainframe.

1.5 THESIS LAYOUT

Throughout this thesis key aspects of the evolution of the Corinth Basin and critical studies of the controls acting upon the system at particular times are considered separately. Each chapter is therefore distinct in geographical/geological and theoretical content. Chapters 3 to 5 take the form of self-contained papers prepared as the basis for publications - the core of chapter 4 is already submitted for publication (Collier in press (c)).

The remainder of chapters 1 and 2 review the theoretical and regional literature relevant to a tectono-sedimentary study of an extensional basin in central Greece. Chapter 3 describes the

Lower Pliocene sedimentary fill in the north of the Corinth Basin. The contemporaneous structural development of the basin is inferred from the sedimentary patterns and features observed. Additional controls acting upon the Lower Pliocene system are discussed in qualitative terms in relation to the structural form and evolution of the basin at that time.

Chapter 4 concentrates on a study of the Corinth Canal. The interaction of the tectonic vertical displacement of the Corinth Isthmus with variation in late Quaternary eustatic sea-level is considered from two directions. Firstly, a computer model is set up which predicts facies geometries as a product of the two variables. Secondly, on the basis of empirical evidence, and by reference to the "known" late Quaternary sea-level curve, the tectonic component to post-depositional relative base-level change is quantified.

Chapter 5 illustrates specific geological case histories from the tectono-sedimentary patterns of the southern Corinth Basin. A facies analysis is presented of shallow marine sediments. The distribution of these deposits was influenced by syn-depositional basin structure and the sequence has been affected by post-depositional faulting. The compatibility of basinwide models of facies distribution with smaller scale intrabasinal tilt block settings is discussed. Problems in the interpretation of syn-rift sedimentary environments are explored, as are problems of isolating the process controls which generated observed geomorphic and sedimentary features.

Chapter 6 provides a summary of the structural and sedimentary evolution of the Corinth Basin. An integrative discussion then follows on the variation in space and time of controls

determining the distribution of sedimentary facies through the basin fill.

1.6 LITERATURE REVIEW - THEORY

1.6.1 Extensional Basin Evolution

An awareness of basin forming processes and the geothermal evolution of an extending basin is necessary to comprehend the range of tectonic actions which may affect basin morphology and hence sediment distribution within that basin.

Early models describing extension of the continental crust emphasized pure shear as the mechanism for thinning the crust and mantle lithosphere (fig. 1.2a). Artemjev & Artyushkov (1971) proposed that the upper crust extends by brittle deformation, with the formation of fault-bounded rifts, whilst the lower crust undergoes ductile attenuation. McKenzie (1978a) quantified the thermal response to uniform stretching of the entire lithosphere by pure shear - for a given and specific set of conditions. Stretching of the continental lithosphere is assumed instantaneous in the model. Isostatic compensation is preserved throughout and lateral heat flow is ignored. The product is an initial fault-controlled subsidence followed by a more gradual and diminishing subsidence rate of the isostatic response to the thermal re-equilibration of the lithosphere. This model has gained popularity due to the simplicity with which an extension factor (β) may be derived from back-stripped sediment thicknesses within a basin (e.g. Sclater & Christie 1980, Wood & Barton 1983). β may also be obtained more directly from crustal scale refraction or reflection surveys.

Figure 1.2

Schematic end-member models for extensional deformation of continental lithosphere.
a) Pure shear model - the upper crust undergoes brittle extension and the lower crust ductile attenuation, over mantle lithosphere attenuated to an equivalent degree.
b) Simple shear model - upper crust brittle extension is accommodated by simple shear through the lithosphere on a low-angle detachment. "Upper plate" and "lower plate" attenuation are thus offset, producing an asymmetric geometry.
After Wernicke (1985) and Buck et al (1988).

a

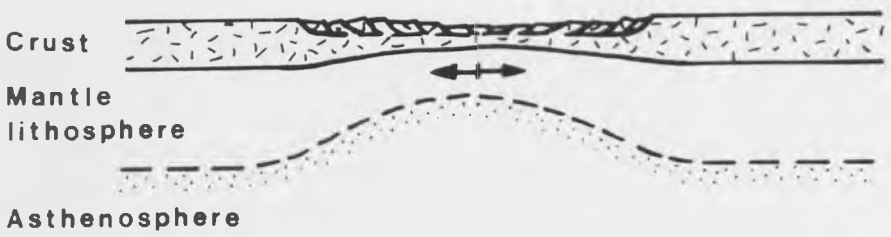
Crust
Mantle
lithosphere
Asthenosphere

b


Crust
Mantle
lithosphere
Asthenosphere

Jarvis & McKenzie (1980) developed the uniform pure shear model to encompass extension events of finite duration. They found that heat flow and resultant subsidence values only differed significantly from the original model if extension continued for more than 15-20 Ma (for given attenuation factors). Steckler & Watts (1980), however, found that lateral heat loss out from the zone of attenuation was an important factor in determining subsidence rates in the early history of a continental margin. Greater syn-rift subsidence values were calculated to result from given extension factors when lateral heat flow was incorporated into the equation. Cochran (1983) developed the model to include the consequences of both finite rifting times and lateral as well as vertical heat flow functions. The effect was that predicted subsidence was increased during the syn-rift phase but diminished through the post-rift phase, as compared with the simple McKenzie (1978a) model. Furthermore, these effects were predicted as being more marked towards the basin margins, and flanking regions (basin footwalls) were shown to undergo uplift of the order of several hundred metres under certain conditions.

It has since been demonstrated that additional convective effects would increase the magnitude (although not the pattern) of isostatic uplift and subsidence across a basin margin, when compared to passive conductive models (Keen 1985, Buck 1986).

Leeder (1983) found that the uniform pure shear model of extension could not explain features of the Jurassic North Sea basin. Leeder proposed that hinterland uplift, intrabasinal uplift and basaltic volcanism, and subsidence of up to c.1km outside the fault-controlled rift necessitated a model based on non-uniform stretching between crust and mantle lithosphere together with possible lithospheric flexuring. Wernicke (1985)

illustrated a structural mechanism for a non-uniform extension model, by offsetting crustal thinning from subcrustal lithospheric thinning along a low-angle detachment - a simple shear model (fig. 1.2b). The net uplift/subsidence response at any locality will be the product of the combined isostatic response to thinning of the crust and to thinning of the mantle lithosphere (McKenzie 1978a, Royden & Keen 1980). Preferential thinning of the mantle lithosphere which is more dense than asthenosphere will cause uplift. Crustal thinning of a greater attenuation factor than of the mantle lithosphere will generate subsidence. Royden & Keen (1980) coined the term tectonic subsidence (McKenzie's initial subsidence) for the response to an initial extensional strain. Thermal subsidence describes the later subsidence produced by conductive cooling of the subcrustal lithosphere.

Buck et al (1988) developed a two-dimensional quantitative demonstration of the consequences of a simple shear model of crustal extension. Heat flow is solved in two dimensions and extension rates are defined. An asymmetric uplift/subsidence profile is generated by the normal-sense simple shear, assuming local Airy isostatic compensation (fig. 1.3). Maximum uplift is predicted to occur in the hangingwall behind the zone of rift subsidence. Two predicted features are that a) the rift will widen by migration back into the lower plate, and b) the major upper plate uplifted shoulder will tend to advance basinwards due to the combined effects of active advective heating of the detachment region and the thermal uplift response to thinning of the mantle lithosphere. Dunbar & Sawyer (1988) predict similar topographic asymmetries across continental lithosphere undergoing simple shear extension. They utilise the finite element method

Figure 1.3

a) Schematic cartoon of parameters expressing the form of lithospheric sections subject to simple shear (Buck et al 1988). W_r = width of zone of crustal thinning.
W_{ss} = surface width of shear zone (dipping at angle theta).
b) Topographic product of simple shear, assuming Airy-type isostatic compensation, for crustal subsidence and thermal uplift caused by the attenuation of the crust and mantle lithosphere. W_r increases with time; model results are shown at 2, 6, 10, 14, 18 and 22 m.y. after rift initiation. W_{ss} is zero (representing a detachment), theta is 15^{o} and the extension rate 1cm/yr. Horizontal width of the topographic section = 1000 km.
c) Topographic product of simple shear. Parameters as in (b), except W_{ss} = 50 km.
After Buck et al (1988).

a

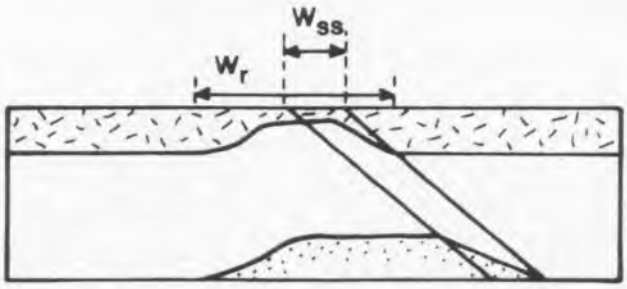

b

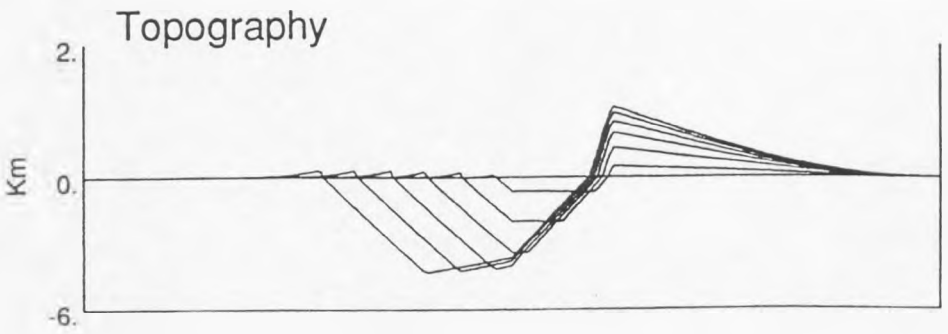

c

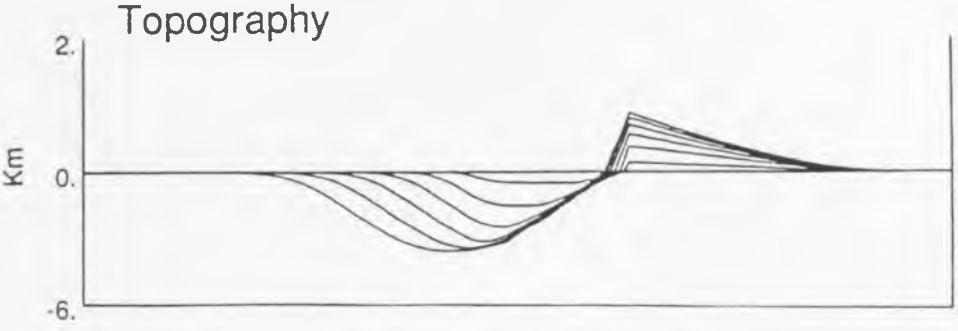

of two-dimensional analysis. This enables the effects of crustal density heterogeneities and variations in initial crustal thickness to be incorporated into the models. Buck et al (1988) point out that pure shear attenuation is more efficient at generating melts than the more widely distributed thermal anomaly produced by simple shear extension.

Recent two-dimensional modelling techniques demonstrate the scope for including geological and geophysical data into basin subsidence models. The interaction of the range of variables acting on the thermo-mechanical basin system requires the full range of conditions to be taken into account, if attempting an analysis of a real basin example (e.g. the Red Sea in Buck et al 1988). These factors include:

a) Pure shear versus simple shear.

b) Finite rates and durations of extension.

c) Possible crustal heterogeneities.

d) Possible active processes of convection or asthenospheric melt addition (e.g. by the partial melting of a subducted oceanic plate).

1.6.2 Structural Framework

It is necessary to understand the geometric range and effects of normal faulting to establish the likely sedimentary response to active tectonism within an extensional basin. Extensional tectonics characteristically generates basin and block morphologies, on a variety of scales. Both vertical displacement and surface tilting is likely to result from any increment of movement on a fault. The prevalence of asymmetric structural forms tends to produce asymmetric subsidence/tilt

vectors. The sedimentary response consequently tends to show asymmetries. Asymmetries may take the form of clinoforms showing downlapping as opposed to offlapping geometries, alluvial surfaces undergoing alluviation or incision, or coastlines being transgressed or regressed according to the structural context (Leeder & Gawthorpe 1987). Such asymmetries allow structural geometries to be deduced from depositional geometries.

Extensional basins bounded by continental crust occur in two principal forms; grabens and half-grabens [simplifying "basins" to linear troughs at high-angle to the direction of maximum tensile stress, so excluding transtensional and pull-apart basins]. Grabens are bounded on two sides by faults, half-graben basins on one side only. Asymmetric grabens are the intermediate, with two basin-bounding faults but of different magnitudes of displacement. Early models emphasized the block and basin morphology of basins (Bott 1971, Artemjev & Artyushkov 1971). Subsequent workers recognised the need for some geometrical mechanism to accommodate fault displacements across the brittle-ductile transition (Morton & Black 1975, Wernicke & Burchfiel 1982). Fault structures could have two end-member forms; listric or planar. In the case of listric normal fault displacements, differential tilt occurs between footwall and hangingwall. Bedding dips steepen into the fault in the hangingwall. In the simplest case of planar faulting, a train of "domino" rotating blocks (Wernicke & Burchfiel 1982), the row of planar fault-bounded blocks will all be tilted by the same amount. Listric faults shallow onto a low-angle decollement. Planar rotational faults must also either shallow onto a detachment surface at depth or undergo accommodatory shear at their roots to compensate for voids that would otherwise be

generated.

Planar Rotational Faults:

The planar rotational fault model has been emphasized in studies of the Basin and Range province (Wernicke 1981, Wernicke & Burchfiel 1982, Gross & Hillmeyer 1982). Gross and Hillmeyer found that the rotation of blocks above a detachment surface could be accommodated by the successive development of new normal faults at steeper angles as pre-existing faults were rotated to lower angles. Proffett (1977) had already described the effect of multiple generations of sub-planar faults. These allowed higher angle rotations of strata and higher extension factors than would be possible for single fault-generation rotating blocks. This is because planar faults become mechanically inefficient and therefore lock after rotation of the fault to a dip of about 30^{o}. This corresponds to the observation of Jackson (1987) that normal faults with dips less than 30^{o} do not move seismically. Any movement on lower angle brittle faults must therefore move aseismically.

Barr (1987) provides a geometrical analysis of the displacement vectors arising from rotation of one member of a domino-train of planar fault-bounded blocks. Assuming ductile deformation of the lower portion of each fault block to avoid the generation of voids, it remains a geometric necessity that footwall regions will be uplifted above the pre-faulting topographic datum (for given initial fault angles and fault-spacings). The problem of void-generation inherent to the theoretical planar-rotation model is most acute at the junction between the domino train and the non-rotating footwall. The space problem can be accommodated by a listric bounding fault (fig. 1.4a), by a model of antithetic normal fault structures opposed to a principal normal fault (fig.

Figure 1.4

a) Schematic diagram of planar "domino" blocks rotating over a detachment against a bounding listric normal fault. The lower portion of each tilt block undergoes ductile deformation to avoid the generation of voids (Barr 1987).
b) Schematic cross-section to illustrate the gross geometry of planar upper crustal faults passing onto a lower angle detachment in the brittle-ductile transition zone. The displacement on this mid-crustal detachment will diminish with depth as an increasing proportion of the extension is taken up by ductile strain (after Eyidogan & Jackson 1985).
c) Asymmetrical footwall and hangingwall reverse drag produced by the displacement gradient on a normal fault dipping at 60° within horizontal beds. Fault radius/maximum displacement = 5. (After Barnett et al 1987).

a

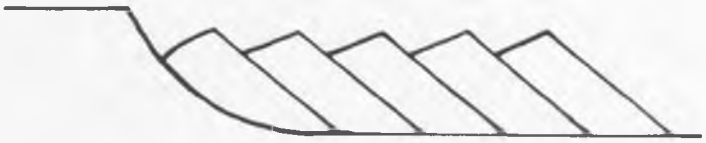

b

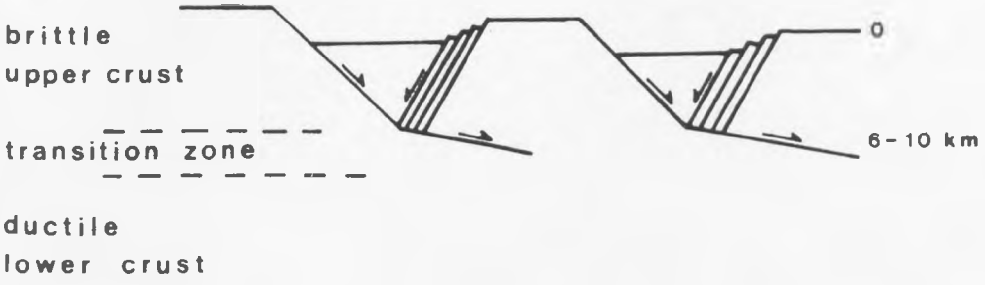
brittle
upper crust
transition zone
ductile
lower crust
0
6-10 km

c

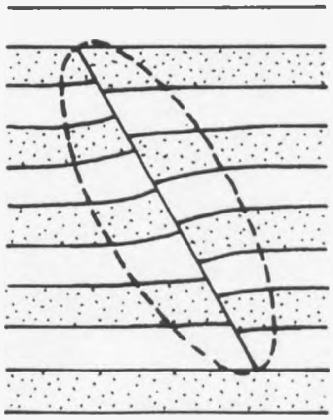

1.4b) or by the internal and heterogeneous deformation (whether ductile or brittle) of the rotating block adjacent to a non-rotating footwall (Barr 1987, Jackson et al 1988). Barnett et al (1987) formalise the ductile deformation that may occur in the vicinity of a planar normal fault nucleated in isolation from other structures, i.e. not linked onto a detachment surface (fig. 1.4c). Such local strain heterogeneities will also occur around the elliptical displacement field of any one displacement event on a fault surface (Watterson 1986).

Listric Faults:

The listric faulting model takes the form of one or more concave-up normal fault surfaces which diminish in dip with depth onto a low-angle or horizontal decollement surface (Cloos 1968, Bally et al 1981, Gibbs 1984a). The decollement may delineate upper crust brittle extension from lower crust ductile attenuation at or near the brittle-ductile transition zone (Wernicke 1981, Brun & Choukroune 1983) or may occur at higher levels within the brittle upper crust, with movement facilitated by the presence of low-friction layers such as evaporite strata (e.g. Gibbs 1984b). Alternatively displacements may be transferred by extensional simple shear zone(s) or "staircase" geometries to the lower crustal or subcrustal domains (Brun & Choukroune 1983, Smythe et al 1982, Gibbs 1987, Buck et al 1988).

The retreat of the hangingwall from the listric fault footwall creates a potential void which must realistically be replaced. Folding of the hangingwall strata accommodates such space problems; hangingwall rollovers ("reverse drag" of Hamblin 1965) occurring over concave-up fault segments and hangingwall synclines developing over convex-up "ramps" (Gibbs 1984a, Williams & Vann 1987). Rollover anticlines are characteristic,

but not definitive, of listric fault geometries (Barnett et al 1987, W. Higgs pers. comm.). Hangingwall strain heterogeneities produced by displacement gradients on a planar fault surface may also produce hangingwall anticlines and synclines. Any modelled fault surface derived from the interpretation of a hangingwall rollover form is limited by some assumption of the character of hangingwall deformation (Wheeler 1987). A variety of graphical and area balance techniques exist for estimating the form of listric normal faults. Each is based on a specific set of assumptions regarding the internal strain history of the hangingwall block in 2-dimensions (Gibbs 1983, White et al 1986, Williams & Vann 1987, Wheeler 1987).

Linkage - Transfer Faults and Zones:

Extensional basins often have structures at a high angle to basin margins. These may correspond to reactivated crustal fractures produced by some earlier orogen of independent stress orientation (e.g. Leeder 1982). Alternatively, they may be integral compartmentalising features of the active graben or half-graben (Gibbs 1984a). Analogous to lateral ramps in thrust tectonics, transfer faults may offset compartments of distinct structural geometry and strain history. An alternative to discretization of compartments by transfer faults is the gradual change of structural tilts/levels across a transfer zone (Leeder et al 1988). As normal faults propogate laterally, so neighbouring en echelon fault segments will overlap and produce interference patterns with complex tilt surfaces (Bosworth 1985). Ultimately, fault block trains in neighbouring "compartments" may develop tilts in opposite directions dependent on the sense of displacement on their respective master-faults (as in Garfunkel & Bartov 1977). Extensional strain magnitudes may vary between

neighbouring compartments, accommodating variation in finite extension along the axis of an extensional basin.

Footwall Uplift:

Vertical movements in response to normal faulting comprise hangingwall subsidence and subordinate footwall uplift. Such movements have been measured geodetically (Savage & Hastie 1966, Hooke 1972, Stein & Barrientos 1985) and relative to sea-level (Jackson et al 1982a).

The footwall uplift component of normal fault displacement may be the product of a combination of processes. Dependent on fault dip, fault spacing and angle of block rotation, there may be a geometric requirement for the footwall crest of a rotating block to undergo net uplift (even after subsequent sediment loading) with any increment of fault displacement (Barr 1987, Jackson et al 1988). Secondly, there may be a component of elastic rebound with the release of strain immediately after slip on the fault plane (Savage & Hastie 1966, Jackson & McKenzie 1983) of a magnitude dependent on fault attitude. Mansinha & Smylie (1971) estimated the elastic footwall uplift of a fault dipping at 45° to be about 10% of the fault throw. Such elastic displacements will be nullified by the subsequent re-establishment of extensional stresses across the fault. So any topographic feature produced by footwall elastic rebound would theoretically be a transient feature and have only periodic influence on sediment distribution. A third potential mechanism for generating footwall uplift is the isostatic response to unloading of the footwall block by hangingwall subsidence/heave. Jackson & McKenzie (1983) calculated that isostatic footwall uplift during normal faulting would amount to about 10% of the

hangingwall subsidence, on a normal fault dipping at 45°. This model assumes local Airy isostatic compensation and that the fault cuts right through the continental crust and so excludes any effects of crustal flexure. The predicted footwall uplift value is strongly dependent on fault dip and hence the extent of unloading of the footwall for any given throw on the fault. If the fault plane were vertical, no local isostatic uplift would effect the footwall block in response to downfaulting of a neighbouring block. A second constraint on the system is the density of material infilling the space vacated by the hangingwall subsidence; air, water or sediment. The greater the contrast in substrate densities across the fault, the greater the ratio of footwall uplift to hangingwall subsidence.

Fault Scarp Degradation:

As has already been stated, the distribution of sediments within a basin will largely be constrained by the structural form of the basin. One feature of actively extending basins which has direct influence on facies patterns is the generation of fault scarps. Such scarps will be the product of fault block rotations and the elastic and isostatic responses to hangingwall downfaulting, as just discussed. In sub-aerial environments, erosion of fault scarps and/or basin floor will also influence topography and subsequent sediment distribution across that surface.

Faulting and the generation of fault scarps produces two distinct environments within the basin. One is the steep footwall scarp which successively exposes fresh fault plane surface area with fault-throw increments. The second is the relatively shallow tilted surface of the hangingwall. This may be exposed basement behind the footwall of a rotating basement tilt block or the

tilted sedimentary surface of the graben/half-graben hangingwall (basin floor). The degree of tilting of both the hangingwall and the area behind the footwall crest (the hangingwall of the next basin in the case of a domino series of tilt blocks) associated with some fault increment diminishes away from the fault plane as the elastic strain component decreases (Savage & Hastie 1966, Stein & Barrientos 1985).

The rate of degradation of any fault scarp will be a function of a number of factors. Firstly, the environment within which the fault scarp is found; sub-aqueous or sub-aerial, and climatic conditions controlling mechanisms of erosion. Secondly, fault dip and the rate of fault displacement will determine rates of erosion and the net product of footwall emergence/footwall erosion. Any gravity-driven erosive mechanism such as stream flow will be a function of slope angle and topographic relief. Bucknam & Anderson (1979) considered the relationship between fault scarp height and slope angle in Quaternary sediments in western Utah. They found that the slope angle is proportional to the scarp height and that any decrease in slope angle for scarps of a given height is a product of the greater age of that scarp. This assumes that fault angles are similar, substrates are similar and the structural evolution of each scarp was similar. At best, such comparisons are therefore only likely to be helpful within any one geological and structural setting.

Schwartz & Coppersmith (1984) recognized the significance of fault recurrence intervals influencing fault scarp topography. In addition, a single fault displacement of magnitude x after some period t may generate greater erosive activity than the sum of erosive activity after y displacements of magnitude x/y

occurring every t/y.

Schwartz & Coppersmith (1984) and Hancock & Barka (1987) point out that clastic wedges accummulated against the base of normal fault scarps will reduce the availability of fault surface to erosion and so modify the rate at which such a scarp will degrade (fig. 1.5). With respect to limestone footwall lithologies of normal faults in western Turkey, Hancock & Barka describe a range of fault-rock and geomorphic modifications to the fault surface which will affect susceptibility to physical and solution weathering processes. These include the generation of pore-space by fault-rock brecciation, pluck holes, comb fracture traces and stream-cut gutters. Stewart and Hancock (in press) also detail processes of subsurface water channeling, bio-erosion and soil/vegetation build-up which will affect denudation rates.

The structural geometry and evolution of an extending graben/half-graben has been shown to be a principal control on basin morphology. Basin boundaries, the relief and attitude of the topographic surface and the development of fault scarps and tilt block chains are all a direct function of structuration. The structural setting of any sediment body, against a footwall, on a hangingwall against a transfer fault or within a transfer zone will determine the facies and architectural evolution of that deposit. This is due to the distinct displacement vectors characteristic of each structural setting (Leeder & Gawthorpe 1987, Leeder et al 1988).

1.6.3 Sedimentary Facies - Concepts, Qualitative Models, Quantitative Simulations

The definition of the facies concept has undergone some evolution

Figure 1.5

Cartoon strip (a - e) illustrating the development of a normal fault zone through bedrock and the resultant alluvial fan. As fault brecciation continues the active slip-plane may migrate into the hangingwall, eventually cutting through the colluvium to produce a complex alluvial fan-fault zone profile. (After Schwartz & Coppersmith 1984 and Hancock & Barka 1987).

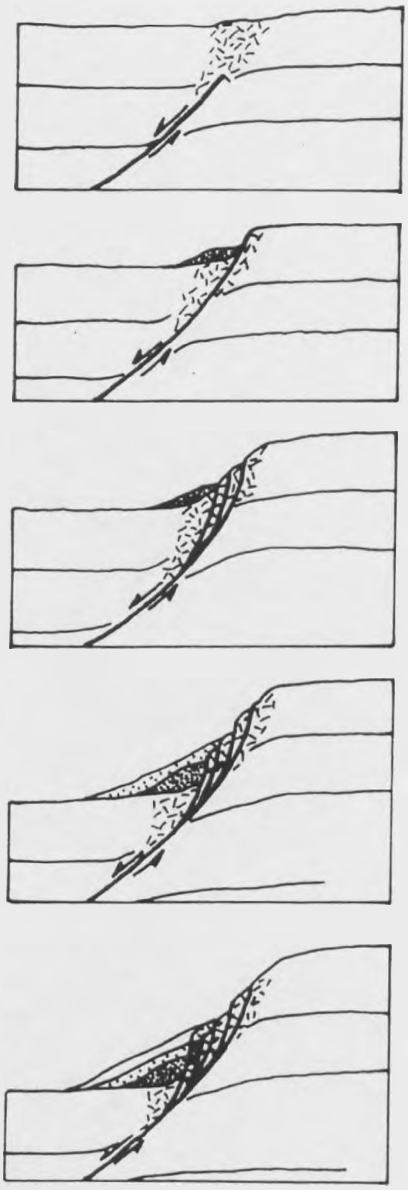
a
b
c
d
e

in the historical literature (Walker 1984). The word derives from the latin facia/facies, meaning the external appearance of an object. A purely descriptive concept is implied. Middleton (1978) detailed this approach as an objective description of the total field, lithological, sedimentary structure and organic aspects of rocks. The facies could be given an informal title (facies A, etc.) or a descriptive title (laminated siltstone facies). Anderton (1985) provides a less restrictive approach to the subject. In addition to the descriptive sedimentary facies, he defined an interpretative sedimentary facies as "A label summarizing the interpretation of the processes and environments of deposition of a certain rock unit". So the descriptive laminated siltstone facies may be an interpretive lacustrine facies or even an interpretive interdistributary bay lacustro-deltaic subfacies. Both descriptive and interpretive facies will usefully be employed through this text. Lithofacies may additionally be used to loosely refer to the descriptive form. The terms facies associations or suites (descriptive or interpretive) will be used to imply spatial relationships between the facies concerned.

One extra point to note is that in the neotectonic environment an apparently interpretive facies may in fact be descriptive. When standing on an active alluvial fan, the sedimentary processes and environment observed become part of the description. Alluvial fan facies in this case becomes a descriptive term.

Facies patterns across some sedimentary basin must be described with three dimensions in mind. At any one time horizon, the topography of the depositional/erosional surface necessitates the inclusion of a vertical dimension reference. The third, vertical dimension is also required to describe the burial

history of a sediment column and any vertical change in facies. But the sedimentary history introduces the fourth dimension of time. Sedimentation rates (the vertical dimension divided by the time dimension) may vary according to sedimentary and structural environment within a basin. Thus facies models and models describing the evolution of sedimentary facies patterns through time should ultimately be related to 3- and 4-dimensional frameworks respectively.

A variety of controls determine the spatial distribution and development of facies within a basin. These may be divided into two distinct suites; sedimentary processes and non-sedimentary controls. The sedimentary controls are here used to imply processes which will be occurring within any environment independent of external influences (such as tectonic activity). Thus within a fluvio-deltaic environment, for example, channel migration, delta progradation and abandonment due to crevasse events (Elliott 1974), diversion of channels into topographic lows produced by the compaction of interdistributary fines (Collier in press (a), Fielding 1984a), and erosion of exposed surfaces are all products of the internal hydrodynamics and resultant architecture of the system. These influences will be modified, however, by non-sedimentary processes such as the tectonic tilting or vertical displacement of the alluvial surface (Bridge & Leeder 1979, Alexander & Leeder 1987). Tectonic activity and the tectonic history of a basin will determine its relief and gradients within the basin. Other non-sedimentary controls include eustacy, climatic conditions and the possible occurrence of volcanism. Hinterland drainage areas and hinterland lithologies are a second order control (themselves determined by the regional tectonic history) which will influence

sediment supply rates and the compositional character of basin deposits.

Field studies of axial river channels have demonstrated that active tectonic tilting may instigate instantaneous avulsion events or may alternatively produce a gradual migration of the channel belt (Alexander & Leeder 1987). The channel belt preferentially migrates downslope while meander loops are preferentially abandoned upslope. Leeder & Gawthorpe (1987) considered tectono-sedimentary interactions within extensional grabens/half-grabens and developed qualitative models for the three- and four-dimensional distribution of sediments for particular environmental settings. Asymmetric tectonic subsidence vectors typical of half-grabens tend to produce asymmetric facies patterns. Structural levels/tilts and structural access to any marine influence will determine whether the basin-fill is chacterised by interior drainage lake development, axial through-drainage or marine sedimentation with or without axial flow. Examples of such systems influenced by extensional fault activity may be found in Surlyk (1978), Sellwood & Netherwood (1984), Fielding (1984a), Gawthorpe (1986), Leeder & Alexander (1987), Ord et al (1988) and Leeder et al (1988).

The deduction of qualitative models of sedimentation in extensional basins by the observation of both modern and ancient tectono-sedimentary systems then allows the development of quantitative models. Sedimentary architecture may be predicted by the quantification of controlling influences on sediment distribution. Such work has so far been concentrated on the simulation of alluvial architectures (Bridge & Leeder 1979, Crane

1982, Alexander 1986a, Collier in press (a)).

Two approaches have been developed for the quantitative simulation of alluvial architecture. Both would be applicable to alternative depositional environments. One approach is to interpolate the detailed facies patterns between borehole-constrained sample columns; probabilistic "stochastic" modelling. The second approach is the simulation of theoretical alluvial sections. Both are limited by how realistic are the assumptions and input data used. Alexander (1986a) points out a functional difference between the two approaches. Stochastic models divide reservoir rock from shale permeability barriers for purposes of reservoir modelling (Haldorsen & Lake 1984). Alluvial section simulations, on the other hand, may make genetic distinctions between channel-belt and overbank facies (Bridge & Leeder 1979).

Early quantitative models were manually operated and simulated positional response of channels to conditions of climate and base-level variation (Allen 1974, 1978) and avulsion periodicity, floodplain width and sedimentation rate (Leeder 1978). Bridge & Leeder (1979) then provided computer simulations of flow-normal alluvial sections to explore the effects of a number of inter-related controls on the resulting architecture. These controls were a) laterally variable aggradation rates, b) contrasting rates of compaction between overbank fines and (non-compacting) channel-belt sands, c) tectonic tilting of the floodplain surface, and d) channel avulsion periodicity as defined by some predetermined non-random distribution. Any asymmetric tilting (half-graben) influence was found to concentrate channel-belt sandbodies towards the actively downfaulted floodplain margin. Crane (1982) further quantified the inherent sedimentary controls on channel avulsion activity. He related avulsion periodicity

to the topography of the floodplain, flood event distribution and mean flood flow velocity. Alexander (1986b) combined the use of geologic data with the theoretical consideration of the tectonic influence on alluvial architecture to develop a predictive model of syn-depositional flow patterns and hence alluvial sandstone body distribution in the subsurface.

The significance of differential compaction rates affecting the topography of an alluvial surface was further investigated by Collier (in press(a)). Two components to the lateral variation in compaction rates are recognised. These are; a) a facies-dependent differential governed by the porosity-depth curve of each lithology within the alluvial section and b) a differential resulting from any underlying basement topography. Two-dimensional architectural simulations across a buried tilt-block topography indicate that asymmetries in facies distribution may continue long after active tilting of the buried basement and alluvial surfaces has ceased. Mathematical descriptions of compaction curves were derived for a variety of lithologies, based on borehole-constrained porosity/depth data of Sclater & Christie (1980), Baldwin (1971) and others. This enabled multi-lithology alluvial sections to be produced, taking into account the within-sequence compaction variables. Computer simulations of simplified Coal Measures alluvial sections, for instance, quantitatively confirm the qualitative observations of Fielding (1984a). These contrast the typically diagonal-offset pattern of sandbody distribution in a "passive" alluvial section from the vertical stacking of sandbodies which characterise tectonically-influenced architectures [with the proviso that vertical stacking of sandbodies may also result from post-faulting basement irregularities, as mentioned above].

A further constraint on sedimentary facies distribution, the position of relative base-level through time, has also been modelled quantitatively. Pitman III (1978) simulated an Atlantic-type passive margin and the migration of a coastline across that margin with changing sea-level. The rate of net coastal transgression or regression was a function not only of whether sea-level was rising or falling but the rate of sea-level rise or fall compared to the rate of subsidence of the continental margin. Sedimentation rates across the continental margin are a further constraint on the system. This approach to modelling base-level change relative to the continental surface subsidence/uplift and sedimentation rates is equally applicable to lacustrine settings as it is to marine settings. Sea-level varies as a function of glacio-eustacy and/or changes in the capacity of ocean basins and/or the output of juvenile water at mid-ocean ridges (Pitman III 1978). Lake volumes may vary in response to changes in climate (changing the supply/evaporation ratio) or local tectonic effects changing the geometry of the lacustrine basin.

Chapter 4 details quantitative stratigraphic modelling of the migration of coastal facies in response to relative base-level changes, as carried out by this author. The effects of glacio-eustatic and tectonic displacement variables have been modelled in relation to given depositional slope angles and sedimentation rates. Where the glacio-eustatic variable in well-constrained through time, i.e. through the late Pleistocene and Holocene, the stratigraphic effects of eustatic variation may be accounted for. This allows the estimation of the tectonic displacement component through time (Chappell 1974, Collier in press (c) and chapter 4

of this thesis).

It should be remembered, however, that even these more advanced simulations are only demonstrations of the potential influence of the specific conditions dealt with by each model.

CHAPTER 2 REGIONAL GEOLOGICAL SETTING

2.1 SUMMARY

Since the Late Miocene the Aegean area has been under approximately north-south extension (relative to its present orientation). The Aegean terrane lies to the north of the Hellenic Trench where north-eastwards subduction of the Mediterranean floor continues. Prior to the Late Miocene the region had been in an Alpine collisional setting characterised by westerly-directed thrusting. This crustal shortening history has left a remnant core of overthickened crust running north-south through central Greece.

During the neotectonic (post-Alpine) history of the area the crust has been attenuated in the concurrently-subsiding Aegean Sea. A system of discrete fault-bounded basins dissect Mesozoic basement sequences on the Greek mainland and Palaeozoic-Palaeogene basement in western Turkey. In central Greece major basin-bounding faults trend E-W or ESE-WNW. Further north in the Aegean a component of dextral strike-slip motion linked to the North Anatolian Fault interacts with extension that produced the North Aegean Trough. The Menderes basins in western Turkey show an analogous structural style and a similar E-W trend to the Gulf of Corinth system in central Greece.

Neogene extensional basins in the Aegean include true half-graben and graben forms but are more commonly asymmetric grabens. Volcanism from Pliocene to historic times has been concentrated in the narrow South Aegean Active Arc (Fytikas et al 1984) and forms a typical subduction-related calc-alkaline suite, predominantly andesites and dacites.

2.2 THE AEGEAN PROVINCE

2.2.1 Pre-Neogene Geology

The origins of the Peloponnese, western and north-central Greece (also much of Albania and Yugoslavia), and SW Anatolia lie in the Apulian platform (fig. 2.1). This was part of a Permo-Mesozoic African promontory within the triangular embayment of Tethys on the Pangean continental margin (Sengor et al 1984b, Robertson & Dixon 1984). Eastern Macedonia, Thrace and northern Anatolia originated from the Cimmerian continental wedge according to the model of Sengor et al (1984b). Laurasian continental elements lie to the north. See also Dewey & Sengor (1979), Mercier (1979) and McKenzie (1978b).

The partial closure of Palaeotethys along the Caucasian Cimmerides is thought to have proceeded during the latest Triassic (Sengor et al 1984b). To the south of the Cimmeride zone, rifting took place from the Upper Permian to Lower Jurassic. Rift events young westwards (Robertson & Dixon 1984), with extension in the southern Turkish area in the Lower Triassic and in the Greek area in the Mid-Triassic (Channel et al 1979). This rifting in the northern branch of Neotethys lay in a back-arc position relative to the Cimmeride orogen (Sengor et al 1984b). The question of when significant areas of Neotethyan oceanic crust first appeared in the southern branch (the proto-Mediterranean) remains uncertain. Evidence for Mesozoic rifting is seen in the Othris (syn. Sub-Pelagonian) Zone of east central Greece. A south-westwards transition from carbonate platform deposits to submarine fan to pelagic deposits includes facies variations and locally-sourced detritus compatible with active extensional faulting in the Early Triassic and the Jurassic (Smith et al 1979).

Figure 2.1

Lower Jurassic plate reconstruction of Pangaea, simplified after Sengor et al (1984b). The shape of the Cimmerian continent has not been palinspastically restored. Continental elements are therfore in relative positions only. Palaeotethyan closure along the Caucasian Cimmerides had commenced by the Late Triassic. Triassic and Lower Jurassic rifting generated the northern branch of Neotethys.
AP = The African Promontory, comprising the Apulian-Anatolide-Tauride Platform
SC = Sakarya continent
TWO = Tanggula-Waser Ocean
ArP = Arabian Promontory


PALAEOTETHYS
N+S
CHINA
PLATFORM
LAURASIA
TWO
CONTINENT
CIMMERIAN
Northern
SC Branch
AP
Southern Branch
NEOTETHYS
ArP
GONDWANA

The occurrence of olistrostromes and palaeoslope reversals in the Late Jurassic/Early Cretaceous, and Early Cretaceous melanges in the Othris Zone (Smith et al 1979) are related to the north-eastward migration of a thrust stack and ophiolite emplacement. Late Jurassic/Early Cretaceous emplacement of ophiolites of Mid-Jurassic origin (Spray et al 1984, Smith & Spray 1984) created western and eastern ophiolite belts either side of the Pelagonian Zone. The number and location of ophiolite root zones that sourced the Greek and Turkish ophiolite belts remains a matter of some controversy (Robertson & Dixon 1984; compare the single root zone of Ricou et al 1984 with the three or four root zones of Sengor & Yilmaz 1981 for ophiolites in western Turkey).

Tethyan strands remained open into the Tertiary. Calc-alkaline volcanism marking subduction zones (Robertson & Dixon 1984) and further cold emplacement of ophiolite slabs (Smith & Spray 1984) mark the complex Late Cretaceous/Palaeogene pattern of Tethyan closure and micro-continental collisional events. The major collision of the Apulian promontory with Eurasia, together with active Neotethyan spreading to the south by the Eocene, caused the anticlockwise rotation of the Apulian continental area (Robertson & Dixon 1984).

Late Eocene to Miocene nappe emplacement occurred across the Aegean region. Three principal metamorphic belts are recognised in the Hellenides by Papanikolaou (1984): 1) An external low-grade metamorphic belt (including high pressure-low temperature mica-schists) currently exposed in the southern Peloponnese and Crete can be linked to the single blueschist domain of the central Cyclades (also Lister et al 1984). 2) A medial metamorphic belt initially comprised a variety of "island-arc-

like" and non-metamorphic fragments (Papanikolaou 1984). These include the Ionian, Gavrovo-Tripolitsa, Pindos and Pelagonian units (Pe-Piper & Piper 1984 and fig. 2.3). Since the Eocene, the Pindos and Parnassos Zones and more easterly non-metamorphic nappes have remained at high structural levels. As a result they have supplied detritus to flysch basins to the west of the Hellenide thrusts. The flysch basins young to the west, reflecting the westwards advance of the Hellenide thrust front (Richter et al 1978). 3) The third, internal, metamorphic belt which covers the area of the Greek North Aegean,. eastern Macedonia and Thrace includes imbricated fragments of Cimmerian origin (after Papanikolaou 1984 and Sengor et al 1984b).

The western Ionian and Pre-Apulian Zones underwent continued compression into the Pliocene (Underhill 1988). This contractional deformation was a product of the Miocene-initiated Hellenic subduction system (Le Pichon & Angelier 1979, 1981, Mercier et al 1979a, Mercier 1981, Spakman et al 1988). Clockwise rotations recorded in the Ionian islands since 5Ma (Kissel et al 1984) probably relate to this Hellenic Arc contraction. The rapid rotations of 5 degrees/Ma inferred by Kissel et al (1984) may have been accommodated by thin-skinned allochthons moving across Triassic evaporite decollements (Underhill 1988).

2.2.2 Neogene Tectonics

A significant change in the Aegean tectonic regime at about the Serravallian-Tortonian boundary marks the onset of the neotectonic regime (Meulenkamp 1985, Sengor et al 1984a). The southern Aegean landmass started to break up and subsidence produced basins across the area of what is now the Aegean Sea.

During the Messinian, sediment supply rates were apparently reduced and typical deposits of the Aegean area include marls and evaporites, reflecting at least in part the Mediterranean salinity crisis (Meulenkamp 1985). A combination of enhanced extensional subsidence and eustatic sea-level rise in the Lower Pliocene led to the submergence of large areas and a palaeogeographical evolution towards the present configuration (fig. 2.2). McKenzie (1978b) inferred a stretching factor of two since the Miocene, on the basis of seismic refraction data which indicates about 30km of continental crust below the southern Aegean. This compares with up to 50km in Greece and western Turkey (Makris 1976). Recent refraction and magnetic studies by M. Hartung and J. Makris (pers. comm.) indicate that continental crust under the Cretan Sea has been attenuated to just 17km. Le Pichon and Angelier (1981) explained the Aegean extension as resulting from roll-back of the Hellenic subduction zone. In contrast, Dewey and Sengor (1979) attributed the N-S extension of the Aegean region to the westwards "extrusion" of the wedge-shaped Greek-Anatolian plate in response to the northward migration of the Arabian plate.

Two principal models exist for the Neogene evolution of the Aegean. The first, proposed by Mercier et al (1976, 1979a, 1983, 1987 and Mercier 1979, 1981, 1983; also Sebrier 1977), entails complex changes in the regional stress field through the Pliocene and Quaternary. During the Pliocene-Lower Pleistocene the internal domain (within the Aegean Arc) is inferred to have been under extension. However, local faulting on the island of Euboea and in the Corinth Basin (Sebrier 1977) with apparent reverse displacements led this research group to interpret a Lower-Mid Pleistocene compressional phase within the central

Figure 2.2

Major neotectonic elements in the Aegean province.
LB = Langhada Basin
AB = Axios Basin
SB = Sporadhes Basin
NAT = North Aegean Trough
NAF = North Anatolian fault zone
AG = Alasehir Graben
BM = Buyuk Menderes Graben
LA = Lamia Basin
GP = Gulf of Patras
GC = Gulf of Corinth
Principal sources:
Mercier et al (1987), Sengor (1987), Ferentinos et al (1981), Jackson et al (1982b), Psilovikos & Syrides (1984), Pavlides & Kilias (1987), Brooks & Williams (1982), Robertson & Dixon (1984).

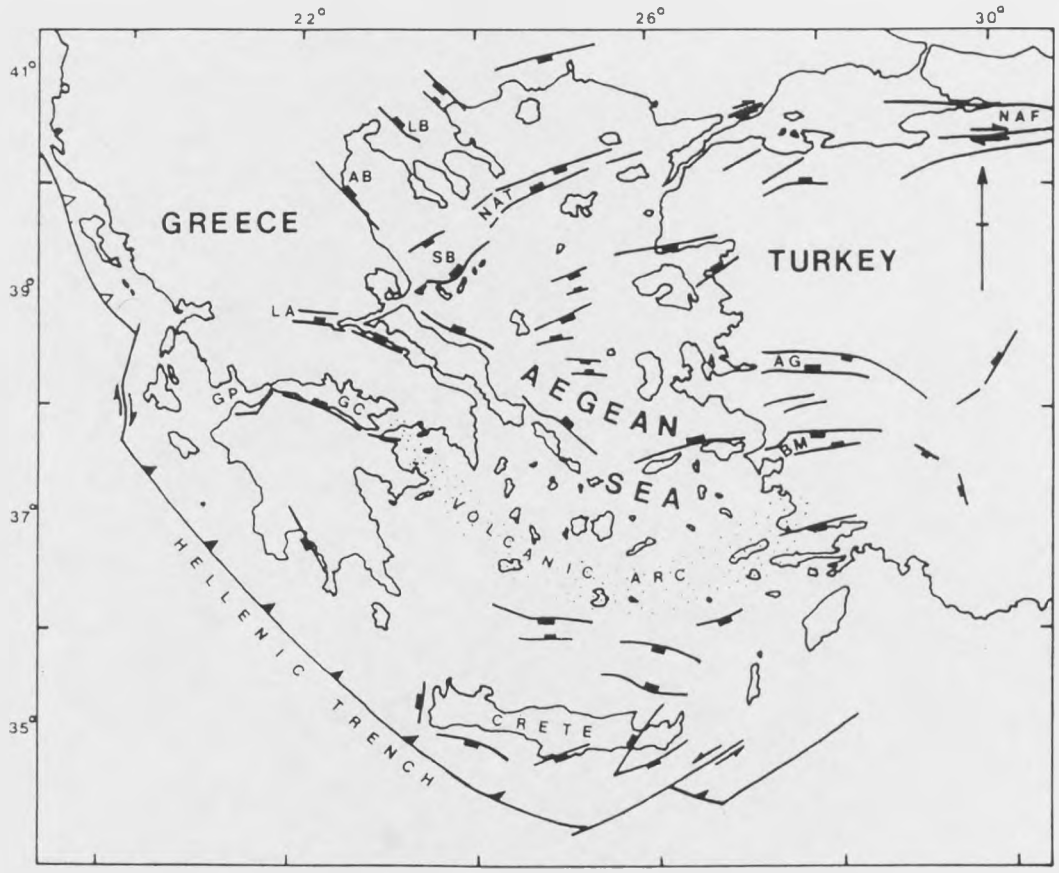
22°
26°
30°
41°
39°
37°
35°
GREECE
TURKEY
AEGEAN
SEA
VOLCANIC ARC
HELLENIC TRENCH
CRETE
LB
AB
NAT
SB
LA
GP
GC
AG
BM
NAF

Aegean. At the same time the western external Ionian Zone was under strong compression. In the Mid- to Late Pleistocene and Holocene the internal domain was inferred to have reverted to an extensional stress regime (Mercier et al 1979a, 1987). The current tensile stress trajectory strikes NW-SE or NNW-SSE over most of the central and western Aegean region (Mercier et al 1987).

The second model for the post-Miocene history of the Aegean was developed by Jackson et al (1982b). They reinterpreted the few structures in the central Aegean with apparent reverse displacements as having extensional origins. These related either to the heterogeneous internal deformation of normal fault hangingwall blocks or to the high-angle rotations that may be achieved by successive normal fault generations (after Profett 1977). This author concurs with the Jackson et al model, in the absence of any observation of faults of reverse displacement and contractional origin in the Corinth Basin or surrounding areas (in contrast to Sebrier 1977).

Normal faulting of listric form is characteristic of the unconsolidated Neogene sedimentary infill of the Aegean extensional basins. Fault planes steepen towards the surface and often continue to curve beyond the vertical and become overturned within 2-3m of the surface, giving an apparent reverse displacement. Such faults are exemplified in the Corinth Canal section (also fig. 3 of Mercier et al 1979b). The reinterpretation of such minor faults as extensional in origin implies that no early Pleistocene compressional phase of tectonics is recorded in the central Aegean. This avoids having to invoke very rapid reversals in the state of lithospheric stress (Jackson et al 1982b).

The structural evolution of the Sporadhes Basin is described by Brooks and Ferentinos (1980) and Ferentinos et al (1981). This Neogene half-graben trends WSW-ENE and forms part of the North Aegean Trough, an elongate extensional basin which may have exploited the crustal weakness of the North Anatolian transcurrent fault trend. Psilovikos and Syrides (1984) contrasted the predominantly marine sedimentary history of the North Aegean basin since the Miocene with the largely continental history of the Axios and Strymon basins to the north. Highly variable humid to semi-arid climatic conditions through the Neogene created the variability of lacustrine environments within these basins (see also Pavlides & Kilias 1987, Brooks & Williams 1982). The active seismicity around Thessaloniki has been described with its regional tectonic implications by Mercier et al (1979b), Soufleris & Stewart (1981), Soufleris et al (1982), Mercier et al (1979b, 1983) and Pavlides and Kilias (1987). These studies showed that the 1978 Thessaloniki earthquakes occurred on pre-existing faults of Quaternary age and that the crust is stretching along a N-S to NNE-SSW direction in the area.

Broadly analagous structural and sedimentary histories have been recorded for the western Anatolian basins (Becker-Platen 1970, Bingol 1976, Dumont et al 1978, Angelier et al 1981, Sengor et al 1984a, Sengor 1987) and the Gulf of Patras (Ferentinos et al 1985, Doutsos et al 1985).

2.3 THE GULF OF CORINTH ASYMMETRIC GRABEN SYSTEM

2.3.1 Geological Setting

The Gulf of Corinth is the major geomorphological trough in central Greece. It is 120km long and up to 27km wide, with a

Figure 2.3

Summary map of the Gulf of Corinth region. The structural complexities of the footwall margin are emphasized, compared with the relatively unstructured northern basin margin. A-B = line of section in figure 2.6.
Diagonal hatching = Neogene-Quaternary syn-rift
Stipple = Palaeogene ophiolites
Mesozoic:
Cross-hatching = Parnassos + Pelagonian Zones
Stipple/dash = Pindos Zone
Irregular dash = Gavrovo-Tripolis Zone
Sources: Sebrier (1977), Bornovas & Rondogianni-Tsiambaou (1983), Gaitanakis et al (1985), Ferentinos et al (1985), Brooks & Ferentinos (1984), Doutsos et al (1985), Pe-Piper & Piper (1984) plus field and Landsat observations.

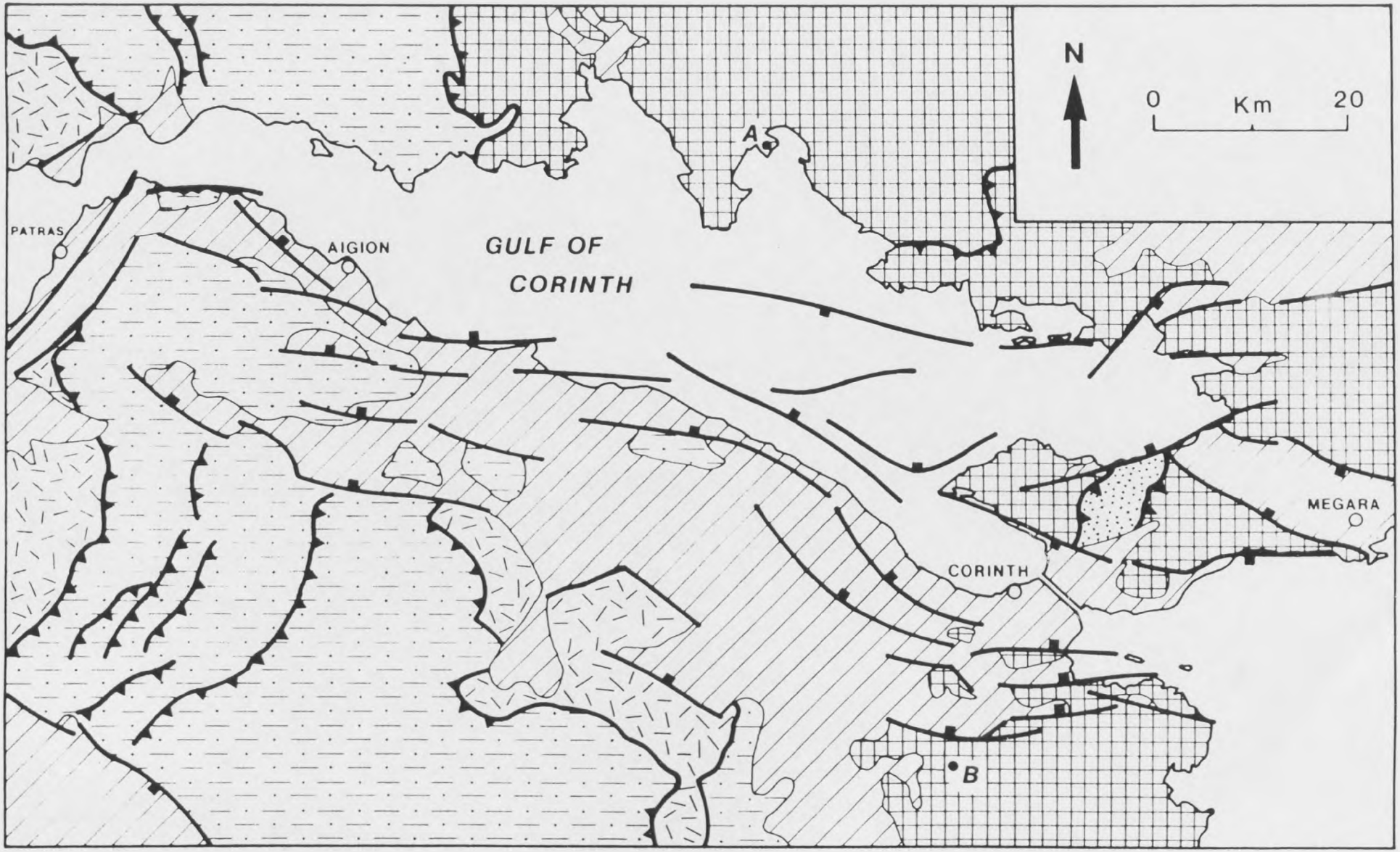
N
0 Km 20
A
PATRAS
AIGION
GULF OF
CORINTH
MEGARA
CORINTH
B

present maximum depth of 869m (Heezen et al 1966). The ESE-WNW trending trough is asymmetric in cross-section, being deepest towards its southern margin (Myrianthis 1984, Perissoratis et al 1986). The bathymetry reflects the southerly tilt of the developing asymmetric graben, the southern margin and the basinal depocentre being controlled by a series of major north-dipping normal faults along the northern Peloponnese coast (fig. 2.3).

The Neogene Gulf of Corinth basin cuts across the north-south structural grain of the Hellenides. Figure 2.3 illustrates the positions of major Hellenide structural zones relative to the Gulf of Corinth. The pre-Neogene "basement" also includes flysch deposits in N-S striking basins associated with Hellenide thrust fronts (Richter et al 1978). Detritus entering the Gulf of Corinth basin system during the Neogene will therefore include first and multi-cycle materials. The 45km thickness of the Hellenide crustal root through central Greece (Makris 1976, Le Pichon & Angelier 1981) implies that a substantial mountain belt of N-S trend existed in the area prior to the Late Miocene onset of extension. The initial basin floor may therefore have been in an intermontane setting, at some undetermined height above sea-level. The continental environment (Collier 1987) of the Drosaton Basin infill, SSW of Aigion (fig. 2.4) probably reflects this original relief.

To the west of the Gulf of Corinth proper, the Gulf of Patras lies between the essentially north-south extended basins of central Greece and the outer arc Ionian Zone (Ferentinos et al 1985, Underhill 1988). At the eastern end of the Gulf of Corinth extension has been taken up across the ESE-WNW trending Corinth Basin and Megara Basin (Theodoropoulos 1968) and the ENE-WSW trending Livadostros Basin (Jackson et al 1982a). These may

Figure 2.4

Structural and location map - the Gulf of Corinth asymmetric graben system.

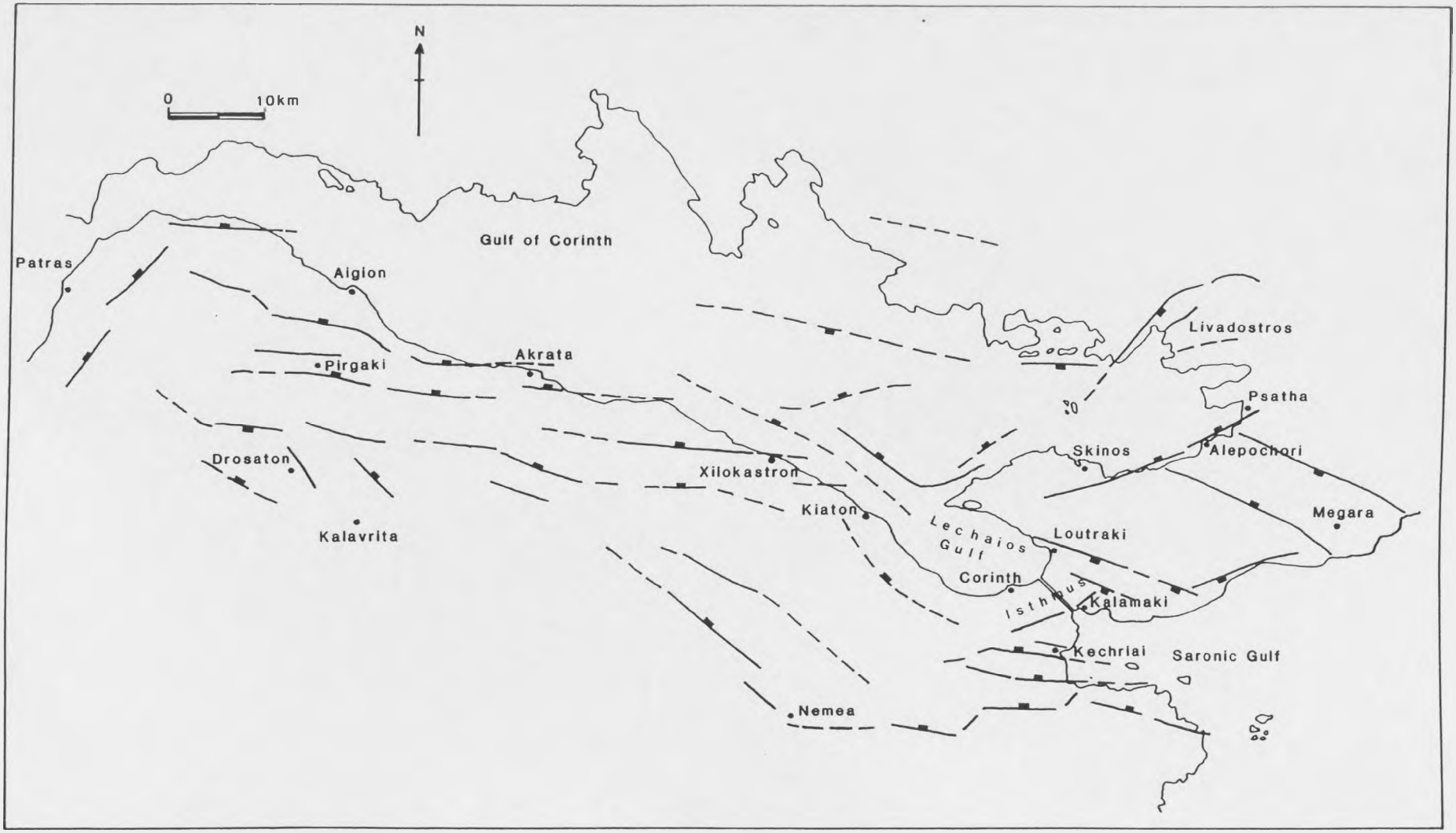
N
0
10km
Gulf of Corinth
Patras
Aigion
Akrata
Pirgaki
Drosaton
Kalavrita
Xilokastron
Kiaton
Lechaios Gulf
Corinth
Isthmus
Kalamaki
Loutraki
Skinos
Livadostros
Psatha
Alepochori
Megara
Kechriai
Saronic Gulf
Nemea

be regarded as sub-basins to the Gulf of Corinth System and the rate of extensional subsidence in each has varied through the Neogene and Recent. The Megara Basin is now inactive and is being passively uptilted on the Skinos Fault (Jackson et al 1982a, Leeder et al 1988).

The Corinth Basin is currently net-erosive across the Isthmus of Corinth but depositional in the Lechaios and Saronic Gulfs (fig. 2.4). The southern margin and basement tilt-blocks of the Corinth Basin comprise chiefly Pelagonian Zone limestones and dolomites of Triassic and Jurassic age (fig. 2.3). The Gerania massif to the north contains both Pelagonian Zone lithologies and a Palaeogene-emplaced ophiolite thrust slice. A complex pulsed history of extensional tectonism in the Corinth Basin is defined by and represented in its Neogene and Recent sedimentary infill.

2.3.2 Plio-Quaternary Stratigraphy

The scope for biostratigraphic subdivision of Neogene and Recent units in the Gulf of Corinth system is severely limited. This is due both to the short time-span involved and the particular environments that have prevailed within the basin system. Much of the basin fill is fluvial and lacustrine or brackish in character, especially in the Pliocene. A "Levantine" freshwater to brackish macrofaunal assemblage includes Viviparus (V. megarensis and V. pulchriformis), Unio, Potamides, Planorbis, Congeria, Melanopsis and Theodoxus (Kollman 1973, Keraudren 1979, Sebrier 1977) but none of the members are time-specific within the Neogene. The Lower Pliocene age associated with the assemblage (Sebrier 1977, Keraudren 1979) is inferred from regional environments at that time being continental. Palynological work (Freyberg 1973, Sebrier 1977) has similarly

Figure 2.5

Pliocene-Recent stratigraphy as used in this thesis. Modified after Harland et al (1982), Berggren & Van Couvering (1974), Sebrier (1977) (a) and Bousquet et al (1976).
Magnetic polarities: black = normal, unshaded = reversed polarity chrons. For biostratigraphic zonal schemes refer to Harland et al (1982) and Berggren & Van Couvering (1974).

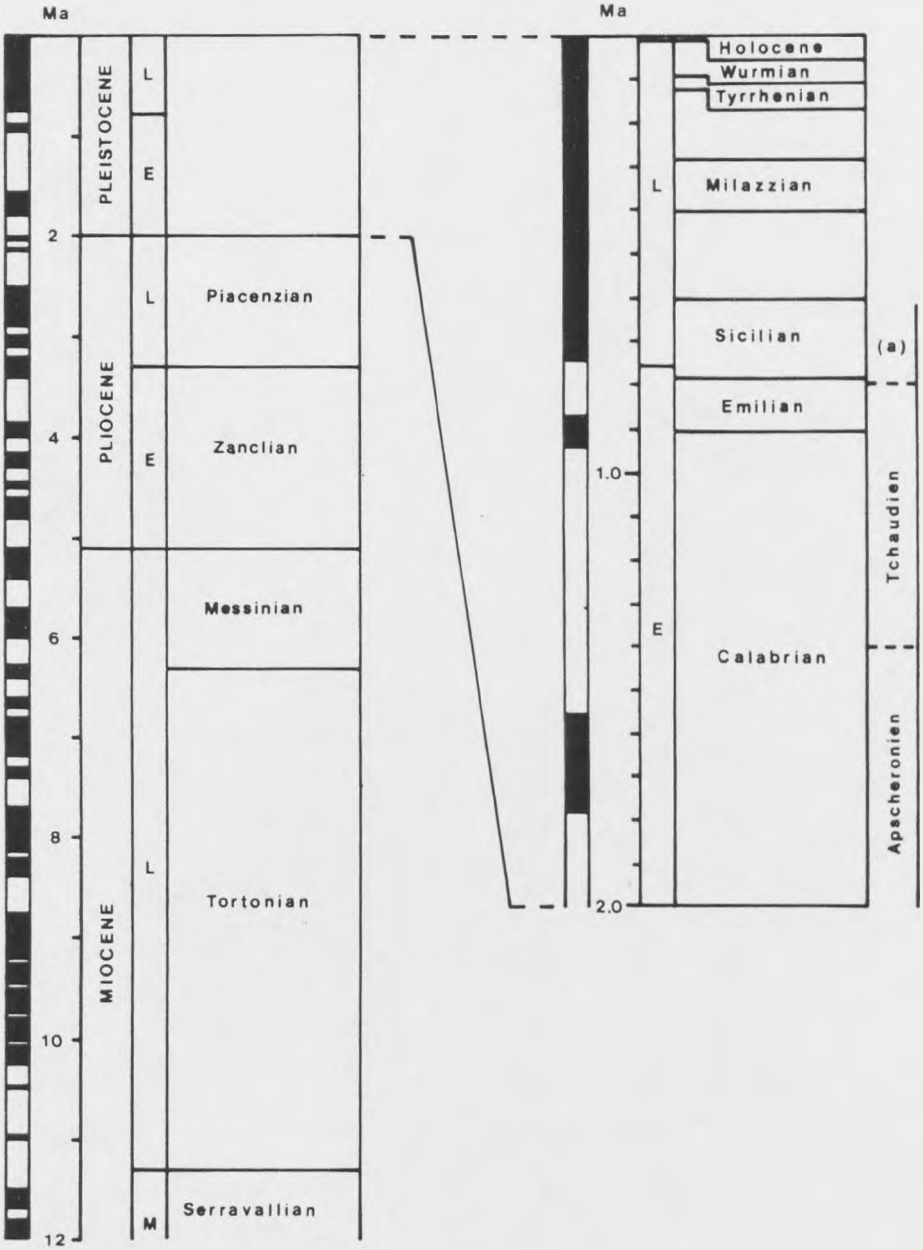
Ma
PLEISTOCENE
PLIOCENE
MIOCENE
L
E
L
E
L
M
2
4
6
8
10
12
Piacenzian
Zanclian
Messinian
Tortonian
Serravallian
Ma
1.0
2.0
L
E
Holocene
Wurmian
Tyrrhenian
Milazzian
Sicilian
Emilian
Calabrian
(a)
Tchaudien
Apscheronien

failed to establish a time framework to which the early structural development of the basins can be accurately related.

Locally, in the Corinth Basin, volcanics within the sedimentary sequence allow some chronostratigraphic division. Isotopic dating has been carried out on hornblendes and biotites of the calc-alkaline andesites and dacites. A Mid-Pliocene volcanic suite of about 3.8 Ma is recognised in the northern Corinth Basin (chapter 3 and Fytikas et al 1976, 1984).

A variety of marine macrofaunal species have historically been used as stratigraphic markers within the Mediterranean Quaternary. Deperet (1913) studied the fauna of deposits recovered from the digging of the Corinth Canal. He found them to include the Senegalese thermophile gastropod Strombus bubonius, and also Conus and Natica lactea (in Blanc 1958), from which he inferred a Tyrrhenian association (fig. 2.5). Keraudren (1979) and others have continued to utilise such associations. Dufaure et al (1975a) and Schroder (1975) have however recognised that Natica lactea may also be found in pre-Tyrrhenian deposits. Conus mediterraneus and Spondylus gaederopus, previously associated with the Tyrrhenian, still occur in the Mediterranean today (Vita-Finzi & King 1985). Their Tyrrhenian association is therefore rejected.

Two further means of dating are relevant to the Gulf of Corinth basins. Isotopic dating of materials may be carried out where feasible, and reference to archaeological sites may give some clues to the relative position of sea-level through the last 3 millenia. Flemming (1968) and Vita-Finzi & King (1985) list the apparent vertical displacements of ancient harbour sites. The ancient town of Kechriai for instance (fig. 2.4) has been

submerged, indicating a relative rise in base-level of c.2m. Such figures may not be refined, however, without a detailed knowledge of minor and local Holocene sea-level fluctuations.

Isotopic dating of macrofaunal elements from Quaternary sediments in the Corinth Basin has been carried out using ^{14}C and U-series disequilibrium techniques. ^{14}C dating of molluscs from terrace sites around the Corinth Isthmus has yielded a variety of Late Pleistocene and Holocene ages (Vita-Finzi & King 1985). But Vita-Finzi (pers. comm.) has pointed out that such dates are highly susceptible to distortion by the recrystallization of original aragonite lattices and by leaching, especially towards the limit of the dating technique. Beach-rock cements may also prove to be a useful source of datable material for the estimation of post-cementation vertical displacements. But again, a detailed knowledge of local Holocene sea-levels would be needed to fully constrain any systematic survey of beach-rocks around the current coastline.

Two U-series dates of molluscs from terraces near Corinth are reported by Sebrier (1977). Ivanovich & Harmon (1982), however, specifically exclude molluscs as being suitable for dating by this technique. New U/Th dates of suitable scleractinian corals from the Corinth Canal area are reported in chapter 4 of this thesis. Future work might include the corroboration (or otherwise) of such dates by Pa/U (Ivanovich & Harmon 1982), He/U and electron spin resonance techniques (Radtke et al 1988).

2.3.3 Gulf of Corinth Structure

The neotectonic structure of the Gulf of Corinth system is dominated by major E-W or ESE-WNW trending normal faults.

Faults in the eastern Gulf of Corinth active in 1981 (Jackson et al 1982a) were found to dip at an average 45° to focal depths of 8-11km. The present Gulf of Corinth is bounded to the south by major north-dipping normal faults whose gross displacement have caused a characteristic asymmetry to the basin. Pre-Neogene basement has been offset by a total of more than 3km across these southern basin margin structures (Brooks & Ferentinos 1984).

Seismic lines across the present central and eastern Gulf of Corinth (Myrianthis 1984, Brooks & Ferentinos 1984, Perrisoratis et al 1986) reveal the presence of south-dipping normal faults towards the northern margin of the basin. An asymmetric graben morphology is therefore described, with thickest Neogene sediment sequences in the southern part of the Gulf of Corinth (Myrianthis 1984).

The basinwide structure has been strongly affected by uplift across northern Peloponnesus (Jackson & McKenzie 1983, Mariolakis & Stiros 1987, Stiros 1986). The rate and cause of this uplift has yet to be fully constrained. The active southern basin margin structures have successively stepped northwards through the Neogene development of the basin. Previous basin margin structures to the south of the present coastal margin faults have become inactive and uplifted in the footwalls of the more recent normal faults (fig. 2.4). Hangingwall depocentres of the early stages of basin evolution have thus been uplifted in the footwalls of later faults. The magnitude and rate of such uplift will remain indeterminate until the early sedimentary infill of the basin is adequately dated and initial relief determined. Figure 2.6 represents an overall cross-section through the Gulf of Corinth asymmetric graben system.

Figure 2.6

Sketch structural section across the Gulf of Corinth asymmetric graben. For location of line A-B refer to figure 2.3. Structure inferred from seismic in Myrianthis (1984), Brooks & Ferentinos (1984), Perissoratis et al (1986). Bathymetric data from Heezen et al (1966).

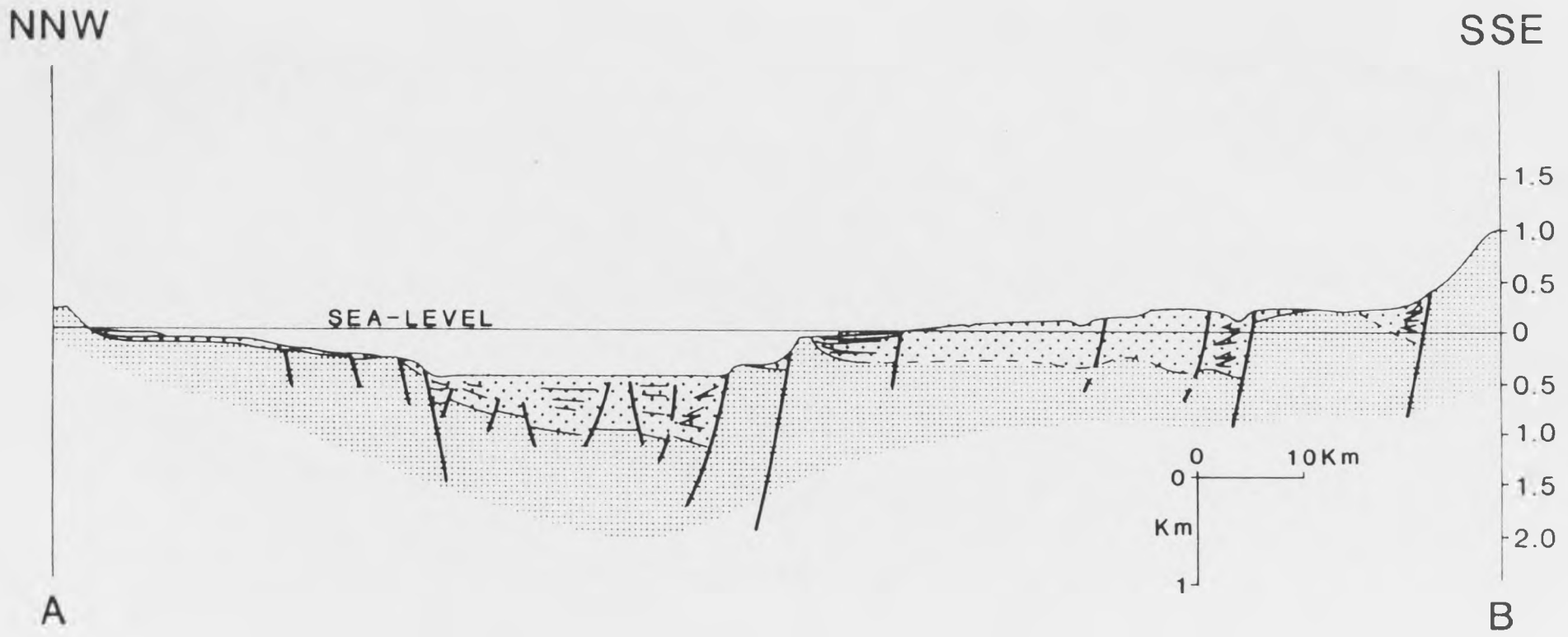
NNW
SSE
SEA-LEVEL
1.5
1.0
0.5
0
0.5
1.0
1.5
2.0
0
10Km
0
Km
1
A
B

The Plio-Quaternary fill of the present Gulf of Corinth exceeds 1km in thickness in the structural depocentres (Myrianthis 1984). In addition to the major normal faults which determine basin morphology, with throws of hundreds of metres or kilometres, the sedimentary fill is subject to normal growth faulting on subordinate synthetic and antithetic structures (Brooks & Ferentinos 1984, Perrisoratis et al 1986). This produces characteristic extensional tilt block chains (e.g. Brooks & Ferentinos 1980, Wernicke & Burchfiel 1982) on a variety of scales (refer to chapter 5).

The seismicity associated with extensional faulting in the Gulf of Corinth periodically triggers substantial submarine slumps on abyssal slopes (Perrisoratis et al 1984). Additional rotational slumps down footwall scarps and down Gilbert delta fronts occur in response to both seismic and storm surge events (Ferentinos et al in press).

CHAPTER 3 CORINTH BASIN - EARLY SYN-RIFT GEOLOGY

3.1 SUMMARY

The oldest exposed Neogene deposits occur in the north-east of the present Corinth Basin. Extensive sections through more than 500m of vertical section are exposed in the Charalampos fault block. The sequence is overlain by dated andesites from which a Lower Pliocene age for the sequence is inferred.

The distribution and architecture of sedimentary facies in the Lower Pliocene sequence describe a syn-depositional basin morphology comprising a structurally-controlled, east-west trending trough. Lateral and axial depositional systems entered this basin. Basin relief initially determined broad environmental conditions and transport gradients determined local depositional style. Basin form and source areas are inferred from palaeoflow and provenance data.

The statistical analysis of fluvial sands of the axial depositional system enables the detailed facies context to be determined. The position of stacked channel sands is inferred to have been controlled by structural deformation of the alluvial surface.

Qualitative comment on structural activity through the period of deposition of the Lower Pliocene sequence follows from the recognition of syn-sedimentary deformation and syn-depositional faulting features. Changes in the average grain size, provenance and transport energy of basinal deposits also allow comment on the structural evolution of the Lower Pliocene Corinth Basin. Seismic activity is inferred to have varied in intensity through time. During episodes of tectonic quiescence

sedimentary processes and differential rates of compaction across the basin floor are postulated to have controlled facies distribution.

3.2 INTRODUCTION

An early syn-rift sequence is preserved in outcrop in the north and north-east of the Corinth Basin. These are the oldest exposed Neogene deposits within the basin (fig. 3.1). Evidence of syn-depositional normal fault activity implies that the sediments were deposited after the onset of the neotectonic N-S extensional regime in latest Miocene or early Pliocene times (Jackson et al 1982b, Mercier et al 1979 and Le Pichon & Angelier 1981). Post-depositional structural displacements have isolated these early syn-rift deposits in an intrabasinal fault block to the north of Agios Charalampos (fig. 3.2). This block is bounded to the south-west and north-west by fault and unconformity contacts with later Neogene sediments. To the east, the sequence lies in possible fault contact against basement. The footwall to the Charalampos fault block comprises the Asprakhomata-Kalamona Formation, which are also the oldest deposits within the block itself. These extend to the north fault-margin of the Corinth Basin.

The only previous sedimentary studies of the early infill to Corinth Basin are the sedimentological studies of Freyberg (1973) and co-workers. Freyberg carried out detailed sediment compositional studies and developed a lithostratigraphy for the sequence, to which he ascribed a Pliocene age. The lack of chronostratigraphic subdivision of the sequence is due to the lack of within-sequence lavas or other isotopically datable

Figure 3.1

Lower Pliocene outcrop (stippled) in relation to the principal neotectonic structural elements of the Corinth Basin.
CFB = Charalampos fault block
AKFB = Asprakhomata-Kalamona fault block
Diagonal hatching = pre-Neogene basement
X = Ano Almiri - Katamalion tilt blocks (see section 5.6.1)

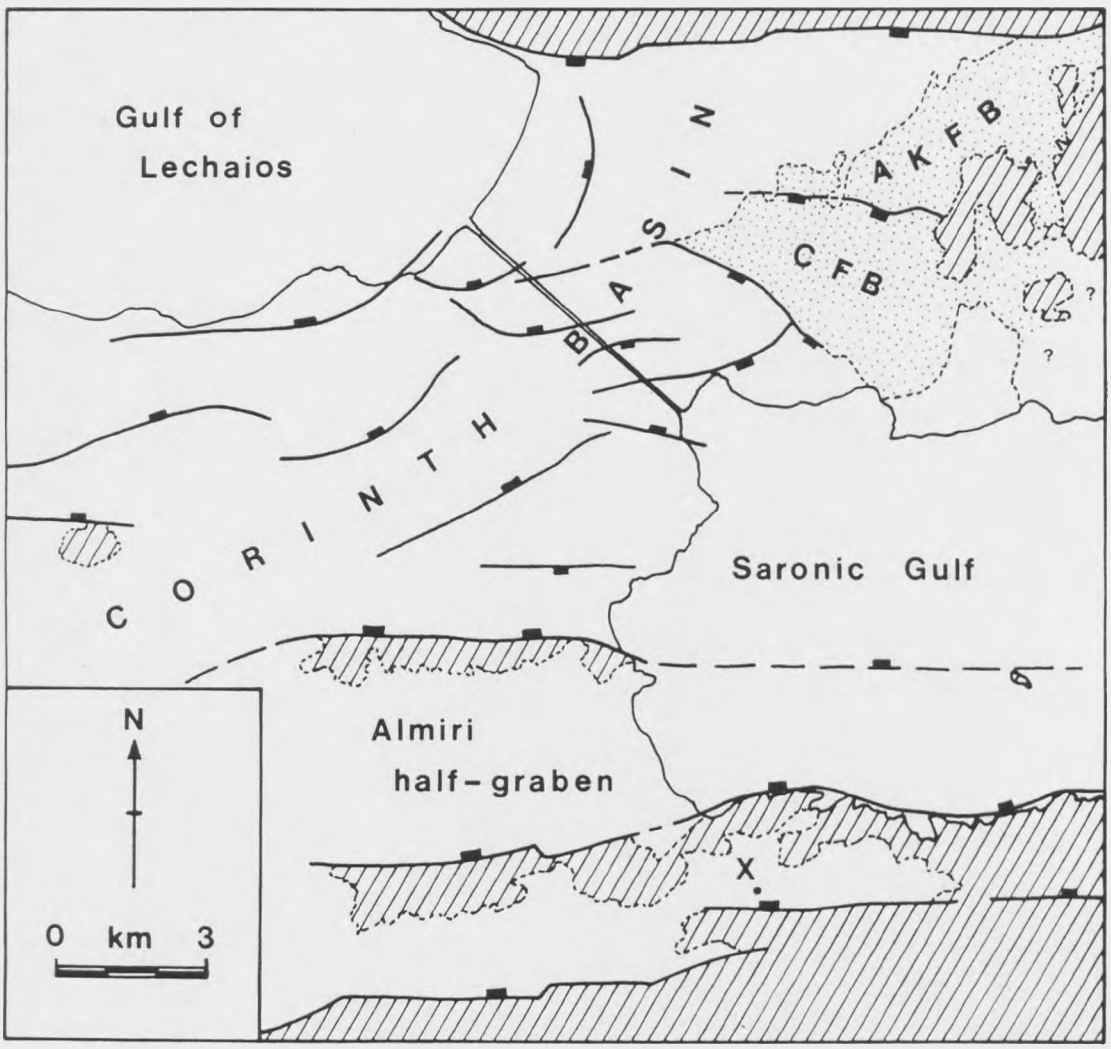
Gulf of
Lechaios
CORINTH BASIN
AKFB
CFB
Saronic Gulf
Almiri
half-graben
X
N
0 km 3

Figure 3.2

Summary map of Lower Pliocene outcrop and structure. Refer to enclosure 1 for detail.
Diagonal hatching = pre-Neogene basement
Stipple = Lower Pliocene outcrop
Unornamented = post-Lower Pliocene sequence sediments
K = Kalamaki
Ag Ch = Church of Agios Charalampos
A-B-C = line of section in figure 3.3
D-E = line of section in figure 3.20
Contours in metres

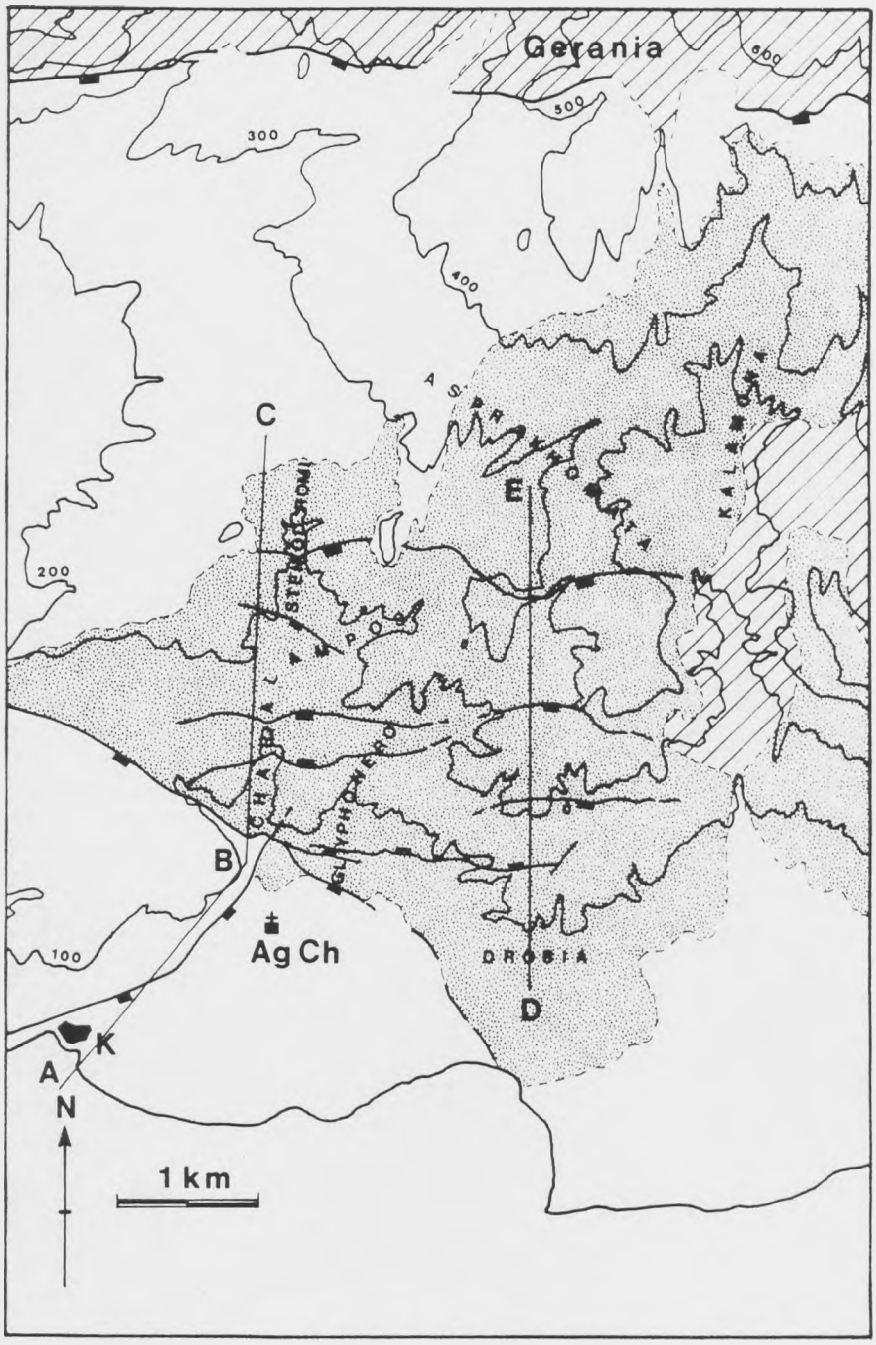
Gerania
600
500
300
400
200
100
C
E
B
D
Ag Ch
DROSIA
K
A
N
1 km

materials and also to the lack of a time-specific micro- or macrofauna. The "Levantine" macrofaunal assemblage of gastropods and bivalves (section 2.3.2) which is characteristic of the Pliocene of the Gulf of Corinth basins (Sebrier 1977) is facies-controlled and does not allow subdivision of the Neogene. Likewise, palynological studies (Sebrier 1977 and Freyberg 1973) and microfaunal analyses (Athersuch for this author and Keraudren 1979) have provided some environmental evidence but not subdivision of the Pliocene stratigraphy. Mid-Pliocene dates have been obtained for andesites which cap the syn-rift sequence within the Charalampos fault block. The sequence is therefore given a Lower Pliocene age.

Facies geometries and palaeoflow data from the Lower Pliocene deposits of the Charalampos fault block describe two major depositional systems. An axial system flows west to east parallel to basin-bounding and intrabasinal normal faults. The second system includes a variety of alluvial fan and fan deltas which supplied sediments into the basin at high angle to fault structures and is termed the lateral system (after Leeder & Gawthorpe 1987). Facies distributions and palaeoflows are used together to outline the asymmetric graben syn-depositional morphology, from their record of palaeoslopes and distributary patterns. Facies and sediment thickness changes across faults and the occurrence of allokinetic syn-sedimentary deformation (Leeder 1987) are used to define episodes of structural and seismic activity within the evolution of the basin.

Exposure of the Lower Pliocene syn-rift sequence of the Corinth Basin presents an ideal showcase through which controls on syn-rift facies architecture can be considered. Syn-depositional

tectonic activity must be expected to have had a strong control on the form of the depositional surface, by local or basinwide tilting and vertical displacement events, and on sediment supply rates, the latter being constrained by changes in the alluvial profiles across basin margin structures. In periods of tectonic inactivity sedimentary processes and compactional subsidence rates across the basin will have largely controlled facies patterns. Climatic conditions will also have determined sediment supply rates and soil development and influenced fluvial transport style.

Observed facies geometries are the product of the competition through time of the above control mechanisms. Facies variations in time and space respond to these controls on a variety of scales. Major basinwide morphologies such as the form and position of the depocentre and the basinwards limits of prograding clinoforms will be a function of subsidence and sedimentation rates averaged through time. On the small scale, individual seismic events or sedimentary flood events, for example, may cause fluvial channel positions to avulse (Bridge & Leeder 1979 and Leeder & Alexander 1987).

The monolithic provenance of the Multi-Coloured Series axial system illustrates the importance of source-area basement control on sediment input rates and character. The unroofing history of the northern margin of the Corinth Basin is partially constrained by the recurrence of these peridotite and serpentinite sands derived from the west of the Charalampos fault block. [It is worth noting here that basement lithology also controls sedimentation style within the modern axial system of the Buyuk Menderes Basin in western Turkey. This asymmetric graben-fill provides a partial analogue to the tectonic and sedimentary

situation within the Corinth Basin in the Lower Pliocene. Lateral and axial systems are controlled both in areal extent and internal architecture by competing tectonic and non-tectonic controls.]

No evidence is available from the Lower Pliocene syn-rift sequence of the Corinth Basin on its topographic level at the time of rift initiation. Evidence exists for a marine incursion into the basin within its Lower Pliocene history. But the absence of internal chronostratigraphic control and known base-level reference points prevents any quantitative analysis of subsidence or sedimentation rates. Qualitative comment may be made however. This chapter, on the basis of observed facies patterns and internal characteristics, lays out evidence for the structural evolution of the Corinth Basin through the Lower Pliocene. The relative significance of the various controls on facies type and distribution are then discussed, with emphasis placed on the difficulties of isolating local and small-scale controls in an area of highly variable tectonic strain and sedimentation rates.

3.3 FACIES ANALYSIS

The setting-up of a facies scheme and the subsequent designation of observed rock types to facies within the scheme is inescapably an iterative process. The definition of facies according to the lithological characteristics of a particular rock is a reasonable aim. Problems may arise, however, when ascribing subsequent samples or rocks in outcrop to the defined facies scheme. The principal danger is that the process becomes a pigeon-holing process through which information is lost rather than gained.

This danger is especially relevant when a considerable range of facies and interpreted environments is involved, as in the case of this study of the Lower Pliocene deposits of the Corinth Basin. Only relatively generalised facies are defined to avoid a cumbersome number of facies across the range of alluvial, lacustrine and marine environments. Indeed, over-classification may generate a false sense of accuracy when rock examples may tend to be forced into a category for which inadequate definitive data is available.

Statistical analysis of facies designations and facies sequences does however allow the validity and significance of lithofacies sequences to be tested. Such an analysis, by Markov chain analysis, is carried out in section 3.5.4, a detailed study of the Multi-Coloured Series Sands. Outcrop quality and the inherent variability of other formations in the Lower Pliocene sequence precludes such detailed analyses having statistically valid numbers of facies transitions. A more general approach is therefore followed. Facies definitions and interpretations are outlined in table 3.1. Broad facies associations are then described in section 3.4. These are based on facies associations in outcrop but are described in a generalised form, because some associations occur in more than one position within the Lower Pliocene stratigraphy. Details of sub-association variants are discussed in the relevant stratigraphic section (3.5). The facies associations described and interpreted in section 3.4 are thus intended as an aid to help clarify stratigraphic interpretations, not as exclusively definitive studies in themselves. Both alluvial and submarine fan environments, for example, might include mass and debris flow conglomerates (facies A1). Environments are thus inferred from

Table 3.1

Facies scheme

*: detailed in section 3.5.4
**: detailed in section 5.3

FACIES CODE	ROCK TYPE, TEXTURE & BED GEOMETRY	SEDIMENTARY STRUCTURES, FAUNA, BIOTURBATION	INTERPRETATION
(With acknowledgements to Miall 1977, 1978, Cant & Walker 1976, Ricci Lucchi 1975, Fielding 1984a, 1984b, Wilson 1975 and after chapter 5 of this thesis)			
A1	massive, disorganised matrix-supported breccias &/or conglomerates as convex-up lenses, sheets or channel fills (<1m to tens of metres thick), poorly sorted	unstructured to variably coarsening-, fining-up & symmetric grain size variation, outsize clasts, syn-sedimentary deformation common	mass and debris flow deposits
A2	massive or crudely bedded conglomerates, erosively-based, clast support, minor sand/fines lenses	crude horizontal bedding, imbrication	longitudinal bars, basal channel deposits
A3	stratified conglomerates	broad, shallow trough cross-beds with imbrication	minor channel fills
A4	stratified conglomerates	planar cross-beds, imbrication	bar forms or minor deltaic growths from pre-existing bars
SS*	scour surfaces ± pebbley lags	---	erosional surfaces interpreted as channel bases
L*	granule or pebble stringers or lenses	---	lag deposits on in-channel reactivation surfaces
P*	medium to v.coarse sand, may be pebbley	planar horizontal or low angle laminations	lower flow regime planar bed flow
A*	medium to v.coarse sand, may be pebbley	variable trough cross-beds, 0.4-1.0m width, 0.1-0.2m depth	lower flow regime dunes
B*	fine to coarse sand	small-scale trough cross-beds, 0.2-0.6m width, 0.05-0.1m depth	unidirectional migrating dunes

C*	fine to coarse sand	large scale (0.5-3m) planar cross-beds	channel bar forms
D*	v.fine to medium sand	small-scale (<0.5m) planar cross-beds, variable palaeoflow directions	upper flow regime bed forms on top of large bed forms, sand flats or in-channel at low stage
E*	v.fine to v.coarse sand, may be pebbley	asymmetric scours <3m width, parting lineations	in-channel erosive features
F*	clays to f.sand	ripple laminations (climbing) in sands, clay interbeds, bioturbation, rootlets	floodplain accretion
G*	v.fine to fine sand	low-angle laminations ± trough cross-beds	overbank accretion
H	lignites, ganisters, carbonaceous muds	plant debris, roots, bioturbation	plant colonised surfaces
I	carbonate nodules & lenticular horizons, humic accummulations	rootlets, prismatic & sphaeroidal texture, bioturbation, layered pedogenic features	soil developments
B1	sandy/conglomeratic sheets (± lobate geometry in plan)	imbrication, planar cross-beds	traction-transported subaqueous deposits, channelised or lobate
B2	channelized, erosively-based sands	planar laminations, trough cross-beds, plant debris, non-marine fauna	fluvial/distributary, mouth-bar or crevasse splay channel
B3	thinly interbedded sands, silts & claystone	planar laminations, bioturbation, freshwater & brackish fauna, plant debris	fluvial/distributary levee or mouth-bar to subaqeous overbank deposits
B4	trough-scoured silts /f.sands within B3, B5 or B6 facies	fining-up, laminated &/or bioturbated scour-fills	current-influenced basin floor deposits
B5a	diffuse-, irregular- or planar-laminated silts & claystones	bioturbation, plant debris, siliceous nodules, freshwater fauna	distal overbanks or lacustrine sediments deposited out of suspension

B5b	diffuse-, irregular- or planar-laminated silts & claystones	bioturbation, plant debris, brackish or marine fauna	interdistributary or estuarine suspension deposits
B6	thinly parallel-bedded heterolithic silts & claystones	varves, plant debris, freshwater fauna	lake floor suspension deposits (oxic where bioturbated)
B7	micrites ± silts & claystones	massive to planar-bedded	basin floor surface water or gravity-supplied suspension deposits
B8	dark claystones	homogeneous or planar-laminated	anoxic basin floor sediments
S1**	texturally mature, matrix-poor conglomerates	variably organised, imbrication	wave-reworked beach deposits
S2**	sands, well-sorted	unidirectional ripple laminations, brackish -marine faunal debris	current-influenced interdistributary or shoreface deposits
S3**	sands, silts	symmetric-ripples, chevron & draped ripple-laminations	wave-reworked shallow water deposits
S4**	sands, well-sorted	trough cross-beds (0.1-0.3m width), bundley, brackish-marine faunal debris	current-influenced estuarine/shoreface sands, wave-modified where bundley
B9	medium sands, well-sorted, isolated non-erosive sheets <2.5m thick	massive, bioturbated	migrating shoreface bars & sand sheets
RLA	"organized" pebbly sands, conglomerates, variable matrix content, poor sorting	un- & coarse-tail-graded, crude lamin-ations, outsize & intra-clasts	sand debris flow, mass & grain flow; high density turbidites
RLD	sand/mud interbeds, moderate to well-sorted sands, 0.03-1m scale beds	variously normal-graded, ripple-, wavy or planar-laminated, burrows in muds, small-scale contortions	low density turbidite or traction + fallout deposits
RLE	sand/mud interbeds, variable sorting, 0.03-0.2m bedding	un- or normal graded c.sands, lower flow regime dunes/laminae	low volume turbidite flow or tail flow deposits

associated facies assemblages, not the facies itself.

3.4 FACIES ASSOCIATIONS

3.4.1 Distal Alluvial Fan: FA1

Description:

The principal characteristic of this facies association is its grain size bimodality between fines and coarse clastics on a metre to decametre scale. Coarse-grade facies are predominantly of relatively organised medium to coarse sands and conglomerates. These may be erosively-based, facies A2 and B2, or as individual or stacked sheets of facies B1 or A4. Planar-laminated, trough cross-bedded and planar cross-bedded sedimentary structures (facies P, A, D) may locally be seen within the sandy units. Coarsening-up packages from B2 to B1 are common. Convex-up surfaces to these and rare A1 lenses are characteristic. These coarse-grained facies occur typically as randomly-stacked channels and lenses within fines of facies I, H and rarely F. Humic pedogenic textures and structures of facies I are particularly common (see section 3.5.1).

Interpretation:

The bimodal character of the facies association between sub-aerial accretionary fines and channelised or sheet sands and conglomerates reflects the switching of channel courses across the alluvial surface. Moderate slopes or proximity to primary source areas are implied by the occasional occurrence of mass or debris flow deposits (A1 conglomerates) in otherwise stream flow-dominated coarse clastic facies. Coarsening-up packages interpreted as medial to distal crevasse splay sequences and flood-sheet coarse clastics reflect the random processes of

fluvial avulsion which distribute channel positions across the distal alluvial fan surface through time.

3.4.2 Fluvial (Braided Stream): FA2

Description:

The principal elements of this association may occur in further association with other facies, in which case the assemblage is ascribed to the relevant facies association FA1, FA2 or FA5. The principal elements in the Lower Pliocene examples occur in two forms: The first is of sands comprising facies P, A, B, C, D, B1 and B2. Erosive surfaces (SS) and pebbly lags (facies L) may be found within the sandy units. For more detailed descriptions of FA2 sandy facies and their sequence organization, see section 3.5.4. The second form is of conglomeratic facies dominated by A2, A3 and A4 facies. Imbrication of the moderate- to well-sorted pebbles and cobbles is common. Planar cross-bedded forms show highly variable orientations. Low-angle laminations occur, but as a minority constituent of observed sedimentary structures which are dominated by planar and broad trough cross-stratification (for example, section 3.5.2). Asymmetric channel forms are infilled by organic debris (facies H) and facies G fines which extend over 5-10m thick conglomerate packages.

Interpretation:

The fluvial interpretation of the sandy facies assemblage is based on their vertical organization (section 3.5.4) and their lateral association with fines of facies F, H and I and spatial relationship to facies associations FA1, FA5/6 and FA3. The conglomeratic sub-association is dominated by stream-flow deposits. The scarcity of lateral accretion bedforms indicates

moderate- to low-sinuosity stream geometries. Low stage or channel-abandonment deposits are characterised by the accretionary deposits of facies G. This inference is supported by plant colonisation features in the form of facies H lignites and ganisters.

3.4.3 Lacustrine: FA3

Description:

Suspension deposits predominate with freshwater faunal elements and occasional siliceous nodule and cemented-horizon developments. Facies B5a laminated silts and claystones include a variety of diffuse-, irregular- and planar-laminations with variably intense bioturbation. End-member facies include heterolithic, apparently varved fines (B6), carbonate-dominated fines (B7) and massive or planar-bedded dark claystones in which evidence for faunal activity is absent (B8). Two sub-associations may be outlined: Firstly, S3 symmetric and draped ripple-laminations may locally be seen within otherwise laminated silt lithologies of facies B5a. Secondly, trough-scours cut B5a or B6 silty deposits and these may be associated with decimetre-scale sandy beds as B3 interbeds or erosively-based (B2) or sheet-like units (facies B1) within the background B5a silts.

Interpretation:

The two characteristics of freshwater influence, as indicated by macrofaunal evidence, and the prevalence of deposition out of suspension suggest sedimentation within a freshwater body away from distributary bodies. A lacustrine setting is inferred. Details of bedding type and lithologies will be a function of source area lithology (e.g. carbonate or siliceous), climatic

conditions affecting the rate of supply of sediment and its annual variability (its capacity to produce varved sedimentation), and basin depth influencing the degree of oxygenation at the basin floor water/sediment interface. The two sub-associations describe variants within the lacustrine environment. Facies S3 records sedimentation at shallow water depths within the wave zone. Current-supplied coarser clastics (B1, B2 and B3) are interpreted as being distal to distributary systems entering the lacustrine basin.

3.4.4 Fluvial-dominated Delta Front: FA4

Description:

The basic form of this facies association may be characterised as a coarsening-up facies sequence from basinal silts/clays to current-influenced sandy or conglomeratic coarse clastics. The waterbody into which the delta distributes sediment may be freshwater- or marine-influenced. The "type" facies sequence (as exemplified by fig. 3.8b) starts with B5a or B5b laminated fines. B3 sandy interbeds may then be cut by erosively-based, current-influenced sands of facies B2. Bioturbated sand and silt/claystone interbeds above interdigitate with low-angle laminated sands of facies G or P. Facies A and/or B trough-bedded sands typically overlie these and may be erosively-based. Facies B trough-bedded sands predominate in sandbodies which range from 1-15m in thickness. Facies F, H or I fines and organic deposits might be expected to roof the sandbodies but these are typically capped by symmetric ripple-laminated and bundley cross-stratified sands (S3 and S4). The facies sequence then reverts to B5b, or more commonly, B5a fines. Less complete facies sequences also occur: Facies P or facies B sands may

occur directly over silts of facies B5a or B4, as in figure 3.8c. Similar abbreviated sequences may also occur with conglomeratic coarse-grade end-members. B5a to B3 silts to sandy interbeds may be overlain by conglomerate sheets (B1). These characteristically show imbrication and planar cross-bed developments (e.g. fig. 3.6b). One further sub-association seen in such conglomeratic FA2 sequences has a 1-5m thick fining-up trend in which B1 conglomerates are overlain by heavily bioturbated fine sands and silts (of facies B3 or F) and lignites (facies H).

Two further variations on the sandy facies coarsening-up theme are worthy of note: Firstly, B5a or B4 silty units are locally succeeded by B3 internally coarsening-up interbeds which grade into facies B trough cross-bedded sands. These may have a symmetric ripple-laminated surface (facies S3) and the whole facies sequence is typically limited to a few metres in thickness. The second, and similar, facies sequence simply consists of B5a silts giving way to B3 sand/silt interbeds, but with these being cut by erosively-based current-influenced sands of facies B2. Again, the facies sequence is limited to a few metres in thickness.

Interpretation:

The classic coarsening-up facies sequence from basinal silts to current-influenced sands is interpreted as a section through a prograding fluvial distributary. Distal sandy interbeds are cut by the advancing mouth-bar channel. Mouth-bar and/or levee deposits comprise interdigitated bioturbated fines and sands with low-angle laminations (plate 3.2b). Fluvial sands in the distributary channel will potentially show the range of detailed

facies that occur in the FA2 fluvial facies association. These are typically capped by wave-influenced sands which are interpreted as representing a period of reworking of the topmost distributary channel sands upon abandonment and submergence of the channel. The abbreviated sequence of facies P and B directly overlying basinal silts (with or without an erosive base) is thought to record an instantaneous distributary channel avulsion event (after Elliott 1974).

Coarsening-up conglomeratic facies sequences are similarly interpreted as fluvial-dominated delta front facies associations. In these cases, however, mouth-bar channel and mouth-bar features are absent. Conglomerates are characteristically sheet-like, leading to the interpretation that channel progradation occurred across lobate conglomeratic sheets dumped ahead of the channel opening. Basin floor gradients must have been low, as with the sandy facies association, to allow rapid distributary progradation without, for instance, the development of avalanche foresets of a Gilbert-type fan delta. The fining-up sand-silt-lignite sub-association probably records the overbank accretionary infill of small interdistributary bay areas or abandoned channels.

Reduced sandy coarsening-up facies sequences are interpreted as interdistributary crevasse splay sequences (after Elliott 1974, Fielding 1984a). The B5a-B4-B3-B2 trend probably denotes a medial section through crevasse splay sequences, while the presence of B2 channelised sands suggests a more proximal locality.

3.4.5 Estuarine: FA5

Description:

Facies association FA5 consists predominantly of variously laminated silts (plus subordinate claystones and fine sands) of facies B5. B4 trough-scoured silts/fine sands also occur. Bioturbation is variable but characterised by 1-2cm vertical burrows. Macro- (and micro-) fauna range from being limited to freshwater gastropod and ostracod species to having a varied marine gastropod, bivalve and foraminiferal assemblage. Additional sedimentary structures include the local occurrence of S3 symmetric ripple-lamination within B3 sand/silt interbeds and the isolated appearance of unstructured, bioturbated sandbodies up to 2.5m in thickness within the background B5 or B3 deposits.

Interpretation:

The range of faunal assemblages suggests a range of freshwater to brackish to marine basinal conditions. The occasional occurrence of wave-modified features (facies S3) and the progradation of FA4 distributary channels into the basinal environment suggest a shallow, low gradient basin floor in the narrow structural trough of the Corinth Basin. Facies B9 sandbodies may represent periodic reworking of sediments by tidal currents, transporting bars or sand sheets across the basin floor.

An awareness of the structural setting allows this association to be interpreted as representing an "estuarine" environment within the confines of the structural graben (see section 3.5.3). An essentially microtidal environment is postulated by analogy with the present Mediterranean. Marine influence at one end of the trough competed with a wedge of freshwater introduced from the

prograding deltaic front at the other end (plus any lateral distributary systems). The position of the saline wedge would have varied with fluvial flow stage.

3.4.6 Proximal Submarine "Fan"/Slope Apron: FA6

Description:

Variously disorganized (facies A1) or organized (facies RLA) conglomerates predominate. The coarsest and most disorganized end-member is of massive, unstructured pebble and cobble conglomerates which are typically matrix-supported. Outsize basement cobbles and boulders are common. Such unstructured units are up to tens of metres in thickness. Any internal channel or erosional surfaces are masked by the lack of structure. Sedimentary dykes are commonly present.

The more organized form of this facies association comprises conglomeratic units of <1-5m thickness which may show crude internal horizontal laminations and grading. These interdigitate with poorly-sorted pebbly sands and typically exhibit matrix-rich asymptotic "toe-sets" (e.g. fig. 3.16). Coarsening-up and fining-up trends occur within individual units, and syn-sedimentary deformation in the form of dykes and contortions are common.

Interpretation:

Debris and mass flow transport characterise the deposits of this facies association. Amalgamated mass flow units are thought to form the bulk of the disorganised units. Discrete mass and debris flow events are represented by the bedded A1 and RLA conglomerates. Channelisation is rarely seen, although this may be a function of the chaotic texture of the conglomerates. The

rapid interdigitation of pebbley "toe-sets" with sandy units suggests dumping of material and freezing of mass flows was common, perhaps at a break of slope.

The mass and debris flow deposits described may occur in either sub-aerial (alluvial) environments or in submarine settings. Reference to their stratigraphic context in the Corinth Basin (section 3.5.5) enables facies association 6 to be interpreted as a submarine "fan" or slope apron setting (the 3-dimensional geometry of which has not been determined). The prevalence of mass and debris flow processes over low-density turbidite or suspension sedimentation suggests a proximal position.

3.4.7 Distal Submarine "Fan": FA7

Description:

Facies association FA7 is characterised by facies RLD and RLE. RLA conglomeratic erosively-based or sheet-like units up to 1m thick may also occur within the assemblage. RLD sand/mud interbeds are laterally extensive over tens of metres and vary from 0.03-1.0m in thickness. They include a variety of sedimentary structures, with ripple-drift laminations and convolute bedding within moderate- to well-sorted sands, and burrows common in the mud intervals. Normal and ungraded sand units up to 0.2m thick may also come into the RLE facies category, where the upper flow regime structures are absent.

Interpretation:

Facies RLD units are interpreted as low-density turbidites (after Ricci Lucchi 1975), the muds being deposited from suspension in the aftermath of turbid flow events. Biogenic colonisation indicated by burrows in these muds suggest longer intervals

between deposition out of turbidity flows at any locality. Facies RLE lower flow regime sandy interbeds are thought to represent low volume turbidites, interbedded again with fallout deposits (Ricci Lucchi 1975).

The facies association typically shows an overall coarsening-up trend, with increasing proportions of RLA conglomeratic and sandy beds, grading into facies association FA6 sequences (e.g. fig. 3.16). The FA7 association is thus ascribed to the more distal regions of a subaqeous fan or apron setting. The submarine title is again based on the stratigraphic context of the facies association within the Corinth Basin (section 3.5.5).

3.5 STRATIGRAPHIC SEQUENCE - DESCRIPTIONS AND INTERPRETATIONS

3.5.1 Asprakhomata-Kalamona Formation

Description:

Those deposits within the Corinth Basin termed the Asprakhomata-Kalamona Formation are thought to be the oldest exposed Neogene basin-fill sediments in the basin. Asprakhomata and Kalamona are local names for hills to the NE of the mapped area (fig. 3.2). Sediments which may be ascribed to the Asprakhomata-Kalamona Formation outcrop in two structurally-separated areas.

The main area of outcrop of Asprakhomata-Kalamona sediments is the intrabasinal fault block to the north of the Charalampos fault block (fig. 3.1 and enclosure 1). This block forms the footwall to the Charalampos fault block. Strata dip consistently, if variably from 5-40°, towards the northern fault-margin of the basin against the Gerania Massif. The lowermost exposed footwall sediments at the fault contact between the

Charalampos and Asprakhomata-Kalamona fault blocks comprise the stratigraphically lowest sediments seen in the basin. No borehole or seismic data is available to ascertain what thickness of basin sediment lies below this outcrop level.

The second outcrop ascribed, tentatively, to the Asprakhomata-Kalamona Formation is in the southern, stratigraphically lowest area of the Charalampos fault block (figs. 3.3 and 3.4). Facies here are analogous to those seen in the Asprakhomata-Kalamona Formation 2km to the north. No internal chronostratigraphic division of the Lower Pliocene is possible in the Corinth Basin, due to the lack of within-sequence and isotopically datable lavas or any time-specific fauna. It is therefore not possible to determine whether deposits at the base of the Charalampos section are time-equivalent to any or which of the deposits in the Asprakhomata-Kalamona fault block. The possibility of a time-gap between the age of the sediments in each area has not been discounted. On the other hand, deposits within the Charalampos section above those here ascribed to the Asprakhomata-Kalamona Formation may be lateral equivalents to more marginal facies observed in the younger, more northerly deposits of the Asprakhomata-Kalamona fault block.

Facies from the Asprakhomata-Kalamona Formation will be described according to location. Three areas will be considered: a) the oldest exposed sediments, outcropping in the footwall to the Charalampos fault block in the Stenodromi and Charalampos valleys, b) the northernmost deposits of the Asprakhomata-Kalamona fault block, against the Gerania basement margin, and c) from the southern, basal exposures of the Charalampos fault block.

a) In the Stenodromi valley, weakly laminated grey muds and

Figure 3.3

South-north cross-section across the Charalampos fault block. See figure 3.2 for position of section.
Unornamented and spaced circles = Holocene and Late Pleistocene fans
Hatch/dot = ?Pliocene-Pleistocene, undifferentiated
V = volcanics (mid-Pliocene)
Heavy stipple = Upper Conglomerates
Medium stipple = Multi-Coloured Series Sands
Light stipple = Multi-Coloured Series "Marls"
Pebble symbol = Agios Charalampos Conglomerates
Dash = Asprakhomata-Kalamona Formation

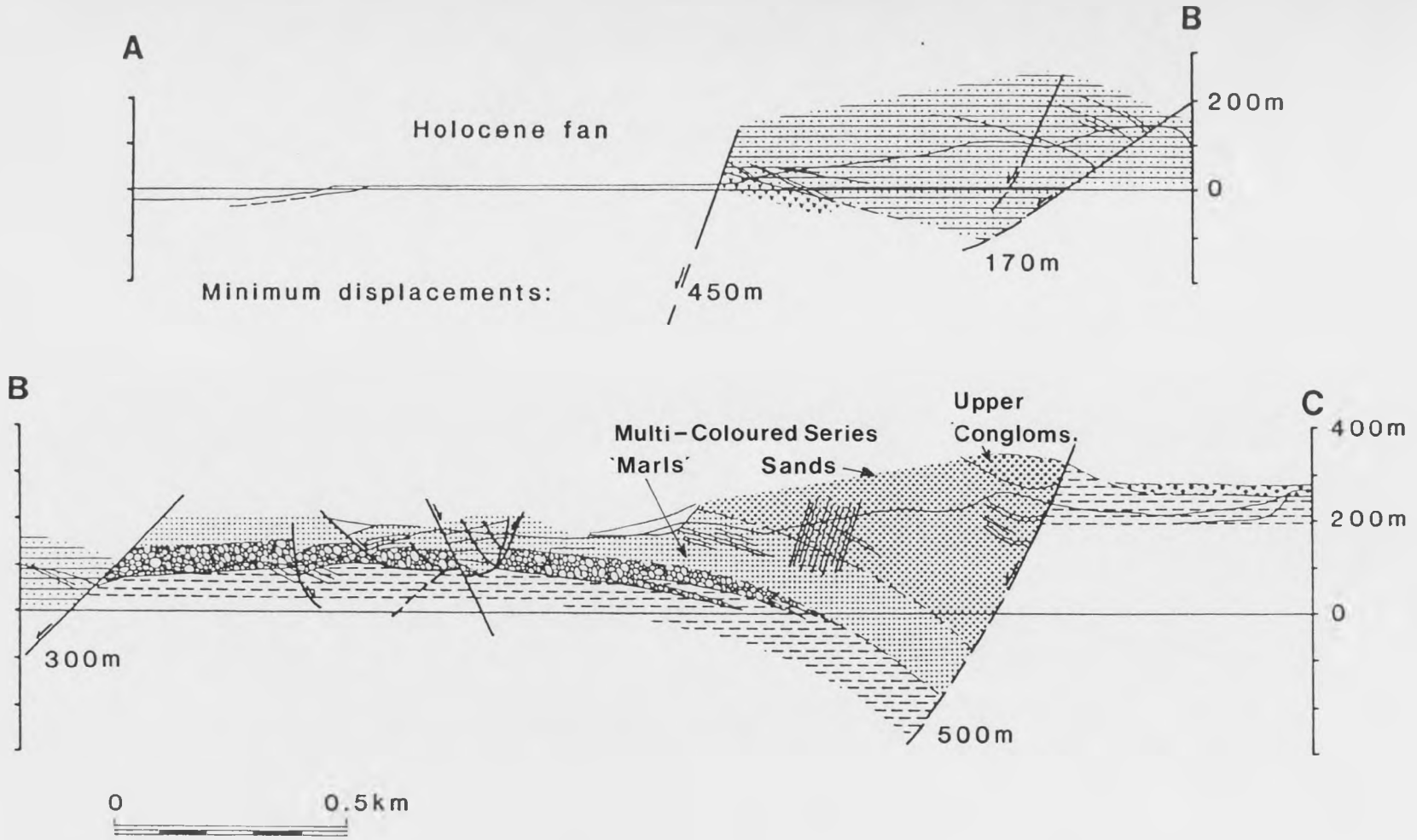

South-North section A-B-C through Pliocene-Recent Corinth Basin sequence, north of Kalamaki.

Figure 3.4

Summary sedimentary log of the Lower Pliocene sequence in the type Charalampos-Stenodromi section. Stratigraphic ornaments as in figure 3.3.
For sedimentary log symbols refer to enclosure 2.

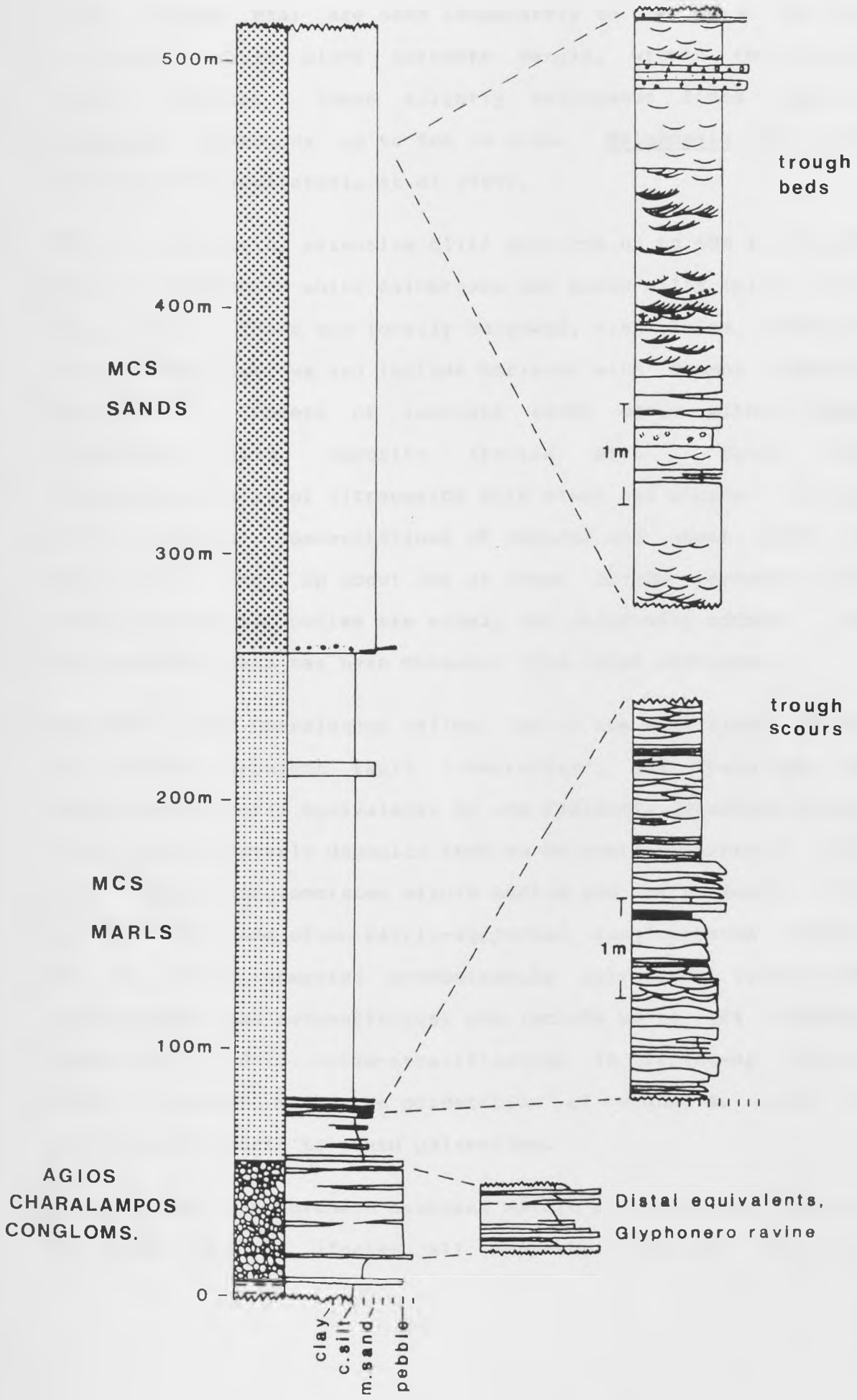
500m
400m
300m
200m
100m
0
MCS
SANDS
MCS
MARLS
AGIOS
CHARALAMPOS
CONGLOMS.
trough
beds
1m
trough
scours
1m
Distal equivalents,
Glyphonero ravine
clay
c.silt
m.sand
pebble

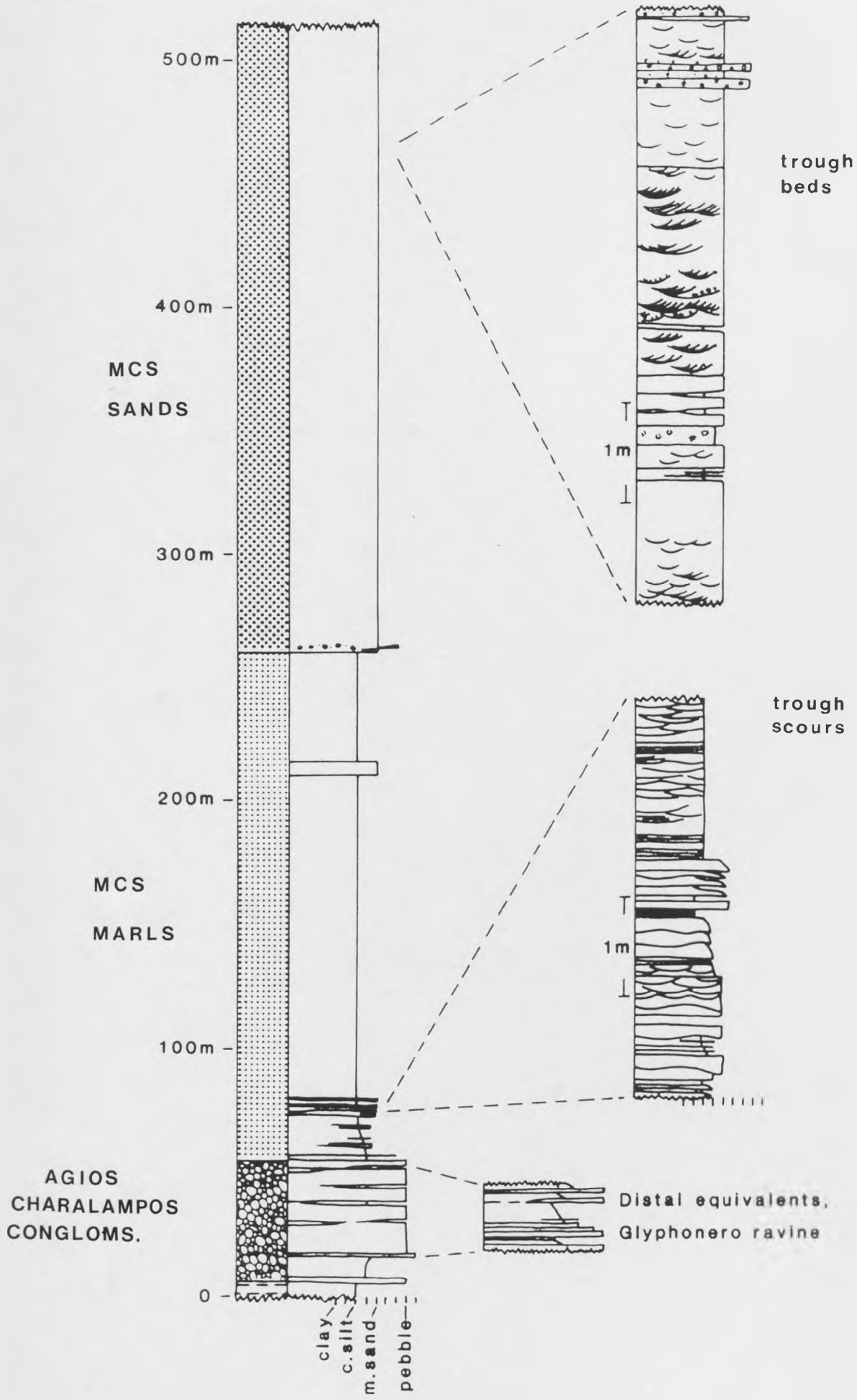
500m
400m
300m
200m
100m
0
MCS
SANDS
MCS
MARLS
AGIOS
CHARALAMPOS
CONGLOMS.
trough
beds
1m
trough
scours
1m
Distal equivalents,
Glyphonero ravine
clay
c.silt
m.sand
pebble

silts (facies B5a) are seen immediately to the north of the Charalampos fault block northern margin, within the stream (waddi) section. These slightly calcareous fines contain Viviparus gastropods up to 4cm in size. Melanopsis has also been reported (Gaitanakis et al 1985).

600m to the north, extensive cliff sections up to 60m in height expose interbedded white calcareous and brown silts (plate 3.1a fig. 3.5a). These are locally burrowed, with 1-2cm irregular sub-vertical burrows and include horizons with common rootlets (facies I). Sheets of immature sands occur within these background silt deposits (facies B1). Sands are characteristically of ultrabasics with minor red cherts. In the cliff sections, concentrations of channel and sheet sands in which sand makes up about 70% of these 10-15m packages (30% fines) in 2-3m sandbodies are widely and diagonally offset. No palaeocurrent data has been obtained from these sections.

Deposits in the Charalampos valley, 1km to the east along strike and without apparent fault interruption, are therefore the approximate lateral equivalents of the sediments described above. These more easterly deposits tend to be coarser overall, with erosive-based conglomerates within medium and coarse sands. The poorly-sorted and often matrix-supported conglomerates (facies A2, B1 and A1) comprise predominantly ultrabasic lithologies (peridotites and serpentinites) and include up to 10% basement limestones. Rare cross-stratification in fining-up channel fills, together with the orientation of channels, imply an approximately north to south palaeoflow.

b) Against the northern basement margin of the Corinth Basin, limestone breccias (facies A1) apparently derived from the

Plate 3.1

a) Asprakhomata-Kalamona Formation deposits in the north side of the Stenodromi ravine, grid ref. approx. 6.10 23.20

b) Agios Charalampos Conglomerates showing asymmetric channel with lignite fill, grid ref. 5.84 21.60

c) Multi-Coloured Series Sands transition zone coarsening-up package, as logged in figure 3.8b, grid ref. 6.90 22.35

d) Outcrop of stacked channel sands, Multi-Coloured Series Sands, grid ref. 6.04 22.21

e) Sedimentary dyke in Upper Conglomerates, grid ref. 7.88 19.93

f) Syn-sedimentary contortions (approx. 5m amplitude) at the Multi-Coloured Series "Marls" to Upper Conglomerates boundary, grid ref. 7.26 20.21

a

b

c

d

e

f

Figure 3.5

Logs: Asprakhomata-Kalamona Formation
a = sketch log (with detail) from Stenodromi ravine (see fig. 3.2)
b = outcrop in southern part of Charalampos fault block, grid ref. 5.67 20.82
c = outcrop in southern part of Charalampos fault block, grid ref. 5.84 20.78

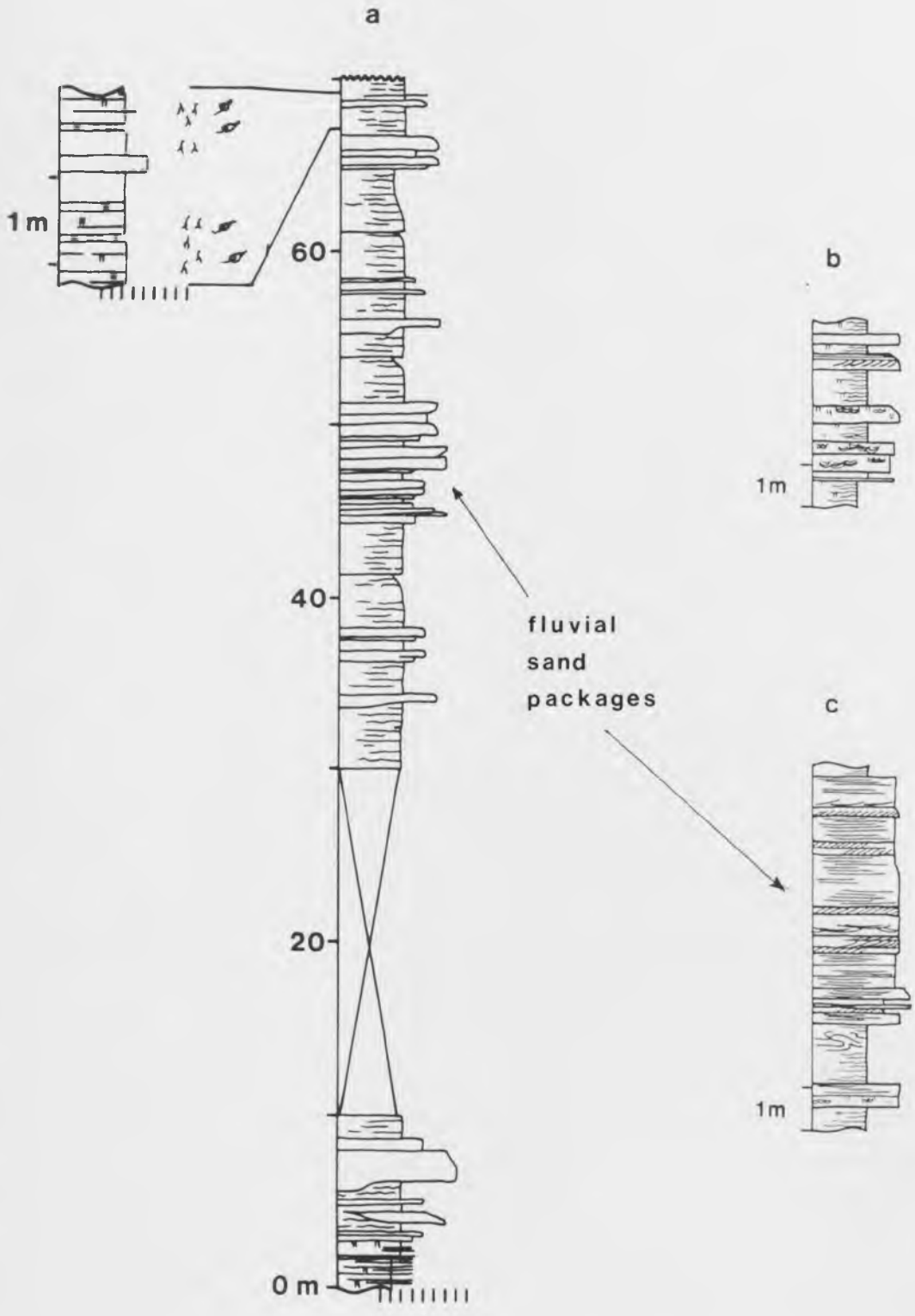
a
1m
60
40
20
0 m
fluvial
sand
packages
b
1m
c
1m

immediate footwall interdigitate out into calcareous silts. These silts are virtually a clastic limestone, and contain variable percentages of scattered pebbles, being predominantly facies B7 and B5, with B1 sandy or pebbley sheets. Calcareous silts and sands are locally intensely bioturbated, whilst elsewhere they include discrete bands of limestone conglomerate.

Angular blocks of basement limestone, up to several tens of metres in scale lie within the calcareous silt and sand background sediment. Other blocks are in fault or slide contact with basement limestone of the apparent footwall. The footwall limestones may themselves be part of a larger scale slide block or olistrostrome which has been downfaulted against the ophiolite thrust sheet to the north (Gaitanakis et al 1985). The point to be emphasized here is the irregularity in style of sedimentation and clastic input of the Asprakhomata-Kalamona Formation against the northern margin of the basin.

c) The lowest stratigraphic units outcropping within the Charalampos fault block are characterised by occasional 1-3m internally complex sandbodies (including facies P, A and D) within a predominantly silt and clay grade matrix, typically of facies B5a and B6. These fines include dark grey shales (B8) but are more commonly planar or wavy-laminated and variably calcareous, grey silts. Bioturbation is minor but present. Laminae are also occasionally disturbed by small-scale dewatering features. Gastropod casts are tentatively identified as Viviparus. Flat-bottomed sand sheets within the fines (fig. 3.5b) include symmetric ripple and 5-10cm bundled trough forms of facies S3 and S4.

Sandbodies within the silt matrix (fig. 3.5c) tend to fine-up

overall. Bedforms are variable within any one body, with planar laminations and planar to trough cross-stratification. Sands are predominantly of limestone detritus, with subordinate cherts and fine-grained siliciclastics.

Interpretation:

Facies encompassed by this formation were all deposited within various lacustrine and alluvial settings. No record of marine influence has been found within these rocks. Because of the likely time separation between outcrop areas, the three locations described will again be treated separately.

a) Lowermost exposed strata in the northern Stenodromi valley are of lacustrine origin, as indicated by the FA3 characteristics of in situ freshwater gastropod fauna and a lack of sedimentary structures associated with current influence. The cliff sections above expose alluvial deposits. Channel and sheet flood sands lie within overbank fines and soils. The diagonal offset pattern of channel sand packages reflects a "passive", i.e. non-fault induced, architecture of distribution (after Bridge & Leeder 1979, Alexander 1986a, Fielding 1984a). The distinct coarser grade alluvial facies association to the east, with clastics supplied from across the northern margin to the basin, suggests that distributaries into the basin were localised, either at the basin margin or by preferential tectonic subsidence within the basin. Either way, facies patterns are consistent with alluvial fan or apron geometries distributing detritus from the northern basement margin to a southerly depocentre inhabited by a freshwater lake of variable size.

b) The subaqueous deposition of planar-laminated, bioturbated marls of facies association 3 against the northern basin margin

indicates that the basin was periodically inundated by a lake - and therefore structurally isolated to the east and west. The occurrence of limestone slide blocks and immature clastics, together with the irregularity of sediment supply into the basin, indicates periodic tectonic activity on the margin fault. The incursion of basement-derived detritus and the inundation of the basin floor by carbonate fines, perhaps enhanced by karstic erosion conditions, frequently interrupted the otherwise passive lake floor sedimentation out of suspension, with its background benthic faunal activity.

c) Asprakhomata-Kalamona sediments of the southern Charalampos fault block may be characterised as lacustrine muds and calcareous silts of facies association 3. Periodic relative base-level changes allowed the incursion of FA2 coarsening-up fluvial sand packages. Lacustrine fines vary from dark grey shales to laminated, possibly varved marls and silts to wave-influenced rippled silts. The lake was apparently oxic; even the darkest grey muds show signs of bioturbation, colouration denoting a reduced carbonate clastic component rather than a lack of oxygen. There is no evidence that water depth exceeded a few tens of metres (or the limits of the photic zone). Clastics were sourced in the southern basement margin to the basin.

3.5.2 Agios Charalampos Conglomerates

Description:

A radiating coarse clastic wedge in the southern part of the Charalampos fault block is termed the Agios Charalampos Conglomerate. In the Charalampos river section, facies B6 heterolithic laminated marls with common epichnial and endichnial morphology burrows (after Martinsson 1970) typify the underlying

strata. The lowest conglomerate unit is of well rounded texturally sorted pebbles of limited lithologic range (B1 or S1); specifically black and grey cherts and indurated limestones. 5m of sands above feature asymptotic cross-stratification (fig. 3.6a).

The Charalampos section through the clinoform is dominated by conglomerates. These coarsen-up overall to cobble grade in the upper 30% of vertical section. Provenance is of polymict basement lithologies (excluding ultrabasics). 5-8m stories are complex, with both sheet-like and erosive channel-based internal surfaces. A3 and A4 cross-stratification and imbrication of the conglomerates is common. Palaeoflows were to the north and north-west on the basis of pebble imbrications. The direction of dip of sets is highly variable, often apparently reversed from one unit to the next in two-dimensional cliff-section. Inter-storey fines and channel-fills are of facies B3 calcareous silts and sands, and facies H lignites (plate 3.1b). Viviparus pulchriformis, Amphimelania ornata and Melanopsis have been recovered from fines within the conglomerate stack (Kollman 1973).

The proportion of Agios Charalampos coarse clastics in the Glyphonero ravine section is substantially reduced, to about 40% (fig. 3.6b). Facies B5a fines are heavily bioturbated, often to a stage where original diffuse bedding and laminae are virtually destroyed. Some of these structureless silts are rich in plant fragments. Two contrasting styles of transition from fines to conglomerate occur. Firstly, heavily bioturbated fine sands and silts fine-up and are capped by a layer of lignite. A laterally extensive (within 30m limits of outcrop) and non-erosive conglomerate sheet (B1) lies directly on the lignites. The

Figure 3.6

Logs: Agios Charalampos Conglomerates
a = log through Charalampos ravine section, grid ref. 5.78 21.57
b = log through Glyphonero ravine section, grid ref. 6.33 20.94

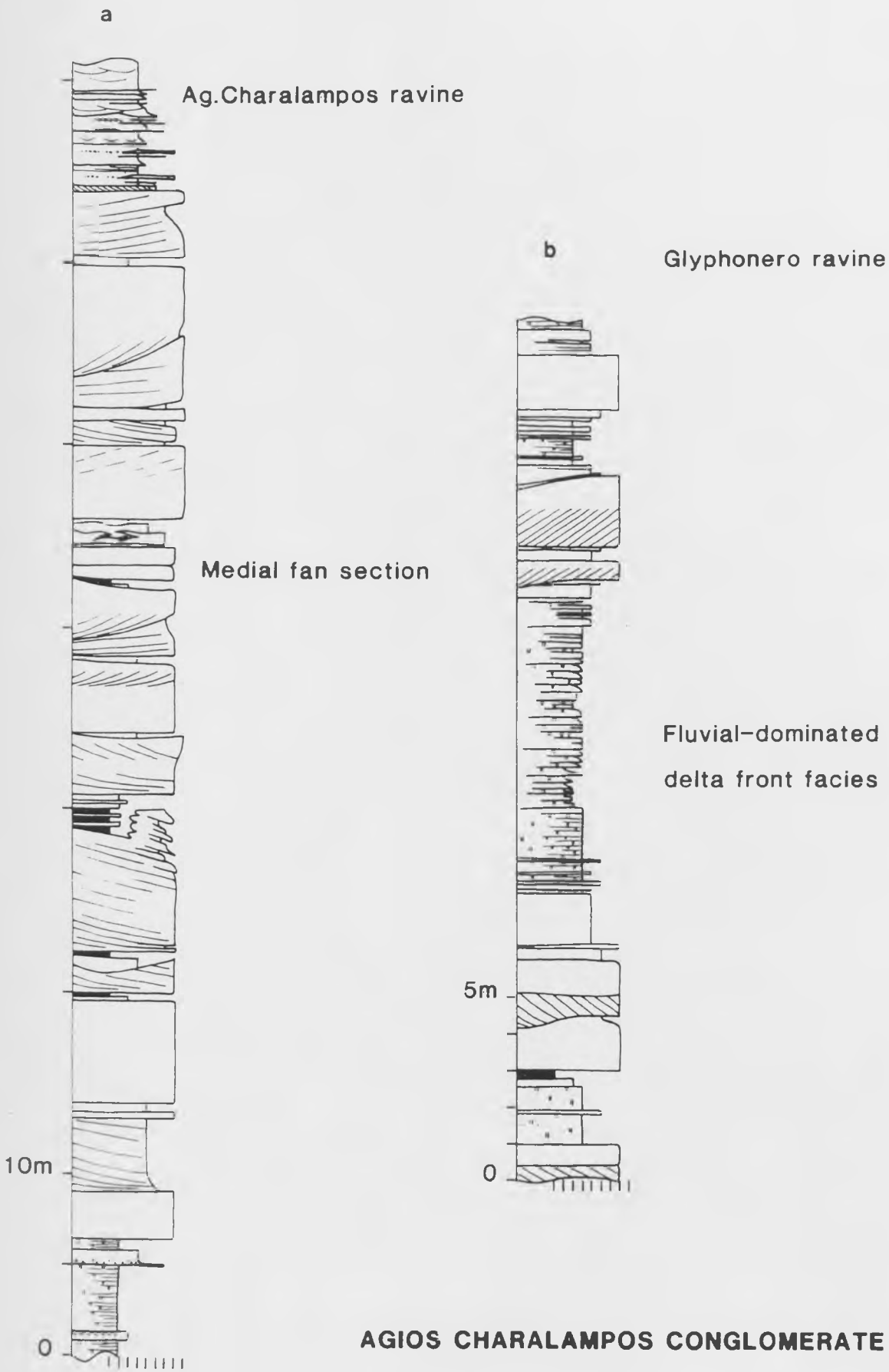

AGIOS CHARALAMPOS CONGLOMERATE

second transition style entails a gradual coarsening-up of silts and sands. There is typically a concurrent diminution in intensity of bioturbation. Initial conglomerate units are erosive-based and cross-stratified. Palaeoflows in this more easterly ravine section were to the north and north-east.

Interpretation:

These conglomerates formed a fan delta emanating from the south side of the basin. The absence of basinal sediment intraclasts excludes the possibilty that the fan was sourced from some intrabasinal topographic feature. Its apex is therefore inferred to have been at the basement margin of the basin. The fan delta prograded rapidly into the shallow lacustrine waterbody indicated by the underlying and laterally-equivalent FA3 Asprakhomata-Kalamona to Multi-Coloured Series fines. Water-depth at the time of initial fan-delta progradation is estimated as between 4 and 12m. The lower figure is the height of asymptotic sets in sands at the base of the Agios Charalampos ravine section (fig. 3.6a). The upper limit is the height between bioturbated silts of the underlying lacustrine facies and the first sub-aerial horizon within the fan deposits, as inferred from the presence of lignites. Relative base-level change is not taken into account in this water-depth estimation.

Lignite- or fines-bounded conglomerate packages within the clinoform are all less than 14m in thickness. This lends further support to the inference that the fan-delta prograded into a shallow waterbody. Lacustrine (FA3) fines or lignites indicate sites of reduced sedimentation rates and lie diachronously between areas of active coarse-clastic lobe deposition on the fan surface and in interdistributary "bay"

settings. The more distal coarse clastic packages (fig. 3.6b) are similar in style to a fluvial-dominated delta front facies, as outlined in facies association 4. Distributary geometries may be analagous to the "goose-foot" patterns of the Ebro Basin Scala Dei alluvial fans (Allen at al 1983). Here, however, interdistributary areas were subaqueous and either a) filled by overbank fines and then lignites or b) filled by prograding and consequently coarsening-up crevasse splay or minor delta developments. The sheet-like base to conglomerates above certain distal fines may reflect a more "coot's foot"-like architecture of shallow sheet lobes advancing from channel or crevasse apices.

The overall coarsening-up trend of the fan-delta conglomerates reflects their continued progradational trend until an abrupt and probably tectonically-induced submergence of the fan surface. Significant incision of the fan surface is not seen, other than by the sedimentary process of channel switching and lateral migration. The fan-delta facies are therefore consistent with a subsiding footwall fan position, as opposed to the incised character of an uplifted or up-tilted hangingwall fan (Leeder et al 1988, Leeder & Gawthorpe 1987). The variety of A4 cross-stratification dip orientations indicates the prevalence of lateral bar and possibly channel bar bedforms. A moderate-sinuosity FA2 braid stream form is therefore suggested. Palaeoflows recorded as pebble imbrications radiate to the north and north-east. This pattern correlates with the northwards and eastwards transition from fan-delta coarse clastics to basinal fines (as seen in outcrop and borehole 5/69 in figure 14 of Freyberg 1973).

3.5.3 Multi-Coloured Series "Marls"

Description:

The title here is retained to conform with the published lithostratigraphy (Gaitanakis et al 1985) for the area. Calcareous silts and fine sands predominate, but with subtle variations in sedimentary detail. Most characteristic are B5a white calcareous silts/sands with diffuse bedding of decimetre scale and occasional B4 trough scours with axes trending approximately east-west (plate 3.2a). Variations include the degree of bioturbation, the local appearance of a limited macrofauna and of siliceous nodules, and the periodic incursion of serpentinite sands of facies B3, B2 and B1.

At the top of the Agios Charalampos Conglomerates in the Charalampos valley, fine calc-arenites abruptly overlie the pebble conglomerates. A few lenses of pebbles and granule stringers occur within the lowermost fine sands (fig. 3.7a) which are variably planar-laminated or homogeneous. Facies D cross-stratification and facies A or B trough sets of varying dimensions within the sands, together with bioturbated fines which fill and drape the troughs, emphasize the inconsistent current regime.

15m up into the Multi-Coloured Series calcareous silts/sands is a 5m package with erosive-based and trough cross-stratified green sands (facies B2, B3 and B1). These are exclusively ultrabasic in composition. Fining-up pulses are typically bioturbated at the top. The sands contain freshwater mussels and Viviparus. The package is terminated equally abruptly as it appeared within the background "marl" sediments.

Some 200m of the Multi-Coloured Series "Marls" occur within the

Plate 3.2

a) Multi-Coloured Series "Marls" with facies B4 trough-scours, grid ref. 5.86 21.77

b) Multi-Coloured Series Sands transition zone - asymptoting surfaces at base of distributary channel sandbody, grid ref. 6.34 22.01

c) Facies B trough cross-beds of Multi-Coloured Series Sands, grid ref. 6.02 22.12

d) Mass and grain flow conglomerate packages of Upper Conglomerates, as shown in upper part of log, figure 3.16. Grid ref. 7.51 21.29

a

b

c

d

Figure 3.7

Logs: Multi-Coloured Series "Marls"
a = log through Charalampos valley, grid refs. 5.84 21.64 to 5.86 21.73
b = detailed log illustrating trough-scour morphologies, grid ref. 5.95 21.81

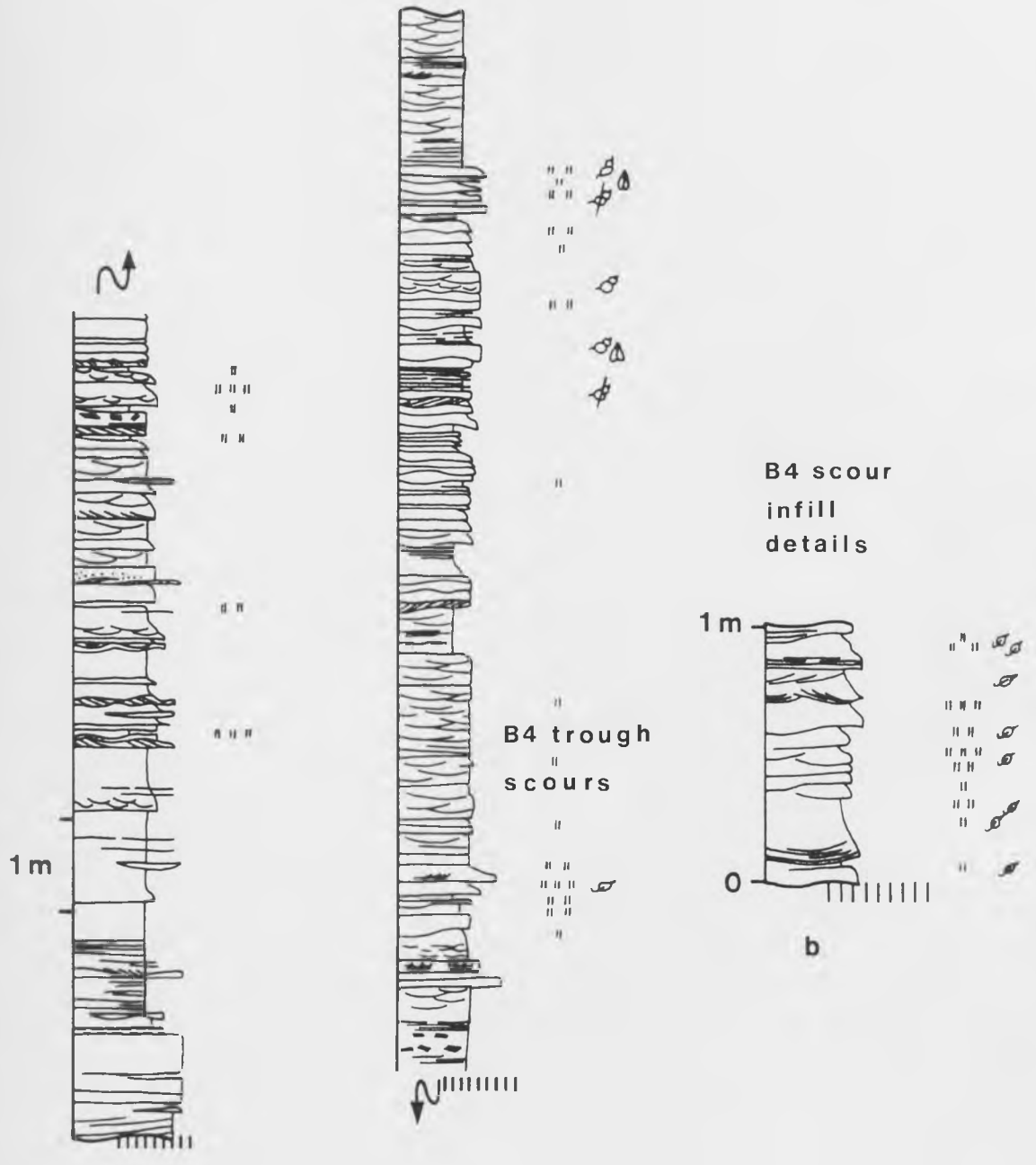
1 m
B4 trough
scours
B4 scour
infill
details
1 m
0
a
b

Charalampos/Stenodromi type-section (fig. 3.4 and Freyberg 1973). 1-10m thick serpentinite sand sheets occur with increasing frequency towards the top of the "marls". These sand sheets are commonly homogeneous but some exhibit planar lamination (facies P) and small-scale trough sets (facies B). The "marls" themselves include two 1m thick nodular horizons. These are characterised by irregular siliceous nodules and 2-15cm thick silica-cemented bands parallel to bedding. The microfauna of the B5a calcareous silts/sands includes gastropod opercula, Cyprideis, Amplocypris, Hemicyprideis and Candona (specimens 5.6.1 and 8.8.4, appendix 1). Details of bedforms and bioturbation associated with the B4 trough scours that are common throughout the Multi-Coloured Series "Marls" are illustrated in figure 3.7b.

Calcareous silts/sands of similar detailed facies extend to the east and south-east deyond the Drosia hills (fig. 3.1 and enclosure 1). A distinct fauna from that seen further west, however, includes ?Tyrrenocythere, ?Aurila, cyprids and ?Herpetocypris reptans (7.6.2, appendix 1). The total thickness of Multi-Coloured Series "Marls" to the east is not evident, their lower limit not being exposed. A minimum thickness of 160m north-east of Drosia can be established.

Interpretation:

Upon submergence of the Lower Pliocene Agios Charalampos fan-delta sedimentation continued in a freshwater environment of facies association 3 or 5 in the western part of the Charalampos fault block, as indicated by its macro- and microfauna. The presence of siliceous nodules in facies B5a is typical of shallow freshwater settings. There remains the possibility, however,

that at least some of the faunal elements are second cycle materials.

Lithic carbonate detritus forms the bulk of the calcareous silts and fine sands. Palaeoflows implied by current-induced bedforms, and the continuity of the coarsening-up profile into the overlying and westerly-derived Multi-Coloured Series Sands above, all conform to a model of west to east transport of sediment within the "Marls". But current activity was discontinuous within the environment of deposition of the "marls". In the west, bioturbated horizons characterise quiescent sedimentation episodes. Facies B4 trough scours and the localised interruption of "marl" deposition by B2 channelised and B1 sheet sands indicate increased current influence.

To the east, faunal elements found in the Drosia hills (e.g. 7.6.2, appendix 1) indicate brackish conditions prevailed at least periodically. Cardium and a varied (though unidentified) fauna of bivalves and gastropods suggest near-normal marine salinities may have been reached (fig. 3.12a). Symmetric and draped ripples amongst "marls" indicate wave activity. A model is therefore proposed of an east-west trending current-dominated (microtidal) estuary, corresponding to facies association 5. This was bounded to the north and south by the basement margins of the basin. Fluvial conditions extended into this estuarine trough from the west, the major source of sediment. Water depths were low, explaining the continuity of freshwater to brackish conditions for several kilometres east of the exclusively current-influenced fluvial facies. Structureless and cross-stratified 1-2m thick sandbodies in the eastern zone of brackish conditions may indicate the development of bar forms at the limit of tidal influence.

3.5.4 Multi-Coloured Series Sands

Description:

Multi-Coloured Series Sand facies may be usefully divided into two types: 1) the transitional facies association at the junction between the Multi-Coloured Series "Marls" and Sands. 2) the bulk of the sands, where uninterrupted by substantial thicknesses of fines.

The Stenodromi valley cuts through a 250m vertical section of green and orange sands (figs. 3.2 and 3.4). To the east, the total thickness of sands decreases as they interdigitate out into Multi-Coloured Series "Marls" through a transitional zone. The position of this zone progrades 2.5km to the east in about 300m of vertical section.

1) The transitional facies suite is summarised as sharp-based or coarsening-up sandbodies isolated within a matrix of calcareous silts and sands (refer to section 3.4.4). The sands are composed of peridotite and serpentinite with subordinate limestones, cherts and bioclastics. Palaeoflows are generally eastwards, but with a high degree of divergence (see map, enclosure 1). The sands contain Viviparus gastropods and Cyprideis ostracods (8.8.2, appendix 1). The basal and upper contacts between "marls" and sands vary between sandbodies and along the length of any one sandbody. Sandbodies have a high length/thickness ratio from west to east, but are relatively narrow north-south (length/thickness ratio of the order of five to ten times greater, where exposed in outcrop).

Figures 3.8a, b and c illustrate some of the variation in facies detail around the transitional zone sandbodies. In figure 3.8a S3 symmetric ripples and mud drapes denote wave activity and

Figure 3.8

Logs: Multi-Coloured Series Sands, transition zone
a = log, grid ref. 6.55 22.36
b = log, grid ref. 6.90 22.35
c = log through distal equivalent of upper sandbody in log b, at grid ref. 7.27 22.16

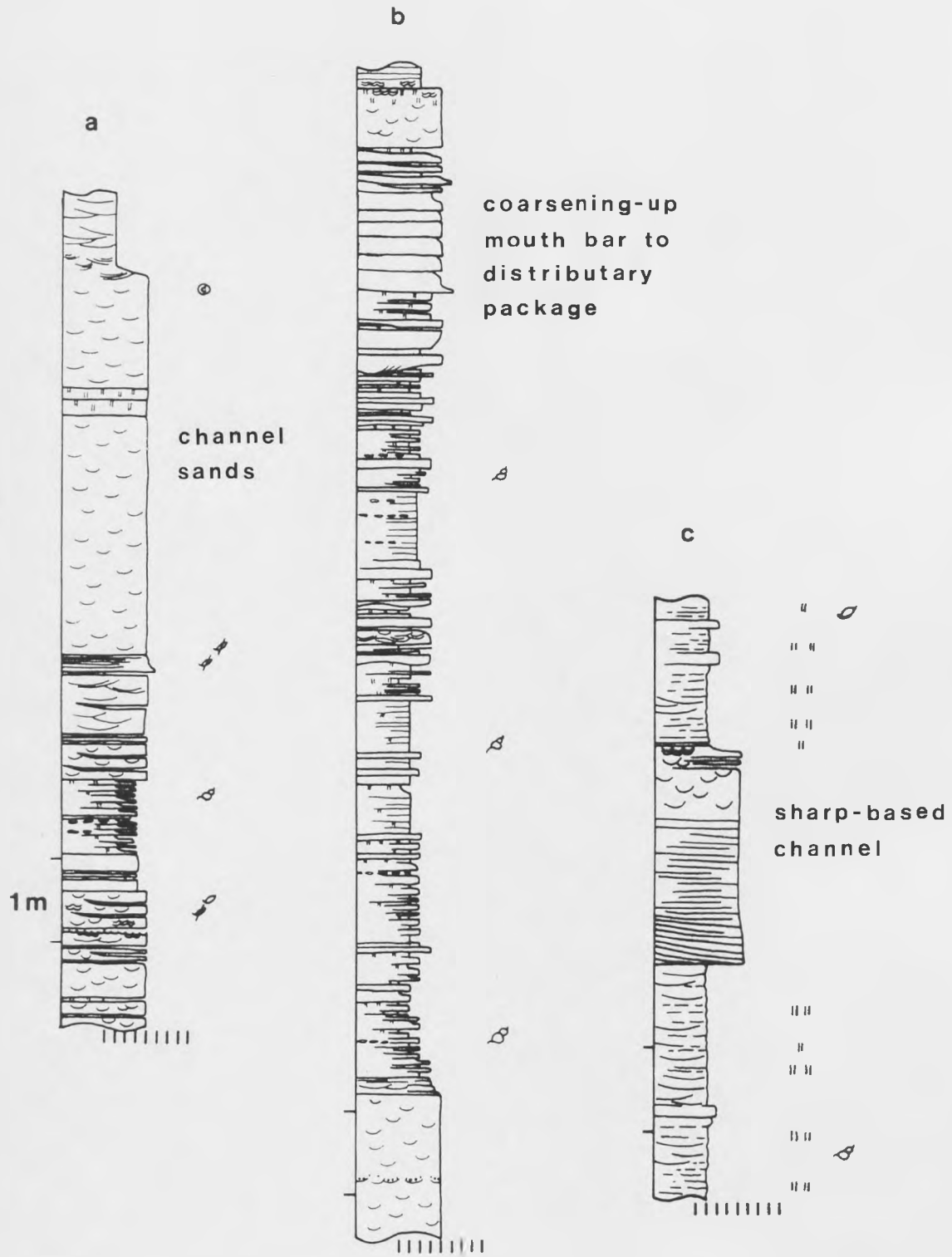
a
b
c
channel
sands
coarsening-up
mouth bar to
distributary
package
sharp-based
channel
1m

reworking of sands across the surface of the lower sand package. Facies B5(a) calcareous silts and fine sands above are bioturbated. Siliceous nodules are developed locally. Facies B and A trough cross-bedded sands interdigitate into the silts to give a coarsening-up pattern beneath the basal coarse-grade and planar-laminated sands (facies P) of the sandbody itself. The major part of this sandbody is pervasively trough cross-stratified (facies B), with bedform dimensions less than 30cm. Trough cross-lamination (S4) of the topmost sands and trough scour fills (B4) in the succeeding calcareous silts indicate continued current influence after the sand supply was cut off.

A more complex coarsening-up package is seen in the upper part of figure 3.8b. Facies B3 interlaminated silts and sands, the fines of which are bioturbated, are cut by a channelised and cross-stratified sand unit of facies B2. Above a 0.8m interval of B3 interbedded sands and bioturbated silts, 0.15-0.3m fining-up sand units dip to the north and south, away from the axis of the sandbody. These bedding surfaces asymptote down and interdigitate out into silts. The same sandbody was logged 400m to the ESE (fig. 3.8c). Sandbody thickness is virtually maintained across that distance. In the latter position, however, facies B2 or P sands with asymptotic internal bedding surfaces (dipping shallowly to the east and south at outcrop) lie conformably but abruptly on the underlying "marls". The upper part of the sandbody is again trough cross-stratified (facies B), with S3 symmetric and draped ripples at its top.

2) The Multi-Coloured Series Sands outcrop almost continuously in the Stenodromi valley in the northern and north-western area of the Charalampos fault block. Only minor incursions occur by

"Marls" from the east. Figure 3.9 illustrates the homogeneity of grain size through this section, and its sedimentary structures, characterised by facies B small-scale trough cross-stratification. Sand composition is predominantly serpentinite. Salger (1973) confirms this. Composition is similar to sands of the transitional facies which are downstream equivalents, palaeoflows within the sands being consistently eastwards (enclosure 1).

Thin ultrabasic and red chert pebble layers (L) occasionally occur, often in association with cross-stratification in the immediately overlying sands. Bioclastic lags of Unio shell fragments also occur. Individual facies A trough scours may also contain granule/pebble or bioclastic lags in the base of their fills. Larger scale bedforms are rare. Facies C cross-bedding does occur, up to 2m in height and with climbing sets on their backs. These are characteristically capped by facies D tabular cross-sets.

Rare B5 calcareous silt packages can be traced laterally through the Multi-Coloured Series Sands. These are continuous to the east into the transition with Multi-Coloured Series "Marls". They are themselves homogeneous to planar-laminated and sometimes bioturbated. Viviparus is common. Kollman (1973) reports a "Levantine" faunal assemblage from the Multi-Coloured Series Sands. Viviparus pulchriformis, Theodoxus micans, T. nivosa, Melanopsis, Congeria, Micromelania elegans, Bulimus, Amphimelania ornata, Unio and Paludina are all reported.

Some sands are rich in bioclastics. Specimen 16.7.2 (appendix 1) contains both Cyprideis and Aurila ostracods, from which a brackish environment has been inferred. 8.8.6 includes

Figure 3.9

Log: Multi-Coloured Series Sands in Stenodromi valley, grid refs. 6.03 22.41 to 6.08 22.53

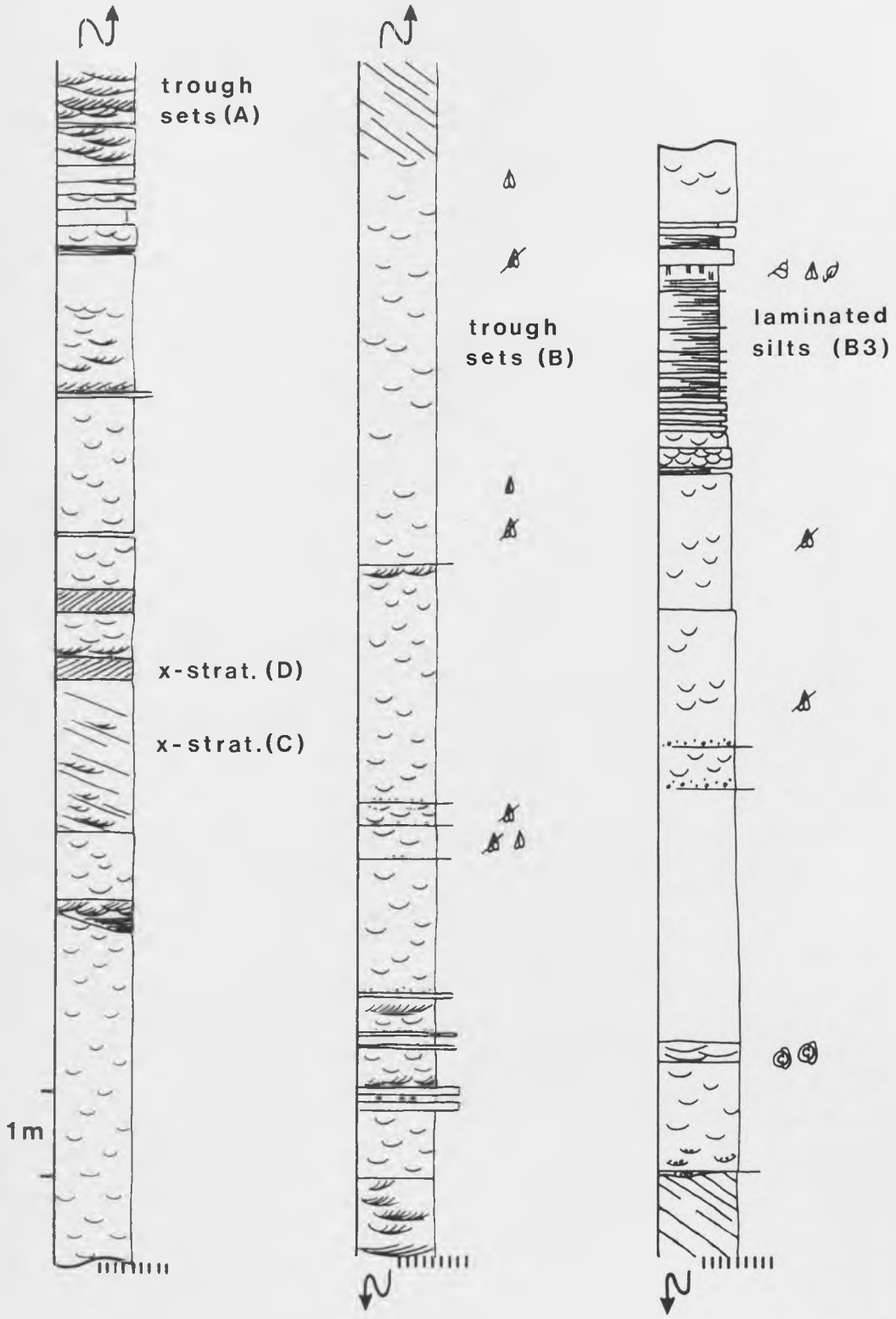
trough
sets (A)
x-strat. (D)
x-strat.(C)
1m
trough
sets (B)
laminated
silts (B3)

Hemicythere and Aurila which would indicate a more marked marine influence. At the same locality, marine foraminifera (unidentified) also occur (slide 49679). Figure 3.10 illustrates typical Multi-Coloured Series Sands in thin section.

Lignites are reported from approximately 20m above the base of the Multi-Coloured Series Sands in a borehole in the Stenodromi valley (borehole 6/69 in figure 14 of Freyberg 1973). However, no lignites are seen in outcrop.

Interpretation:

The Multi-Coloured Series Sands represent the eastwards progradation of the axial fluvial facies association (FA2) along the "estuarine" basement-bounded trough described in section 3.5.3. The transitional facies association represents a fluvial-dominated delta front. This transitional zone environment will be discussed first.

1) Multi-Coloured Series transitional zone - FA4:

The detailed form of the interdistributary fines to distributary channel sand transition (facies association 4) is a function of the sedimentary process by which the change occurred (Elliott 1974). Overbank flooding, crevasse events and avulsion or the lateral migration of the channel position may all occur. Furthermore, the log profile of, say, a sandbody redirected into an interdistributary area by a crevasse event out of a precedent distributary channel will vary laterally (Fielding 1984a & b).

Figure 3.8a illustrates the abandonment characteristics of wave-reworking and silt-draping across the top of one trough-bedded distributary sandbody. Interdistributary fines above are characterised by a pulsed style of sedimentation with fining-up units and sand sheets probably introduced by overbank flood

Figure 3.10

Photomicrograph of Multi-Coloured Series Sands:
Serpentinite sands with isopachous cement rims. Hydrocarbons passed through and infiltrated fractures in grains prior to development of pore-filling sparite. Late secondary porosity.
Scale bar = 0.5mm. Unstained thin section (48600), PPL.
Facies B sands, Stenodromi valley, grid ref. 5.98 22.07

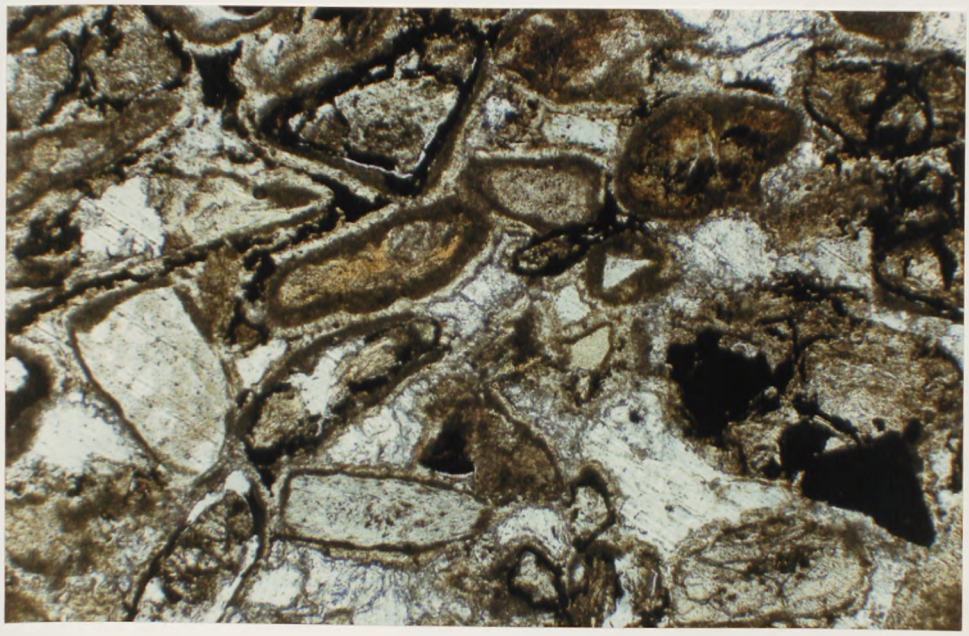

events.

Above, facies B trough cross-stratified sands which interdigitate into B3 calcareous fines probably represent distal mouth bar deposits. The logged outcrop trends approximately parallel to the direction of flow. Any erosive base to the mouth bar sands may therefore be obscured in outcrop. Alternatively, the irregularity of current influence in these sands may imply a minor mouth bar/crevasse channel origin. The occurrence of planar-laminated sands (facies P) marks the basal deposits of the distributary channel proper. The bulk of the channel sands are monotonously trough cross-stratified (facies B). The presence of bioturbated horizons denote periods of reduced current influence and the possible advance of brackish basin waters into the channel.

A more characteristic coarsening-up progradational package is seen in log 3.8b (also plate 3.1c). The erosive base of a mouth bar channel is evident. Fining-up units of mouth bar/levee sands dip and wedge out to north and south, at high angle to the channel axis. A relatively thin unit of facies B trough-bedded channel sands is preserved here. The upper part of the channel deposits may have been reworked by wave action following channel abandonment. But the same distributary channel may be traced 400m to the east where it forms a sharp-based sandbody sitting within basinal silts (fig. 3.8c). Low-angle laminations in the basal sands may be lateral accretion surfaces (flow-normal sections are not available at this locality). These low-angle surfaces also asymptote to the east, parallel to the overall flow trend (also plate 3.2b). Characteristic facies B trough-bedded sands of the distributary channel outcrop above. The topmost

sands have been subject to reworking. Silt drapes across trough beds and symmetric draped ripples (facies S3) indicate wave action influenced this abandonment facies.

The basinal calcareous silts above and below the distributary sandbody exhibit a range of bedding types. B5 planar laminations, diffuse planar bedding, B4 trough scours and bioturbation of variable intensity all imply considerable variation in current influence. Both Viviparus gastropods of freshwater/brackish affinity and marine bivalves are found within the basinal fines. This illustrates one of several problems encountered in the detailed interpretation of fluvial-dominated deltaic facies. These include:

1) Fluvial stage variability; a saline wedge may migrate up the distributary channel at times of low river stage (Wright & Coleman 1974). The saline wedge will then be flushed out to or beyond the mouth bar at high stage.

2) Climatic control on saline wedge position; any broader time-scale variation in fluvial discharge which may reflect climatic trends will also control the relative position of the saline wedge at the delta front.

3) Reworking of marine fauna across the alluvial surface, following any temporary marine transgression onto the delta plain.

4) Transport of freshwater fauna into the brackish/marine environment.

The range of processes often prohibits the exclusive interpretation of detailed environments within and around the delta front. Macro- and microfauna of freshwater and/or brackish and/or marine environments occur together as a product

of any combination of the above processes.

2) Multi-Coloured Series Sands - FA2:

The subdivision of facies within the c.350m thickness of virtually continuous Multi-Coloured Series Sands is necessary to understand the detailed environment in which they were deposited. The approach of Cant & Walker (1976) has been adopted. This requires some familiarity with the facies prior to setting up proposed facies divisions, as some interpretational input is inherent to the allocation of each unit to a facies type. The following detailed facies scheme (summarised within table 3.1) is proposed, modified after Cant & Walker (1976). This allows the comparison of results with their description and interpretation of the Devonian Battery Point Sandstone in Quebec, which shows some similarities to the Multi-Coloured Series Sands sequence.

SS - Scoured surfaces, with or without associated pebble/granule lag deposits. These incising erosional surfaces are interpreted as fluvial channel bases. A scoured surface is strictly an "event" facies rather than a lithofacies, but has genetic meaning and is therefore distinguished.

L - Lags of pebbles or granules. These occur as lenses or layers up to 0.05m thick or as diffuse stringers within medium sands. Such lags fine up or become more diffuse upwards very rapidly (within 0.1m). They are interpreted as in-channel reactivation surfaces, denoting variation in fluvial discharge.

P - Planar horizontal or very low angle laminated sands.

A - Variable trough cross-bedded facies. Poorly to well defined trough cross-bedding with troughs 0.4-1.0m in width and about 0.1-0.2m in depth. Troughs occasionally show a climbing habit

and may contain basal pebble/granule lags.

B - Well-defined trough cross-bedded facies (plate 3.2c). Troughs are on average smaller than in facies A, widths ranging from 0.2-0.6m, depths from about 0.05-0.1m. Troughs are stacked more regularly than in facies A. In plan view internal cross strata are highly arcuate. Facies B makes up the majority of the exposed fluvial sand sequence. Trough cross-beds are typically delineated by bioclasts (gastropod and locally foraminiferal fragments). Where these are absent the facies may appear homogeneous due to the high level of grain size sorting in the sepentinite sands.

C - Large scale, planar-tabular cross-bedded facies. Just two 1.8-2.2m high cross sets are recognised in 2 sq. km. of outcrop. One is capped by small-scale cross sets of facies D while the other is truncated by an erosive scour surface (SS). Basal contacts of the cross sets are angular to slightly asymptotic parallel/sub-parallel to flow. Diffuse cross-bed layers occasionally include small-scale, climbing, trough-like sets.

D - Small-scale planar-tabular cross-bedded facies. Sets are 0.15-0.25m in height, isolated and rare. Palaeocurrents are more variable than facies A and B.

E, F, G - Asymmetrical scours up to 3m in width (E), sandstones with climbing ripple cosets (F) and upper flow regime low-angle stratified sands (G) of Cant & Walker (1976) are not observed in the Multi-Coloured Series Sands.

B3 - Laminated calcareous silts (with thin sand interlaminae) appear both gradationally and abruptly over sands, usually of facies B. The thicker silt developments may be bioturbated and

contain freshwater/brackish molluscs. This facies records periods of terminated current activity. This might imply the isolation of a channel segment as a small lake on the alluvial surface or the transgression by the basinal environment onto the delta plain.

The statistical analysis of observed transitions between the facies described may allow an overall genetic/environmental association to be inferred. The log in figure 3.9 is used for this purpose as it typifies the Multi-Coloured Series Sands facies. Indeed the logged section is from the Stenodromi valley which Freyberg (1973) described as the type section.

If there is a sequential link between observed facies this may be determined by a Markov chain analysis of the observed facies sequence (Miall 1973, Cant & Walker 1976). The essence of this technique is to establish whether or not any transition has a greater than random probability of occurrence. If so then some genetic linkage may be deduced. The first step is to list the vertical sequence of facies recorded in the logged section (table 3.2). These facies transitions may be pictorially represented by a flow diagram of observed facies relationships (fig. 3.15). Certain trends stand out at this stage (as they do at outcrop). Facies B trough-bedded sands, the volumetric majority of the sequence, tend to overlie basal scours and lags or facies A variably trough cross-stratified sands. Facies B also alternates with lag deposits and facies H silts. Overall a left to right evolution in figure 3.11 might be inferred. But is this real or the product of random facies transitions?

A transition probability matrix (table 3.4) is calculated from the observed transition count matrix (table 3.3). The lower

Figure 3.11

Observed facies relationship diagram, Multi-Coloured Series Sands. Abrupt facies transitions are marked as continuous arrows, gradational transitions as dashed arrows.

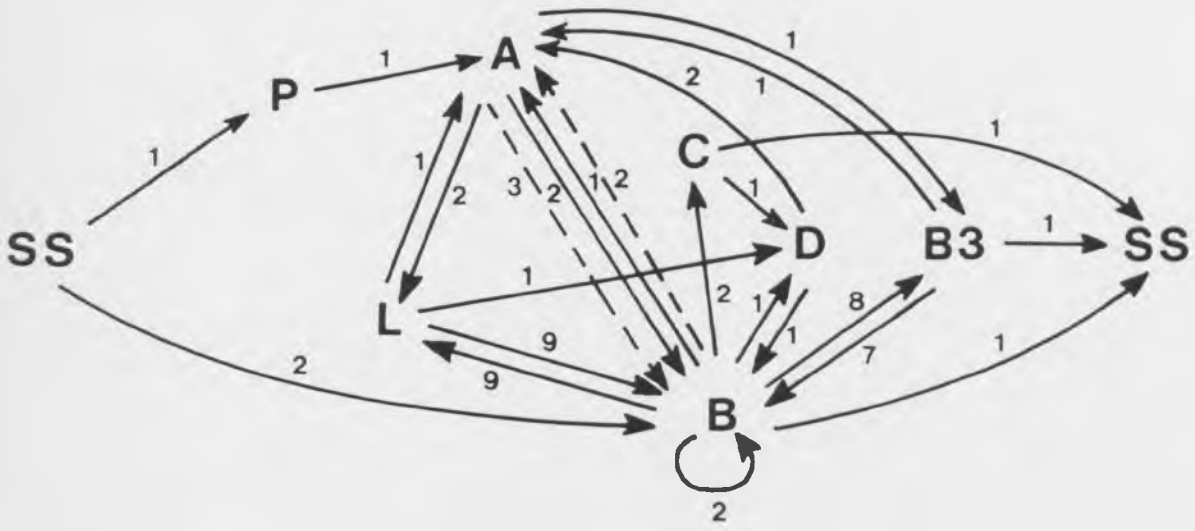
SS
P
A
L
C
D
B3
SS
B
1
2
3
9
8
7

Tables 3.2 - 3.4

TABLE 3.2

Vertical sequence of facies observed in logged section, fig. 3.9. Sequence reads from base upward. Scoured surfaces and lags are included as "event" facies. Transitions from one lithofacies into itself (in parentheses) are excluded for the purposes of Markov chain analysis.
. = SS : = L , = sharp boundary ,, = gradational boundary

B.P,A,B,C,D,A,,B,D,B,B3.B:D,A,,B,B3,B,B3,B,B3,B,A,B3,A,B:A,,B:
B:B,,A:B:B:B:B,,A:B,C.B(,B,)B:B:B,B3,B,B3,B,B3,B,B3,B

TABLE 3.3

f_{ij} Transition count matrix

	SS	L	P	A	B	C	D	B3	Row sum
SS	0	0	1	0	2	0	0	0	3
L	0	0	0	1	9	0	1	0	11
P	0	0	0	1	0	0	0	0	1
A	0	2	0	0	5	0	0	1	8
B	1	9	0	3	0	2	1	8	24
C	1	0	0	0	0	0	1	0	2
D	0	0	0	2	1	0	0	0	3
B3	1	0	0	1	7	0	0	0	9
									61

TABLE 3.4

p_{ij} Observed transition probability matrix

	SS	L	P	A	B	C	D	B3
SS	-	-	.333	-	.667	-	-	-
L	-	-	-	.091	.818	-	.091	-
P	-	-	-	1.00	-	-	-	-
A	-	.250	-	-	.625	-	-	.125
B	.042	.375	-	.125	-	.083	.042	.333
C	.500	-	-	-	-	-	.500	-
D	-	-	-	.667	.333	-	-	-
B3	.111	-	-	.111	.777	-	-	-

Tables 3.5 - 3.7

TABLE 3.5

The frequencies of each facies and the total number of observed facies summed from the vertical sequence row data:

SS	L	P	A	B	C	D	B3		T
3	11	1	8	25	2	3	9	=	62

TABLE 3.6

r_{ij} Random transition probability matrix

	SS	L	P	A	B	C	D	B3
SS	0	.186	.017	.136	.424	.034	.051	.153
L	.059	0	.020	.157	.490	.039	.059	.176
P	.049	.180	0	.131	.410	.033	.049	.147
A	.056	.204	.019	0	.463	.037	.056	.167
B	.081	.297	.027	.216	0	.054	.081	.243
C	.050	.183	.017	.133	.417	0	.050	.150
D	.051	.186	.017	.136	.424	.034	0	.153
B3	.057	.208	.019	.151	.472	.038	.057	0

TABLE 3.7

d_{ij} Difference matrix

	SS	L	P	A	B	C	D	B3
SS	0	-.186	.316	-.136	.243	-.034	-.051	-.153
L	-.059	0	-.020	-.066	.328	-.039	.032	-.176
P	-.049	-.180	0	.869	-.410	-.033	-.049	-.147
A	-.056	.046	-.019	0	.162	-.037	-.056	-.167
B	-.039	.078	-.027	-.091	0	.029	-.039	.090
C	.450	-.183	-.017	-.133	-.417	0	.450	-.150
D	-.051	-.186	-.017	.531	-.084	-.034	0	-.153
B3	.054	-.208	-.019	-.040	.305	-.038	-.057	0

facies of each transition couplet is given by the row number (i) and the upper facies by the column number (j). Transitions are picked only when facies change in character. Therefore no account is taken of bed thickness. This emphasizes the control on couplets by depositional process (Miall 1973, 1984). This is termed the embedded chain method.

A random probability matrix (r_{ij}, table 3.6) is then calculated for comparison with the observed transition probability matrix (p_{ij}). This assumes the same abundance of each facies as observed (table 3.5) but in a random sequence (after Cant & Walker 1976). [Equation (1) of Miall (1973) is specifically avoided as a means of calculating this random probability matrix as the equation does not relate directly to the relative abundances of facies present.] For the embedded chain method in which i=j transitions are not permitted;

$$r_{ij} = J/(T-I) \qquad \text{Equation 3.1}$$

where J is the observed frequency of the upper facies, I is the observed frequency of the lower facies and T equals the total number of recorded facies.

A difference matrix (table 3.7) is next calculated to highlight transitions which occur with a greater than random frequency:

$$d_{ij} = p_{ij} - r_{ij} \qquad \text{Equation 3.2}$$

The most negative d_{ij} values highlight the least likely transitions. From the difference matrix (d_{ij}), a new facies relationship diagram may be constructed (fig. 3.12). This illustrates only those transitions which occur more frequently than random, with a d_{ij} value greater than 0.05. Dotted arrows show difference probabilities in the range 0.05 to 0.10, light

Figure 3.12

Analysed facies relationship diagram, Multi-Coloured Series Sands. Only transitions that occur more frequently than random are shown, with a d_{ij} value greater than 0.05.
Dashed arrows show probabilities in the range 0.05 to 0.10;
light arrows 0.10 to 0.30;
heavy arrows greater than 0.30.
Inferred fluvial settings are indicated.

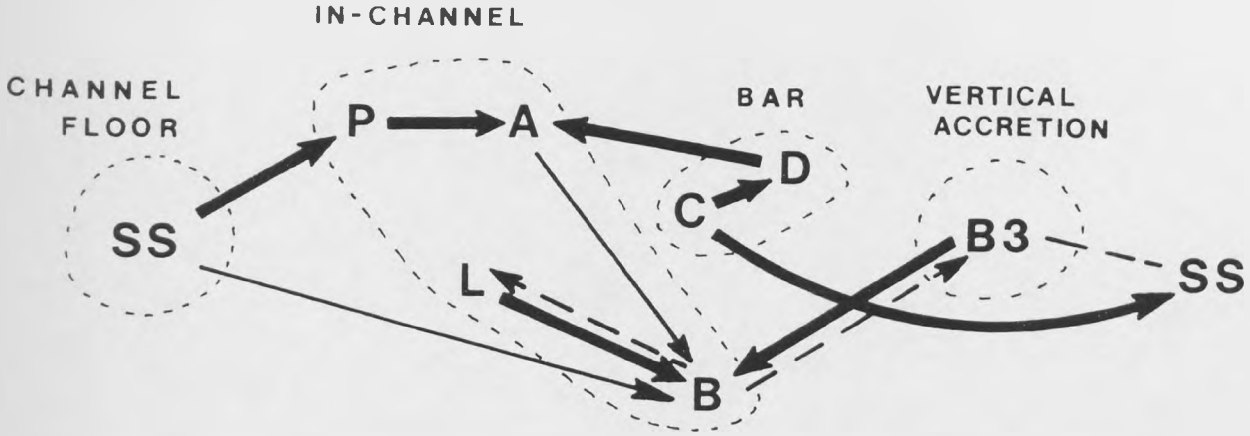
IN-CHANNEL
CHANNEL FLOOR
BAR
VERTICAL ACCRETION
P
A
D
C
SS
L
B3
SS
B

arrows 0.10 to 0.30 and heavy arrows greater than 0.30.

Within any one stratigraphic succession the significance of the difference matrix values may be assessed by means of a chi-square test (following method 1 of Miall 1973):

$$\chi^2 = \sum_{ij}^{n} \left(f_{ij} - I_{r_{ij}} \right)^2 / I_{r_{ij}} = 70.2 \qquad \text{Equation 3.3}$$

where n equals the rank of the matrix (8 in this case). A null result would imply the f_{ij} observations equalled a purely random transition result. If χ^2 exceeds the critical value for the specified number of degrees of freedom, the null hypothesis is rejected. The number of degrees of freedom equals the number of non-zero values in the r_{ij} matrix ($n^2 - n$) minus the rank of the matrix. That is:

$$df = n^2 - 2n = 48 \qquad \text{Equation 3.4}$$

From a table of chi-square values, for 48 degrees of freedom, the critical value at the 95% confidence level is 65.3. The non-random distribution of facies transitions is therefore statistically real.

But what are the environmental implications of the facies relationships of figure 3.12? An overall left to right facies development is confirmed as the dominant trend between any two channel-bounding scour surfaces. Above a scour surface (interpreted as a channel base) the tendency is for planar-laminated facies A to be overlain by larger-scale trough cross-stratified facies A and then facies B trough bedded sands. This corresponds to the expected shallowing/increasing flow velocity transition within a channel environment. At the same time bar forms occur (2m high cross sets of facies C) which are typically

capped by small-scale planar or tabular cross-stratification (facies D). These may be inundated by further trough bedded channel sands or cut by the erosive base of a succeeding channel.

The alternation of facies B trough bedded sands with lag deposits (L) and laminated/bioturbated silts (B3) suggests some variability in flow discharge rates. Facies L is taken to represent falling to rising stage reactivation events within the channel sands, although some lag deposits may accummulate in the lee of constructing bedforms. The facies B3 to B transition represents increasing discharge and B to B3 diminishing discharge. With falling flow stage, the basinal saline wedge advances up-channel and basinal silt deposition may periodically have advanced up-channel and onto the delta plain.

The Multi-Coloured Series Sands are interpreted as a lower delta plain fluvial channel-dominated sequence. A model sequence is summarised in figure 3.13. A low-sinuosity channel character is inferred from the lack of lateral accretion surfaces. This model sequence has distinct similarities with the Battery Point Sandstone described by Cant & Walker (1976). The major difference is the absence of Cant & Walker's upper flow stage and accretionary facies E to G in the Multi-Coloured Series Sands. This lack of channel margin and alluvial plain/overbank facies would seem to support the hypothesis that the observed Multi-Coloured Series Sands are exclusively within-channel deposits. Outcrop position is therefore inferred to run parallel to and within the structurally constrained depocentre of the Multi-Coloured Series axial system. North-south outcrop in the Multi-Coloured Series Sands is limited to less than 1km. It is therefore not evident whether, as one end-member possibility,

Figure 3.13

Multi-Coloured Series Sands - braided fluvial facies association. Idealised log after Markov chain analysis. [Vertical scale does not represent exact facies proportions.]

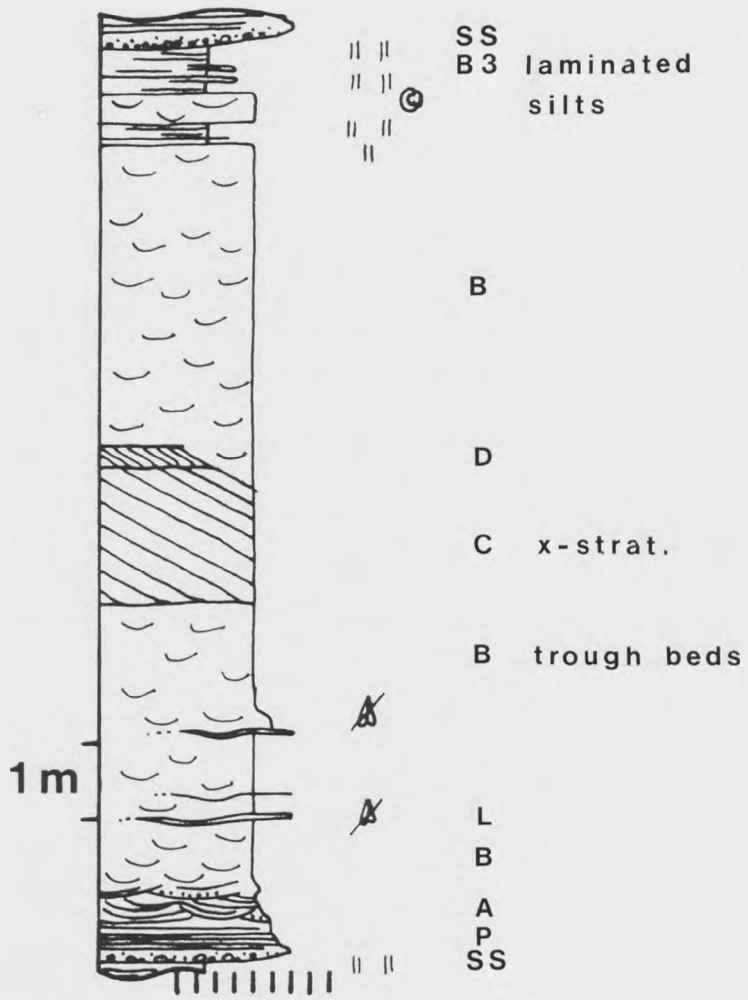
SS
B3 laminated
silts
B
D
C x-strat.
B trough beds
1m
L
B
A
P
SS

axial channel sands covered the width of the syn-depositional basin or whether outcrop happens to correspond to a vertically-stacked channel belt controlled by syn-depositional normal faulting (after Bridge & Leeder 1979).

One or two cautionary points should be made regarding the statistical analysis of the fluvial sands. Firstly, some difference probability (d_{ij}) values may be distorted by low facies frequencies. For example, the precursor to facies C is not represented in the inferred facies relationship diagram (fig. 3.12). This is because facies C only occurs twice in the test section. Although in both cases the large scale cross sets occur above trough bedded sands of facies B, the resultant d_{ij} value is only marginally above random. A second limitation of the chain analysis is that this does not take into account any materials lost by erosion out of the section. A field-based interpretation is required as to whether Cant & Walker's facies E to G were never present or alternatively were truncated by subsequent channel bases. In this case, truncation seems unlikely. The scour surfaces seen in outcrop are not sharply incising and the preservation of calcareous fines beneath these surfaces also suggests that near-complete channel fill packages have been preserved. The Multi-Coloured Series Sands in outcrop therefore appear to record exclusively mid-channel FA2 fluvial sands (plate 3.1d).

3.5.5 Upper Conglomerates

Description:

The Lower Pliocene sequence of the Charalampos fault block coarsens-up abruptly with the appearance of conglomerates over the Multi-Coloured Series into the north and east areas of the

fault block (i.e. all exposed areas of this stratigraphic level). Major syn-sedimentary deformation features are locally seen at this level, such as the 5-8m contortions illustrated in plate 3.1f. Facies vary considerably within the Upper Conglomerates, as a product of pre-existing environmental differences across the area. Conglomerates in the north are channelised within palaeosol and sandy background sediments and so form an FA1 assemblage. In the east, FA6 conglomerates exhibit a range of mass and grain flow characteristics and are associated with FA7 turbidites.

In the north-west, coarse-grained sands of the Multi-Coloured Series (facies association 2) are incised by channels 1-2.8m wide and 0.3-0.8m deep (fig. 3.14a). These contain facies A1 very poorly sorted conglomerates which are matrix-supported and clast-supported conglomerates of facies A2 and B1. Clasts are of polymict basement types but also include Multi-Coloured Series Sand intraclasts. Channel trends and clast imbrication suggest south-westerly palaeoflows.

Where the Charalampos valley crosses the northern margin of the Charalampos fault block (fig. 3.2), the uppermost sands of the Multi-Coloured Series in the fault hangingwall include 0.5m thick horizons of syn-sedimentary contortions. A few metres above, conglomerates appear in the sequence. These occur as facies A1 and B1 coarsening-up sheets which can be demonstrated to be non-erosive and convex-up over several tens of metres. Conglomerates, predominantly red cherts and ultrabasics, also fill minor sharply-incising channel cuts (facies A2). These occur within sandy and humic brown soil horizons of facies I (fig. 3.14b).

Figure 3.14

Logs: Upper Conglomerates
a = sketch log of sheet conglomerates above Multi-Coloured Series Sands, grid ref. 5.74 22.59
b = sketch log of erosive-based, sheet and convex-up conglomerates amongst pedogenic developments, grid ref. 7.18 22.66

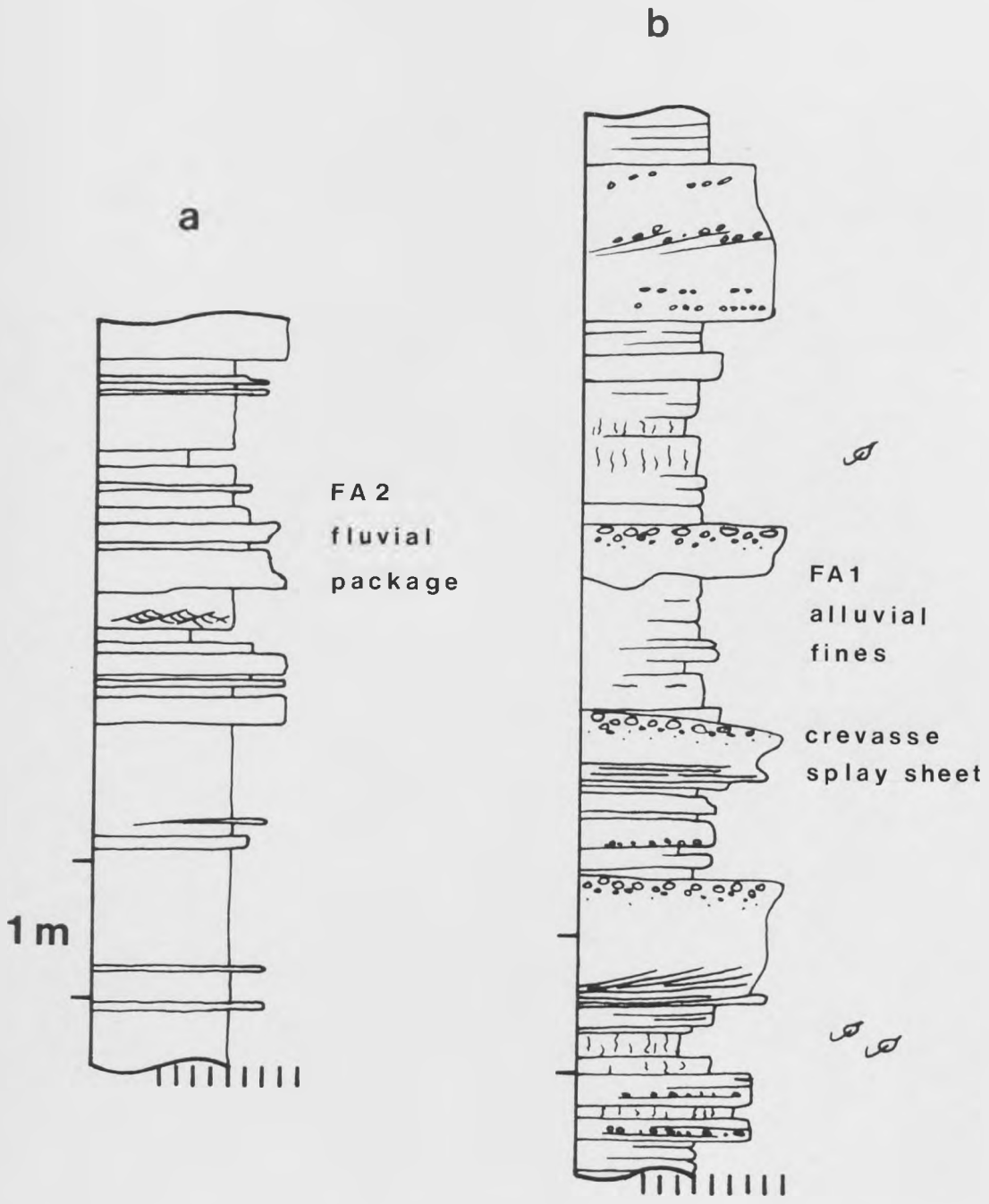
a
b
FA 2
fluvial
package
1 m
FA1
alluvial
fines
crevasse
splay sheet

Contrasting facies transitions occur to the east of the limit of the Multi-Coloured Series Sands. A range of transitional styles from Multi-Coloured Series "Marls" to conglomerates occur, according to conditions including water depth and transport energy (related to depositional slope). Figure 3.12a illustrates the gradational form of the transition in the south of the outcrop area, in the Drosia hills. The upper deposits of the Multi-Coloured Series "Marls" were here demonstrably under marine influence. Facies B5b diffusely-bedded calcareous silts contain a varied gastropod and bivalve fauna, including Cardium. Metre-thick sandbodies (facies B9 and S4) contain concentrations of reworked foraminifera. The first conglomerates appear as isolated thin sheets but rapidly pass up into irregularly-structured conglomerates of facies RLA. Up to cobble grade, these conglomerates are variously grain- or matrix-supported and show a variety of coarsening-up, symmetric or fining-up grain-size distributions within each unit. Thin pebbly sand intervals are both planar- and cross-laminated.

600m to the NNE the incursion of conglomerates over Multi-Coloured Series sands and silts appears to be more abrupt (fig. 3.15b). Facies B9 1-2m thick sandbodies occur within the Multi-Coloured Series deposits. These are frequently homogeneous, but small-scale trough cross-stratification and planar-laminated sands are also present. The sands contain macrofaunal elements derived from both freshwater (Unio) and marine (foraminifera) environments. Intervening silts are variably planar, diffusely and wavy-laminated, and interbedded with fine sands, so comprising facies B5 and B3. Within limits of outcrop, the conglomerate incursion appears to be instantaneous. A4 cross-stratified granule and pebble units up to 2m thick vary widely in

Figure 3.15

Logs: Multi-Coloured Series "Marls" to Upper Conglomerates transition
a = log, grid ref. 7.43 19.43
b = log, grid ref. 7.56 19.96
M = matrix-supported
G = grain-supported

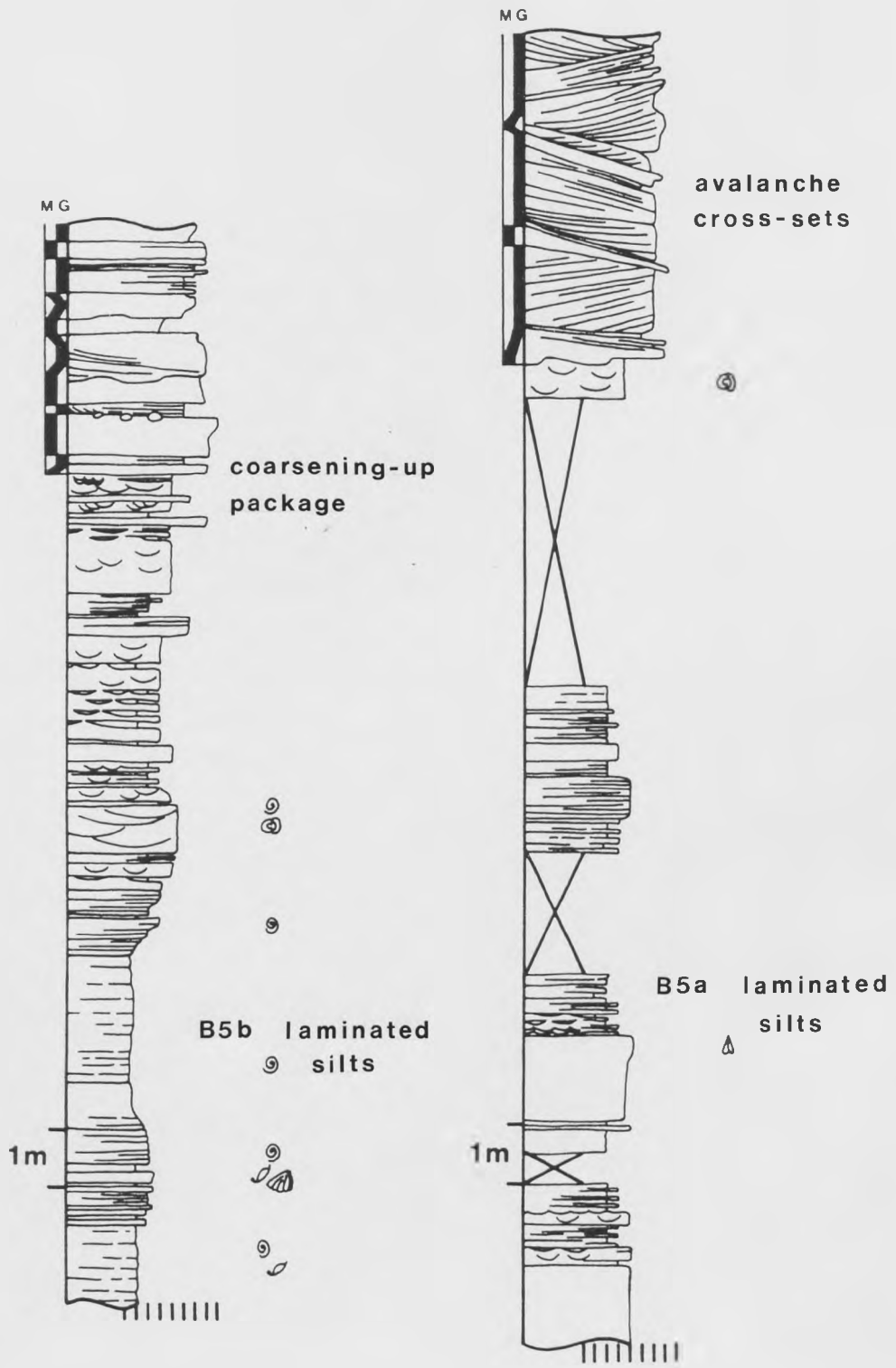
MG
coarsening-up
package
B5b laminated
silts
1m
MG
avalanche
cross-sets
B5a laminated
silts
1m

dip orientation. Textures show a range of grain- and matrix-support, often evolving from either to the other downslope. Individual sets vary in coarsening-up and symmetrically-coarsening character, again evolving down-set. Pebbles are mainly sub-spherical and 75% ultrabasic in composition (with 15% limestone, 5% red cherts and minor silici-clastics). Imbrication of pebbles is rare, discoidal clasts tending to be aligned parallel to depositional dip surfaces. Where imbrication does occur, transport downslope of the set is indicated.

A further and distinct character to the conglomerate incursion is seen 800m to the north-west (fig. 3.16). Multi-Coloured Series "Marls" with occasional sand units give way to interbedded calcareous silts and 10cm fining-up fine sand to silt beds of facies RLE and RLD. Facies RLD ripple co-sets are common in the silts immediately above the fining-up beds. Small-scale contortions and slumps also affect the silts. The tops of silt beds are frequently bioturbated. An overall coarsening-up trend leads to a predominance of 20-30cm fining-up sand units and then assorted granule to cobble conglomerate units of facies RLA. These generally coarsen-up but consistently and symmetrically-graded beds also occur. Coarsening-up packages are frequently preceded by the interdigitation of calcareous sands with matrix-supported pebbly conglomerates. The matrix is of heavily calcareous sand and silt. This material also makes up the matrix-fill of sedimentary dykes which are locally intruded into the poorly-structured RLA conglomerates. Above the section logged in figure 3.16 the sequence is dominated by poorly-structured pebble and cobble conglomerates of facies A1. Ultrabasic lithologies predominate with subordinate limestones, cherts and siliciclastics. Sedimentary structures are rare.

Figure 3.16

Log: Coarsening-up package from turbidites to mass and grain flow deposits of the Upper Conglomerates. Grid ref. 7.51 21.29
M = matrix-supported
G = grain-supported

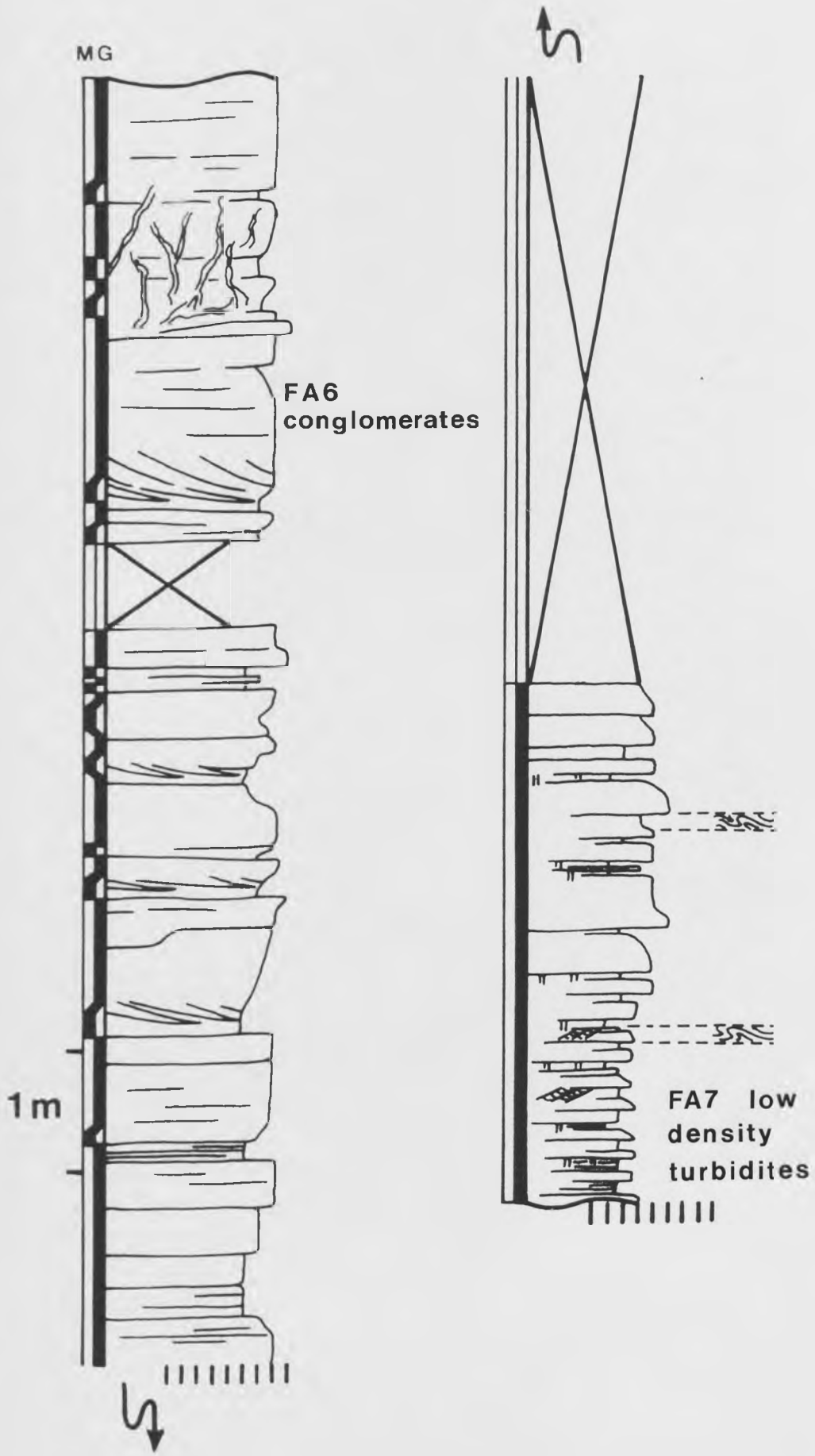
MG
FA6
conglomerates
1m
FA7 low
density
turbidites

But syn-sedimentary deformation in the form of sedimentary dykes up to 1m in width locally reaches high intensity (plate 3.1e).

Interpretation:

The appearance of conglomeratic channel-fills and lenses onto the northern part of the Charalampos fault block, together with channel orientations, pebble imbrications and lithologies indicate an incursion of coarse clastics from the north. The bimodal character of these coarse-grained sediments (transported by both stream and mass flow processes) within background sand and soil accummulations suggests a distal alluvial fan setting (facies association 1). Features include coarsening- and convex-up lenses of conglomerate which are thought to record crevasse splay events over the alluvial surface.

Further to the east, there is an equivalent record of coarse clastics which prograded rapidly into the basin at this time, with a corresponding increase in the energy of transport processes. In the Drosia hills (fig. 3.15a), mass flow conglomerates invaded an area previously in a shallow marine environment and dominated by fine-grained sedimentation. A similar relationship of coarse clastics advancing over shallow basinal deposits of facies association 5 is represented in figure 3.15b. The avalanche foresets of the conglomeratic units here suggest the dropping of bedload materials across some topographic feature, such as an intrabasinal fault scarp.

To the north of the north-dipping normal fault at grid ref. 7.63 20.36 (enclosure 1), the transition to coarse clastic sedimentation has a distinct form. An estuarine facies association (FA5) grades upwards into low-density (and low-volume) turbidites of facies association 7, perhaps suggesting a

contemporaneous increase in topographic gradients into the basin centre. The turbidites coarsen upwards (fig. 3.16) into conglomeratic high density turbidite, mass and debris flow units of facies association 6 and ultimately massive, unstructured mass and debris flow deposits. This coarsening-up trend is interpreted as a prograding distal to proximal submarine fan (or slope apron) sequence, representing the progradational incursion of the Upper Conglomerates into the basinal depocentre.

3.5.6 Andesites

Description:

Igneous rocks intrude and overlie the sedimentary sequence described so far in the western part of the Charalampos fault block. A sub-vertical pipe cross-cuts Multi-Coloured Series deposits at grid ref. 4.23 21.82 (enclosure 1). Ropey lavas with pebbles incorporated into the knots of lava have been recovered from the hill above. Freyberg (1973) reports a thickness of more than 70m of intermediate volcanics in a borehole 0.5km to the west (borehole 1/68, his fig. 10). Figure 3.17 presents a photomicrograph of a sample taken from the former outcrop site. Zoned plagioclases (maximum An_{50}) are the predominant silicate phenocrysts, with subordinate orthoclase and minor globular quartz phenocrysts. Ferromagnesians include common hornblende and c.10% biotite, with minor Fe oxide octohedra. A biotite concentrate was dated by the K-Ar method, as detailed in figure 3.17.

A second andesite outcrop occurs at grid ref. 5.10 19.63. It too has been dated, as an extracted hornblende concentrate, to test whether this texturally and compositionally similar andesite

Figure 3.17

Photomicrograph of andesite sample 48596 from grid ref. 4.15 21.86
Scale bar = 0.5mm. See text for description.
Results of K-Ar dating of andesite samples 48596 and 48597 (grid ref. 5.05 19.56).
Dating was carried out by D. Rex, University of Leeds.
Constants used:

λ_β: 4.962×10^{-10} yr^{-1}

λ_e: 0.581×10^{-10} yr^{-1}

$^{40}K = 0.01167$ atom %

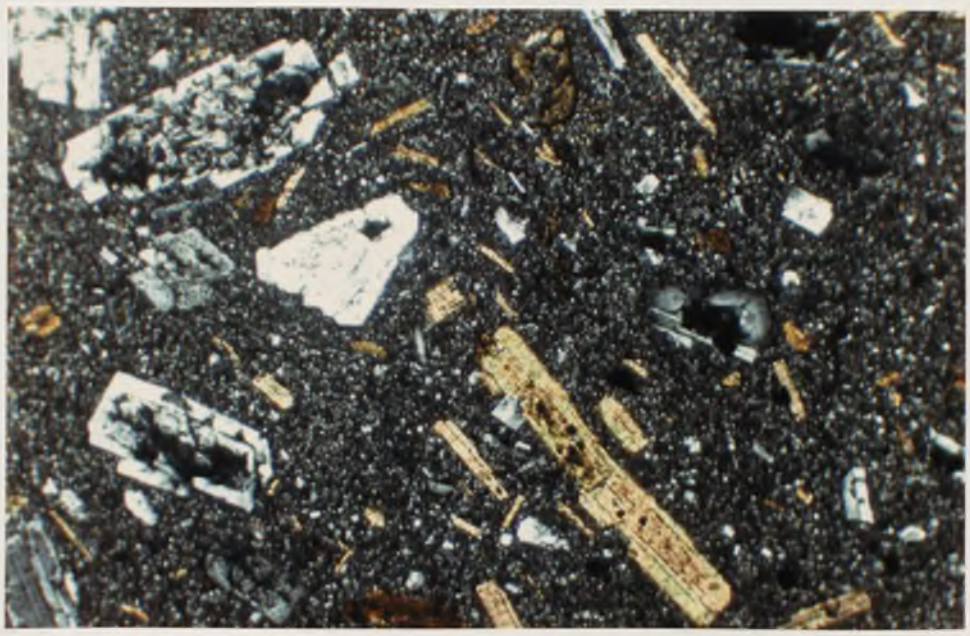

Sample	No.	%K	Ar No.	Vol. ^{40}Ar rad. cc STP / g x 10^{-5}	% ^{40}Ar rad.	Age m.y.
Biotite	48596	6.612	3988	0.09307	30.4	3.62 ± 0.18
Hornblende	48597	0.317	3987	0.00495	5.1	4.00 ± 0.40

belongs to the same suite as sample 48596.

Interpretation:

The andesite suite of the northern Corinth Basin displays a typical chemical character for calc-alkaline volcanics of the south Aegean volcanic arc (Fytikas et al 1984). This suite forms the westernmost outcrops of arc volcanics in the Aegean area. The similar dates obtained from the two dated samples (overlapping within error margins) suggests that these do probably relate to a single suite of volcanic lavas. This Mid-Pliocene age corresponds to one further date recorded from volcanics in the area, 3.95 ± 0.2 Ma (Bellon et al 1979, Fytikas et al 1984). A Lower Pliocene age is therefore inferred for the underlying sedimentary sequence, this syn-rift sequence having been deposited since the regional onset of extension towards the end of the Miocene (see section 2.2.2).

3.6 SPATIAL VARIATION IN FACIES

Two principal facies suites can be distinguished through the Lower Pliocene basin fill. The distinguishing feature of each suite is its general sense of palaeoflow, as measured in relation to the basin structure. Axial and lateral facies suites result from deposition from flow respectively parallel to and at high angle to basin-bounding structures (after Leeder & Gawthorpe 1987). This is the case for both half-graben and graben extensional basin morphologies, and indeed also for foreland basins being overridden by an advancing thrust front. The distinction may be made on a basinwide scale, as here, or in relation to facies around smaller scale intrabasinal tilt blocks, as in chapter 5. A third facies suite might be distinguished, a basinal suite without unidirectional current influence.

Normal faults bounding extensional basins actively control subsidence. With any increment of normal fault displacement the topographic gradient across the structure will be increased. Thus, the highest topographic gradients tend to be across the active fault structures. This leads to a tendency for lateral facies to be the product of relatively high energy transport processes. Depositional surfaces may be relatively steep, as compared with the lower gradients of the axial suite. These are controlled by the longitudinal topographic gradient into the structural trough, parallel to controlling structures. A genetic relationship may be drawn, then, between observed facies and their structural context within a fault-bounded basin. [The same would apply to non-tectonic settings such as the sedimentary infill of a karst-generated basin].

3.7 STRUCTURAL EVOLUTION OF THE LOWER PLIOCENE CORINTH BASIN

3.7.1 Basin Form

The sedimentary facies and their geometries within the basin fill reflect the basin morphology at the time the sediments were deposited. Inferences may therefore be drawn on basin form from sedimentary facies distribution. The record of palaeoflow directions, characteristic sediment provenances and the development of marginal clinoforms are all utilised in such an analysis.

The oldest deposits in the basin, those of the Asprakhomata-Kalamona Formation, are the least well defined in terms of their time and space relationships. General comments may be made, however, on basin form at the time these sediments were

deposited. Periodically fault activity affected the northern basin margin, introducing limestone basement blocks and olistrostromes into the alluvial-lacustrine environment. From the regional context, this faulting is taken to have been extensional. The structural trough may have been of graben or half-graben form at this stage. The southern margin to the Lower Pliocene basin is not seen in outcrop. It has subsequently been downfaulted beneath the present Saronic Gulf (see Chapter 5). Palaeoflows in fluvial sands of the Asprakhomata-Kalamona Formation in the southernmost Lower Pliocene have a south to north sense. Any normal faulting at the southern basin margin was therefore insufficient to nullify the northerly tilt of the basin floor at this locality. Facies across the basin were variously alluvial or lacustrine. The combination of structuration and climatic fluctuations would have determined the condition at any particular time.

The spatial distribution of facies is better defined, although only within the confines of the Charalampos fault block, through the episode of deposition represented by the Agios Charalampos Conglomerate and the Multi-Coloured Series. The Agios Charalampos Conglomerate fan-delta prograded abruptly northwards into the basin. There is a sharp grain size gradient off the fan-delta. The pebble and cobble coarse clastics on the fan-top interdigitate and grade out into sands towards the centre of the Charalampos fault block (in outcrop and in borehole 6/69, Freyberg 1973). This would suggest a relatively steep depositional gradient across the southern basin margin. Initial progradation of the fan could only have occurred if sediment supply rates onto the fan exceeded the space generated by the local subsidence rate (assuming constant base-level). To

maintain the areal coverage of the fan the sediment supply rate from the south would have been proportional to the local subsidence rate (± any base-level change). Subsequent retreat of the fan-delta could have resulted from a marked increase in the local rate of subsidence (although sediment supply might alternatively have been cut off). Given a constant sediment supply rate across a basin footwall margin, the "capture" of coarse clastic wedges close into the footwall in this way characterises basins undergoing rapid tectonic subsidence.

The relatively constant west-east grain size distribution across some 4km of Multi-Coloured Series Sands contrasts with the rapid northwards diminution of grain size of the Agios Charalampos clastics. Together with the easterly palaeocurrent directions paralleling basin structures within the Multi-Coloured Series Sands, this supports the interpretation of the Multi-Coloured Series Sands as an axial fluvial system. The Agios Charalampos fan-delta is interpreted as a lateral sediment distribution system (fig. 3.18).

The Multi-Coloured Series as a whole has a distinct bimodal character, both in grain size and in provenance. The Multi-Coloured Series "Marls" represent the fine-grained background sedimentation of the brackish/marine basin. Their carbonate detritus may derive from both the north and south margins of the trough. The Multi-Coloured Series Sands are almost exclusively (>90%) serpentinite. At this time, therefore, there must have been a basement ophiolite source exposed to the west. At modern outcrop levels the only significant ophiolite sheet in the vicinity lies above an east-dipping thrust ramp in the Gerania massif to the north of the basin (fig. 2.3). No ophiolites are currently exposed to the south of the basin. A model is

Figure 3.18

Schematic block cartoon of the structural form and sedimentary architecture of the Corinth Basin in the Lower Pliocene, at time of progradation of the Upper Conglomerates. This followed submergence and westwards retreat of the Multi-Coloured Series fluvio-deltaic front.
Lower units shown:
White: Multi-Coloured Series "Marls"
Brown: Agios Charalampos Conglomerate "coot's foot" delta
Greens: Asprakhomata-Kalamona Formation lacustrine (pale) and alluvial (dark) deposits
Purple: Ophiolite thrust sheet in northern basement margin footwall

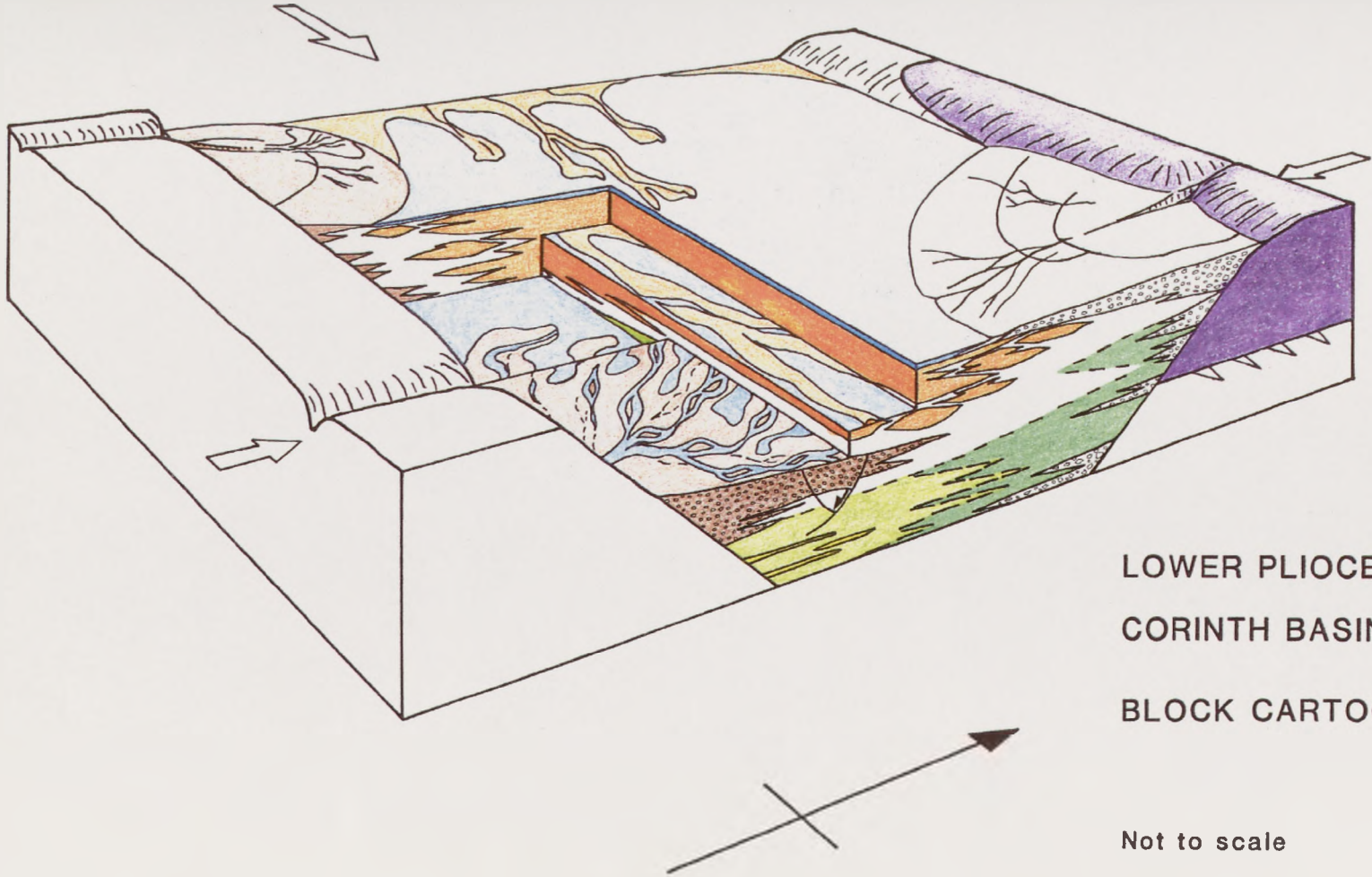

LOWER PLIOCENE,

CORINTH BASIN

BLOCK CARTOON

Not to scale

proposed which entails a westerly continuation of the currently exposed ophiolite, perhaps lying over a thrust flat. This is thought to have been exposed and unroofed in the Lower Pliocene, supplying the serpentinite detritus to the Multi-Coloured Series Sands. A second inferrence to be drawn from the monolithic provenance of the axial fluvial system is that there was no access to the Corinth Basin at this time from the wider Gulf of Corinth basin further to the west. Had there been so, polymict basement lithologies from the surrounding source regions would be expected in the axial fluvial system.

The fluvial-dominated character of the Agios Charalampos Conglomerate and the Multi-Coloured Series Sand delta fronts suggest that the contemporaneous basin floor was shallow. No Gilbert delta morphologies are observed which typify the present steep margins and deep basins around the Aegean (Ferentinos et al in press, Aksu & Piper 1987, Piper & Panagos 1981). This shallow base-level to basin floor relief would have enhanced the rate of progradation of delta fronts when compared with similar sediment volumes entering a deeper basinal environment. The axial system, for example, prograded 2.5km in about 300m of vertical section. The shallow basin floor gradients also determined the detailed facies geometries of the deltaic distributaries; the sheet-like lobes of the Agios Charalampos "coot's foot" delta and the long (>0.5km) distributary channels of the Multi-Coloured Series delta front. Wave/storm influence would have been limited by these relatively shallow depths and by the topographic confines of the trough embayment limiting the fetch of waves (other than from the east).

One problem with commenting on the context of the Multi-Coloured

Series axial system is that the width of the fluvial channel belt is not evident. Lateral equivalents to the north have been eroded off the more northerly fault block (the footwall to the Charalampos fault block). Lateral equivalents to the south have been downfaulted post-deposition below present outcrop levels. However, it seems likely that high intrabasinal subsidence rates would have been needed to maintain the position of the axial channel belt (after Bridge & Leeder 1979). Recognising the rapid progradation of this axial system then suggests a significant pulse of serpentinite sand was supplied, perhaps facilitated by the ease of erosion of the ophiolite source, to allow progradation to overcome subsidence values. Such a qualitative comparison would be modified by any base-level change across this depositional episode.

Basin form was apparently modified at the time the Upper Conglomerates were supplied to the basin. Basinal deposits in the east lose all sign of shallow depths below base-level (such as wave-modified symmetric ripples). Mass flow and turbidite deposits suggest increased gradients into the basinal environment. At the same time distal alluvial fan deposits advanced southwards over the Multi-Coloured Series Sands. These have a polymict basement provenance including ophiolitic materials derived from the north. At any locality there is an overall coarsening-up tendency from basinal silts of the Multi-Coloured Series "Marls" to the axial Multi-Coloured Series Sands (in the west and north) to conglomerates, whether of alluvial or sub-aqueous origin.

3.7.2 Structural Evolution

The interpretation of structural activity in the geological

record is largely dependent on the separation of syn-depositional and post-depositional faults. Definitive criteria for the recognition of tectonic growth faulting is limited to the draping/burial of fault features and sediment thickness and/or facies changes across structures. Even then, only wedge thickening of a bed in the hangingwall to a normal fault describes "syn-depositional" fault movement with respect to that bed, whilst broader "syn-sedimentary" features such as draping and facies changes across a fault may continue after movement has ceased (Ord et al 1988). Additional circumstantial evidence may be collected which may support an interpretation of tectonic activity. These include; palaeocurrent directions being modified to coincide with structurally-influenced slope trends, the occurrence of large-scale soft-sediment deformation features ("allokinetic" features requiring external energy input, sensu Leeder 1987), and "event" facies such as slumps, slides and olistrostromes (Gawthorpe & Clemmey 1985, Perissoratis et al 1984). Syn-sedimentary deformation features such as sediment volcanoes, and other "event" facies, may be specific in defining the lithostratigraphic timing of seismic activity. Aseismic fault activity would not be represented by these latter features.

A further problem in defining episodes of tectonic activity in relation to the Lower Pliocene Corinth Basin fill is that the relationship of stratigraphy to basin margins is not seen. No stratigraphic correlation is possible between basin margin footwalls and the basin fill. Therefore it is not possible to determine directly periods of tectonic activity on the basin margin faults. Such movements have to be inferred from the nature of the basin fill.

As has already been described, facies patterns indicate the Lower Pliocene basin trended east-west. The northern margin was at least periodically active during the deposition of the Asprakhomata-Kalamona Formation. Hence the presence of basement slide blocks and mass flow "event" deposits in the proximal hangingwall. It is realised that the mass flow deposits may be the immediate product of storm or flash flood events, but even then the availability of coarse clastics for transport in such flows may be an indirect indication of footwall exposure by fault activity.

No intrabasinal faults are recorded syn-deposition of the Asprakhomata-Kalamona Formation. Nor does sandbody architecture within fluvial deposits of the Formation appear to reflect intrabasinal structuration. Channel belt sandbodies in the northern Stenodromi ravine, for instance, show "passive" diagonal offset patterns as opposed to the vertical stacking of sandbodies which characterises subsiding hangingwalls (Bridge & Leeder 1979, Fielding 1984a, Collier in press (a)).

The lateral incursion of a fan system, such as the Agios Charalampos fan-delta, does not in itself define a period of increased tectonic activity. Other means exist to trigger the nucleation and progradation of such a clinoform. For instance, non-tectonic erosion through a footwall scarp may access a source area behind the footwall, generating a surge in the sediment supply rate across the margin. Alternatively, erosional unroofing of a footwall scarp may expose a less resistant basement lithology at some locality along the footwall and so increase the local sediment supply rate. In the case of the Agios Charalampos fan-delta, however, the basal conglomerates lie unconformably on Asprakhomata-Kalamona strata which had been

tilted down to the south. The angular discontinuity is seen in outcrops in the Charalampos valley. The Agios Charalampos clinoform incursion therefore corresponds to downfaulting of the southern part of the basin. No soft-sediment deformation is seen in the delta deposits but this will be at least partly due to the coarse grained character of the deposits. Pebble/cobble conglomerates are the least susceptible grain sizes to syn-sedimentary deformation.

The virtually instantaneous retreat of the Agios Charalampos fan delta may imply that the southern part of the basin underwent more rapid submergence and was inundated by basinal "marls" at this time. Alternatively the sediment supply route may have been diverted into a new structural low further to the south.

A syn-depositional fault complex is seen within the Multi-Coloured Series "Marls" just above the Agios Charalampos Conglomerates in the Charalampos ravine (fig. 3.19). Synthetic and antithetic faults accommodate growth which is facilitated by extension across a shallow and sub-horizontal decollement. "Marls" thicken as wedge-shaped horizons into a south-dipping normal fault. Isolated blocks and resedimented conglomerates from the syn-depositionally exposed footwall occur within the "marl" horizons. An interesting feature of the structure is the difference in style of fault block between the coherent calcareous fines and step-faulted blocks in the coarse clastics (fig. 3.19). The occurrence of this growth fault complex just above the Agios Charalampos Conglomerates seems to support the hypothesis that the fan-delta retreated due to the accelerated subsidence of the basin floor.

No other growth faults or syn-sedimentary deformation features

Figure 3.19

Line drawing after photo-montages of a syn-depositional growth fault complex in the Charalampos valley affecting Agios Charalampos Conglomerates and the lowermost units of the Multi-Coloured Series "Marls". Note evidence for conglomerates having been reworked off exposed structural highs into "marls" at points marked R.
North-south section from 5.92 21.53 to 5.92 21.18.

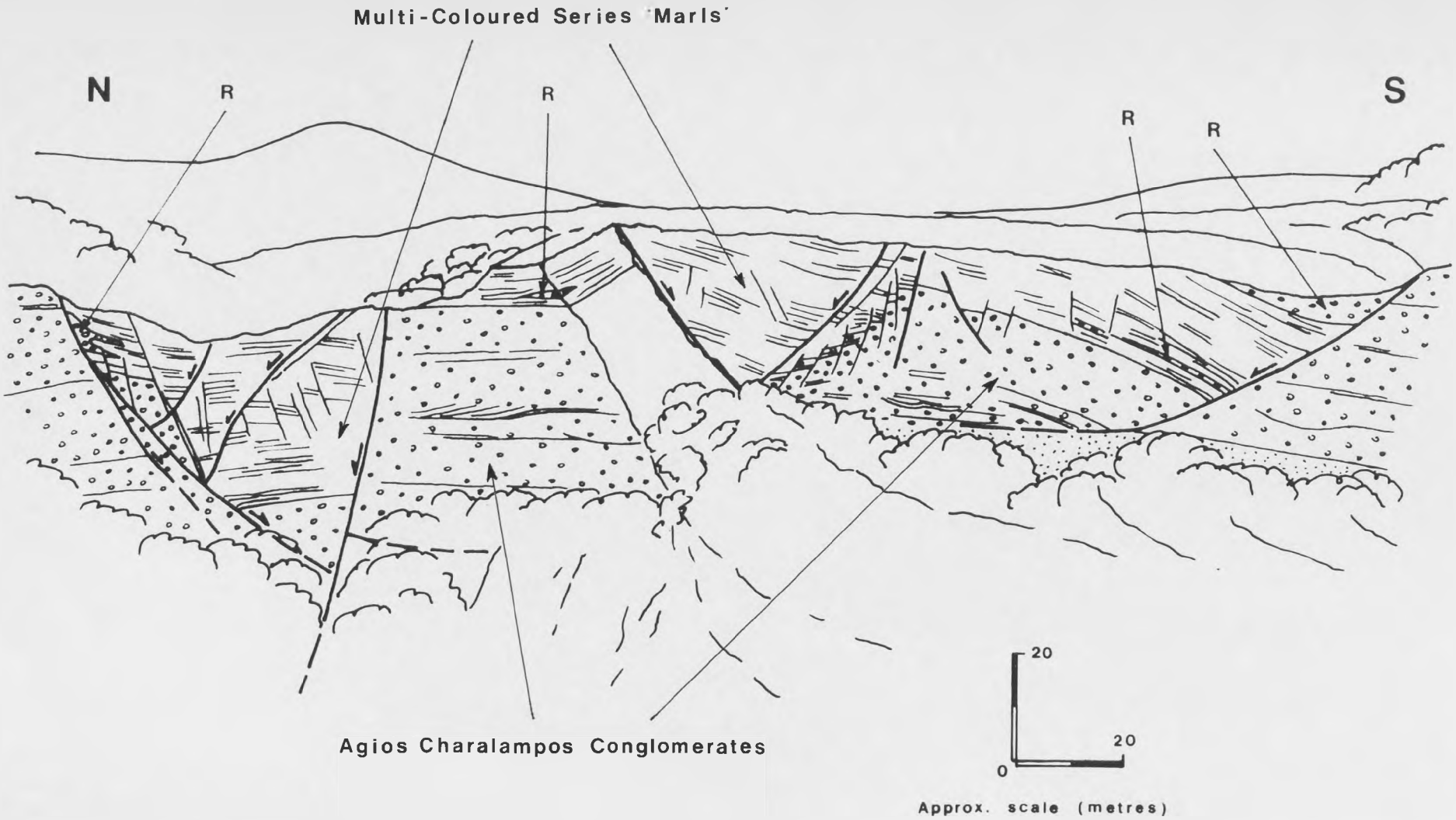
Multi-Coloured Series 'Marls'
N
S
R
R
R
R
Agios Charalampos Conglomerates
20
20
0
Approx. scale (metres)

are recognised through the bulk of the Multi-Coloured Series exposure. Except in the uppermost exposed Multi-Coloured Series Sands. Here, just below the appearance of southwards-transported alluvial fan deposits, sedimentary contorions are seen on a scale of 0.5m. Their occurence is rare as a proportion of total outcrop area, but this may be because these, in the centre of the basin, were some distance from the seismic epicentre. A low Allokinetic Deformation Number, <0.1, would be deduced in the terms of Leeder (1987). However, this evidence of renewed/increased seismic activity correlates with a variety of other corroborating features at this stratigraphic level:

1) The southwards advance of lateral fan systems from the northern basin margin, possibly responding to increased topographic relief generated by faulting at that margin.

2) The apparent increase in depth of deposition of basinal facies.

3) The increase in energy to mass and turbidite flow processes of basinal deposits.

4) The marine inundation of the axial Multi-Coloured Series delta front.

5) The relatively widespread occurrence of allokinetic features, most notably sedimentary dykes and volcanoes within the mass flow deposits of the Upper Conglomerates. Locally, these sedimentary dykes are up to 1m in width and >4m in height (plate 3.1e).

6) The occurrence of syn-sedimentary contortions at the boundary between Multi-Coloured Series "Marls" and overlying Upper Conglomerates. These contortions are >5m in amplitude (plate 3.1f).

7) The 5° angular unconformity at the base of the Upper

Conglomerates at grid ref. 7.28 20.21 (enclosure 1), which describes an eroded tilt block surface. Syn-depositional rotation of this tilt-block coincides with the facies variation across a north-dipping normal fault just to the north. Facies to the north of this fault exhibit higher energy mass flow and turbidite styles (fig. 3.16). Grain flow facies predominate to the south (fig. 3.15). This fault at grid ref. 7.63 20.63 is therefore interpreted as an intrabasinal growth fault which controlled facies style to north and south (fig. 3.20).

8) The apparent predominance of southerly palaeoflow directions through the Upper Conglomerates, which imply that the basin floor underwent tilting to the south. Active normal faulting was therefore probably greater on the southern basin margin at this time.

These features all corroborate the interpretation that an increased rate of tectonic collapse of the graben generated the incursion of conglomerates into the basin at this time. The synchronous relative base-level rise is thus ascribed to tectonic collapse, rather than necessitating (although not discounting) any eustatic sea-level rise.

Highly-rotated fault blocks within the Upper Conglomerates (fig. 3.20) have in the past been interpreted as olistrostromes (Gaitanakis et al 1985). This slide block model requires that the toe of the slide block sits on the sediment surface downslope of what is a sedimentary growth fault. Compressional features are common in the toe regions of such structures (e.g. Perissoratis et al 1984). No onlapped toe, nor any significant compressional features have been observed by this author within these highly rotated fault blocks. An alternative model is that

Figure 3.20

South-north cross-section across the eastern part of the Charalampos fault block. Refer to figure 3.2 for position of section D-E. An alternative to the tilted basement block explanation for the ophiolite outcrop is that this outcrop exposes an ophiolitic olistrostrome derived from a basement high to the north or east.
Pebble symbol = Upper Conglomerates
Stipple = Multi-Coloured Series Sands
Parallel hatching = Multi-Coloured Series "Marls"
Dash = Asprakhomata-Kalamona Formation
Vertical hatching = basement ophiolite

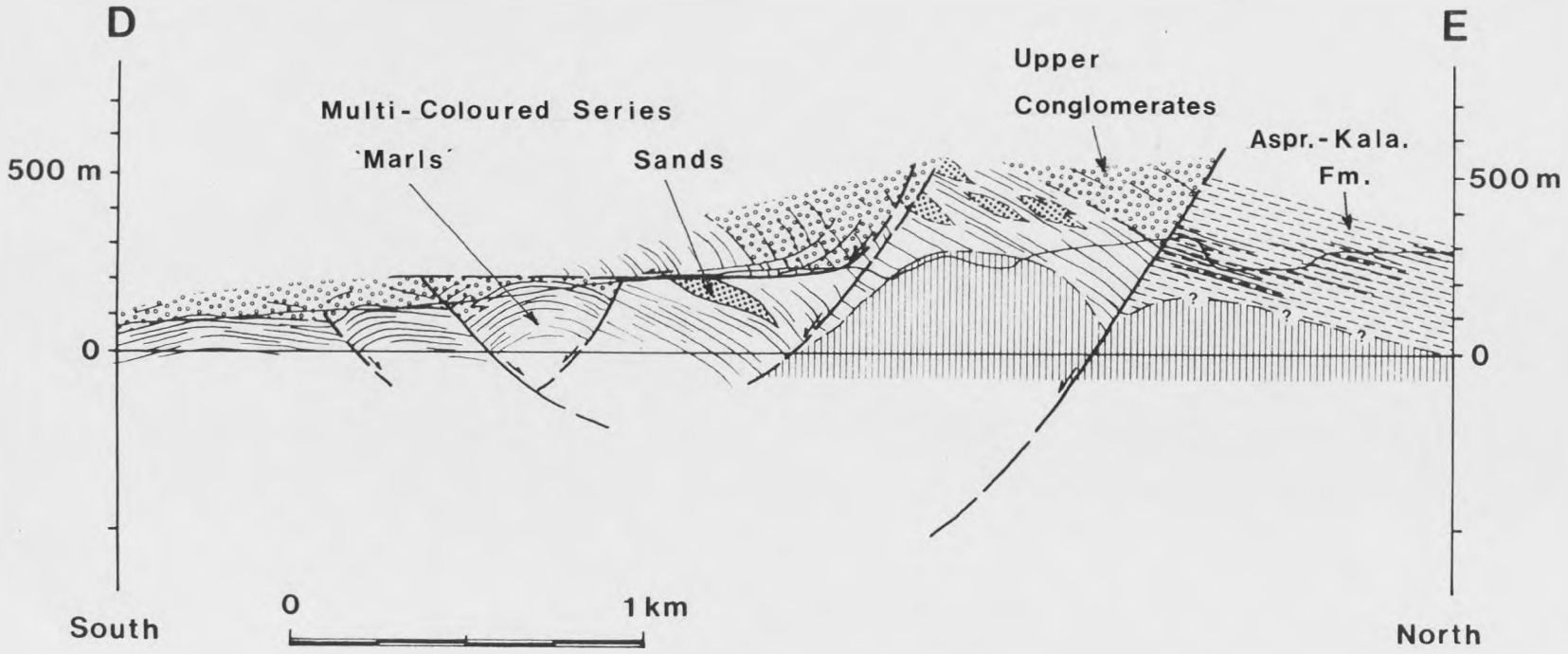
D
E
Upper
Conglomerates
Multi-Coloured Series
'Marls'
Sands
Aspr.-Kala.
Fm.
500 m
0
500 m
0
0
1 km
South
North

these blocks represent exhumed tectonic fault blocks linked into the intrabasinal flat-and-ramp normal fault structure (after Gibbs 1987). Such faulting may have been syn-depositional or post-depositional in relation to the Lower Pliocene sequence. In the Glyphonero ravine, at least three generations of north-dipping normal faults have rotated beds to very high angles (as in the classic Basin and Range example, Proffett 1977), to sub-vertical and even beyond the vertical.

Post-depositional faulting on south-dipping normal faults has generated the pervasive northerly dips across the Lower Pliocene outcrop area (enclosure 1). The fault at the north edge of the Charalampos fault block (figs. 3.3 and 3.20) is interpreted as listric because it has a characteristic rollover anticline in its hangingwall (although this is not definitive of listric faults; see section 1.6.2). Any estimate of the depth to the assumed decollement surface depends on the assumed mechanism of hangingwall deformation (Wheeler 1987). This dependence is illustrated by the difference between depth to decollement values calculated according to two models of hangingwall deformation. Assuming constant displacement on the fault surface (after Williams & Vann 1987) a value of 370m below present sea-level is obtained. However, a brittle fracture zone dips 72^{o} S in the hangingwall (fig. 3.3). Assuming hangingwall deformation was accommodated by shear parallel to this fracture zone and assuming constant heave, then a depth to decollement estimate of 1910m is derived.

Since the Lower Pliocene the northern Corinth Basin has undergone net uplift. This despite the observed post-depositional normal faulting. Uplift is inferred on the basis of marine deposits occurring up to at least 300m above present sea-level north of

Drosia. Present sea-level is thought to be about the maximum eustatic base-level, as climate is currently in an interglacial state.

The major post-depositional normal faults affecting the Lower Pliocene outcrop in the Corinth Basin step the sequence down to the south. South of the Charalampos fault block the sequence and the southern basement margin which existed in the Lower Pliocene have been downfaulted since the Mid-Pliocene and submerged below the Saronic Gulf as recently as the Quaternary (see Chapter 5).

3.8 DISCUSSION: CONTROLS ON THE EVOLUTION OF FACIES GEOMETRIES

As outlined in sections 3.6 and 3.7.1, the structural framework will be a major factor in determining facies patterns in an actively rifting basin. Axial and lateral distribution systems will reflect basin structure. This is certainly the case with the Lower Pliocene deposits of the Corinth Basin. A potential influence on this system, however, is the precedent drainage pattern in the area. Did the Corinth Basin develop through the exploitation of an existing E-W intermontane basin or did the rift basin cut across any pre-existing trough(s)? No evidence is available to comment on either possibility other than to point out that the rift basin crosses at high angle to the precedent N-S Hellenide structural trend. If the basin cut across north- or south-flowing drainage systems then the initial lateral fans entering the rift basin were probably located at its intersection with antecedent drainage basins (Leeder et al 1988). This is apparently the case further to the west in the present Gulf of Corinth for instance, where the Aigion fan-delta is supplied by a

drainage system flowing north, through the uplifting footwall, from the North Peloponnese.

A second control on the basinal facies of the early syn-rift is the relief of the area at the onset of extension. Subsidence initiated at sea-level will immediately introduce a marine environment to the basin. Continental/lacustrine facies will accummulate on the other hand, if the basin floor is still above the syn-depositional sea-level during subsidence. In the Corinth Basin the earliest demonstrably marine deposits are of the Multi-Coloured Series. Subsidence to the contemporaneous sea-level has not been demonstrated prior to this. Unfortunately, no seismic has been shot across the northern Corinth Basin and there are no Lower Pliocene stratigraphic markers in the basin footwalls. Therefore it is not possible to estimate the amount of subsidence which had occurred by the time the Multi-Coloured Series was deposited. This may have been substantial, given the Hellenide intermontane setting and the presence, even after a prolonged extensional history, of overthickened crust beneath the basin (Makris 1985).

Modification of the syn-rift sediment distribution pattern results from an interaction between a number of processes. Modification of facies geometries may take the form of the progradation or retreat of distribution systems (whether lateral or axial), vertical aggradation or erosion. In two-dimensional cross-section, such changes may be described by the relationship between three principal factors at any locality (fig. 3.21):

a) dS/dt; the rate of subsidence (or uplift) with time. This will include tectonic subsidence plus any isostatic subsidence due to sediment (or water) loading and compactional subsidence.

b) dD/dt; the rate of deposition (vertical aggradation) at the

Figure 3.21

Outline flow diagram illustrating the intimate cause and effect relationships between mechanisms controlling the distribution of sediments within a tectonically active basin
dS/dt = rate of tectonic displacement, here including isostatic adjustment to sediment or water loading and unloading
dD/dt = rate of deposition
dSL/dt = rate of change in sea-level

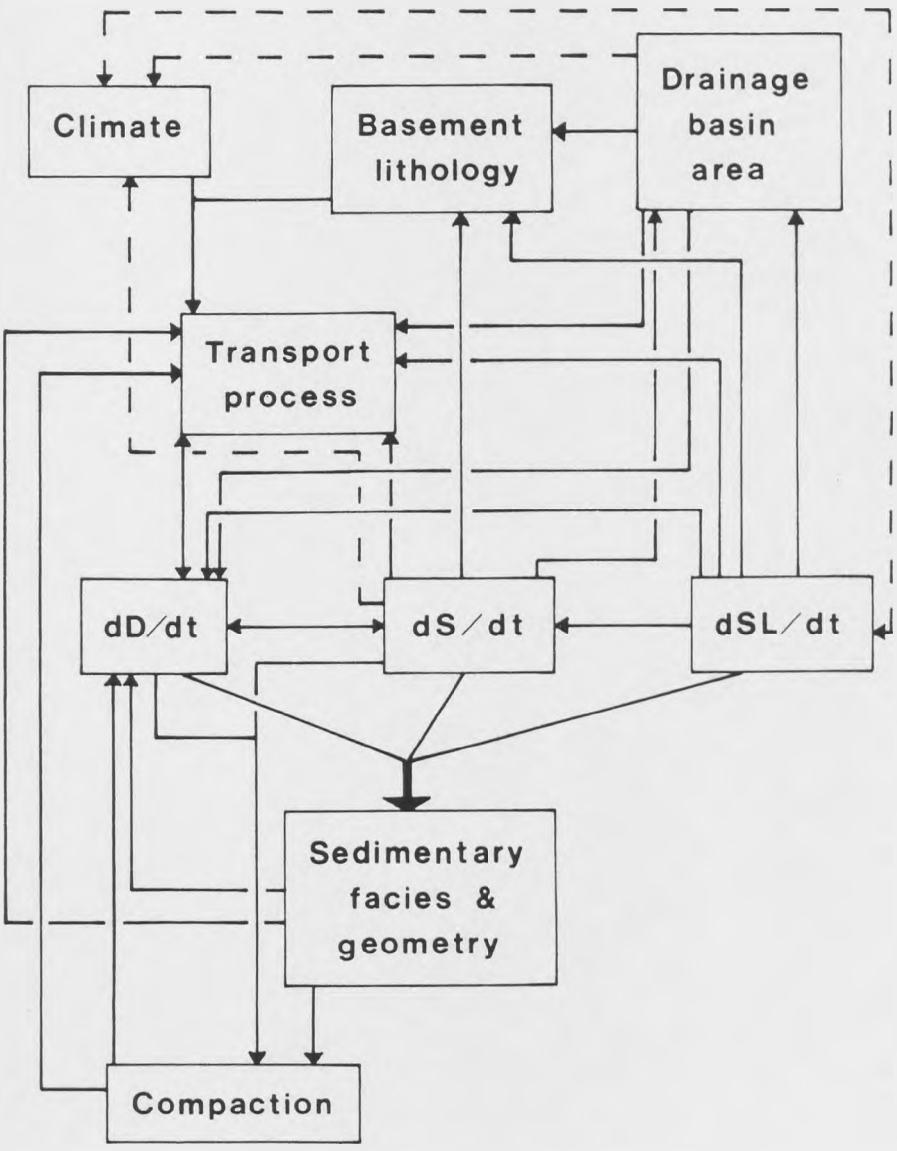
Climate
Basement lithology
Drainage basin area
Transport process
dD/dt
dS/dt
dSL/dt
Sedimentary facies & geometry
Compaction

locality with time.

c) dSL/dt; any change in eustatic sea-level (or lacustrine base-level) with time.

Extensional faulting will control dS/dt but at any locality this value is the resultant of a vertical displacement and a tilt vector on some fault(s) (plus a loading effect). dD/dt will be a function of sediment supply into the basin, depositional slope and sedimentary transport process. Sediment supply is itself a product of hinterland structure/drainage area/pre-rift geomorphology, source lithology and climate (fig. 3.21). Any change in base-level (dSL/dt) will be most significant at and near the coastline. Chapter 4 explores further the interaction of these three principal parameters.

In the syn-rift, structural activity would be expected to be the major control on overall facies geometries. But in periods of structural quiescence, non-tectonic controls such as fluvial constructive and migration processes and compaction of the sediment pile will prevail. The Buyuk Menderes axial river system in western Turkey illustrates this point. This meandering river flows west along an asymmetric graben in the Aegean (Sengor et al 1984a, Dumont et al 1978). The subsidence of this active basin is controlled principally by normal faulting on its northern margin, against the Menderes Massif. A statistical bias of channel belt positions towards the northern margin would be expected in cross-section. But two factors mitigate against this. Firstly, footwall fans locally prograde off the northern footwall, pushing the axial system basinwards. Secondly, random migration of the channel belt across the alluvial plain continues when tectonic tilting of the alluvial surface fails to capture the channel in a structural low.

The Buyuk Menderes delta front has prograded about 15km in 2000 years, isolating Ancient Greek ports inland (Russell 1954). This rapid sediment supply rate and the very constructive nature of the micaceous silt load of the axial river combine to cause the very rapid switching of channel positions (fig. 3.22). This sedimentary migration by meandering, flood and crevasse splay events changes channel position one or two orders of magnitude more frequently than the recurrence time for major seismic events in the basin. Seismic deformation of the hangingwall may therefore periodically lead to capture of the axial channel belt, and so generate a statistical concentration of channel bodies towards the northern margin in cross-section. But in intervening aseismic episodes the dominant control on channel architecture appears to be sedimentary process. Furthermore, even when normal faulting creates a relative low in the hangingwall, the channel may not be captured if there is not a consistent gradient down from the channel to the topographic low. This may explain the present continuation of channel position to the southern side of the basin (west of Soke, fig. 3.22) while a topographic low against the northern margin fault is occupied by marsh and lagoonal environments.

The Buyuk Menderes Basin provides a useful analogy to conditions prevalent when the Multi-Coloured Series was deposited in the Corinth Basin. The overall architecture and the maintenance of channel belt position was probably a product of the tectonic deformation of the alluvial surface. But the detailed position of distributary channel sandbodies at the delta front would have been controlled by a combination of tectonic influence and sedimentary processes of avulsion, crevasse events and minor

Figure 3.22

Sketch map outlining the change in position of the Buyuk Menderes distributary channel through time.
Dotted line = distributary channel as published in Russell (1954).
Dashed line = active channel published on geological map of Pamir (1974).
Solid line = distributary channel published in Kulen (1975) and the approximate course in May 1988.
Refer to figure 2.2 for position of Buyuk Menderes graben in western Turkey.

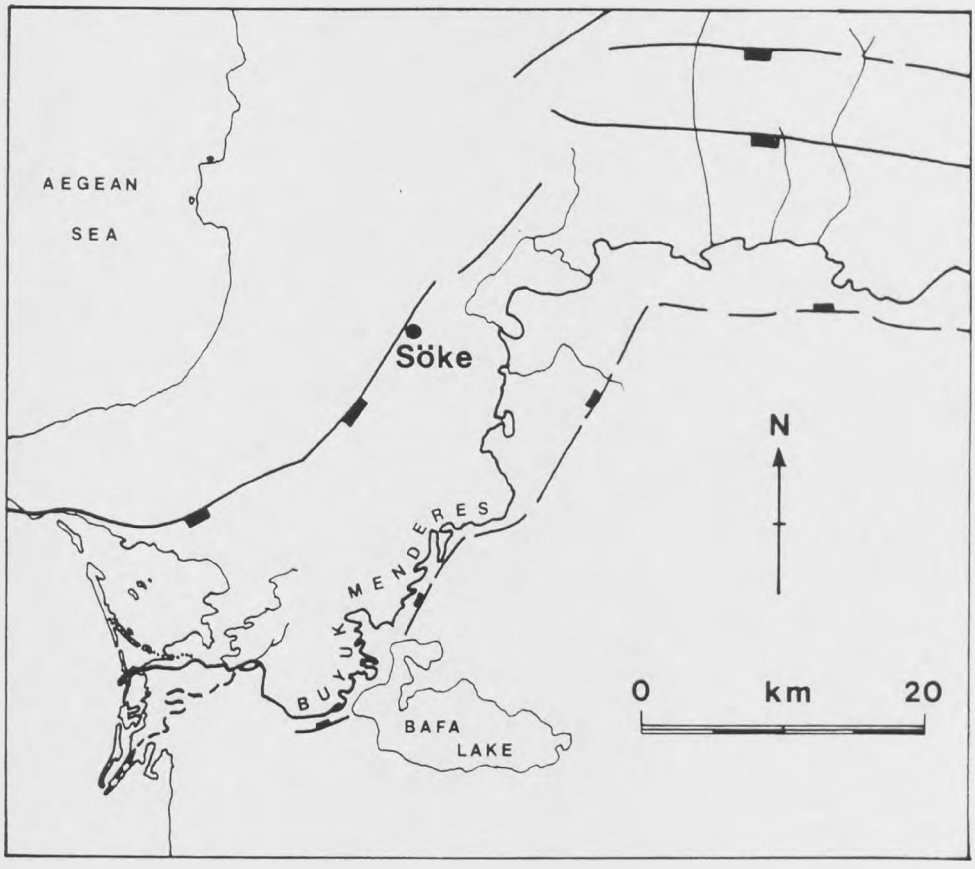
AEGEAN
SEA
Söke
BUYUK MENDERES
BAFA
LAKE
N
0
km
20

delta construction.

The axial progradation of the Multi-Coloured Series Sands may have been enhanced by any synchronous fall in sea-level. No erosion or incision of the alluvial surface is seen, however, so any fall in sea-level (dSL/dt) must have been exceeded by the rate of subsidence of the alluvial surface (dS/dt). Without a closely-constrained history of sea-level and without accurate dating of the sediments, it is not possible to confirm or exclude such a component of sea-level change.

Similarly, it is not possible to isolate what controlled the abrupt progradation of the axial Multi-Coloured Series Sands. Progradation may be triggered by a) structural activity increasing gradients and/or relief in the source area, b) a change in climate to more erosive conditions, c) access being gained to a larger drainage area by incision or structural access to more distal supplies, or d) less resistant lithologies being exposed at source. There is no evidence for any marked climatic change through the Lower Pliocene sequence. Humic soils, lignites and the continuity of fluvial deposits suggest that moderate rainfall conditions prevailed throughout. Structural activity in the hinterland might increase sediment supply, but a wider source area would be expected to generate a wider variety of clast lithologies. It is the monolithic nature of the serpentinite sands which is unique to the axial sands within the Lower Pliocene sequence. This suggests it was unroofing of a non-resistant ophiolite sheet that controlled sediment supply and hence the rate of progradation of the axial system.

3.9 CONCLUSIONS

The earliest syn-rift deposits exposed in the Corinth Basin are designated to the Lower Pliocene. They are capped by andesites dated as Mid-Pliocene. Facies patterns within the Lower Pliocene sequence describe an east-west trough, bounded by faults to north and south.

The lowermost sediments exposed are variably fluvio-lacustrine. These were downlapped from the south by a coarse clastic wedge, the Agios Charalampos fan-delta, which prograded out into basinal calcareous silts of a brackish/marine "estuarine" embayment. High sediment influx rates into an axial fluvial system prograded serpentinite sands from west to east along the trough. Markov chain analysis of fluvial sands outcropping in the Charalampos fault block defines these as being almost exclusively mid-channel deposits of a low-sinuosity braid river. Shallow basin morphology produced fluvial-dominated delta front styles. An episode of relatively abrupt tectonic subsidence then caused the progradation of coarse clastics into the basin centre and the retreat of the axial fluvial system. This was inundated by marine conditions.

Detailed facies geometries reflect the interaction of tectonic and non-tectonic controls on sediment distribution.

CHAPTER 4 THE CORINTH ISTHMUS - LATE QUATERNARY TECTONIC AND EUSTATIC INTERACTIONS

4.1 SUMMARY

The late Quaternary sedimentology and palaeogeography of the Corinth Isthmus in central Greece is re-interpreted. A series of beach-to-shoreface sub-sequences are seen, each with an internal fining-up character. These are superimposed upon a coastal facies belt which has prograded to the west.

Computer modelling illustrates the interaction of tectonic displacements and eustatic sea-level variation as controls on facies patterns. Late Pleistocene-Holocene facies geometries are predicted on the basis of published sea-level data over that time interval. On coastlines undergoing tectonic uplift, such as the Isthmus of Corinth, depositional patterns may be characterised by transgressive sediment wedges. These sub-sequences merge basinwards, below sea-level minima. Each transgression relates to a major eustatic sea-level peak. Such first order models are modified by variations in the rate of tectonic deformation, the second control on relative sea-level position.

Modelled facies patterns are tested on the basis of new $^{230}Th/^{234}U$ dates attained from Scleractinian corals of the Corinth canal area. Dated sub-sequence sediments correspond in age to Late Pleistocene eustatic highs and observed facies patterns correlate with the major Late Pleistocene-Holocene eustatic transgressions of c. 100 ka periodicity. Episodes of intrabasinal normal faulting are isolated from a structural history otherwise dominated by uplift across the Isthmus. Quantification of post-depositional vertical tectonic

displacements may be achieved. This is done by estimating the eustatic base-level at the time of deposition of a dated horizon. This depositional level is then subtracted from its present outcrop level. Using available $^{230}Th/^{234}U$ dates to establish syn-depositional base-levels, minimum uplift rates of the order of 0.3m per ka are calculated across the area since deposition.

4.2 INTRODUCTION

Within an actively extending basin, facies patterns are partly controlled by the structural geometry of the basin and by its history of fault displacement and tilt events (Leeder & Gawthorpe 1987). This has already been demonstrated with respect to the Lower Pliocene of the Corinth Basin. Potentially, the facies zone most sensitive to tectonic deformation is the alluvial-to-marine transition belt, represented by the coastline. Relative displacements of sea-level (base-level) of a few metres or less may produce a significant change in facies. Such a situation is exemplified by the drowning of alluvial sediments by marsh/lagoonal facies behind a transgressive beach barrier at Skinos, central Greece (fig. 4.1), on the subsiding hangingwall to an active normal fault (Jackson et al 1982a, Leeder et al 1988).

However, despite these fundamental tectonic controls, coastal Quaternary sediments of syn-rift basins such as those in central Greece, and elsewhere, are strongly affected by eustacy caused by the periodic growth and diminution of the global ice-caps. The problem therefore arises, when considering the distribution of facies in an active tectonic setting during a period of significant sea-level variability, as to how to determine whether one or other or both controls produced observed facies patterns.

Figure 4.1

Structural map of the Isthmus of Corinth. All faults are extensional. X-Y = section outlined in figure 4.2. Lines a-e refer to cross-sections in figure 4.11; f = sample site 87.29.8.1. Inset outlines the Corinth Basin with major bounding faults at Loutraki (L) and Kechriae (K). C = Corinth; S = Skinos.

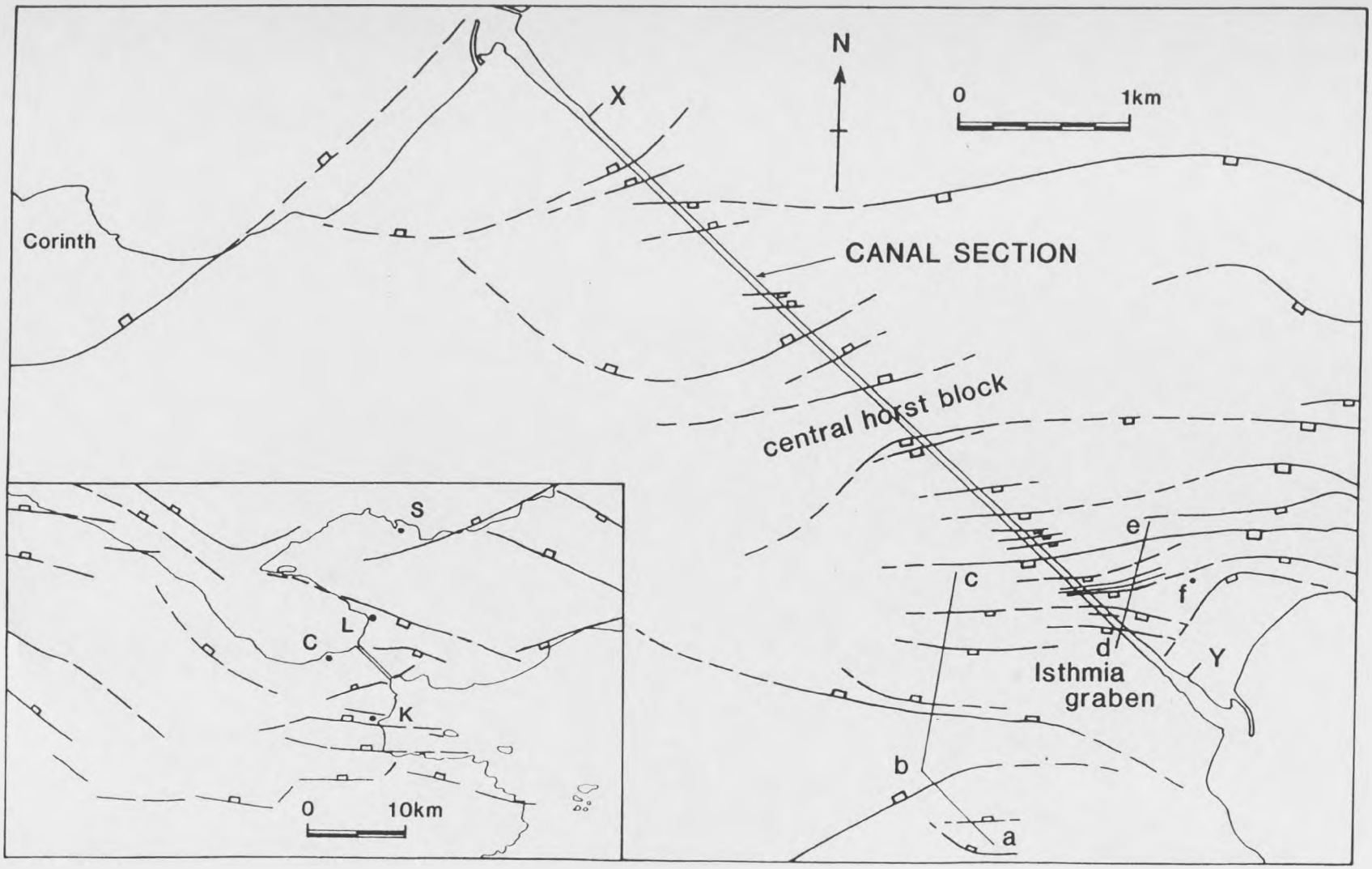
N
0
1km
X
Corinth
CANAL SECTION
central horst block
S
L
C
K
0
10km
e
c
f
d
Y
Isthmia
graben
b
a

The aims of this chapter are threefold. Firstly, to discuss in theoretical terms the interaction of eustatic and tectonic controls on base-level and their consequent influence on sedimentation style. Secondly, to consider the observed facies patterns in the classic canal exposures of the Corinth Isthmus.

Thirdly, an attempt is made, through the use of radiometric ages determined for corals by uranium-series disequilibrium dating, to determine sea-level at time of deposition of the marine sediments within the canal section. This is done by referring to the reasonably well-constrained sea-level curve for the late Pleistocene and Holocene (Chappell & Shackleton 1986, Shackleton 1987, Imbrie et al 1984) and allows quantification of post-depositional tectonic displacements across the Corinth Isthmus.

4.3 THE QUATERNARY CORINTH BASIN

The present Corinth Basin is an asymmetric graben with a complex intrabasinal structure (fig. 4.1). Late Pleistocene and Holocene deposits outcrop around the southern Corinth Basin, across the Isthmus and in areas of the northern Corinth Basin around the unroofed Lower Pliocene sequence. The area remains seismically active, undergoing normal faulting in response to approximately N-S extension (Jackson et al 1982a, Jackson et al 1982b, Vita-Finzi & King 1985).

The Quaternary stratigraphic section on the Corinth Isthmus is made accessible by the excavation of the Corinth Canal (fig. 4.2). The canal provides a unique opportunity to study sediments in alluvial-to-shoreface facies in magnificent cliff sections 5.8 km long and up to 90m in height. As discussed below the Isthmus of Corinth is currently undergoing uplift.

Recent marine deposits are found more than 100m above the maximum Quaternary sea-level.

Freyberg (1973) studied the Neogene sedimentary history of the Corinth Isthmus. Freyberg recognised that eustatic variation influenced facies patterns in the canal area. Freyberg described two marine to freshwater "cycles" in his Kalamaki strata (considered as part of the "Corinth Marls" in this thesis). He assumed a eustatic control to the inundation of Kalamaki strata and of cliffs in the canal section by his Hauptkonglomerat (the 1st marine sub-sequence in this chapter). A relative sea-level fall is then recognised. This allowed cliffs to be cut prior to transgression by the upper Hauptkonglomerat (renamed the 2nd sub-sequence). Freyberg inferred transport of these sediments was from the east on the basis of a SE to NW fining in grain size. He also postulated that the conglomerates were influenced by tidal currents in an enclosed strait. A Tyrrhenian age was attributed to the Gelbsandhorizont (3rd sub-sequence) by Freyberg (1973). Details of Freyberg's stratigraphic boundaries together with environmental and palaeogeographical interpretations for the late Quaternary of the area are substantially modified in this work.

The new facies interpretation may be summarised as repeated beach-to-shoreface sub-sequences each of which fines up internally. Each sub-sequence overlies an erosive or alluvial surface. This pattern is superimposed upon an overall westwards-progradation of the coastline. The term sub-sequence is here used to describe a facies suite bounded by local unconformity surfaces which do not extend across the entire basin (after Hubbard et al 1985).

Figure 4.2

Cartoon section of the Corinth canal. a = "Corinth Marl" lacustrine-to-marine transitional sequence; b = 1st marine sub-sequence; c = 2nd marine sub-sequence; d = 3rd marine sub-sequence; e = 4th marine sub-sequence; f = 5th sub-sequence (including Holocene). All sub-sequence boundaries are unconformable. A-D mark cliffs in unconformity surfaces. Refer to figure 4.1 for positions of X and Y. Lateral equivalents of coral sample 87.29.8.1 are arrowed. Other coral sample localities are as shown.

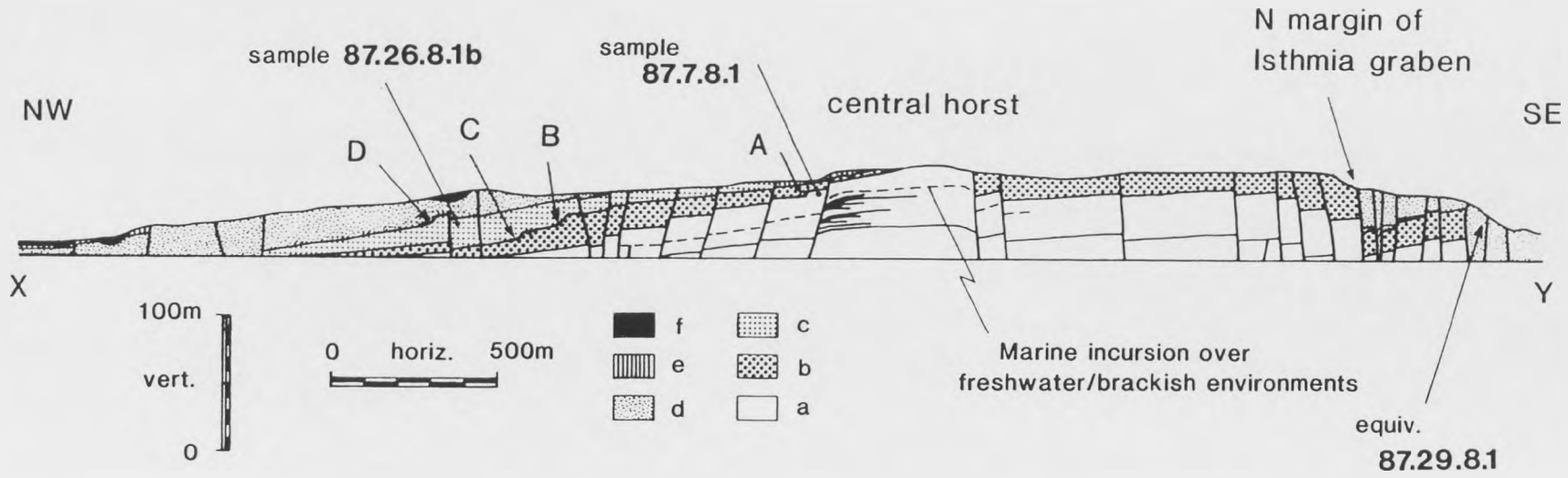
sample 87.26.8.1b
sample
87.7.8.1
N margin of
Isthmia graben
NW
central horst
SE
D
C
B
A
X
Y
100m
vert.
0
0 horiz. 500m
f
e
d
c
b
a
Marine incursion over
freshwater/brackish environments
equiv.
87.29.8.1

No direct evidence is available on the mechanism of uplift of the Isthmus of Corinth. The Isthmus is too distant from the active Skinos fault to be subject to footwall uplift of the magnitude required (cf. Jackson & McKenzie 1983, Jackson et al 1982a and Jackson et al 1982b). This author has found no genetically compressive structures to support one hypothesis that the area is within a torsional compressive regime (Mariolakis & Stiros 1987). All observed faulting, including structures that would lie within the compressive field of the proposed stress ellipse of the Mariolakis & Stiros model, are extensional and are most simply explained by relation to an essentially N-S or NNE-SSW extensional stress field (Jackson et al 1982b, Vita-Finzi & King 1985).

Uplift of the Isthmus is one of two tectonic displacement vectors affecting the Isthmus area. The other is extensional fault-induced subsidence. This latter may be accompanied by block rotations. Subsidence will occur either in response to downfaulting on local, intrabasinal normal faults or basinwide as a product of downfaulting on the major E-W trending basin-bounding normal faults at Kechriae and Loutraki (fig. 4.1, inset). Both means of fault displacement may occur seismically, with at times measurable individual increments of relative base-level change (Jackson et al 1982a) or aseismically, in which case tectonically-induced relative base-level change will be gradational. It is not known whether the regional uplift is steady or irregular.

4.4 MODELLING EUSTACY-CONTROLLED STRATIGRAPHIC PROFILES

World-wide variations in sea-level during the late Quaternary have had a marked effect on coastal geomorphologies and

depositional histories. During falling and lowstand episodes, erosion of previously submerged surfaces has taken place and alluvial profiles have been incised. Wave-cut platforms, datable if colonised by a suitable marine biota, record stillstand levels. Repeated stillstand events have generated stepped coastal profiles on coastlines undergoing rapid tectonic uplift (e.g. Chappell 1974, Bender et al 1979). Passive margins similarly reveal unconformities and transgressive sequences produced by sea-level fluctuation (Pickett et al 1985).

The late Quaternary sea-level curve is reasonably well constrained as a record of base-level variation through time (Shackleton 1987). Independent studies have produced consistent curves against which local variations are one or two orders of magnitude less than the amplitude of major global glacio-eustatic fluctuations. [Imbrie 1985, Imbrie et al (1984), Chappell & Shackleton (1986), Emiliani (1978) and Hays et al (1976)]. Geomorphological studies have been correlated with a variety of other features such as the chemical composition of equatorial Pacific sediments and taxonomic assemblages of Caribbean plankton (Lockwood 1985).

$d\,^{18}O$ isotope values have varied in time in relation to temperature conditions and changes in global ice volume (Shackleton 1987, Chappell & Shackleton 1986, Shackleton & Opdyke 1973). The record of lowstand levels on passive margins allows the correlation of sea-level with the $d\,^{18}O$ record (as approximated in fig. 4.12).

Two approaches may be used to assess the influence of sea-level variation on stratigraphic profiles. Firstly, theoretical modelling can be carried out to predict the position of a

coastline (and the associated suite of coastal facies) as a function of sea-level. To this end, the three principal factors discussed in the last chapter are considered; that is a) the rate of subsidence/uplift with time (dS/dt), b) the rate of change in eustatic base-level with time (dSL/dt), and c) the rate of deposition at any locality (dD/dt). Sea-level and the depositional surface are referred to axes in space. The two parameters of deposition rate, and the rate of coastal subsidence (whether tectonic or due to sediment loading or both) are predetermined.

The second approach, possible in relation to sediments of late Pleistocene and Holocene age, is to equate observed facies patterns and radiometrically dated horizons with the known sea-level curve (e.g. Chappell 1974, Keraudren & Sorel 1987).

The computer modelling outlined in the following section utilises the first approach. Simulated stratigraphic sections are produced which represent the progradation/retreat of a coastal beach profile through time. 2-dimensional modelling allows a reasonable representation of this environment. Lateral variations in sediment supply along the coastline are assumed neglible for the purposes of this modelling. This contrasts with a more complex situation around distributary systems, such as fan deltas, where 3-dimensional geometries create inherent variations in sediment distribution rates through time.

4.4.1 Computer Modelling

The first, theoretical approach to analysing the response of coastal position to eustatic variation was set up as follows. The objective was to develop a model that simulated 2-dimensional

stratigraphic sections through deposits laid down in a tectonically active basin during periods of changing sea-level. The variables involved, referred to x and y axes in space, are:

1) Sea-level change with time (+dSL/dt for rising sea-level, -dSL/dt for falling sea-level).

2) Subsidence (-dS/dt) or uplift (+dS/dt) with time.

3) Vertical deposition rate with time (dD/dt).

4) Depositional slope angle, theta (held as a constant within each model).

Consider the position of a coastline, C, a point where sea-level intersects a depositional surface inclined at an angle theta. Changing the sea-level (SL) variable alone will cause C to migrate along the depositional surface (fig. 4.3a). The horizontal displacement of C is given by -dSL/tan theta. The vertical displacement of C is given by dSL. If sea-level lowers, the coastline will thus migrate seawards (i.e. regression) and a rise in sea-level will generate landward migration of the coastline (transgression).

Subsidence or uplift of the depositional surface, with other variables set to zero, will similarly cause the position of the coastline to change. The third variable, sedimentation rate, will also affect the position of the coastline. Taking an example in which sea-level is constant and there is no tectonic displacement of the coastal profile, a net supply of sediment onto the depositional surface will cause progradation of the coastline (and generate a coarsening-up prograding beach sequence). The position of the coastline in space, for given slope angle, is therefore a function of the three variables of rate of tectonic displacement, rate of change in sea-level and rate of deposition (fig. 4.3a). In two dimensions, the change

Figure 4.3

a) Diagram illustrating the migration of a coastline across a depositional slope (in dip section) as a function of the change in sea-level (dSL), tectonic displacement (dS) and depositional thickness (dD) across some time interval t-t' (i.e. dt).
b) Diagram illustrating the same situation as in (a), but with the original coastline position subsiding by dS/dt and being buried within the stratigraphic section.

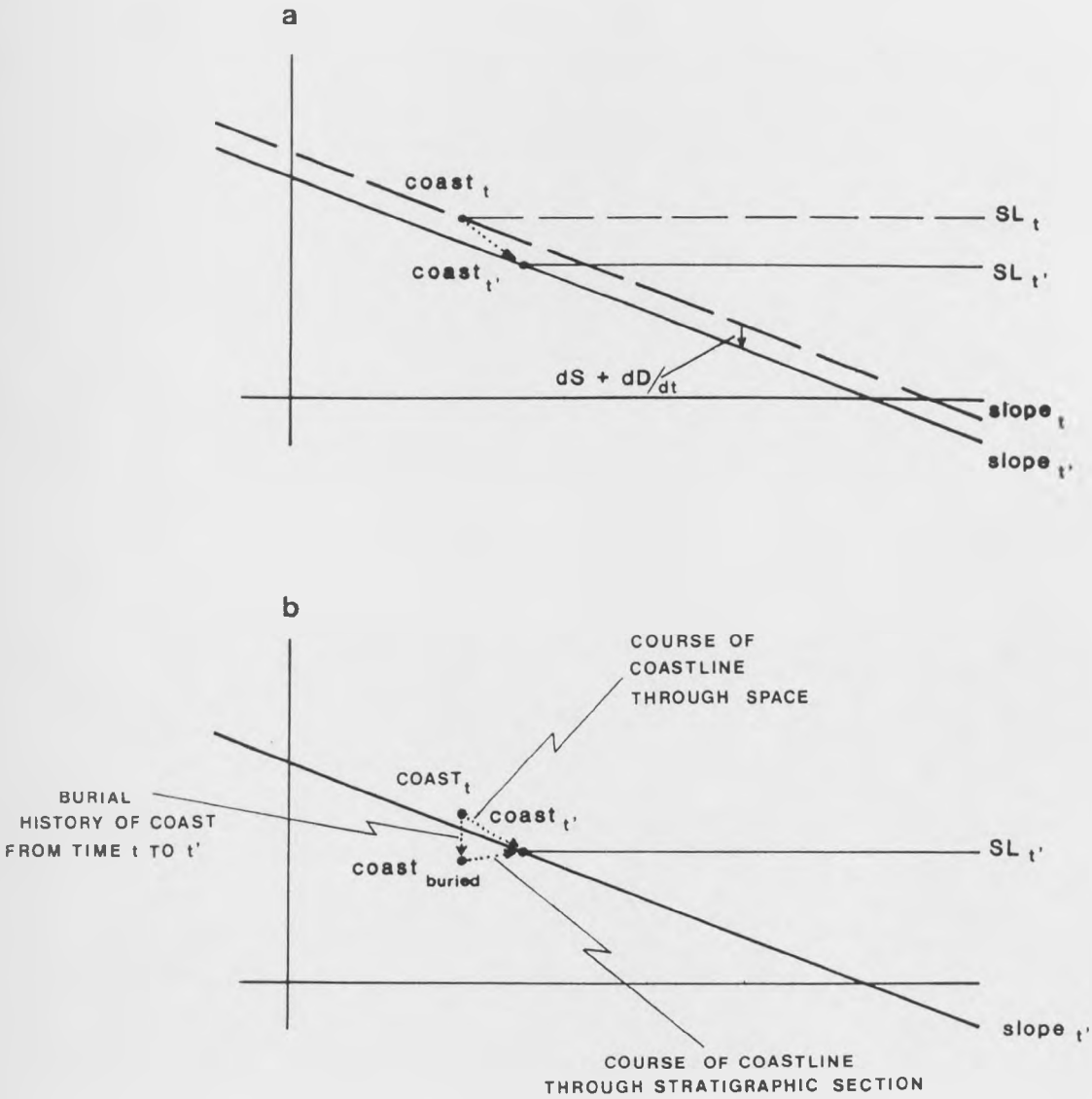
a
coast t
SL t
coast t'
SL t'
dS + dD/dt
slope t
slope t'
b
COURSE OF
COASTLINE
THROUGH SPACE
COAST t
coast t'
BURIAL
HISTORY OF COAST
FROM TIME t TO t'
coast buried
SL t'
slope t'
COURSE OF COASTLINE
THROUGH STRATIGRAPHIC SECTION

in the position of the coastline on a depositional slope of angle theta across some time increment t to t' is given by:

$$C'_{(x,y)} = \{[(-dSL+dS+dD)/dt]/ \tan \text{theta} , dSL/dt\} + C_{(x,y)} \qquad \text{Equation 4.1}$$

where $C_{(x,y)}$ is the position of the coast at time t and $C'_{(x,y)}$ the position of the coast at time t'.

With each increment of deposition (dD/dt), the previous coastline positions are buried by dD/dt. The position against 2-dimensional reference axes of previous coastlines, however, will be governed by the tectonic displacement of the section (fig. 4.3b):

$$C_{\text{buried } (x,y)} = (0 , dS/dt) + C_{(x,y)} \qquad \text{Equation 4.2}$$

A stratigraphic section may therefore be constructed, by computing the sequential tectonic displacement of all previous coast position co-ordinates, after each successive time increment (fig. 4.4). Each variable within the computer modelling may either be defined as a constant, or via some equation, or by the digitisation of a graph as used, for example, to describe the irregular variation in sea-level through the Late Quaternary. The models presented here neglect any isostatic compensation for water and sediment loading or unloading. Sedimentary compaction within the stratigraphic profiles is also ignored.

Figure 4.5 illustrates the migration of a coastline through a simulated stratigraphic cross-section. The position of the coast varies according to the interaction of tectonic deformation and sea-level variation. In this case the area is modelled as

Figure 4.4

Summary flow diagram for computing the migration pathway of a coastline through a stratigraphic profile.

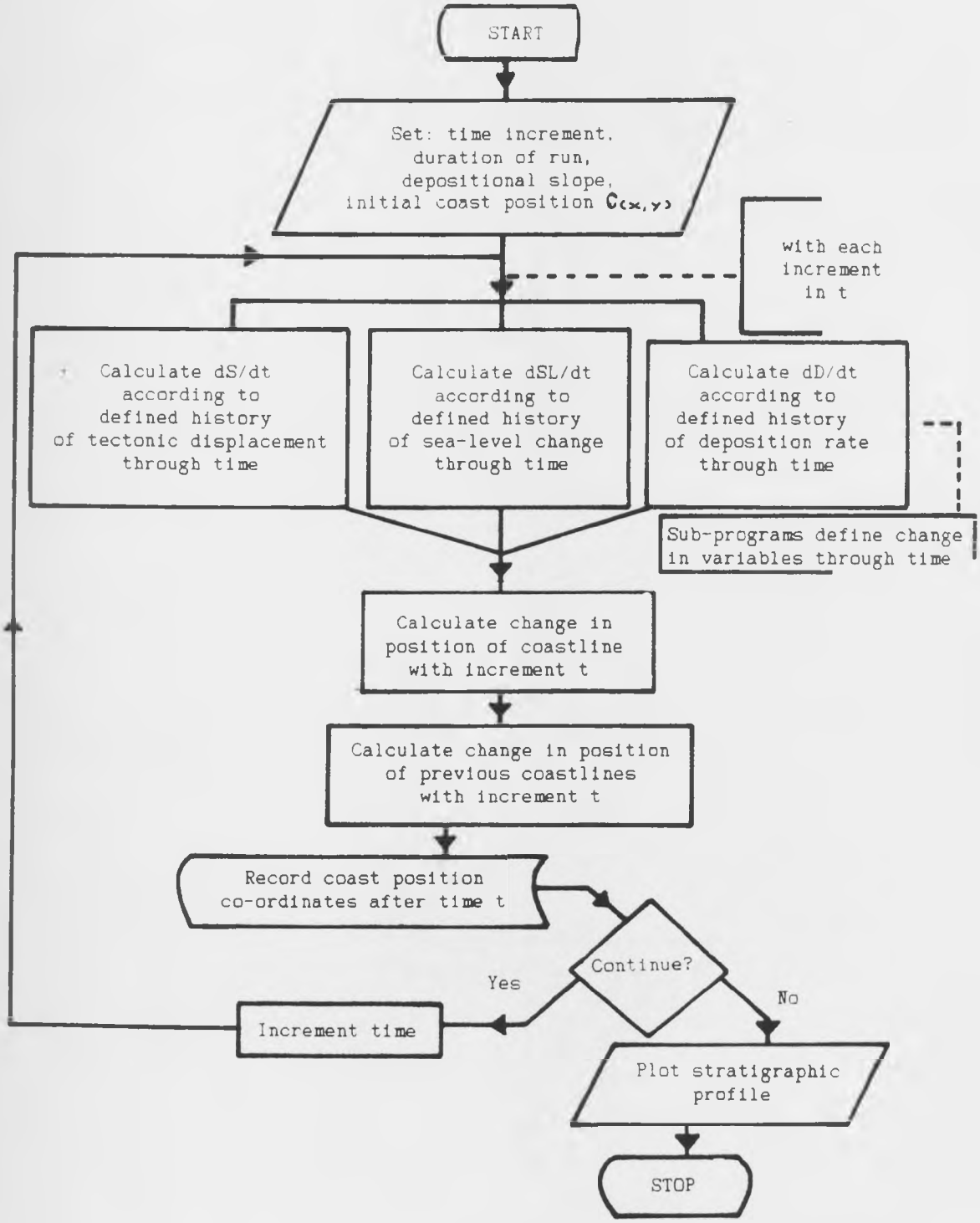
START
Set: time increment,
duration of run,
depositional slope,
initial coast position C(x,y)
with each
increment
in t
Calculate dS/dt
according to
defined history
of tectonic displacement
through time
Calculate dSL/dt
according to
defined history
of sea-level change
through time
Calculate dD/dt
according to
defined history
of deposition rate
through time
Sub-programs define change
in variables through time
Calculate change in
position of coastline
with increment t
Calculate change in position
of previous coastlines
with increment t
Record coast position
co-ordinates after time t
Continue?
Yes
No
Increment time
Plot stratigraphic
profile
STOP

Figure 4.5

Modelled stratigraphic profile showing repeated transgression and regression of a coast through time, on a depositional surface dipping 2° from left to right. A = the present position of coastal facies deposited 430 ka b.p.; B = the present coastline; C = a subordinate transgressive-regressive cycle. Change in sea-level is defined by the sea-level curve illustrated in fig. 4.12. Tectonic uplift rate = constant 0.3m per ka. Deposition rate = constant 0.2m per ka. Roman numerals refer to predicted transgressive peaks of respective oxygen isotope stages. Vertical and horizontal scales in metres.

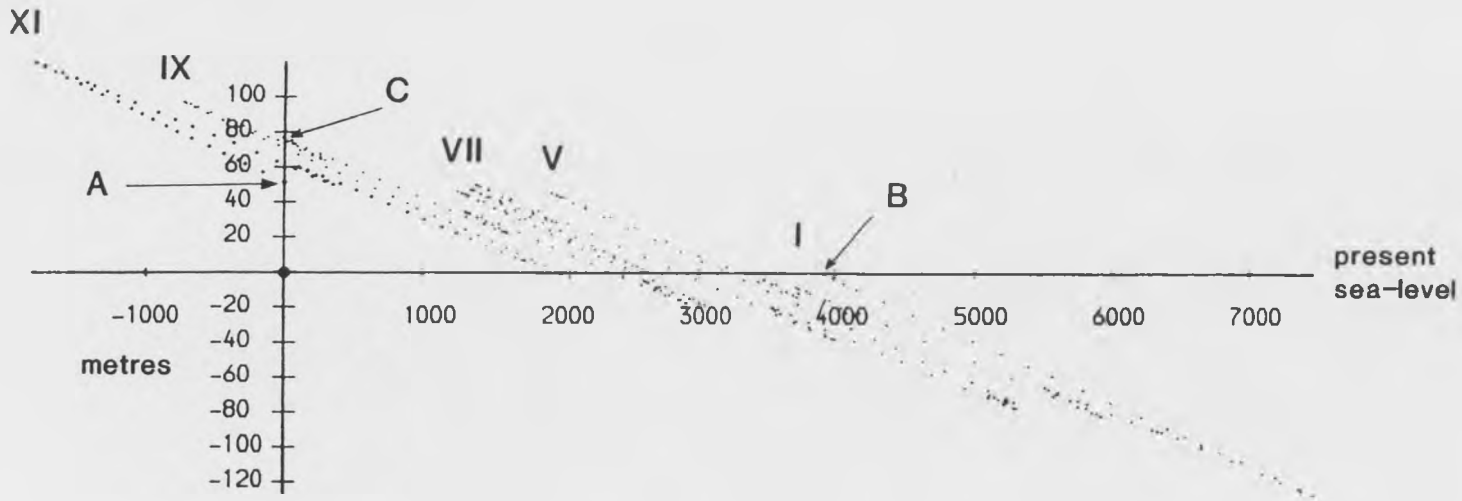
XI
IX
VII
V
I
A
B
C
100
80
60
40
20
-20
-40
-60
-80
-100
-120
metres
-1000
1000
2000
3000
4000
5000
6000
7000
present
sea-level

undergoing tectonic uplift at a constant rate of 0.3m per ka. The sea-level history utilised in the model is illustrated in figure 4.12, the sea-level curve for the last 430 ka based on oxygen isotope data from Imbrie et al (1984). Two further assumptions in the model are that deposition occurred at a constant rate of 0.2m per ka throughout the modelled period and that the depositional slope dipped by 2^{o} (from left to right in the diagram). Five major marine transgressions are predicted by the model. These correspond to the c.100 ka cycle eustatic highs of ^{18}O stages XI, IX, VII, V and I. Minor stillstand events (e.g. at C, fig. 4.5) are predicted to occur in response to subordinate eustatic fluctuations.

When studying an actively extending area such as the Corinth Basin, the assumption of a constant deformation rate is clearly invalid. But, as indicated by figure 4.5, Late Pleistocene-Holocene sea-level fluctuations are likely to dominate the controls on sedimentary facies positions across this period. These eustatic fluctuations must therefore be subtracted from the record if the aim is to isolate the structural control on facies migration.

By way of contrast with figure 4.5, figure 4.6 illustrates the position of coastal facies through a stratigraphic profile generated in a tectonically subsiding area. Slope angle at 2^{o} and a sea-level history based on the Imbrie et al (1984) curve are kept the same as in the model in figure 4.5. Deposition rate is defined as a constant 1.0m per ka. Tectonic subsidence is defined as a constant (negative) 2.5m per ka. Overall, the model predicts a gross transgression due to the relative rise in base-level. This is punctuated by regressive phases corresponding to the more significant eustatic regressions of the

Figure 4.6

Modelled stratigraphic profile with parameters as in figure 4.5 except:
Tectonic subsidence rate = constant -2.5m per ka.
Deposition rate = constant 1.0m per ka.

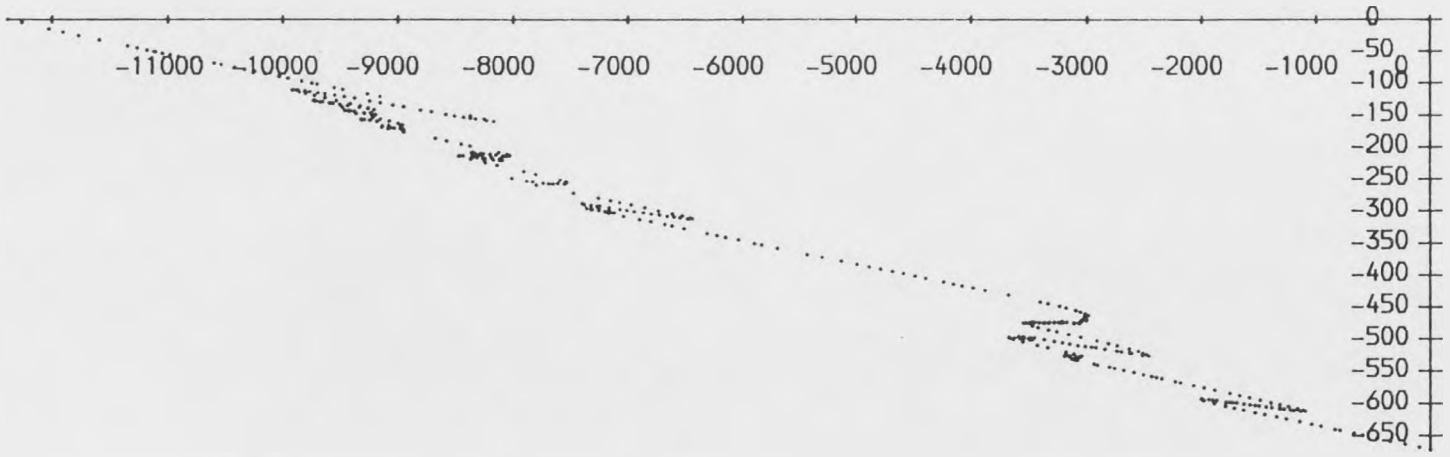

slope	2°
dSL/dt	defined by Chappell & Shackleton 1986 SL curve
dS/dt	-2.5m per 1000 years
dD/dt	1.0m per 1000 years

Late Quaternary. This pattern contrasts with the overall regression where the coastal profile is undergoing uplift, as modelled in figure 4.5. Major eustatic trangressions are superimposed, when dSL/dt exceeds (dS/dt+dD/dt).

4.5 SEDIMENTARY FACIES

A formal facies analysis, defining and interpreting facies and facies associations, will not be presented in this chapter for the canal sediments. Instead, the facies observed are described and interpreted in their stratigraphic context. This will serve to emphasize the repetitious nature of each sub-sequence and allow attention to be focused on any variations from the fining-up sub-sequence theme.

4.5.1 "Corinth Marl" Lacustrine-to-Marine Transitional Sequence

The oldest sediments exposed in the canal section are at the base of the central horst block (fig. 4.2). Dominated on the north-west by white and grey calcareous silts, these are loosely termed the Corinth Marls (Freyberg 1973). There is an upwards transition within the central horst block from freshwater or brackish facies to a marine environment. Figure 4.7a illustrates the typically diffusely planar-bedded habit of the calcareous silts of the non-marine basinal environment, inhabited by Viviparus sp. Trough scour forms represent periods of current influence across the basin floor, where these may have been distal to fluvial-deltaic input to the basin. The internally trough cross-stratified, coarsening-up fluvial package (fig. 4.7a) denotes the further advance of this progradational event in response to a climatically or tectonically-induced lake-level change.

Figure 4.7

Sedimentary logs through the "Corinth Marl" lacustrine-to-marine transitional sequence. Log a = NE Corinth canal bank in middle of central horst block, 19-38m above present sea-level. Basinal marls with periodic current influence and prograding fluvial packages. Log b = NE bank above log a, 53-74m above sea-level. Marine incursion into lacustrine marls. Intra-sequence discontinuities generated by faulting at margins of central horst block. 1st marine sub-sequence unconformably above.

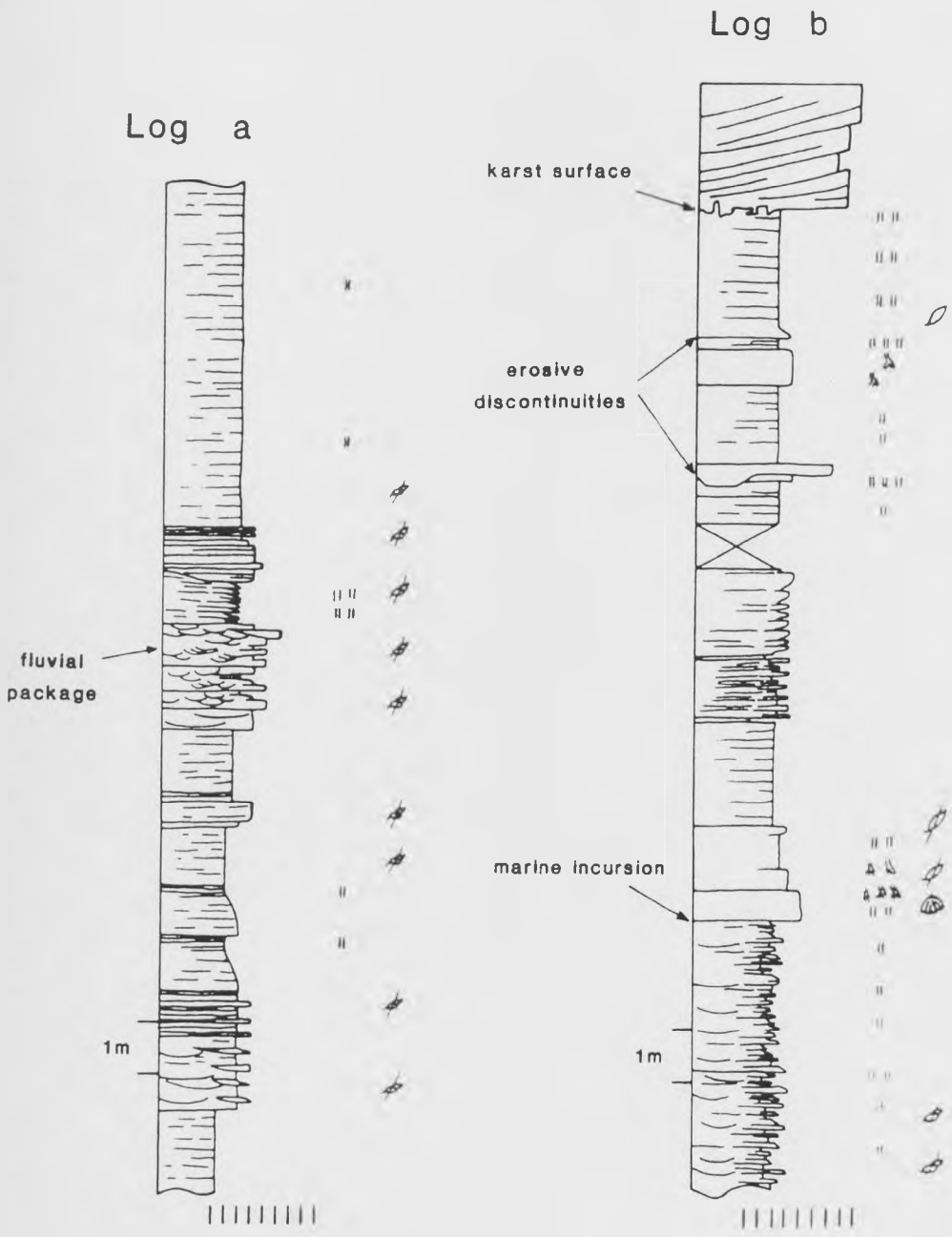
Log a
fluvial
package
1m
Log b
karst surface
erosive
discontinuities
marine incursion
1m

In the upper part of the central horst block a marine incursion is recognised, with the appearance first of Cardium sp. and then of a more varied marine bivalve fauna (fig. 4.7b). Bioturbation is locally intense. Lateral equivalents coarsen towards the south-eastern half of the canal section and include conglomerates of westerly-dipping beach/shoreface sets. This facies association is thought to represent a prograding, westerly-dipping depositional surface, with sediments fining away from a coast lying to the east or south-east.

Erosive discontinuities within the interbedded marine silts and sands mark normal drag deformation of the footwalls to the horst-bounding normal faults (plate 4.1 and fig. 4.8). In the hangingwall of the fault controlling the north-west margin of the central horst block, corresponding wedges of coarser clastics and syn-sedimentary slumping occurred as a response to the within-sequence seismic activity.

Demonstrably in situ corals at the north-west end of the central horst block (87.7.8.1, fig. 4.2) give a U-series result consistent with their being older than 350 ka in age (table 4.1 and section 4.6.2 for discussion).

The Corinth Marl/marine sequence is terminated by a major erosive unconformity. Block rotations beneath this surface record further tectonic displacements prior to or during this erosive episode. The erosive surface was emergent across most of the central horst block and to the south-east. It was first calcretised and then subject to karstic dissolution. This suggests that during the period of emergence climate varied from semi-arid to a more temperate climate, with higher rates of precipitation. Close to the north-western margin of the central

Plate 4.1

Photo-montage of the SW bank of the Corinth canal, NW from the central horst block. See figure 4.8 for details and interpretation.

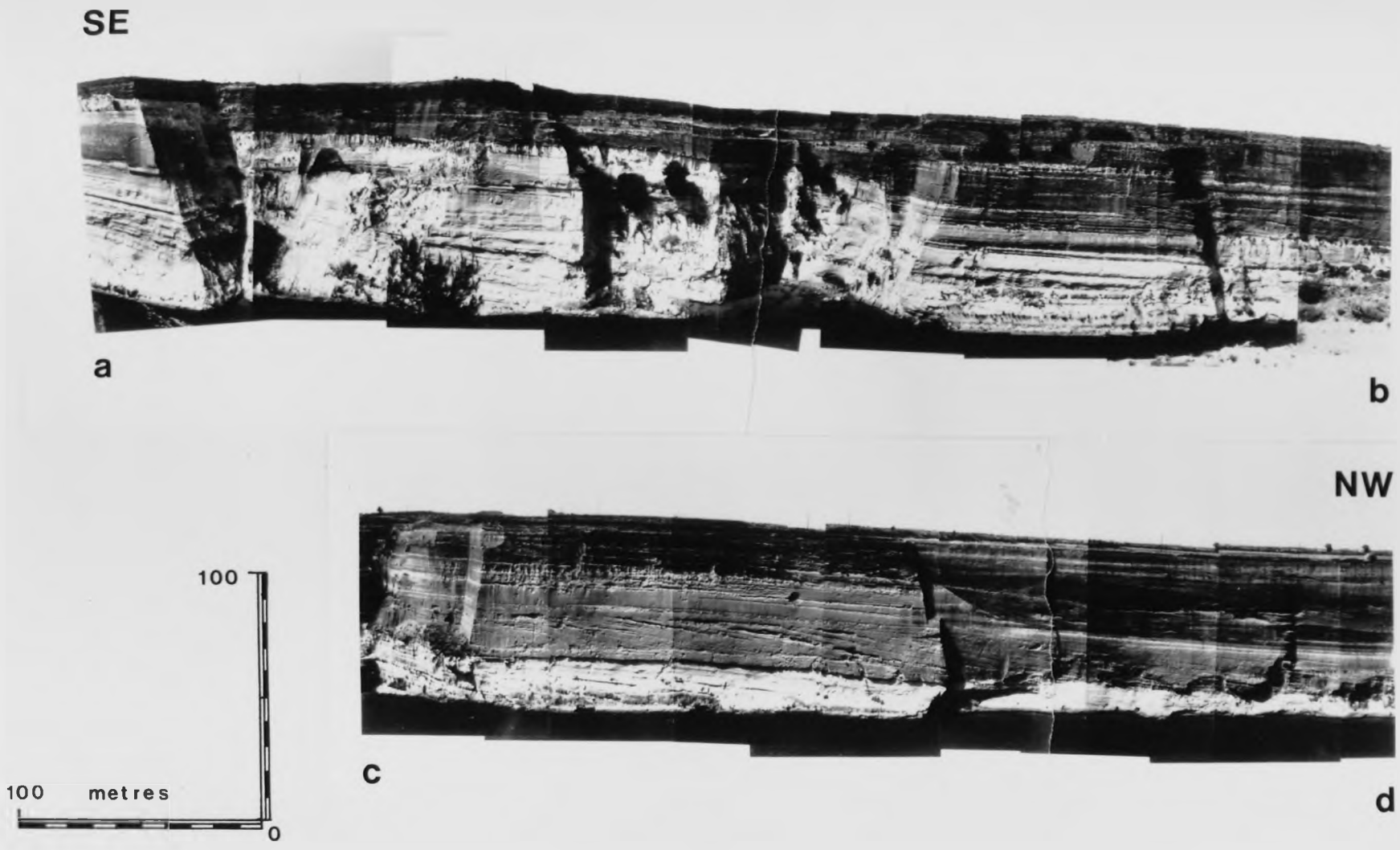
SE
a
b
NW
c
d
100
100 metres
0

Figure 4.8

Line-drawing of the SW bank of the Corinth canal, NW from the central horst block. Heavy lines indicate faults and unconformities separating sub-sequences. The lower unconformity with cliff marked A separates the "Corinth Marl" sequence from the 1st marine sub-sequence. The upper unconformity, with cliffs at B and C, is transgressed by the 2nd sub-sequence.

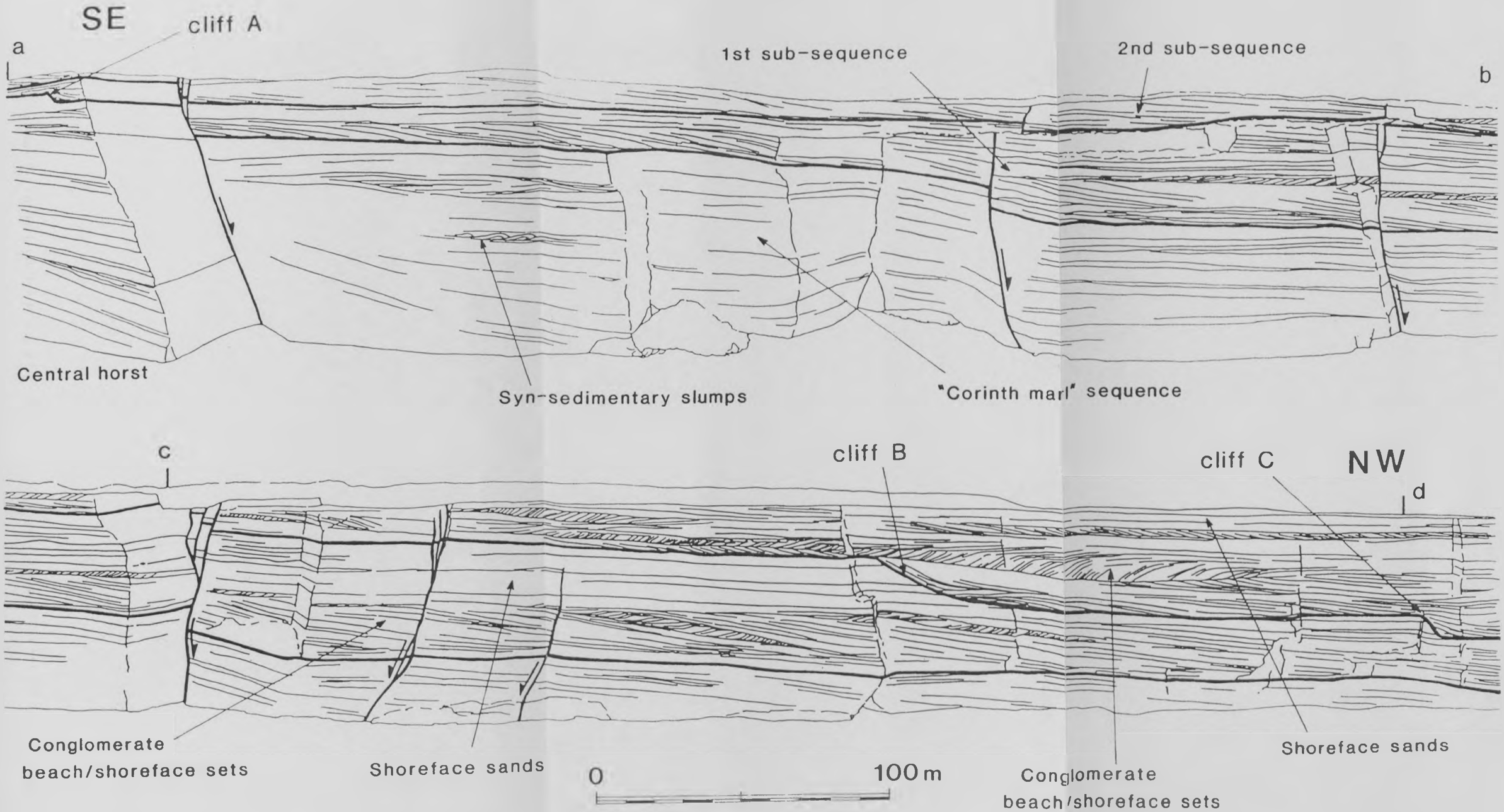
SE
cliff A
a
1st sub-sequence
2nd sub-sequence
b
Central horst
Syn-sedimentary slumps
"Corinth marl" sequence
c
cliff B
cliff C
NW
d
Conglomerate
beach/shoreface sets
Shoreface sands
0
100 m
Conglomerate
beach/shoreface sets
Shoreface sands

horst block, a 2m high cliff marks the limit of a wave-cut platform that is the basinwards continuation of the sequence-top unconformity.

4.5.2 1st Sub-Sequence

The 1st marine sub-sequence (figs. 4.2 & 4.8) is initiated by an aggrading wedge of pebble conglomerates that is at first bounded to the south-east by the cliff-line already described. These conglomerates, of mixed limestone, ultrabasic, chert and assorted "basement" siliciclastic lithologies, contain rare molluscan-bored pebbles and echinoderm fragments. The conglomerates transgressed the central horst block and extended to the south-eastern half of the canal area, where there are west-dipping sets similar to those NW of the central horst. The shallow west-dipping surfaces within the conglomerates may thin or thicken downslope. Occasional climbing dune forms represent beach slope surfaces, the dune forms being interpreted as storm berms. The assemblage of sedimentary structures and the gross fining-up to shoreface facies suggests that this package represents an aggradational sub-sequence produced by a relative rise in base-level.

High-energy, probably wave-reworked shelly sands above the beach conglomerates give way to bundled trough-sets and silt-draped symmetric ripple surfaces of the upper shoreface (fig. 4.9). A 0.5 - 1.0m band of hummocky cross-stratification confirms that sedimentation at this level within the sub-sequence occurred within the zone of storm-wave influence. Concave-up surfaces with half-wavelengths of 5 - 10m bound a complex internal structure of scour surfaces, ripple cosets and bundled trough cross-stratification. Immediately above the HCS horizon, the

Figure 4.9

Log from NE bank of the Corinth canal, 400m NW of the central horst block, 35-55m above present sea-level. 1st marine sub-sequence beach/shoreface conglomerates fine up to shoreface sands with variable storm and wave influence. 2nd sub-sequence conglomerates above. The unconformity between is hidden due to reworking of sands from the top of the 1st sub-sequence.
A = 1st sub-sequence beach/upper shoreface sets
B = 1st sub-sequence shoreface sands
C = 2nd sub-sequence beach/shoreface sets
D = depositional dip direction
LA = pebble long axes
I = pebble imbrications

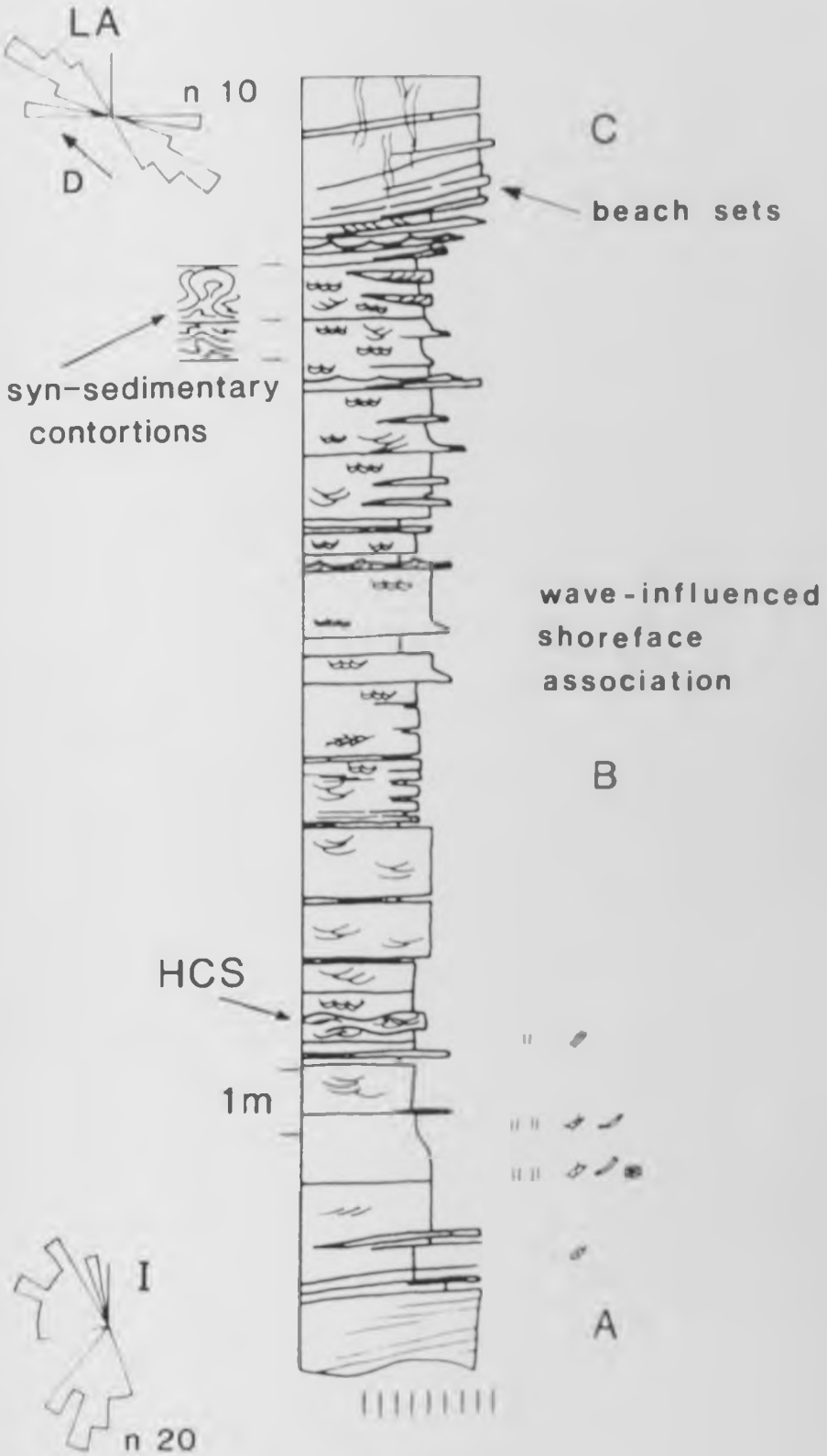
LA
n 10
D
C
beach sets
syn-sedimentary
contortions
wave-influenced
shoreface
association
B
HCS
1m
I
n 20
A

trough cross-stratified sands (with scattered small pebbles) contain only rare draped ripples. Further up the sub-sequence, draped symmetric ripples and chevron ripples indicate a shoaling trend back into upper shoreface facies. This may reflect the progradation of the coastal facies suite during a relative highstand stage.

4.5.3 2nd Sub-Sequence

The 2nd marine sub-sequence lies unconformably on the 1st sub-sequence. Cliffs are cut into the unconformity surface 750 and 900m NW of the central horst block (B and C, fig. 4.8). These represent the upper limit of wave-cut platforms cut during base-level stillstand events. The contact between the two sub-sequences on the central horst block is sharply and irregularly erosive, indicative of subaerial exposure in the intervening period.

The beach-to-shoreface NW-dipping sets of the 2nd sub-sequence onlap to the SE at least onto the central horst. Lithologies are predominantly ultrabasic, implying derivation from the northern margin to the Corinth Basin where an ophiolite thrust sheet is being unroofed. There is evidence for palaeoseismicity within the conglomerates, with sedimentary contortions and dykes (fig. 4.9). The timing of this seismicity is not clear, but the need for a liquifiable calcareous mud fraction to supply the sedimentary dyke matrix implies that this was a syn- or pene-sedimentary event.

The fining-up character of the sub-sequence suggests an overall rise in relative sea-level. The variety of progradational and aggradational structures seen within the beach/shoreface conglomerates (fig. 4.8) with variously migrating bar forms,

suggests that minor changes in relative base-level occurred within the period of deposition of the sub-sequence. It is not possible to distinguish on this scale between eustatic or tectonically-induced fluctuations in relative base-level.

Colonies of Scleractinian corals occur towards the top of the 2nd sub-sequence within a calcareous mud substrate. These Acropora corals have been dated at c. 312 ka (87.26.8.1b, table 4.1).

4.5.4 3rd Sub-sequence

The base of this sub-sequence is again an erosive unconformity (fig. 4.2, with buried marine terrace marked D). The 3rd sub-sequence has a fining-up character similar to those underlying it (fig. 4.10). Beach-to-shoreface asymptotic sets dip and fine to the WNW. The mature, well-sorted coarse clastics within these sets are imbricated down-dip but also up-dip, indicating tidal or storm wave-induced current reversals. Lithologies are polymict basement types, but red cherts locally comprise up to 50% of the clasts.

Higher up the unit, shoreface sands are well-sorted and often heavily bioturbated. They include a varied marine fauna with bivalves Glycymeris glycymeris, Pinna sp., Pecten sp., Lutraria sp. and Cardium sp. together with serpulids and Archimediella sp. Sedimentary features include 0.2m climbing-dune cosets and common trough cross-stratification. Vertical burrows of Solen sp. up to 0.2m deep locally almost destroy the original planar-lamination of the sand substrate.

At the SE end of the canal section, at least 70m of yellow sands with a varied marine fauna were deposited in the Isthmia Graben (fig. 4.11). This marine incursion was at least in part

Figure 4.10

Log from NE bank of the Corinth canal, immediately NW of cliff D (fig. 4.2), with base approx. 27m above present sea-level. Fining-up package of 3rd transgressive sub-sequence. The 3rd sub-sequence unconformably overlies the 2nd sub-sequence at erosional surface marked A.

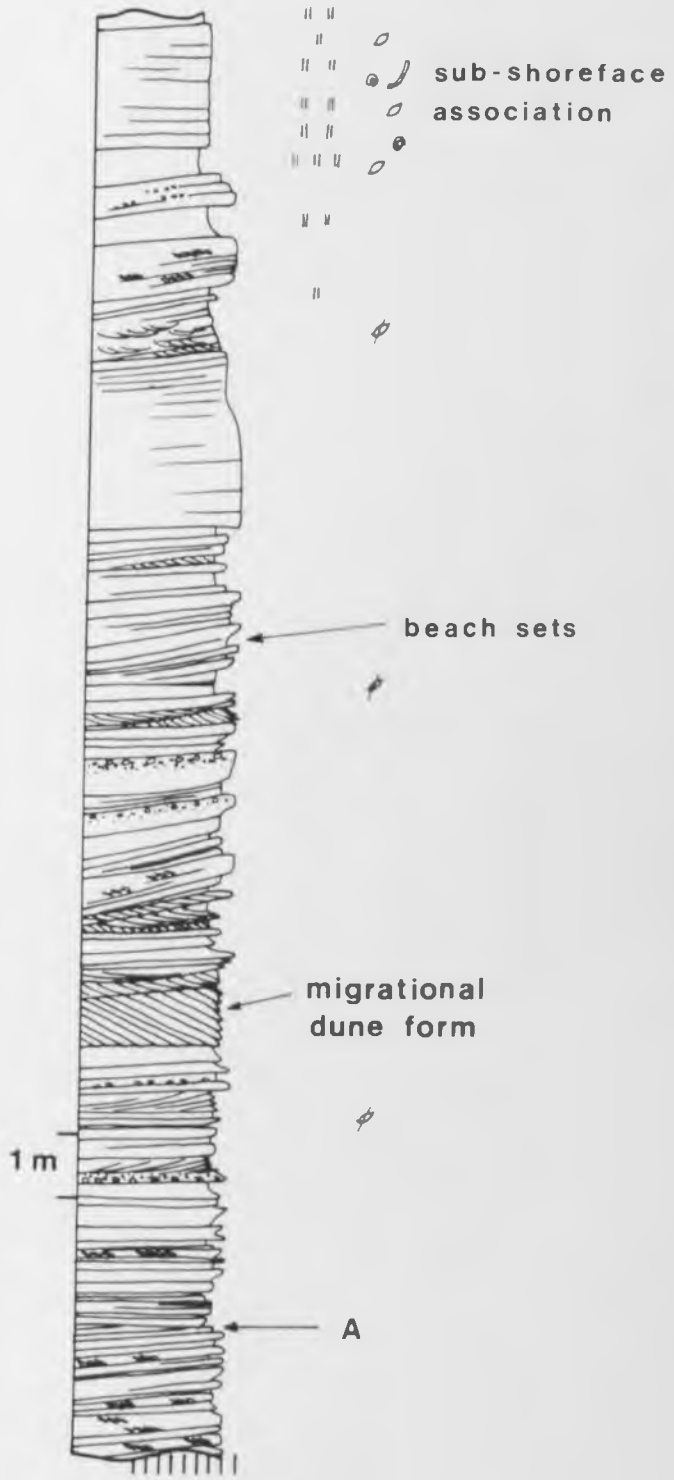
sub-shoreface
association
beach sets
migrational
dune form
1 m
A

Figure 4.11

Cross-section through the intrabasinal Isthmia Graben. Graben-bounding faults X and Y are interpreted as listric in form on the basis of observed hangingwall rollovers. For the positions of lines a-c and d-e refer to figure 4.1. A = "Corinth Marl"; B = 1st sub-sequence; D = 3rd (and/or 4th) sub-sequence.

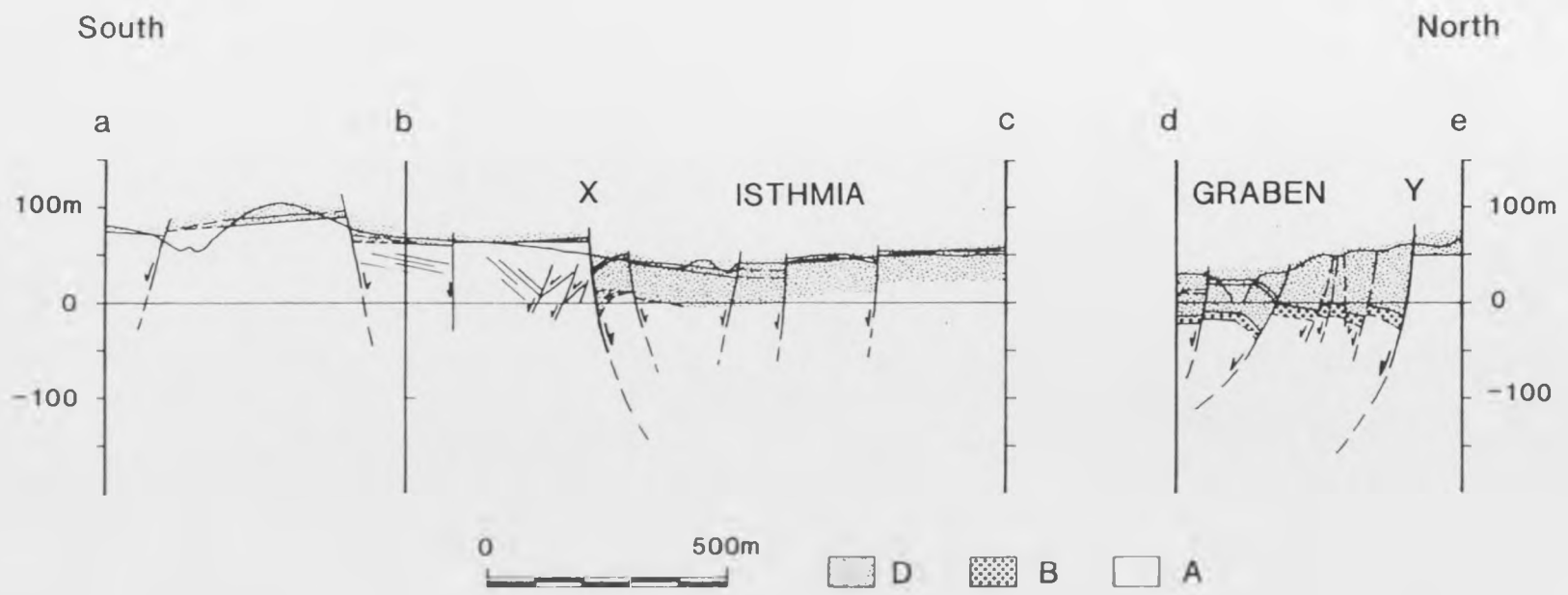
South
North
a
b
c
d
e
X
ISTHMIA
GRABEN
Y
100m
0
−100
100m
0
−100
0
500m
D
B
A

facilitated by normal faulting. Alluvium-infilled growth wedges developed in the hangingwalls to normal faults at the base of the sub-sequence. Corals from these yellow sands, near the SE end of the canal (87.29.8.1, fig. 4.1), have been dated at 205 +13 - 12 ka (table 4.1).

4.5.5 4th Sub-Sequence

At the NW end of the canal, soil profiles developed above the marine deposits of the 3rd sub-sequence indicate that a relative fall in base-level occurred before deposition of the 4th sub-sequence. This more limited sub-sequence comprises oolitic calc-arenites and contains the marine gastropod Natica sp., and is interpreted as another marine transgression onto the Corinth Isthmus from the west.

The 4th sub-sequence oolites are only 2-3m thick, although sand waves of the same material (facies S8 or S9 in the terminology of chapter 5) increase this value to c. 3-4m.

4.5.6 5th Sub-Sequence; Holocene

The oolites of the 4th sub-sequence are overlain by alluvium, soils and fluvial peridotitic sands which are probably early Holocene in age as they extend across beach-rock which is itself continuous into the present beach environment.

Since present sea-level was attained, beach conglomerates and sands have prograded extensively to the west and east of the Isthmus. They probably overlie a wave-cut platform that marks the initial Holocene eustatic highstand. The beach sediments underwent beachrock cementation in the shallow waters above this platform (at depths of c. 0.5-2m). Beachrock is now exposed up to 0.5m above present mean sea-level at both the NW and SE ends

of the canal. Such exposure implies a relative base-level fall since the early Holocene of c. 1-2.5m, whether by eustatic fall or tectonic uplift or some combination of the two.

The beachrocks are overlain by up to 6m of alluvial deposits, perhaps reflecting earlier Holocene climatic conditions that enhanced rates of erosion. The sands and soils are distal to an alluvial fan east of the town of Loutraki, which supplies ophiolite-derived material into the basin from the northern footwall margin to the basin.

4.6 DATING OF CANAL SEDIMENTS

4.6.1 Previous Chronostratigraphy

The Quaternary lacustrine and marine sediments of the Corinth Basin present problems when trying to establish a chronostratigraphy. Varied ostracod and foraminifera faunas are recognised but all assemblages, whilst providing useful environmental indicators, fail to allow any subdivision of the vertical stratigraphy (appendix 1). As discussed in section 2.3.2, attempts have been made to subdivide the Pleistocene on the basis of macrofaunal elements, e.g. associating the gastropod Natica lactea with the Tyrrhenian (Freyberg 1973, Sebrier 1977, Keraudren 1979). Such elements have since been shown (Vita-Finzi & King 1985) to reflect environmental conditions and are not time-specific as previously suggested.

A number of ^{14}C dates have been generated from bivalves in the canal region (Vita-Finzi & King 1985). It should be recognised, however, that evidence should be presented that sample specimens have not undergone recrystallization of their original aragonite.

Such alteration would generate meaningless dates. Only one ^{14}C date, of 38,320 +1590 -1340 years b.p., has been obtained from sediments in the canal section itself (sample 302a of Vita-Finzi & King 1985).

4.6.2 U-Series Disequilibrium Dating

New geochronological data are presented from uranium-series disequilibrium dating of Scleractinian corals (Acropora sp.) found in the marine sediments of the canal area. U-series dating of corals is possible owimg to their assimilation of uranium of a similar isotopic composition to the sea water in which they grew (Ivanovich & Harmon 1982, Bender et al 1979). Marine waters have an average initial $^{234}U/^{238}U$ activity ratio of 1.14 $\pm$ 0.02 (Ivanovich & Harmon 1982). ^{230}Th, the daughter isotope of ^{234}U, is highly insoluble in near-surface sea water and therefore virtually absent in living corals. With decay of ^{234}U to ^{230}Th, the relationship of $^{230}Th/^{234}U$ with $^{234}U/^{238}U$ activity ratios changes with time along a curve for a given initial $^{234}U/^{238}U$ ratio, assuming a closed system. The age of the coral can therefore be calculated, with a practicable limit to the method at about 350 ka.

One potential problem with the dating method arises if the coral aragonite has suffered any dissolution. In this case ^{234}U would be leached out but the highly insoluble ^{230}Th would remain, so that results would become distorted. Samples are therefore examined for signs of possible dissolution.

Coral samples were washed and then cleaned in an ultrasonic acetone bath. Specimens were analysed by x-ray diffraction to identify and reject coral samples whose original aragonite

structure was recrystallized to calcite or contaminated by detrital or calcite cements (appendix 2). Examination of corals under SEM (plate 4.2) established that some samples had suffered some vadose dissolution. These were rejected, as the daughter isotope ^{234}U would be preferentially leached compared with ^{230}Th. These rigorous sample preparations, although not infallible, provide a reasonable degree of confidence in the results obtained when supported by back-calculated initial $^{234}U/^{238}U$ activity ratios which are realistic and self-consistent (within analytical error). Samples listed in table 4.1 met the above criteria and also have similar U contents to living coral specimens, a further prerequisite of reliable dating material.

Th ratios provide a further check on whether a sample is a suitable specimen for dating. The presence of ^{232}Th in a sample relates to the degree of contamination by detrital calcite. The occurrence of ^{232}Th would imply an initial presence of non-radiogenic ^{230}Th, i.e. ^{230}Th derived from an earlier sediment rather than from the decay of ^{234}U taken up by the coral from its sea water environment. 87.7.8.1, 87.29.8.1 and 87.26.8.1b (table 4.1) have acceptably high $^{230}Th/^{232}Th$ ratios.

87.29.8.1 and 87.26.8.1b give finite dates of good quality. Their implied initial $^{234}U/^{238}U$ ratios are identical (within analytical error). This value is higher than that of average sea water (1.14 $\pm$ 0.02, Ivanovich & Harmon 1982), though results overlap at 1 σ. But it is worth noting that freshwater typically has a $^{234}U/^{238}U$ activity ratio in the range 1.2 - 1.3. It is reasonable to expect higher than average $^{234}U/^{238}U$ values in near-surface waters on the coast of a landlocked gulf such as in the Corinth Basin during the late Pleistocene. Umemoto

Plate 4.2

Scanning electron micrographs of coral specimens:
a) Sample 87.29.8.1 showing radial aragonite structure and clean, smooth surfaces to septum. x200 at 5kV.
b) Sample 87.7.8.1 revealing radiating needle structure of aragonite at high magnification. x1100 at 5kV.
c) Sample 87.26.8.1a with some dissolution of original aragonite suggested by the rough septal surfaces. Some blocky detrital calcite may be seen. The anomalous age of >350 ka for this sample was therefore rejected.

a

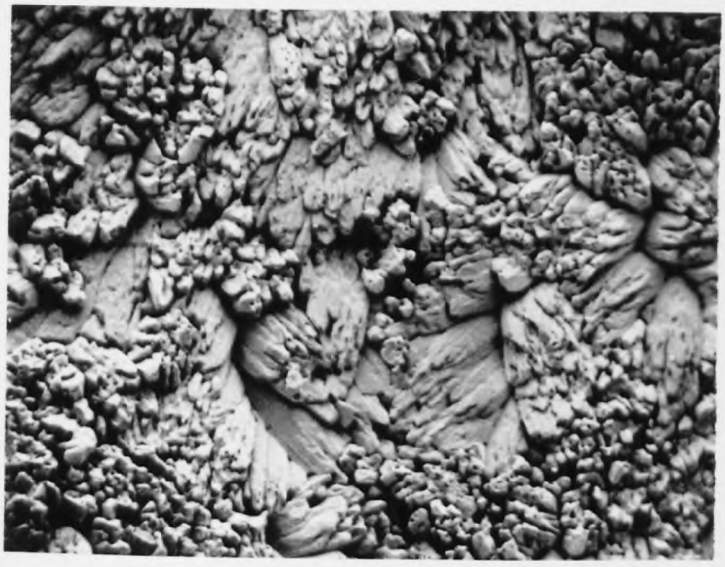

b

c

Table 4.1

U-series results for Acropora sp. corals from the Corinth canal area. See text for discussion of results. Analytical procedures were similar to those detailed in Ivanovich & Harmon (1982) and Atkinson et al (1978). 87.7.8.1 was prepared as an homogenised powder; coral fragments were hand-picked from 87.29.8.1 and 87.26.8.1b. Samples were dissolved in 2M HNO_3. A $^{232}U/^{228}Th$ spike solution was added during dissolution. The addition of a few milligrams of Fe allowed the U and Th to be coprecipitated with $Fe(OH)_3$ at pH10. The precipitate was washed and taken up in HCl. U and Th were separated and purified on ion exchange columns, then electroplated onto stainless steel discs. Isotope activities were measured by α-particle spectrometry. Error margins (bracketed) are based on counting statistics at 1σ. This author is grateful to Dr Tim Atkinson of the University of East Anglia for carrying out these analyses. UEA numbers are his laboratory analysis reference numbers.

	87.7.8.1 (UEA 305)	87.29.8.1 (UEA 316)	87.26.8.1b (UEA 318)
U concentration (ppm)	2.525	2.936	3.268
$^{234}U/^{238}U$	1.06 (0.01)	1.11 (0.02)	1.08 (0.01)
$(^{234}U/^{238}U)_o$	-----	1.19 (0.04)	1.19 (0.04)
$^{230}Th/^{232}Th$	124.1 (9.0)	105.7 (8.4)	113.9 (10.4)
$^{230}Th/^{234}U$	(1.15 (0.02))	0.87 (0.02)	0.97 (0.02)
Age (years)	(>350 000)	205 200 $^{+13\,000}_{-11\,700}$	311 800 $^{+33\,400}_{-25\,800}$

(1965) and Koide & Goldberg (1965) have recorded $^{234}U/^{238}U$ activity ratios as high as 1.18 ± 0.01 at near-coastal sites in surface waters subject to freshwater influence. The data derived from 87.29.8.1 and 87.26.8.1b are therefore consistent with the geological setting and thought to be reliable.

The analysis of 87.7.8.1, from the central horst block below the first unconformity (fig. 4.2), reveals a $^{230}Th/^{234}U$ value greater than that expected from a closed system sample, even of infinite age (given an initial $^{234}U/^{238}U$ activity ratio in the range of marine waters). The high value may be due to preferential leaching of ^{234}U over ^{230}Th. The high $^{230}Th/^{232}Th$ ratio of 124 ± 9 seems to exclude the possibility of significant detrital-sourced non-radiogenic ^{230}Th affecting the sample.

It is possible to obtain an approximate age of 87.7.8.1 from its $^{234}U/^{238}U$ ratio if one assumes this ratio would have been maintained during any leaching, i.e. that the two isotopes are equally soluble. For this calculation the initial $^{234}U/^{238}U$ value for sea water is taken to have been the same as that calculated for 87.29.8.1 and 87.26.8.1b, as the samples come from similar depositional and palaeogeographic settings. The age of the sample can be calculated from the equation:

$$\left[\frac{^{234}U}{^{238}U} - 1\right] = \left[\left(\frac{^{234}U}{^{238}U}\right)_o - 1\right] e^{-\lambda_{234} t} \qquad \text{Equation 4.3}$$

If $^{234}U/^{238}U = 1.0601 \pm 0.0095$, $(^{234}U/^{238}U)_o = 1.19 \pm 0.04$ and $\lambda_{234} = 2.7946 \times 10^{-6}\ a^{-1}$ then t = 412 +130 (+62) -137 (-53) ka.
Errors are the maximum margins for ± 1σ of the sea water ratio combined with ± 1σ of the measured $^{234}U/^{238}U$ activity ratio. Bracketed errors are for $^{234}U/^{238}U$ alone. This apparent age is beyond the accurate range of the dating method. A date older

than 350 ka conforms to the stratigraphic relation of 87.7.8.1 to 87.26.8.1b (fig. 4.2).

It should be stressed that the rare occurrence of corals in the Corinth canal area has limited the number of dates available so far to those given in table 4.1. But these geologically self-consistent results are considered by this author to outweigh the only available ^{14}C result already mentioned, which is itself near the limit of the ^{14}C dating technique.

4.7 DISTINCTION OF EUSTATIC AND TECTONIC CONTROLS

4.7.1 Interpretation of U-Series Results

The U-series dates of samples 87.29.8.1 and 87.26.8.1b correlate with $d^{18}O$ isotope stratigraphy peaks VII and IX respectively (refer to fig. 4.12). The most complete stratigraphic section, in the canal section to the NW of the central horst block, includes four sub-sequences starting with that dated at 312 +33 - 26 ka. Given the occurrence of the sub-sequence to the SE with an age of c.205 ka (peak VII), these four sub-sequences are interpreted as corresponding to the major eustatic highstands of oxygen isotope stage peaks IX, VII, V and I (Holocene). This sequence of major transgressive events is in agreement with the predicted stratigraphic profiles of coastal migration on an uplifting coastline (fig. 4.5). The observed sub-sequence geometries are therefore related to major eustatic sea-level fluctuations of c.100 ka wavelength. Cliffs cut into the sub-sequence bounding uncomformity surfaces probably relate to subordinate sea-level peak and/or trough stillstand events. However, the tectonic control of these latter features cannot be discounted, given the limits of available chronological

Figure 4.12

Oxygen isotope data (Imbrie at al 1984) and inferred sea-level curve for the Late Quaternary. For quantification of uplift rates:
a = depositional depth;
b = the difference between syn-depositional sea-level and present sea-level;
c = present outcrop height above sea-level;
d = extensional subsidence;
e = minimum uplift rate;
f = uplift rate.

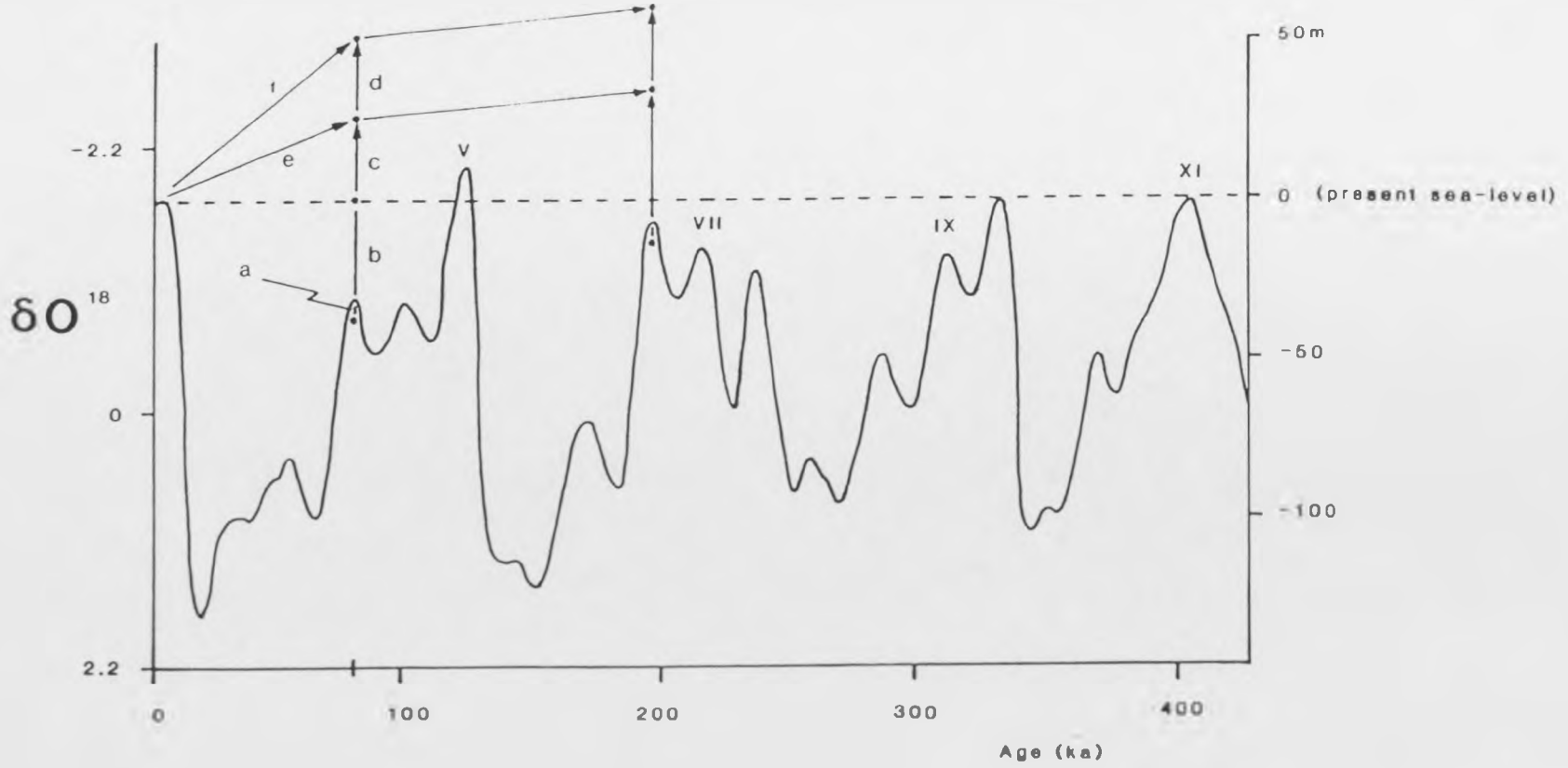
δO 18
-2.2
0
2.2
a
b
c
d
e
f
V
VII
IX
XI
50m
0 (present sea-level)
-50
-100
0
100
200
300
400
Age (ka)

constraint.

If a similar sequence of events is extrapolated back in time, then the 1st sub-sequence might tentatively be ascribed an age of c.400 ka, equivalent to $d^{18}O$ stage peak XI. The marine deposits at the top of the "Corinth Marl" sequence may in turn be c.500 ka in age.

4.7.2 Structural Evolution of the Corinth Isthmus

Periods of normal fault activity which have affected the canal sediments in the late Quaternary can be defined as follows: Tilt block rotations and consequent unconformities occurred during the depositional history of the "Corinth Marl" lacustrine-to-marine sequence and during the unconformity interval prior to the deposition of the 1st transgressive sub-sequence.

At the SE end of the canal normal growth faulting controlled the thickness of the 3rd sub-sequence. Syn-sedimentary faulting was concentrated on specific structures, generating the intrabasinal Isthmia Graben (fig. 4.11). This rapid tectonic subsidence of the eastern Isthmus, which accentuated the effects of the syn-sedimentary eustatic base-level rise, relates to the latest Quaternary tectonic collapse of the Saronic Gulf. The eastern area of the Corinth Basin was a structural high, supplying sediment onto the southern Corinth Isthmus until late in the Quaternary depositional history of the basin (section 5.6). Minor effects of normal faulting are observed in the 3rd sub-sequence to the NW of the central horst (fig. 4.2).

The remaining normal faulting and reactivation events on precedent structures in the canal section are post-depositional. Additional extensional subsidence has occurred across the Corinth

Basin through the Late Quaternary. Unfortunately, the total subsidence value cannot be directly calculated owing to the lack of stratigraphic markers in the basin margin footwalls.

4.8 QUANTIFICATION OF TECTONIC DISPLACEMENTS

An attempt can be made on the basis of available U-series age data to quantify the tectonic component to relative base-level change, i.e. to quantify the net rate of uplift of the Isthmus of Corinth. This is achieved by subtraction of estimated syn-depositional eustatic base-level from the observed present outcrop level of dated sediments.

The post-depositional tectonic displacement of a dated Late Quaternary sediment may be estimated in the following way. The depth below sea level at which the dated sediment was deposited must first be estimated (factor a in fig. 4.12). The Acropora sp. corals of the Corinth area probably lived in a water depth of 10 $\pm$ 10m, in which Scleractinians thrive, although some species can range into the lower levels of the photic zone. Dating of the sediment allows the estimation of sea-level at the time of deposition by reference to the late Quaternary sea-level curve, factor b (fig. 4.12). For the Corinth canal examples, highest sea-level values within the date error margin are utilised so that this factor is a minimum value. The difference between present sea-level and the current height of outcrop of the dated sediment is termed factor c. The summation of factors a, b and c determines the minimum uplift rate averaged across the time interval since deposition (e, fig. 4.12).

If syn-depositional sea-level were lower than the ascribed peak, then the subsequent uplift would be greater than the rate as calculated. If the site had been subject to any post-

Figure 4.13

Graph of minimum uplift rates estimated for dated Corinth Isthmus sediments.

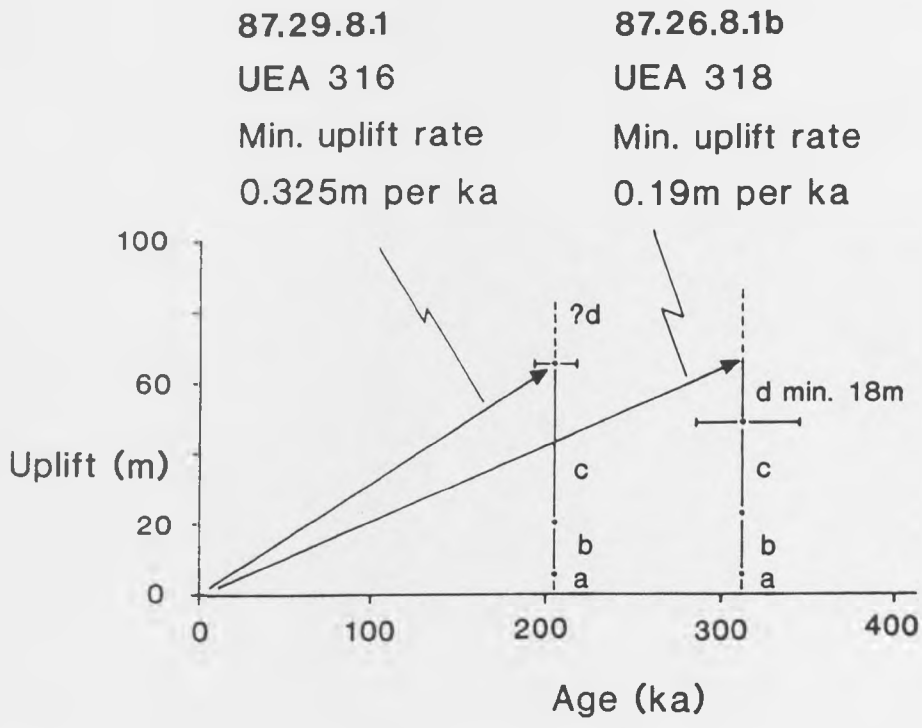
87.29.8.1
UEA 316
Min. uplift rate
0.325m per ka
87.26.8.1b
UEA 318
Min. uplift rate
0.19m per ka
100
60
20
0
Uplift (m)
?d
d min. 18m
c
c
b
b
a
a
0
100
200
300
400
Age (ka)

depositional subsidence, in competition with the background tectonic uplift in the case of the Corinth Isthmus, then a factor d (fig. 4.12) equal to the post-depositional subsidence would have to be added to attain the true uplift rate (f). This component d cannot be quantified for sample 87.29.8.1. A minimum value for d of 18m represents the summation of post-depositional down-faulting displacements on normal faults between 87.26.8.1b and the central horst block (faults are sub-vertical and rotations neglible).

Figure 4.13 presents minimum tectonic uplift rates calculated on the basis of dated corals 87.29.8.1 and 87.26.8.1b. Error margins on the age of 87.7.8.1 preclude any worthwhile result. It must be emphasized that the 0.325m per ka uplift rate inferred from 87.29.8.1 is a minimum value averaged over the last c. 205 ka. The tectonic uplift of the Isthmus has not necessarily been at a constant rate and spasmodic post-depositional extension which is recognised may have resulted in spasmodic subsidence in competition with the uplift vector. Further good quality dates from the area will improve the constraint of structural deformation rates through time.

4.9 CONCLUSIONS

First order models of expected stratigraphic profiles may be simulated by relating known sea-level fluctuations for the Late Quaternary to specific tectonic and depositional settings. Two-dimensional cross-sections represent the migration of a coastal beach profile in response to eustatic sea-level variation for the last 430 ka. On an uplifting coastline facies geometries are characterised by major transgressive events correlating with the transgressive peaks of eustatic cycles of c. 100 ka duration.

Deposition rather than erosion is facilitated by the rate of eustatic sea-level rise exceeding the rate of tectonic uplift.

The sedimentary facies of the Corinth canal area, central Greece are re-interpreted as repeated fining-up beach-to-shoreface transgressional sub-sequences. Each sub-sequence is bounded by unconformity surfaces on the Corinth Isthmus. Further to the west, sub-sequences merge into one variably lacustrine or marine sequence below the base-level minimum.

Scleractinian corals recovered from the canal area have been successfully dated using the U-series disequilibrium method. Available dates correspond to Late Pleistocene eustatic base-level maxima and appear to confirm that the observed marine sub-sequences were deposited during the transgressive peaks of c. 100 ka eustatic cycles.

Episodes of syn-sedimentary normal faulting are identified within the Late Quaternary history of the Corinth Isthmus, including the development of the 1km wide Isthmia Graben. Post-depositional vertical tectonic displacements of dated sediments may be quantified after estimation and subtraction of syn-depositional sea-level. At locality 87.29.8.1, a minimum uplift rate of 0.325m per ka is derived, averaged over the last c. 205 ka. This figure is in excess of post-depositional extensional subsidence rates in the central Corinth Basin.

CHAPTER 5 RECENT EVOLUTION OF THE SOUTHERN CORINTH BASIN

5.1 SUMMARY

A facies scheme is outlined for marine deposits outcropping in the southern Corinth Basin. Facies associations range from beach to shelf environments. Shoal developments of oolites are common and tidal currents generated large-scale bedforms including tidal sand waves and a 2.7km long longitudinal sand wave.

The distribution of marine facies is interpreted to have been controlled by a syn-sedimentary fault-induced topography. Beach and oolitic facies occupy structural highs. Structural features modified tidal currents, generating velocities above 1m s^{-1} by the concentration of flow through an inferred narrow connection between the Gulf of Corinth and the Aegean Sea to the east.

Extensional faulting after a relative sea-level fall produced a train of 200-400m scale tilt blocks with growth-infills of alluvial sediment. Ooarenites were reworked off tilt block footwall crests and supplied laterally into structural lows. Braid stream deposits were transported east to west through structural lows. The implications of these facies patterns are discussed in terms of the post-depositional uplift of the southern Isthmus and the relative subsidence of the Saronic Gulf area.

5.2 INTRODUCTION

This chapter considers further the Late Pleistocene - Holocene history of the Corinth Basin. Specifically, a sedimentary

analysis is carried out of marine sediments in the southern Corinth Basin. These are inferred to be of Late Pleistocene age. The deposits are then considered in relation to their syn-depositional structural and eustatic environment. The structural deformation of the southern part of the basin is described since deposition of the marine sediments. The synchronous effects of eustatic base-level changes and climatic variation are included in this discussion of the recent evolution of the basin.

A second theme developed in this chapter relates to the range of scales at which structuration may affect sedimentary facies patterns. Extensional tilt block trains are shown to have controlled facies geometries at certain times and localities within the basin history. Chapter 3 explored the distribution of facies on a basinwide scale in an evolving extensional graben (or half-graben). Here, analagous features of lateral distribution systems and axial transport systems are described around intrabasinal fault blocks of a few hundreds or even tens of metres in scale.

The southern Corinth Basin has, like the central Isthmus discussed in chapter 4, undergone uplift in its recent history. Marine deposits occur up to 140m above present sea-level (fig. 5.1). This figure therefore represents the minimum uplift since deposition of those sediments, assuming present sea-level is near the eustatic base-level maximum. This uplift has provided the opportunity to study further the pattern of syn-rift sedimentation direct from outcrop.

A single marine (sub-) sequence is exposed in the south of the basin. This lies unconformably on predominantly fluvio-

Figure 5.1

Areal distribution of marine facies in the southern Corinth Basin. The map records facies inferred to have been deposited at the relative sea-level highstand position.
a, b and c locate logs in figure 5.2.
AC = Ancient Corinth
Ex = Examilia
X = Xilokeriza
K = Kechriae
Contours at 100m intervals

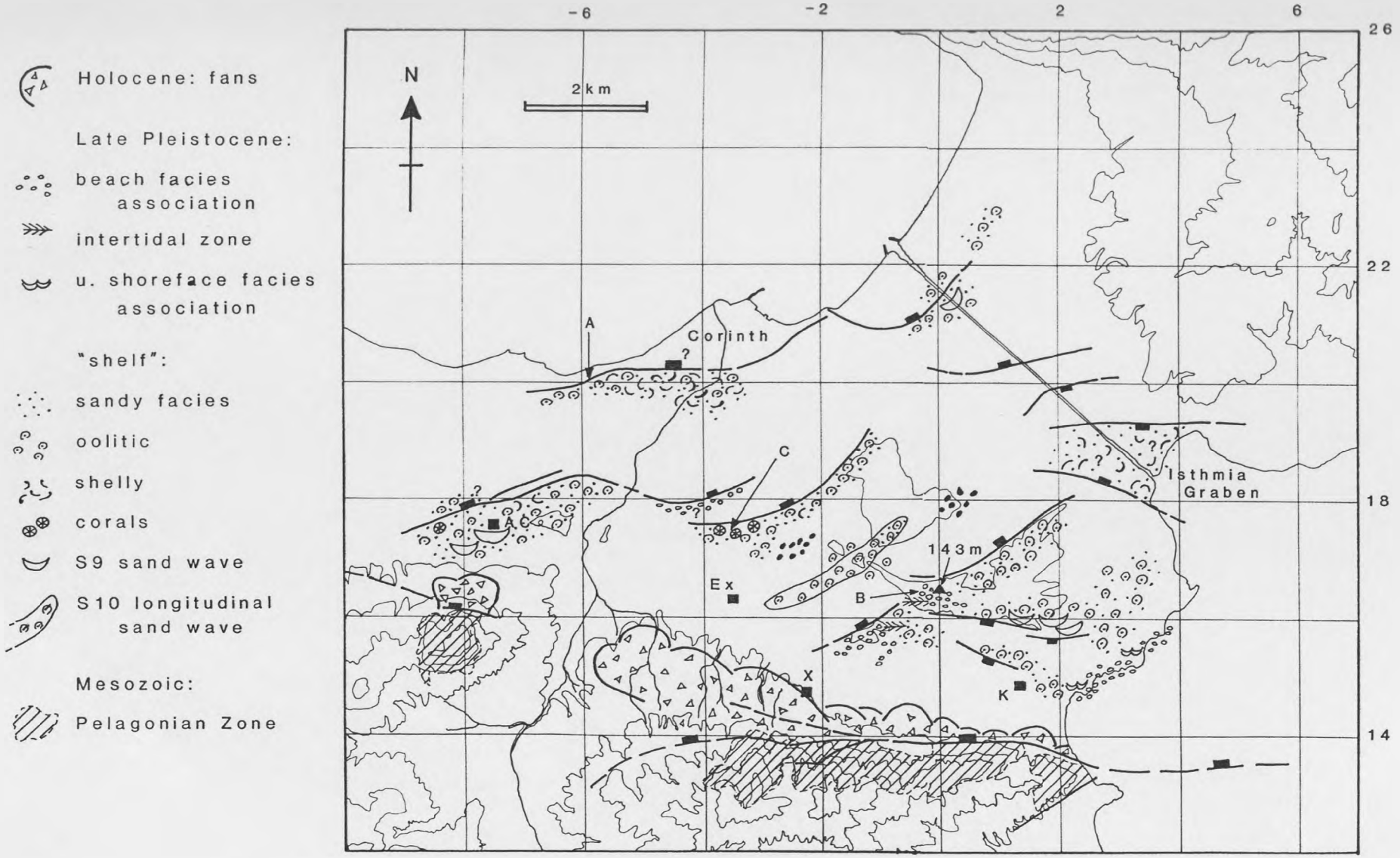
Holocene: fans
Late Pleistocene:
beach facies association
intertidal zone
u. shoreface facies association
"shelf":
sandy facies
oolitic
shelly
corals
S9 sand wave
S10 longitudinal sand wave
Mesozoic:
Pelagonian Zone
-6
-2
2
6
26
22
18
14
N
2km
A
Corinth
?
C
Isthmia Graben
143m
Ex
B
X
K

lacustrine deposits characterised by the "Corinth Marls" (e.g. 13.9.1, appendix 1). Alluvial fines to streamflow conglomerates extend into the assumed-lacustrine marl sediments around the village of Ancient Corinth. Further to the north, however, basinal calcareous muds include a marine microfauna (10.5.1, appendix 1), indicating the presence of hidden stratigraphic and/or environmental boundaries within the "Corinth Marls".

The age of the deposits exposed to the south of Corinth is poorly constrained. Stratigraphic studies of Freyberg (1973) and others have relied on chronological associations of certain macrofaunal members, such as the gastropod Strombus bubonius which has been associated with the Tyrrhenian (Keraudren 1979). The dangers and inadequacies of this approach have already been discussed in chapter 2. As have the only previous U-Th dates on molluscs from the area, as given in Sebrier (1977). The following study ascribes a Late Pleistocene and possibly Tyrrhenian age to the marine deposits exposed across the southern Corinth Basin. This is based on the lateral continuity of marine facies towards the 4th marine sub-sequence of the canal section. The oolitic facies unique to this 4th sub-sequence in the canal is additionally common to the marine deposits exposed south of the Isthmus. The tectono-eustatic "event stratigraphy" allied to the currently available U-Th dates from the canal area supports the Tyrrhenian age inferrence. Isotopic dating of suitable materials will have to be carried out to provide independent evidence on these interpretations. At the time of writing, this author is awaiting the results of U-Th dating on coral samples from marine deposits 3km south of Corinth.

The first part of this chapter describes the range of facies seen

in the marine sub-sequence across the southern Corinth Basin. The beach to shoreface range of facies associations is distinct from those characterising the 1st to 3rd marine sub-sequences in the canal section. The distribution of facies across the southern area is then related to the syn-depositional structure of the southern part of the basin. Additional eustatic and climatic controls on facies style and distribution are then discussed in relation to the marine sub-sequence and subsequent deposits.

The structural development of the southern Corinth Basin is outlined, emphasizing the importance of fault block rotations in determining facies patterns in three dimensions. And the combined effects of structuration, eustatic and climatic variation are then considered in a broader discussion on the Late Pleistocene - Holocene evolution of the basin.

5.3 FACIES DESCRIPTIONS AND INTERPRETATIONS - MARINE DEPOSITS OF THE SOUTHERN CORINTH BASIN

5.3.1 Conglomerate Facies S1

Description:

This facies encompasses a range of conglomerates. These vary in grain size and in degree of organisation. The common characteristics are that the conglomerates are texturally mature and poor in matrix fines. Grain size varies from granule to large pebble grade. Grain size sorting is good and clasts are typically rounded to very rounded with a high degree of sphericity. Provenance is essentially from the Pelagonian Zone Mesozoic lithologies to the south, being dominated by micritic

carbonates, with red, grey and black cherts and further fine-grained siliciclastics. Towards the Corinth Isthmus the proportion of serpentinites increases. Basin sediment intraclasts are rare. Additional features include rare marine bioclastics (notably echinoid remnants) and molluscan-borings to some clasts. Bedforms are variably developed. The range is from apparently disorganised conglomerate lenses and beds up to 0.4m in thickness to well-structured cross-stratified units 0.1 - 0.7m thick in which clast imbrication (often bi-directional) is common.

Interpretation:

The high maturity of this conglomerate facies suggests a high energy environment with a prolonged history of clast reworking. The open-matrix texture supports this requirement, further emphasizing the extreme sorting that characterises the facies. A marine influence is suggested by the faunal remains, the presence of molluscan-bored clasts typifying the littoral zone. A beach conglomerate facies is therefore inferred, as this environment covers the range of textures and bedforms observed. The continuity of this facies into the sub-littoral shoreface environments is not, however, excluded. The common occurrence of conglomerate facies S1 directly over the Top "Corinth Marl" unconformity complies with this interpretation, these basal conglomerates representing a transient beach environment of a transgressive coastline (fig. 5.2a and plate 5.1a).

5.3.2 Unidirectional and Herringbone Cross-Bedded Facies S2

Description:

This range of unidirectional and herringbone cross-bed forms

Figure 5.2

Selected logs through marine sub-sequence sediments. See figure 5.1 for locations.
a = log, grid ref. -5.80 20.10 (Greek national 1:50,000 grid)
b = log, grid ref. 0.30 16.37
c = log, grid ref. -3.52 17.55

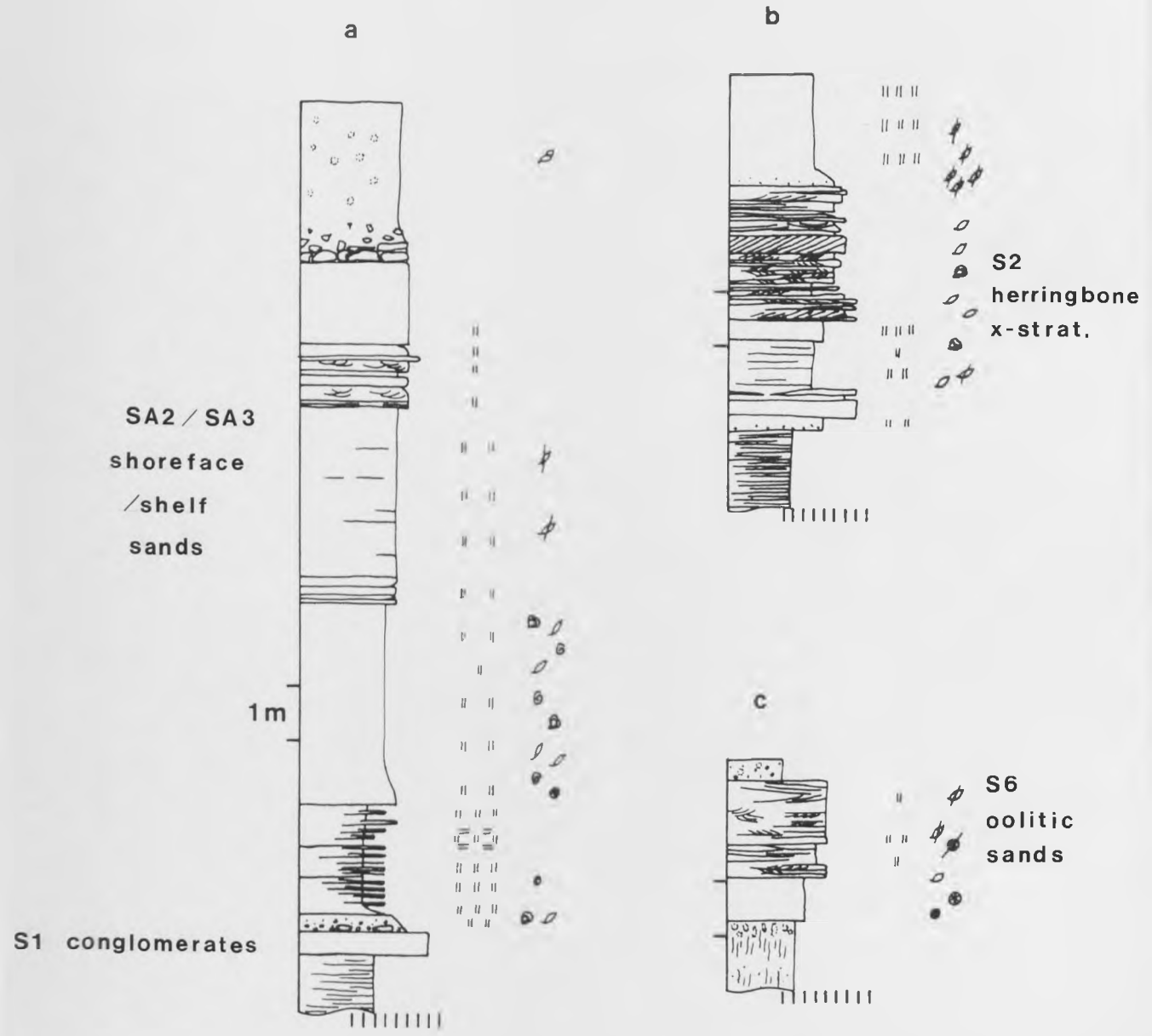
a
b
SA2 / SA3
shoreface
/shelf
sands
1m
S1 conglomerates
S2
herringbone
x-strat.
c
S6
oolitic
sands

Plate 5.1

a) Facies S1 basal conglomerates, with S5/6 facies above. 1st Corinth scarp (see log, fig. 5.1a), grid ref. -5.78 20.10

b) Facies S2 herringbone cross-beds, see fig. 5.2b, grid ref. 0.30 16.37

c) Photomicrograph of oolitic sands from facies S10 longitudinal sand wave, grid ref. -2.42 16.28
Slide 49774, XPL, scale bar = 0.5mm

d) Facies S7 cross-stratification at base of S9 sand wave, see fig. 5.4, grid ref. 2.20 15.68

e) Facies S9 (type A) sand wave, grid ref. 2.40 15.75

f) Internal bedding surfaces of south-facing sets facies S10 longitudinal sand wave, grid ref. -2.35 16.33

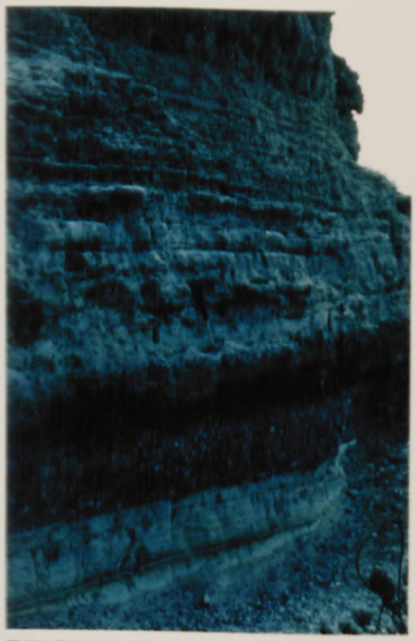

a

b

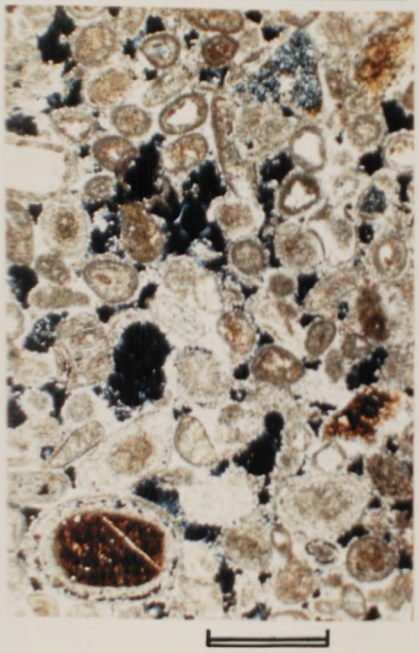

c

d

f

e

occurs within a grain size range from fine sand to granule grade. Cross-bedding units are planar and vary from 2 to 15cm in height. Textural sorting is good, with coarser grade deposits being matrix-poor. Asymmetric ripple trains in lenses, single planar cross-beds and climbing ripple sets are included in facies S2. Herringbone cross-bedded units exhibit opposing directions of foreset laminae in adjacent layers (plate 5.1b, fig. 5.2b). The two directions of foreset dip are typically at approximately 180° to each other.

Interpretation:

The well-sorted nature of these sand-granule units suggests significant high energy reworking, such as by wave action. The generation of unidirectional ripple cross-beds indicates that unidirectional current shear stress prevailed during the period in which the cross-bedded unit was deposited. Longshore currents and rip currents at high angle to a shore may produce such an environment as a product of wave motions. Alternatively, a dominant tidal current might have generated shear stresses sufficient to produce ripple laminae whilst the opposing tidal current was insufficiently strong to generate the bedform. The herringbone units suggest that opposing tidal currents were both sufficient to generate ripple foreset laminae. A littoral to sub-littoral environment is inferred.

5.3.3 Symmetric-Rippled Sand Facies S3.

Description:

Included in this facies is a range of symmetric and draped ripple lamination morphologies. Ripples are developed in fine to medium sands and often occur in association with planar-laminated

sands (facies S5). Drapes are typically of calcareous silts. The sands themselves are of mixed carbonate and siliceous composition. Ripples show a continuum from facies S2 asymmetric to symmetric ripples, but it is those with high symmetry indices (horizontal length of stoss side / horizontal length of lee side) which are included in this facies. There is also a trend from stacked symmetric ripples to bundled, larger trough cross-beds (facies S4). Symmetric ripples range in dimension from about 2 to 5cm in height and 3 to 10cm in wavelength. The internal structures of symmetric ripple stacks include chevron overlaps in ripple crests and troughs, aggradational sand layers parallel to underlying ripple forms, and eroded ripple crests. Alternatively, symmetric ripple surfaces may discordantly cross-cut underlying ripple forms in which foreset laminae may be unidirectional. Silt drapes may parallel ripple laminae or preferentially infill ripple troughs.

Interpretation:

The bi-directional current influence indicated by symmetric ripples signifies the prevalence of tidal or wave action, both of which will occur in the littoral or shallow sub-littoral zone. The variety of internal lamination geometry reflects a range in the relative strengths of forward and backward currents. An internally symmetric chevron structure may occur if both forward and backward currents are strong enough to produce foreset laminae. Aggradational chevron ripples will develop given two conditions; adequate sediment supply and ripple laminae being in-phase with both current motions. The internal symmetry of ripple laminations will decrease with increased asymmetry of opposing current strengths. Unidirectional foreset laminae in ripples of symmetric morphology will result when the lesser

current motion is sufficient to maintain the symmetric external form but insufficient to generate foreset laminae.

5.3.4 Trough Cross-Bedded Facies S4

Description:

Trough cross-beds occur in sediments across sand and granule grades. The sparcity of 3-dimensional outcrop precludes the subdivision of trough bedforms according to morphologies in plan view. Facies S4 incorporates a range of cross-bedding types, therefore, with bedding scale varying from about 5 to 10cm in height and 10 to 30cm in width. One special case may be recognised, which shows relatively symmetric trough cross-bedding and typically exhibits a "bundled" trough habit with vertical (aggradational) cross-bedding growth. Marine shell fragments locally occur in association with facies S4, as lag concentrations on trough bed surfaces.

Interpretation:

A marine environment is inferred from the occurrence of marine bioclastics within facies S4. The trough cross-bedding is interpreted as the product of the migration and accretion of ripples in the upper shoreface and beach face. Trough cross-bedding is particularly common in the breaker and inner rough zones of the beach face in a high wave energy environment (H.E. Clifton, pers. comm.). Ripples reflect the asymmetry of wave currents down the beach face, while bundled, in-phase trough beds suggest a more oscillatory wave-dominated current influence.

5.3.5 Planar-Laminated Sand Facies S5

Description:

Facies S5 covers a basket of detailed planar-lamination forms. These include fining-up and non-graded laminae and diffusely-bedded units. The composition of the clastics may be dominated by carbonate, siliciclastics, serpentinites or by ooarenites. Grain sizes exhibiting planar-laminated beds range from coarse silt to granule and small pebble grades. Bioturbation of Skolithos facies (Seilacher 1967) may be absent or strongly developed to the point where primary sedimentary structures are totally destroyed. Marine gastropods and bivalves may locally be found in situ, though more commonly are fragmented as diffuse bioclastics.

Interpretation:

The variety of planar-lamination forms present reflects the range of environments and current mechanisms under which they formed. Laminations in fine to medium sands on a 1-2mm scale, with alternations in grain size and/or composition are common on beaches subject to wave action (H.E. Clifton, pers. comm.). The swash and backwash action of waves both supplies and sorts the sands. Where planar laminations of facies S5 occur in association with current ripple laminations (S2), the parallel bedding probably records deposition below the critical velocity of ripple formation, i.e. as lower stage plane beds. Fining-up and relatively diffuse planar beds may result from sedimentation out of suspension. The suspension of sediment may be achieved by wave or storm action, and grading will probably develop given an episodic alternation of suspension and sedimentation events. The degree of modification of planar-laminations by macrofaunal

burrowing will be a function of two interacting parameters; the rate of sediment supply (and remobilisation) over the depositional surface and the intensity of faunal activity.

5.3.6 Oolitic Sand Facies S6

Description:

Facies S6 encompasses a range of oolitic sands, predominantly of medium to coarse sand grade but including locally granule grade pisoliths. Ooids may make up more than 90% of the sediment detritus (e.g. plate 5.1c) or may be a minor component within a clastic sand. Ooids are most commonly nucleated around micritic carbonate. Other nuclei include siliciclastics, serpentinite grains and shelly fragments. In the best developed oolites, grain size sorting is good and oolitic rims are well developed and highly spherical. However, their is a range of oolite qualities down to unevenly developed ooids within clastic sands in which ooids are irregular in form and frequently fragmented. Pisoliths and grapestone aggregates also occur locally. Sedimentary structures developed within oolitic sands include S5 planar laminations and S7-10 cross-beds, in which case the ooarenites are described in these respective categories. S6 ooarenites are typically homogeneous and unstructured, with variable signs of bioturbation. They may contain shelly detritus and may locally be coralliferous. Oolites and pisolites locally occur as minor constituents within pebbley units poor in fines.

Interpretation:

S6 ooarenites are interpreted as having formed in high energy, relatively shallow shelf environments. Wave action and/or tidal

currents would have provided the energy to rework the developing ooids. Oolite formation resulted from the combination of carbonate-saturated waters and high water temperatures, conditions that would have suited high rates of algal activity. Ooid production would been concentrated in shoal areas. Ooarenite sedimentation may have occurred at some distance from these generative shoals, as storm and/or tide action reworked the ooids into deeper shelf environments. Pisolite growth probably records ooid generation in less continuously energetic environments, marginal to the main shoal environments. Grapestone developments may denote multiple ooid development-accummulation-storm reworking events. The occurrence of pisolitic pebbly units poor in fines is inferred to represent lags in between large scale S9 and S10 sand wave bedforms.

5.3.7 Large-Scale Planar Cross-Bedded Facies S7

Description:

These cross-bed forms are by definition bounded by planar (or sub-planar) surfaces. They are developed in medium to coarse grade sands. They range from 20-40cm in scale. Foreset laminae may be slightly concave-up or planar (plate 5.1d). Foreset orientations may be locally consistent or highly variable when associated with larger scale bedforms of facies S9 and S10.

Interpretation:

Large-scale planar cross-beds are produced by the preservation of current-induced megaripple and dune bedforms. For a given grain size, megaripples are generated by higher current velocities than would produce small-scale current ripples (unidirectional cross-

beds of facies S2). Alternatively, the relatively coarse sand grade material involved may determine the tendency to form megaripples or dunes, as against small-scale current ripples that might by generated in finer sands for the given current velocity. The shape of foresets will be controlled by the current velocity over the bedform and the bedload/suspension ratio (after Jopling 1965). An angular to concave-up foreset trend, for instance, denotes increased velocity as a greater proportion of material is taken up in suspension and carried forward to create a bottomset. Megaripple or dune orientations record the direction of maximum current velocity at the time of bedform generation.

5.3.8 Large-Scale Dune Facies S8

Description:

These dune forms are developed in medium to coarse grade sands. They vary in scale from about 0.5-3.0m. S8 dunes may lie directly on a planar surface or alternatively exhibit an aggrading habit, with a foreset and toeset developed (see fig. 5.4). The facies is locally associated with S9 sand waves, being developed on stoss surfaces of these large scale bedforms. In such cases, implied palaeocurrents are similar to those of the parent sand wave.

Interpretation:

The development of dune bedforms characterises the mid to upper flow regime. The angle of climb over the lower bounding surface will be determined by the rate of sedimentation against rate of migration of the dune form. Where associated with S9 sand waves, the evolution of S8 dunes indicates flow separation over a dune (perhaps of facies S7) which has encroached onto the stoss

surface of the sand wave in an unsteady flow environment. The dune then grows as it migrates up the sand wave, having set up the second order flow separation cell. Where S8 dunes are formed in isolation, they again indicate preferred growth of smaller-scale bedforms and may represent features that under appropriate conditions would have evolved into S9 sand waves.

5.3.9 Sand Wave Facies S9

Description:

Sand waves with a variety of detailed internal morphologies occur across the southern Corinth Basin and as far north as the canal on the Isthmus. They occur in calcarenites which are frequently, though variably, oolitic. The medium to coarse sand grade clastics which form the bulk of the arenites and the nuclei of the ooarenites are micritic carbonate and predominantly of basement origin, with subordinate bioclastics (molluscan, gastropod, echinoid and foraminiferal fragments). Sand waves range from 5 to 10m in height. The simplest morphology, type A (plate 5.1e), is of a simple dune form 5 to 8m in height with a low-angle climbing habit. The dune-crest is preserved above long foresets which dip at 20-25° and thin bottomsets which do not include smaller-scale ripple or dune forms. The example in plate 5.1e shows only limited developments of low-angle, convex-up erosional surfaces across the dune-crests and upper foresets. No small-scale bedforms are seen on the dune surface or within the foresets. Skolithos bioturbation of varied intensity is developed in the foresets. A variation to the type A sand wave may be seen in unique 3-dimensional outcrop on the Ancient Corinth archaeological site. The Fountain of Glauke is cut out of a sand wave at least 7.5m in height, exposing S- and SE-

dipping beds of the stoss side of the bedform. Sets of 5-30cm thickness both thin and thicken downslope, and are bounded by either convex-up or planar surfaces. Some are heavily bioturbated, others not. Small-scale contortions and brittle failure features are seen locally within individual foreset beds. The Fountain of Glauke sand wave has a north-facing, transverse dune geometry and in plan view is diagonally offset from a neighbouring sand wave under the NE corner of the Temple of Apollo (fig. 5.3).

A more complex type B sand wave morphology is seen to the north of the village of Kechriae (fig. 5.4). Large bedforms 6 to 10m in height comprise stoss-side sets dipping at about 8-10° and steep foresets dipping at about 18-20°. The foresets, however, include marked erosive discontinuities. No thick mud drapes are found across these surfaces, but some grain size variation, fining-up to coarse silt grade material occurs within individual 5-15cm sets. Bioturbation intensity varies considerably between sets. Smaller-scale dune forms of facies S8 migrate in piggy-back fashion over the primary duneform. Smaller-scale cross-stratification of facies S7 characterises the bottomset region. Current directions indicated by these small-scale bedforms are highly variable, but predominantly oppose the facing-direction of the primary S9 foresets (fig. 5.4).

Interpretation:

The association of bioturbated oolitic arenites with marine bioclastics in sand waves suggests these bedforms were produced in a marine environment. Tide-influence is inferred as the energy source for generating the sand wave bedforms. These require bottom currents of the order of 1.0 to 1.2 $m\ s^{-1}$ (Allen

Figure 5.3

Block cartoon illustrating bedforms in outcrop and interpreted sedimentary geometries on the Ancient Corinth archaeological site. Two north-facing facies S9 sand waves are diagonally offset. These are onlapped by interdigitated soils (irregular vertical hatching) and oolitic sands reworked off the exposed bedforms (light stipple). Bioturbated coarse sand (heavy stipple) and cross-stratified ooarenites above mark an apparent temporary resubmergence of the bedforms.

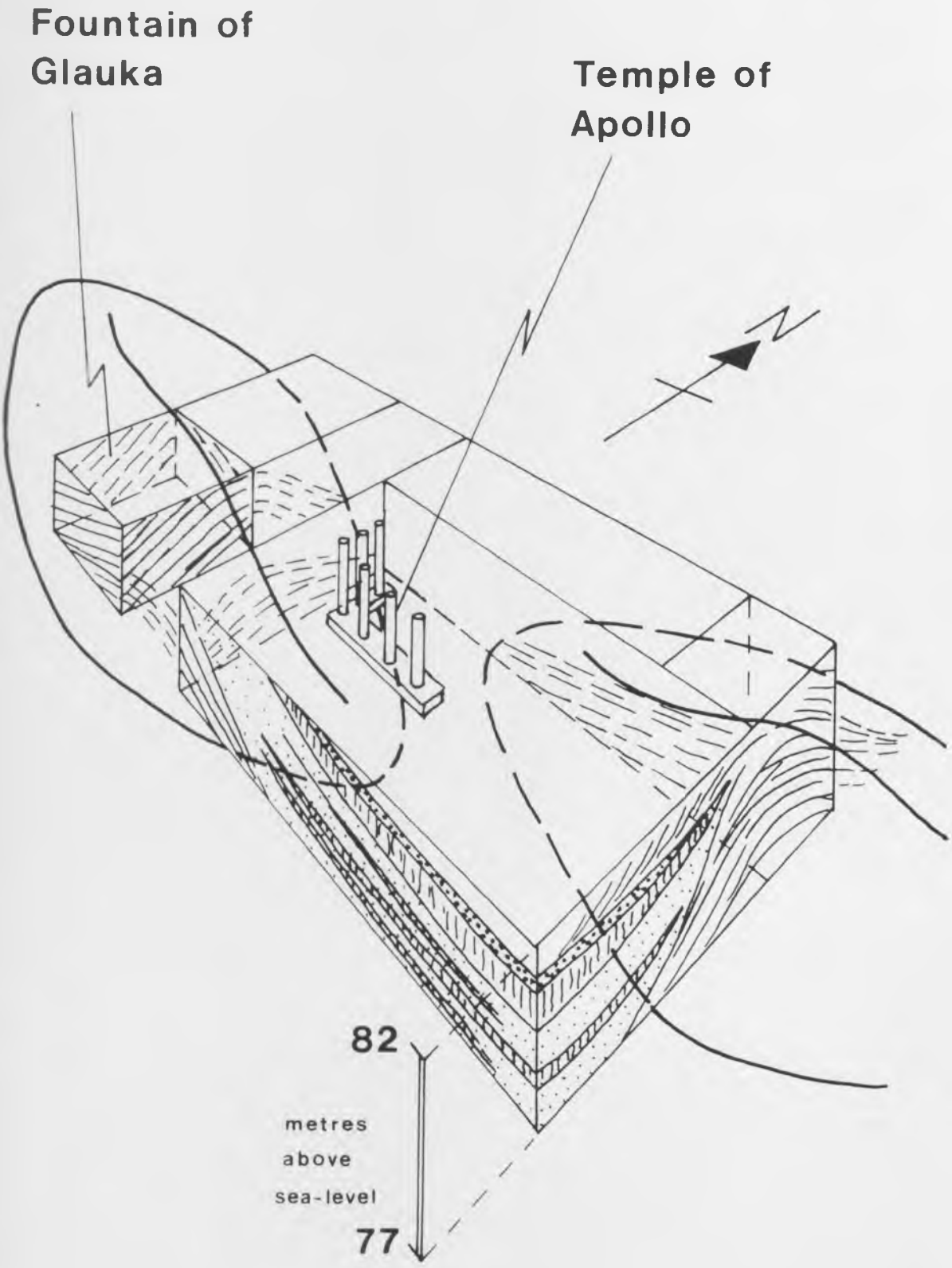
Fountain of Glauka
Temple of Apollo
N
82
metres above sea-level
77

Figure 5.4

Line drawing after photo-montage of a facies S9 (type B) sand wave 1km NE of Kechriae (grid ref. 2.20 15.68). A S8 dune is seen on the stoss side of the S9 sand wave, towards the left of the illustration.
[Palaeocurrent rose is not area-compensated.]


N
n=19
S9
S8
S7
3
m
0

1980). The external morphology of the sand wave is increasingly asymmetrical with increased time-velocity asymmetry of the tidal currents across the bedform. Their internal structure similarly depends on the strength of currents affecting the bedform.

The type A sand waves observed approximate to the class I and class II internal morphologies of Allen (1980). Bedforms are highly asymmetrical, indicating that bottom currents were effectively unidirectional. Any currents opposing the direction of sand wave migration were insufficiently strong to generate ripple or dune forms. Foreset accummulation was by avalanching of materials beyond the dune-crest. The climbing habit seen in some examples indicates a high rate of net deposition (over transport), analogous to the conditions needed for small-scale climbing ripple cross-lamination to develop. The variable intensity of bioturbation within sets reflects the more detailed spasmodic rate of sediment supply onto the foresets. The occurrence of convex-up erosive discontinuities may denote sediment reactivation with variation in flow stage, at least in the case of intermediates between type A and type B sand waves. Or such surfaces may reflect minor, random current direction fluctuations across the sand wave surface (Allen 1980).

The more complex internal structure of type B sand waves represents a correspondingly more complex interaction of current and sediment supply rates. The overall structure is again unidirectional. Facies S7 small-scale back-sets indicate flow separation in the lee of the sand wave and resultant backflow up the bottomsets. Locally intense bioturbation and erosive discontinuities again may reflect the periodic abandonment of sediment transport at low stage. The overtaking of large sand

waves by smaller S8 dunes may record an unsteady flow regime. This would concur with the prevalence of major low-angle reactivation surfaces. Type B sand waves come into the class III (and tend towards the class IV) category of Allen (1980).

5.3.10 Longitudinal Sand Wave Facies S10

Description:

One laterally extensive bedform may be seen ENE-NE of the village of Examilia (fig. 5.5). The feature is approximately 2.7km long and would originally have been 15-20m in height. The maximum present outcrop height is about 11m, because the core of the bedform was quarried out for building stone about 2,000 yr b.p. The WSW and NE ends of the slightly arcuate feature include complex superimposed convex-up discontinuities. Convex-up and planar discontinuities are seen within the body of the bedform (plate 5.1f) but these are relatively rare. The external, calcretised surface and internal bedding reflect a near-symmetric cross-sectional geometry. To the NW, sets of ooarenites bedded on a 5-20cm scale dip by 20-25°. Sets locally include small-scale S2 cross-lamination of variable orientation, but with palaeocurrents tending to parallel the trend of the S10 bedform. 100m to the NW of the bedform axis, bedding surfaces are shallow-dipping to sub-horizontal. These shallow-dipping "bottomsets" asymptote away from the main bedform. On the SE side of the bedform, sets dip to the SE as steeply as 30°. No small-scale cross-stratification was observed on this side. A few hundred metres from the WSW end of the longitudinal sand wave, the bedform crest is essentially aggradational, but includes a number of convex-up slightly erosive surfaces which cross the crest. Along the flanks of the feature, sets are bounded by second

Figure 5.5

Map of facies S10 longitudinal sand wave. Dashed line approximately delineates bedform, beyond which bedding surfaces dip at less than 5°.
Contours in metres.

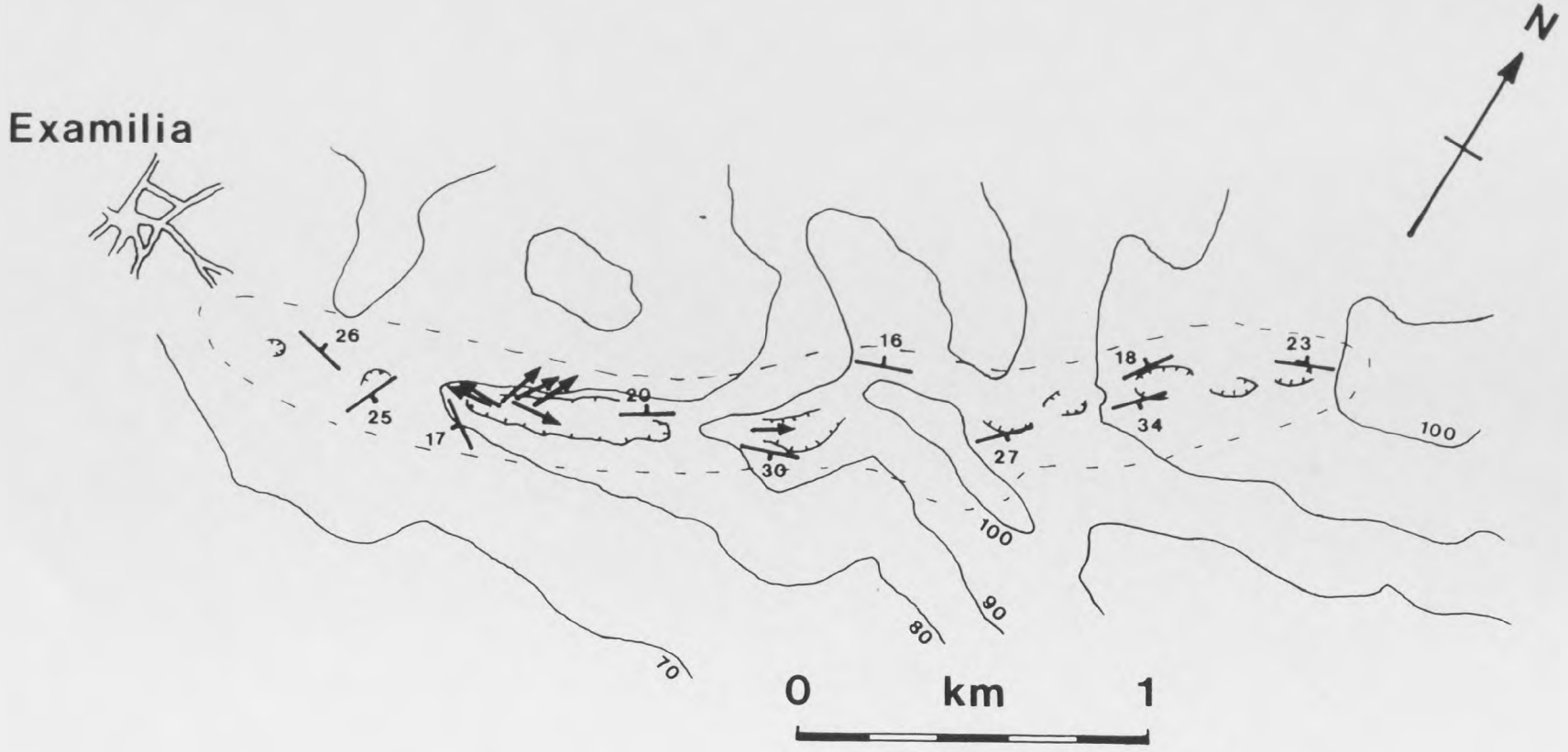
Examilia
N
26
25
17
20
30
16
27
18
34
23
100
100
90
80
70
0
km
1

order planar and convex-up erosive surfaces. The sorting and oolitic character of the sands in the central region of the longitudinal sand wave are exemplified by plate 5.1c. The predominant nucleus lithology is micritic carbonate, with subordinate serpentinite sands and siliciclastics. Towards the NE end of the bedform, oolitic coatings tend to be less well developed and the percentage of serpentinite nuclei increases to 20-25%.

Interpretation:

A marine, tide-influenced environment is inferred from the occurrence of this bedform. The term longitudinal sand wave is coined to signify the similarity of internal structure with tidal sand waves (e.g. facies S9) and to indicate the overall bedform geometry. The near-symmetry in cross-section of the feature suggests that an analogy might be drawn with an aeolian seif dune. These dunes are elongate, almost straight and oriented parallel to the prevailing wind direction. The ridge profile is continuous but may be serrated. Sand is supplied alternately to opposite sides of the seif dune, generating two foreset cross-bedding dips at c.180° to each other. Topographic features adjacent to and parallel to the longitudinal sand wave may have set up the longitudinal current cells necessary to generate the linear structure. Internally, details of foreset structure reflect similar processes as affect the sets of S9 sand waves. The accummulation of fines and layers of intense bioturbation probably signify periods of reduced sediment supply. The thinning and thickening of individual sets downslope may be a product of resedimentation after avalanching of material off the crest. Second order bounding surfaces may record either random

reorientations of current direction over the bedform surface or more marked variations in the overall flow conditions. Some preferred sense of transport parallel to the ridge axis is noted from the sedimentary structures observed. The variety of orientation of S2 cross-bedding over the NW flank of the bedform may either reflect tidal current reversals or more localised current cells and back-flows.

5.4 FACIES ASSOCIATIONS - MARINE DEPOSITS OF THE SOUTHERN CORINTH BASIN

5.4.1 Beach Facies Association

Description:

This association has a coarse clastic average grain size, and is typically the coarsest grade of the three facies associations. Conglomerates of facies S1 with high textural maturity are most characteristic of the facies association. These are typically basal to a sequence which may include unidirectional and herringbone cross-beds (S2), symmetric-rippled sands (S3) and planar-laminated clastics (S5), interbedded on a decimetre to metre scale. A fining-up trend is common, as is a tendency to fine down depositional slope (as seen in the beach-shoreface sets of the canal section, chapter 4). The basal S1 conglomerates often lie directly on an erosive unconformity across which outsized basement and second cycle sediment cobbles and boulders are occasionally scattered. Berms characteristic of the upslope conglomerates of the canal section have not been seen in the southern Corinth Basin, but this may be due to the relatively limited outcrop compared with the canal. Planar-laminated coarse sands and granules (S5) are frequently intimately related

to S1 conglomerates. They are also frequently interbedded with facies S2 and S3. Herringbone cross-beds of S2 are relatively rare and always limited in vertical extent to less than 2m. Bioturbation of the sandy facies within the association is highly variable but generally less intense than in associations SA2 and SA3. Boundaries between facies in the SA1 association are usually abrupt and interdigitate rapidly up- and down-slope. Fauna is rarely preserved intact. Fragments are of a littoral to shallow marine echinoid-bivalve-(±gastropod) assemblage.

Interpretation:

A number of features lead to the characterisation of this association as representing a (marine) beach environment. The high textural maturity of each facies reflects the reworking by storm, wave and tidal action. The landwards-coarsening grain size trend denotes the overall transport of coarse clastics up the shoreface during storm recovery stages (H.E. Clifton, pers. comm.) and the lower energy winnowing of fines by backwash currents to leave matrix-poor sediments on the beach backshore. Bioturbation is limited and fauna fragmented by the repeated reworking inherent to beach processes. Herringbone cross-beds (S2) themselves define the action of both ebb and flood tidal flows. Their limited preservation potential results from a requirement for very high sediment supply rates to record rapid tidal fluctuations allied to episodes of reduced reworking.

The fining-up trend typical of the beach face association SA1 reflects the transgressive character of the sub-sequence in the southern Corinth Basin. A relative rise in sea-level is implied. A progradational beach sequence during a relative stillstand would have a contrasting coarsening-up character at

any locality. Local variations from this fining-up habit will be a function of the three principal variables discussed in previous chapters; local rates of tectonic displacement, rates of eustatic base-level change, and rates of sediment supply to the beach face, in this case. A prograding beach will not show a marked coarsening-up trend, for instance, if no coarse clastics are being supplied onto the beach face. It is not possible, within the scale of the sub-sequence, to isolate the effects of tectonic from eustatic minor base-level changes. No distributary facies have been isolated in outcrops of the marine deposits in the southern Corinth Basin. All sediment transport is therefore inferred to have been by longshore and onshore current action.

5.4.2 Shoreface Facies Association SA2

Description:

Sandy facies with a range of small-scale sedimentary structures characterise facies association SA2. Symmetric ripples (S3) and bundled trough cross-beds (S4) are common. Both are commonly interbedded with planar-bedded sands (S5), with occasional appearances of unidirectional-rippled sands (S2). Textural sorting is good, but a bimodal character is often seen with rippled sands of S3 and trough-bedded sands draped by calcareous silts. Shelly lags and irregular epichnial burrows (Martinsson 1970) are more common than in the beach association SA1.

There is a gradational change from the SA1 beach association to facies association SA2. The matrix-poor conglomerates S1 are generally lost and there is a fining trend to sandier facies with silt/mud drapes. Beds are more laterally extensive to a scale

of tens of metres. The overall fining-up character that typifies the sequence with the SA2 association above the SA1 beach association continues through this association. Immediately above the SA1 association, planar-laminations (S5) and subordinate unidirectional ripples (S2) are the dominant facies. Bioturbation is limited. S2 ripples tend to give way to a predominance of S3 symmetric-rippled sands which are interbedded with planar-laminated sands (S5) and which are commonly silt-draped. Trough cross-bedded sands (S4) then enter the association, often interbedded with S5 laminae but also occurring within more homogeneous, bioturbated sands.

Interpretation:

The S2-S5 facies association describes a shoreface environment. This typically lies above and is therefore transgressive across the coarse clastic beach deposits. By definition the shoreface is below the intertidal zone which is dominated by planar-laminated sands (S5) with small-scale ripples (S2). However, the intertidal to sub-tidal boundary is not distinct. Rather, there is a gradation to the upper shoreface sub-association in which wave-modified ripples (S3) occur in association with bedforms generated by on- and offshore currents (S2 and S5). In the mid- to lower-shoreface sub-associations wave action provides the dominant energy source and the predomiance of wave-modified ripples (S3) and trough beds of bundled structure (S4) reflect this. The episodic variation in the depth of wave influence, due to storm activity, leads to the bimodality of sedimentary structures with resedimentation occurring in the energetic storm phase and the settling out of fines occurring when bottom currents can no longer remobilise sands. The increasing, but

still variable, degree of bioturbation towards the lower shoreface is similarly inferred to reflect the reduced and episodic occurrence of wave action with increasing depth. Planar cross-stratification of facies S7 might be expected to develop in the form of bars migrating up the shoreface during storms. The lack of such bar forms may be a product of erosion during the recovery stage after a storm and merely reflect the low preservation potential of such features. The transition from the shoreface association to the offshore or shelf environment (SA3) is again gradational (fig. 5.6).

5.4.3 Shelf Facies Association SA3

Description:

This facies association is distinguished from the shoreface association (SA2) principally according to the absence of wave-induced small-scale sedimentary structures. It therefore encompasses a range of offshore slope (below the wave-base) and shelf environments. A number of sub-associations may be described according to grain size, the presence or absence of ooids in sandy facies and possible evidence for these having been resedimented, the relative intensities of bioturbation, the occurrence of in situ faunas, and the presence and geometry of bedforms. For the purposes of this study, some outline trends and associations will suffice.

Two main sub-associations may be described, according to the presence or absence of large-scale (S8-S10) bedforms. Where these are absent, variably oolitic sands predominate. These may include planar-laminations or be intensely bioturbated, usually with simple vertical burrows. Alternatively, well-developed

Figure 5.6

Chart of facies occurrence in associations SA1 to SA3

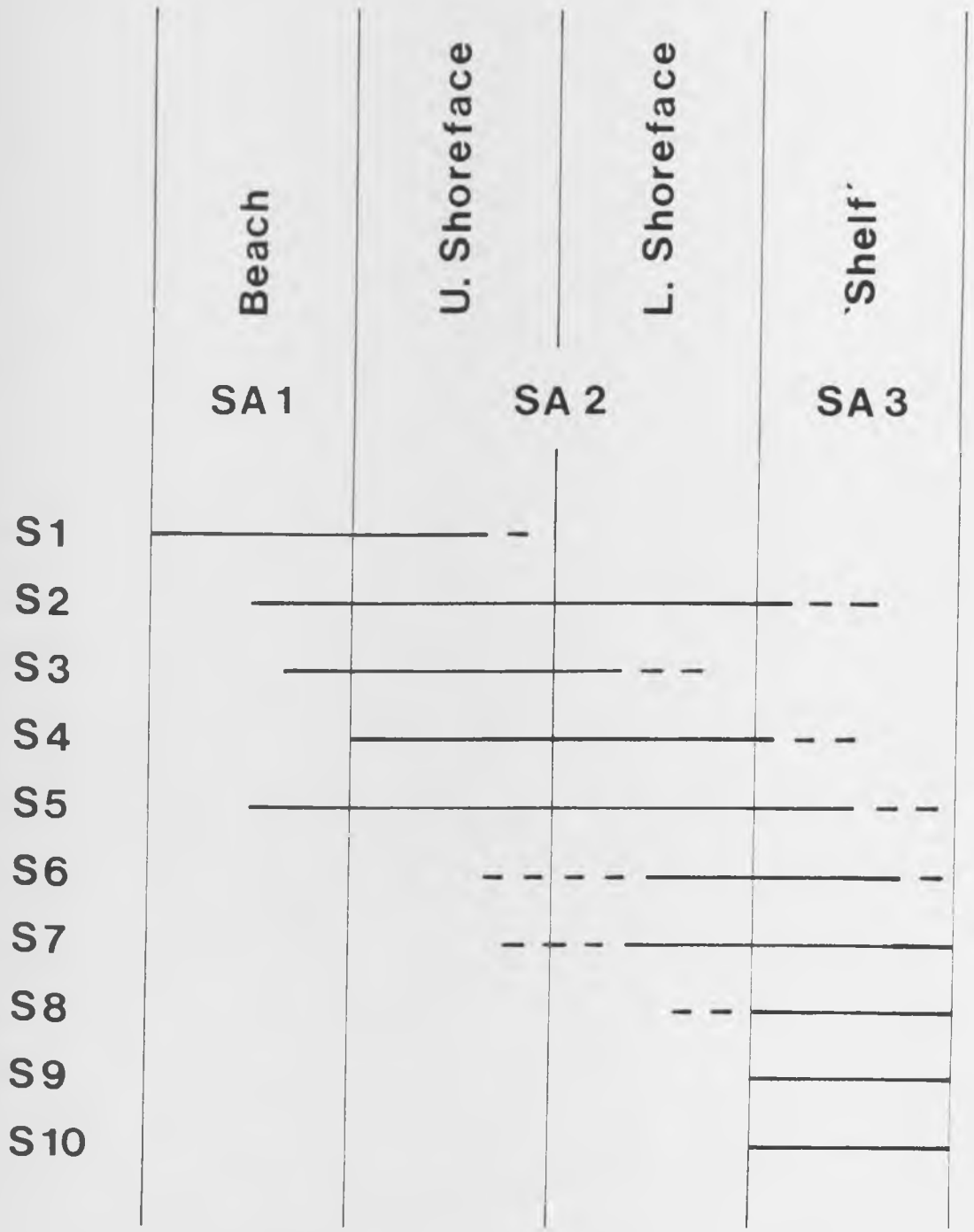
Beach
U. Shoreface
L. Shoreface
'Shelf'
SA 1
SA 2
SA 3
S1
S2
S3
S4
S5
S6
S7
S8
S9
S10

oolitic sands may be virtually homogeneous, with only rare S2 or S5 structures. Silty units of facies B3 or B5b (table 3.1) may occur in association with S6 sands. Coralliferous horizons and shelly accummulations are also seen.

S9 oolitic sand waves typically occur within a surrounding "carpet" of S5 and S6 oolitic sands. Facies S7 planar cross-stratification and S8 dune forms record palaeocurrent trends around the larger bedforms. Levels of bioturbation vary within the background ooarenites, as on the sand waves themselves, with 3-5cm laminations occasionally being alternately bioturbated and non-bioturbated.

The S10 longitudinal sand wave ENE of Examilia (fig. 5.5) is not surrounded by a significant thickness of the oolitic sands of which it is constructed. Instead, pebble lags are seen, locally with a pisolitic component. An in situ fauna is not seen and bioclastics are widely disseminated in this area.

Interpretation:

The range of detailed facies associations occuring within this broad "shelf" classification indicates a variety of current, sediment supply and faunal regimes. The sub-association which does not include large-scale bedforms clearly does not represent the conditions of high sediment supply rate combined with high current velocities needed to generate S8-S10 structures. Current energy may have been locally high, however, to generate smaller-scale cross-stratification features and to disseminate bioclastic materials. Below the wave base, tidal currents are inferred to be the energy source. Reduced current influence and sediment supply rates are represented by the silty and bioturbated facies.

As described in section 5.3.9, the S9 sand wave morphology develops when bottom currents exceed about 1.0m s^{-1}. The comparable vertical scale and internal structure of the S10 longitudinal sand wave suggests a similar current velocity requirement. These tidal bedforms therefore represent environments of enhanced tidal currents within an overall microtidal (Mediterranean) environment. The abundance of oolitic sands around S9 sand waves implies that sediment continued to be supplied to these sand wave fields as the large-scale bedforms aggraded. In contrast, the sparcity of clastics around the S10 longitudinal sand wave suggests that this may represent essentially an environment of sediment reworking, perhaps re-organising sands from the immediate surroundings as the relative sea-level rise continued and established the necessary longitudinal current cells to generate the longitudinal bedform.

The estimation of water depth remains a problem for the sediments in this facies association. Where scleractinian corals occur in situ, a relatively shallow water depth, within the upper photic zone, is indicated. The establishment of tidal currents strong enough to produce S9 and S10 bedforms does not in itself define a shallow water depth. Colella & D'Alessandro (1988) describe S9-type sand waves which currently occupy the floor of the Messina Straits at depths of 3-400m. What these bedforms do indicate, as in the Messina example, is a requirement for some syn-depositional geomorphological feature which could funnel tidal currents and so enhance current velocities. The absence of deep-sea faunal elements, hemipelagic fines or turbiditic deposits in the marine sub-sequence as exposed in the southern Corinth Basin suggests that the water depths seen in the Messina

Strait did not apply. The present topographic differentials between marine deposits (of up to 140m) across the southern part of the Corinth Basin may represent a maximum estimate for their syn-depositional depth range, given that this topography has been accentuated by subsequent structuration (sections 5.6 and 5.7).

5.5 MARINE FACIES DISTRIBUTION AND SYN-SEDIMENTARY STRUCTURE

Figure 5.1 summarises the areal facies distribution of the latest Pleistocene marine sub-sequence across the southern Corinth Basin. This survey attempts to take into account the inherent diachroneity within a transgressive sequence (facies S1 basal conglomerates are common across the whole area). The facies mapped are those inferred to have been deposited at the relative highstand level. As such they approximate to the "deepest water facies" at any locality.

To determine whether or not syn-depositional faulting or the pre-existing structural and topographic form of the basin influenced facies patterns within these deposits, it is necessary to distinguish three categories of currently-observed faults:

a) Fault scarps which existed prior to deposition of the marine sub-sequence. Although not active within the period of deposition of the marine deposits, such features would have had a syn-sedimentary influence on facies distribution.

b) Structures active during deposition of the marine sub-sequence, i.e. syn-depositional faults (sensu Ord et al 1988).

c) Post-depositional faults.

No definitive evidence has been obtained of syn-depositional fault activity within the marine deposits across most of the

southern area. Only in the basal deposits of the sub-sequence in the 1st Corinth scarp is there a record of syn-depositional seismicity. Here, marls below the sub-sequence unconformity are contorted and calcareous muds were extruded through and ponded on the surface of basal conglomerates of the transgressive sub-sequence. Even here though, no facies control by syn-depositional structuration is distinguished within the marine sub-sequence.

Elsewhere across the southern Corinth Basin there is an apparent correlation of facies with the present topographic expressions of several of the more significant intrabasinal normal faults (fig. 5.1). These are therefore inferred to have been pre-existing features (which may or may not have been reactivated subsequently).

The most complete and characteristic transgressive facies sequence is seen in the 1st Corinth scarp (fig. 5.2a). [Although the possibility of two sub-sequences being represented in the 1st Corinth scarp, with a hidden unconformity, has not been discounted.] A fining-up trend is seen from basal conglomerates (interpreted as beach conglomerates of facies S1) to shoreface and then shelf deposits. By way of contrast, close to the present highest topographic point in the southern Corinth Basin the sub-sequence is represented by a limited upper shoreface and beach facies association with a predominance of S1 conglomerates and herringbone cross-stratification horizons representing the intertidal zone (see fig. 5.2b). There is no marked erosion of these marine sub-sequence deposits and this locality is therefore inferred to have been a syn-depositional topographic high. Conglomerates interpreted as facies S1 also

occur on the crest of a ridge 2km north of Examilia (fig. 5.1). This position is inferred to have have been a footwall high at time of deposition, only briefly transgressed if at all. Similar beach facies association deposits are observed east of Kechriae (section C'-D', fig. 5.7) and represent a coastline to the east (refer to sections 5.6 and 5.7).

Oolitic sands are widespread across the southern part of the basin. Thickest accummulations, of at least 8m, occur in the east of the area and include S2 cross-beds and locally S8 dune forms. This area is interpreted as having been a shoal area with active current-reworking of the oolites and high carbonate productivity. Elsewhere, S6 oolites are common on the crests of E-W to NE-SW topographic features (fig. 5.1) which are interpreted to have been areas of positive relief at the time of marine transgression and therefore relatively shallow shoal areas. The proximity of S6 oolites to beach facies associations north of Examilia, 2km NW of Kechriae and ENE of Kechriae supports this inference. In situ scleractinian coral colonies also occur on these topographic ridges, near Ancient Corinth and 1.5km north of Examilia (fig. 5.1). This supports the interpretation of a shallow water (upper photic zone) environment at these localities.

Facies S9 sand waves outcrop exclusively on top of topographic highs. A genetic link is therefore suggested, locating these sand waves on syn-depositional highs across which tidal currents were accelerated. Sand waves 1.5km NE of Kechriae (fig. 5.4 and plate 5.1e) face north, indicating that the dominant tidal current direction was from south to north at this locality. Dominant palaeocurrent directions elsewhere are less well defined, but S9 sand waves at Ancient Corinth appear to face northwards (fig.

5.3) while a sand wave exposed at the NW end of the canal and sitting on top of a shelf feature in the canal section faces approximately north-west.

It is not evident whether the topographic escarpment immediately north of Ancient Corinth (termed the second Corinth scarp, Freyberg 1973) and the escarpment behind Corinth town (the first Corinth scarp) originated as wave-cut platforms or as fault-scarps. The sub-sequence is not fully exposed below either feature and so any facies or sedimentary thickness change across these features is not seen. Topographic escarpments east of Examilia and in the canal section are, however, demonstrably faulted. A component of these displacements may be post-depositional, but the marine facies distribution suggests that the features existed at the time of marine inundation, as described above. Fault brecciation of ooarenites at the western end of the Ancient Corinth archaeological site suggests that normal fault activity has occurred on the second Corinth scarp since deposition of the marine sub-sequence, and faulting may therefore provide the simplest explanation for the pre-existence of a topographic high on which S9 sand waves developed.

One further marine facies shows a close correlation with present fault structures which are therefore inferred to have controlled the geomorphology of the area prior to marine transgression. The facies S10 longitudinal sand wave runs parallel to and in between two NW-dipping normal faults. The feature is therefore interpreted as having developed on the hangingwall of a pre-existing intrabasinal tilt block. Tidal currents are thought to have been constrained and possibly enhanced by the structural trough, current cells being set up parallel to the east-north-

east to north-east fault trend (refer to section 5.3.10).

As discussed in section 5.4.3, the evolution of large-scale sand waves in a microtidal Mediterranean environment requires some syn-sedimentary geomorphological arrangement which funnelled and so enhanced tidal currents. In the case of the Late Pleistocene palaeogeography of the Corinth Basin, there is strong evidence for there having been a basement high in the Saronic area to the east of Kechriae (see sections 5.6 and 5.7). Two palaeogeographic models may be suggested, however. Firstly, the Gulf of Corinth may only have been accessed from open sea conditions at its western end through the strait north of Patras. A circulatory tidal current system may then have been set up within the Gulf. The second and preferred model is that there was an eastwards connection to the Aegean Sea, to the north of Kechriae, probably through the structural low of the Isthmia Graben (figs. 4.11 and 5.1). Such a narrow connection would have a greater tendency to accelerate tidal currents than the circulatory model around the Gulf. The distribution and orientation of tidal bedforms in the southern Corinth Basin are therefore inferred to relate to current systems around the entrance to this narrow strait.

5.6 EXTENSIONAL TILT BLOCK FAULTING AND SYN-TECTONIC SEDIMENTATION POST-DEPOSTION OF THE MARINE SUB-SEQUENCE

A complex history of sedimentation and seismicity has affected the southern Corinth Basin since deposition of the latest Pleistocene marine sub-sequence. Net uplift across the area during this period has led to the exposure of these deposits above present sea-level. At many localities, there is no record

of sedimentation above the marine sub-sequence. In other places oolitic sands of the sub-sequence are buried beneath alluvial facies which indicate a relative fall in base-level (fall in sea-level, tectonic uplift or both) in the interval between deposition of the two units.

Marine sub-sequence sediments on structural and depositional highs, such as to the north and east-north-east of the village of Examilia (fig. 5.1), are generally the youngest exposed sediments. The top 1-2m of these oolitic calcarenites are characteristically calcretised. Early calcretisation of the surface of the facies S10 longitudinal sand wave is inferred as the mechanism by which the topography of this bedform has been preserved. The same applies to certain S9 sand waves, such as those seen on the Ancient Corinth archaeological site which were subsequently onlapped by alluvial deposits (fig 5.3). The calcretisation episode implies a period of relatively arid climatic conditions prevailed soon after deposition of the marine sub-sequence and relative sea-level fall.

The most complete exposures through alluvial facies deposited above the marine sub-sequence are seen on the road from Isthmia to Kechriae (fig. 5.7). These deposits are characterised by a combination of three facies sub-associations:

a) The first is of moderate- to well-sorted conglomerates which occur as individual or stacked erosively-based facies A2 units (table 3.1), or rarely as planar cross-bedded facies A4 units. Isolated convex-up conglomerate sheets also occur, these having an internal coarsening-up tendency (log 2, fig. 5.8). The conglomerates are of basement limestone provenance, with minor basement cherts, and without any basinal sediment intraclasts.

Figure 5.7

Isthmia-Kechriae cross-section.
Blue = Corinth "marls"
Buff = beach association deposits of the marine sub-sequence (section C'-D')
Orange = marine sub-sequence deposits
Green = alluvial sediments
Red = coarse grade conglomeratic sheet

KECHRIAI - ISTHMIA SECTION

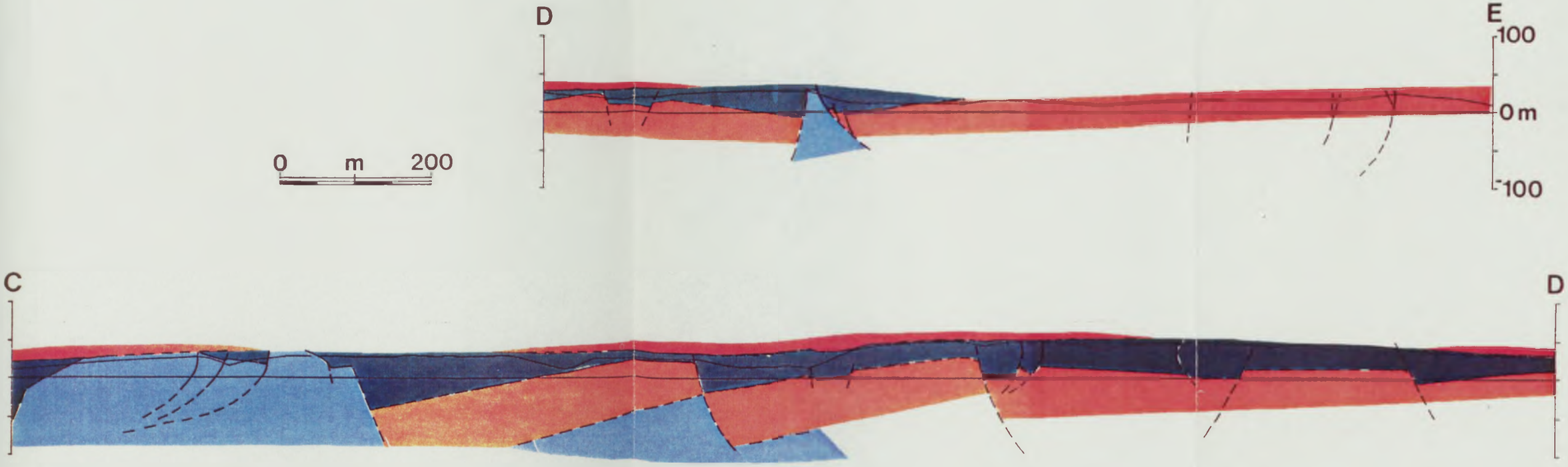

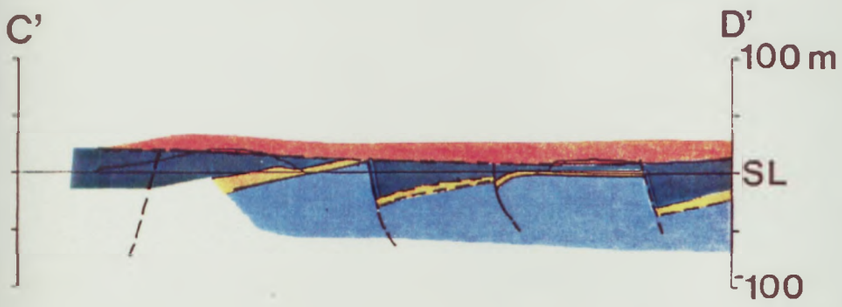

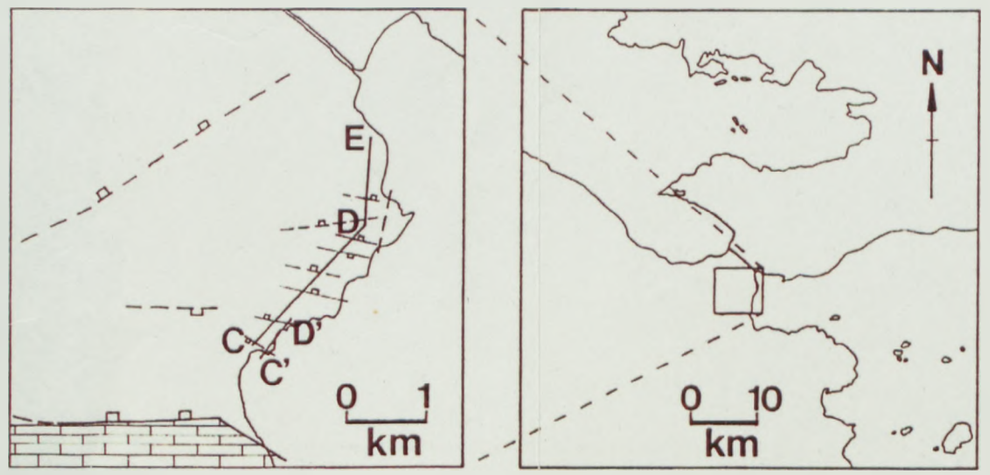

Figure 5.8

Detail of Isthmia-Kechriae cross-section (from section C-D, fig. 5.7).
Orange = marine sub-sequence ooarenites
Green = stream gravels and soils
Yellow = oolitic sands reworked off structural highs within an alluvial environment
Red = fluvial conglomerate sheet
Positions of logs are indicted on section

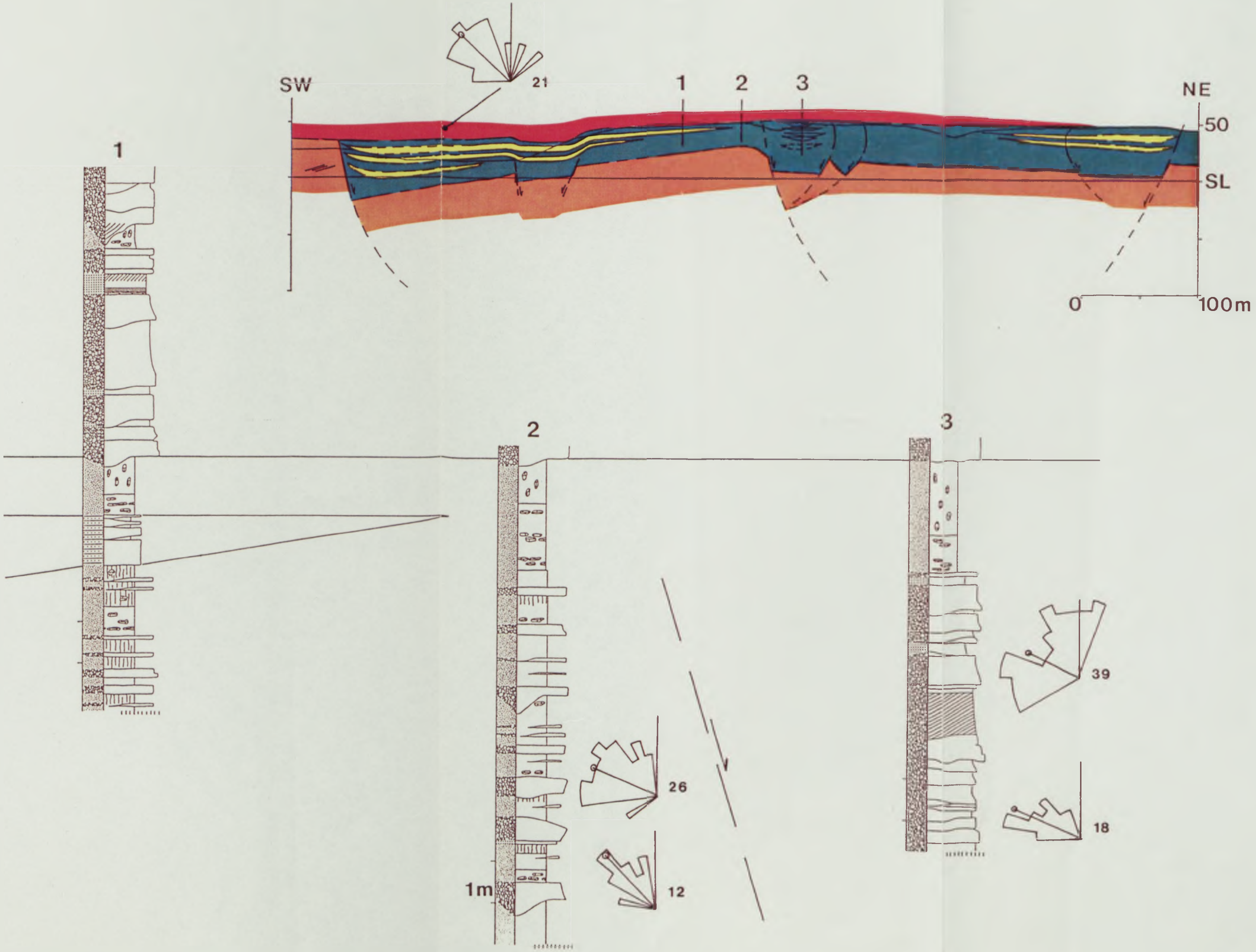
SW
21
1
2
3
NE
50
SL
0
100m
1
2
3
1m
26
12
39
18

b) The second facies sub-association consists of the sandy and silty matrix within which the conglomerate units sit. Reddened B2 sand and silt sheets and lenses are interbedded with variably mature facies I soil developments. Prismatic and sphaeroidal textures are common within silts which contain abundant rootlets. Thicker facies I developments of 2-3m in thickness include extensive carbonate nodule horizons. These facies I accummulations, however, include an abundant marine foraminiferal microfauna of (30.4.2, appendix 1). Fresh or brackish water ostracods (30.4.2, appendix 1) are also found.

c) The third member of the alluvial facies association comprises homogeneous oolitic sand sheets up to 2-3m in thickness. The sheets are generally of a wedge geometry and interdigitate out into facies B3 sand/silt interbeds. The sand wedges are characterised by having a high percentage of fractured ooids (up to 30% in thin section) and contain a marine microfauna (30.4.1, appendix 1).

Sediments of the marine sub-sequence along the Isthmia-Kechriae section have been subject to normal faulting since deposition (fig. 5.7), so generating a train of extensional tilt blocks. There is no evidence for this faulting having commenced during deposition of the marine facies. The alluvial deposits described above infill the topographic lows produced during tilt block rotation. But the alluvial deposits are not in angular discontinuity with the underlying tilt block surface, which would imply a post-rotation infill. Instead, the repeated wedge thickening of oolitic sand sheets towards tilt block footwalls indicates syn-depositional rotation of the tilt blocks with respect to the alluvial fill (see detailed section, fig. 5.8). With each increment of fault block rotation and emergence of

footwall crests, so erosion of marine ooarenites off these structural highs supplied the second cycle sands of the oolitic sand sheets within the alluvial environment. This contrasting origin and depositional environment of the sand and soil wedges explains their bimodal marine and freshwater faunal content. The alternative scenario of the sand wedges representing repeated marine incursions which reworked materials on the alluvial surface would necessitate a very complex history of base-level change and would neither explain the homogeneity of the oolitic sand wedge facies nor its block rotation-related depositional geometry.

The reworked sand wedges describe an essentially lateral distribution of materials off normal fault tilt blocks into the 200-400m scale half-graben and graben structural lows. The east to west palaeocurrents recorded from pebble imbrications in sub-association (a) conglomerates in the structural lows indicate an axial transport system, paralleling the approximately E-W normal faults (inset, fig. 5.7). These conglomeratic units are concentrated in the structurally-constrained lows of the syn-tectonic topography. Log 3 (fig. 5.8) illustrates a package of stacked channel conglomerates. This package is interpreted as overlying a small graben structure. Log 3 contrasts with the log 2 pattern of isolated conglomerate sheets and lenses within a matrix of overbank fines. Here, relatively few channels occur over the buried structural high. Crevasse splay convex-up B1 lenses were probably sourced from the main channel belt immediately to the north. No conglomerates are seen above other footwall crests within the syn-tectonic alluvial deposits, indicating sub-aerial exposure of these footwall highs, which allowed erosion of these latter footwall crests (fig. 5.9).

Figure 5.9

Line drawing after photo-montage of eroded footwall crest onlapped by second cycle oolitic sands (stippled). These were deposited in an alluvial environment and interdigitate with soils which have well-developed carbonate nodule horizons. The marine ooarenites of the eroded fault block exhibit S7 and S8 bedforms. Detail from Isthmia-Kechriae road section, grid ref. 2.75 15.40. Heavy line marks the footwall crest unconformity.

MARINE SANDS OF TILT-BLOCK ONLAPPED BY ALLUVIAL SEQUENCE

The Isthmia-Kechriae tilt block train and its syn-tectonic alluvial infill is conformably capped by a sheet-like incursion of A2 crudely organised conglomerates. Pebble imbrictions again indicate derivation from the east. These conglomerates, however, post-date the major part of the fault block rotations, as they are not displaced by the block-bounding normal faults (fig. 5.7). The conglomerates are only affected by relatively minor downwarping over buried structures (fig. 5.8).

The westerly stream flow direction of the axial system within the syn-tectonic alluvial deposits indicates a westerly tilt to the syn-depositional basin floor. It also requires a basement limestone source at a higher structural level to the east. The Saronic Gulf currently lies to the east, with water depths in excess of 100m just 2-3km east of the present coastline. A reversal of the topographic dip and the preferential subsidence of a Saronic basement source area must therefore be inferred since the time of deposition of the alluvial deposits described. [The thin veneer of Quaternary sediment recorded in the western Saronic Gulf by a recent shallow seismic survey (D. Papanikolaou, pers. comm.) accords with this model.]

The westerly course of the syn-tectonic axial system cannot be traced in outcrop. Structural highs to the north of Kechriae which apparently existed as early as during deposition of the latest Pleistocene marine sub-sequence (section 5.5) would probably have deflected the stream course into the more southerly Kechriae hangingwall graben, perhaps linking into the north-flowing Solomos River further to the west.

6% extension is estimated across the Isthmia-Kechriae tilt block section, assuming a domino block geometry (after Barr 1987),

since deposition of the latest Pleistocene marine deposits. Normal faulting has also taken place during this period further to the west and north on the Isthmus. For example, growth faulting is evident within alluvial deposits in road sections 1.5km ENE of Ancient Corinth (grid ref. -6.20 17.75). But the major part of such faulting probably reactivated pre-existing structures (fig. 5.1) and may not be isolated in the way that is possible along the Isthmia-Kechriae section.

5.6.1 A Small-scale Tilt Block Analogy

This section considers a road section outcrop on the main Corinth-Epidaurus road, 2km SE of the village of Kato Almiri at Greek national 1:50,000 grid ref. 4.65 9.25 (fig. 3.1). These sediments form part of an extensional half-graben infill sequence, the age of which remains unspecified within the Neogene. The 80m long section exposes a series of conglomerates interbedded with soils and sand/silty horizons which are overlain by clays at the ESE end of the section. These strata have been subjected to intense extensional deformation of both brittle and ductile character.

Figure 5.10 presents a line drawing traced from a photo-montage of the road section. Heavy lines trace the more significant faults and unconformity surfaces within the outcrop. Three rotated tilt blocks are delineated within interbedded conglomerates and reddened fines. The facies involved are moderate- to well-sorted limestone conglomerate sheets of facies B1 (table 3.1) interbeddded with facies I red silty or sandy units with variably developed prismatic and sphaeroidal pedogenic textures, small (1-2cm) carbonate nodules, and common rootlets

Figure 5.10

Line drawing after photo-montage and schematic section with graphic logs of the Ano Almiri - Katamalion tilt block section.
Grid ref. 4.65 9.25 (see X, fig. 3.1).
Heavy lines denote faults which controlled facies distribution and unconformity surfaces.

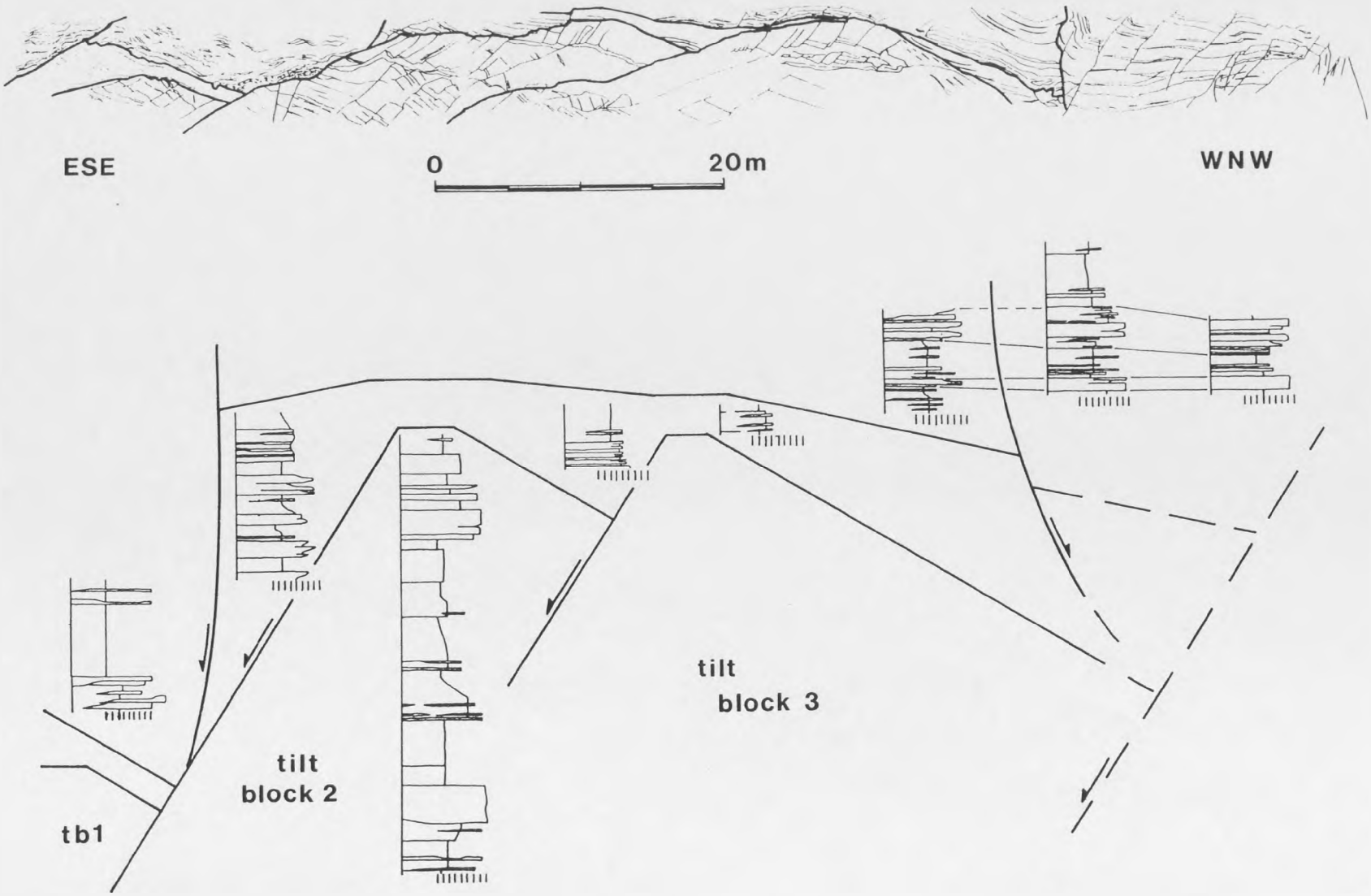
ESE
0
20m
WNW
tilt
block 3
tilt
block 2
tb1

and carbonaceous fragments. Laterally-equivalent units may be traced between fault blocks 1, 2 and 3, these fault blocks being 12-25m in length in the line of section.

Each tilt block contains two marked unconformities which appear to be contemporaneous between the blocks. Each surface is erosive over tilt block footwall crests (uptilted during block rotation) and downlapped by a growth-fill wedge in downtilted areas. The occurrence of two angular unconformities across all three exposed tilt blocks suggests that the "domino" fault block train was subjected to two major pulses of extensional rotation. Each fault block is internally dissected into smaller-scale blocks 1-2m in width. These have undergone further rotation in relation to their containing 10-20m scale tilt blocks. The two suites of faults (one at each scale) combine to achieve rotations of bedding surfaces to dips of up to 55-60°. The generation of voids during the rotation of essentially planar fault blocks is avoided by the ductile flow of soil horizons which separate layers of dominoes which remained coherent and so deformed by brittle faulting.

The tilt block train steps down to the SSE. The structural low is infilled by olive, brown and white-coloured variably calcareous clays (figs. 5.10 and 5.11). The clays have accommodated continued extension by ductile boudinage between tilt block-bounding faults. Figure 5.11 illustrates a dip-section extrapolated from the road section. It is clear that preferential downfaulting to the SSE has allowed the transgression (or isolated infill of the structural low) by lacustrine clays (26.4.1/2/3, appendix 1). The proximity of Pelagonian Zone limestones just 30m to the south of the road

Figure 5.11

Inferred dip-section of the Ano Almiri - Katamalion tilt block section.
Dash = lacustrine clays
Unornamented = fluvial deposits
Brick symbol = basement limestone

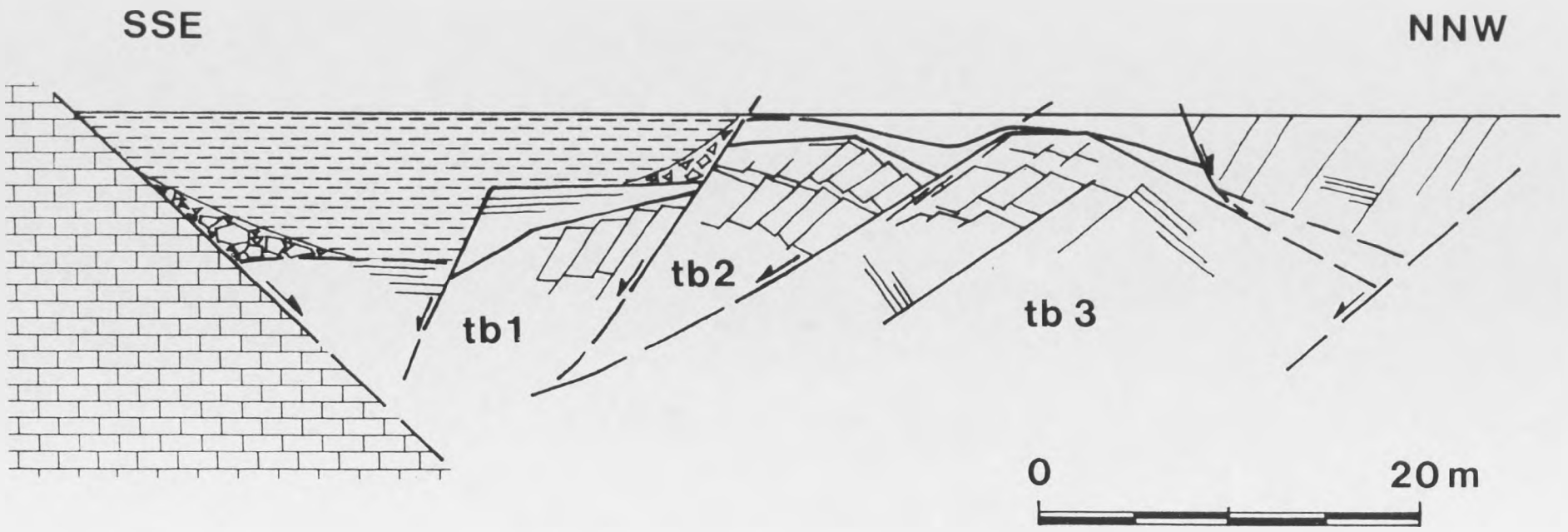
SSE
NNW
tb1
tb2
tb 3
0
20 m

section suggests that the high local extension factor, calculated to be 1.76 across the dip section (after Barr 1987 for domino block rotations), represents the accommodation of strain localised in the immediate hangingwall to a major basement bounding fault.

The principle analogies to be drawn between the small-scale tilt block train of this road section and the tilt block train of the Kechriae-Isthmia cross-section (section 5.6) are as follows:

1) The related styles of brittle deformation: Planar fault-bounded blocks necessarily rotated together (to avoid space generation). Time-equivalent unconformity surfaces and growth-infill wedges may thus be traced across adjacent blocks.

2) Void generation beneath rotating blocks in the small-scale example was avoided by ductile deformation of accommodating horizons of soils and clays. A similar mechanism may have accommodated rotation of blocks of an order of magnitude greater scale in the Kechriae-Isthmia section. Clays/fines, possibly overpressured, or any evaporite horizons within the stratigraphic sequence (after Underhill 1988) may have acted as accommodatory decollement horizons.

One contrast in sedimentary response to tilt block rotation events between the two scales is that the small-scale section does not exhibit a segregated growth-infill architecture of lateral and axial distribution systems. In the Kechriae-Isthmia section the contrast in facies between tilt blocks (marine ooarenites) and hangingwall fills (alluvial facies) allows the recognition of laterally-derived reworked sands and axially-supplied 1st cycle alluvial deposits. The continuity of facies between the tilt blocks in the small-scale example with its growth-infill facies precludes the separation of 1st and 2nd

cycle materials.

The lacustrine incursion into the structural low of the Ano Almiri-Katamalion small-scale domino train marks the cessation of coarse clastic supply into this area.

5.7 DISTINCTION OF CONTROLS ON FACIES PATTERNS - EUSTACY, STRUCTURATION AND CLIMATE

The lack of chronostratigraphic data from the southern Corinth Basin currently precludes a full quantification of tectonic displacements since deposition of the marine sub-sequence. This is because syn-depositional sea-level values cannot be empirically determined. Qualitative inferences may be made, however, regarding the histories of relative base-level change at different localities in the southern Corinth Basin.

Across the Isthmus of Corinth and to the south of the Lechaios Gulf the marine deposits described in sections 5.3 - 5.5 describe a transgressive sub-sequence and thus imply a relative rise in base-level across this area. Given the known cyclicity of sea-level variation through the Late Quaternary, the simplest model scenario would relate this relative base-level rise to a eustatic transgressive phase. Particularly as the marine facies exposed on the southern Corinth Basin are laterally continuous into the 4th marine sub-sequence of the canal section. By relation to the interpreted event stratigraphy of the canal area, this marine sub-sequence is tentatively related to the Late Pleistocene sea-level peak of oxygen isotope stage V (Tyrrhenian). These marine deposits currently outcrop to 140m above present sea-level. If the age inferred above proves to be accurate, this would imply a

net uplift rate averaged over the time interval since deposition in excess of 1m per ka.

As described in section 5.6, deposits of the transgressive subsequence underwent extensional block faulting after their deposition. This would suggest an episode of active tectonic subsidence. Subsequent uplift rates would therefore have had to have been correspondingly higher to uplift these deposits to current outcrop levels. The relative fall in base-level indicated by the change from marine to subsequent alluvial sedimentation indicates that any tectonic subsidence rate was exceeded by the rate of sea-level fall at this time. Again, accepting the tentative isotope stage V age of the marine deposits given above, this would suggest that the block rotation episode took place during the Wurmian eustatic regression phase (see fig. 4.12). This position is illustrated in cartoon form in figure 5.12. In the southern Isthmus area extensional subsidence generated a tilt block topography which controlled the pattern of deposition from westerly-directed braid streams. The 1st cycle basement clastics of these syn-tectonic alluvial deposits imply an area of higher relief with basement existing to the east, in the area now occupied by the Saronic Gulf.

The present situation is illustrated in figure 5.13. Extensional faults are relatively inactive over the southern Isthmus area. Intrabasinal uplift has raised the topography to current levels. Differentials in tectonic displacement across the southern Corinth Basin have reversed the topographic gradient so that streams now flow east into the Saronic Gulf. The presence of the Saronic Gulf to the east of the Isthmus implies that the reversal of topographic gradient continues to the east. In the previous situation (fig. 5.12) the Saronic area was a

Figure 5.12

Block cartoon illustrating the structural and eustatic position in the southern Corinth Basin during tilt block faulting and alluvial deposition.

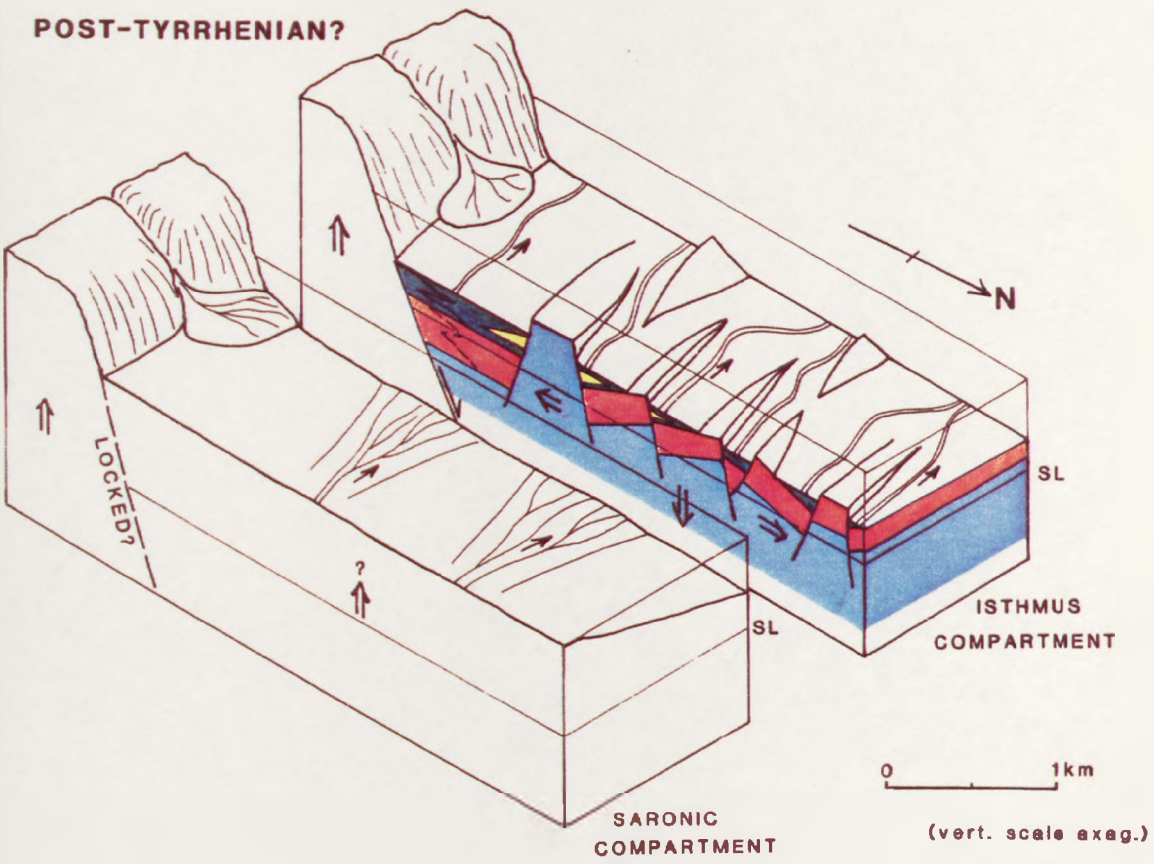
POST-TYRRHENIAN?
N
SL
LOCKED?
?
SL
ISTHMUS
COMPARTMENT
0
1km
SARONIC
COMPARTMENT
(vert. scale exag.)

Figure 5.13

Block cartoon of the present structural and eustatic position in the southern Corinth Basin.

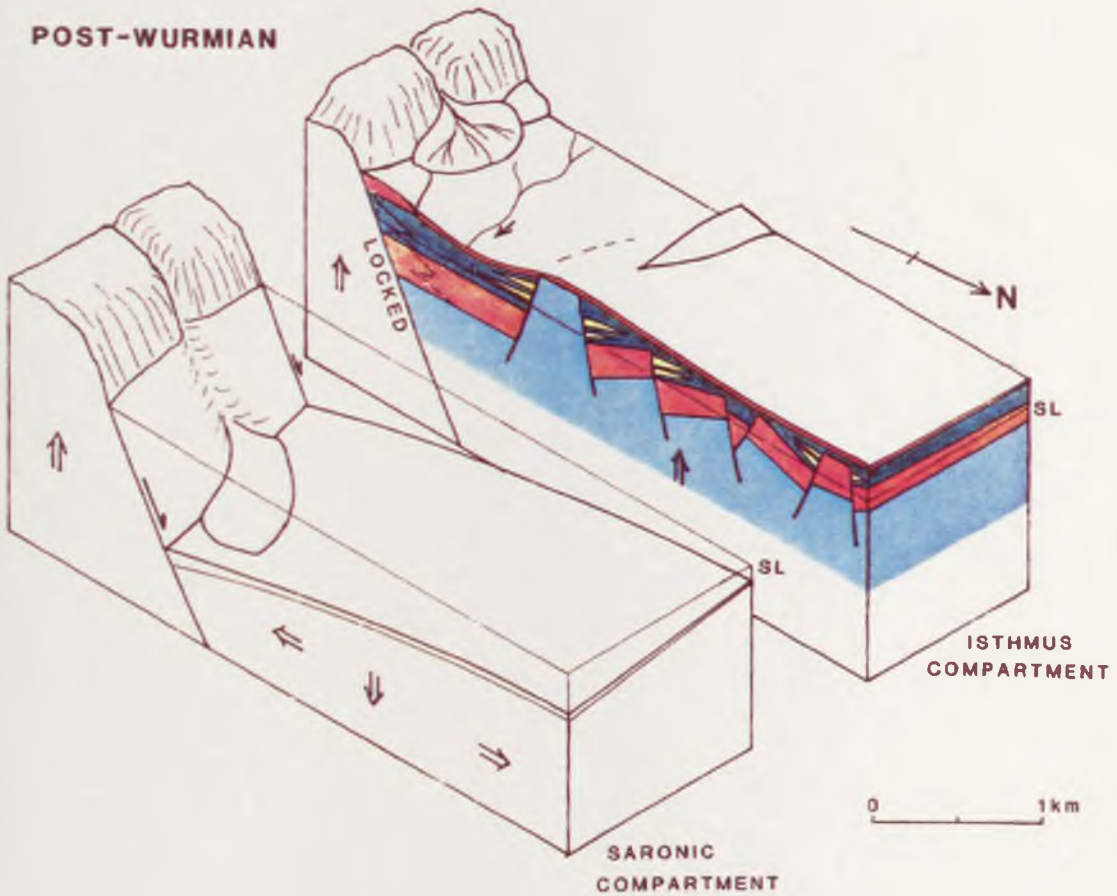
POST-WURMIAN
LOCKED
N
SL
SL
ISTHMUS
COMPARTMENT
0
1 km
SARONIC
COMPARTMENT

relative high supplying detritus to the west. Now it is a relative low accepting sediment from the west. The Saronic Gulf deepens to the east, to depths of more than 180m 11km to the east of Kechriae. Preferential tectonic subsidence of the Saronic area, with subsidence vectors increasing eastwards, is therefore indicated over the period since it supplied sediment onto the southern Isthmus area. These differential subsidence/uplift histories between the Saronic and Isthmus areas of the Corinth Basin suggest a structural "compartmentalisation" of the basin. Compartmentalisation is primarily achieved, however, by displacement gradients on E-W basin-bounding faults. There is no evidence of N-S trending transfer faults (sensu Gibbs 1984a) separating the southern Isthmus from the Saronic Gulf.

Any estimation of the rate of tectonic displacement of the western Saronic Gulf must take into account the position of base-level at the time the area was a relative high supplying sediment westwards onto the southern Isthmus. If, as suggested above, sea-level was at a relative low-stage at the time, then the western Saronic Gulf has not necessarily undergone any subsidence. Instead the two areas have effectively been rotated about a sub-horizontal and approximately N-S axis, the Isthmus undergoing uplift and the Saronic Gulf subsidence with normal fault displacement values increasing eastwards.

The Lechaios Gulf to the west of the Corinth Isthmus continues to undergo active tectonic subsidence. It is the inactivity of extensional faulting across the Isthmus since the last block-faulting episode (fig. 5.12) which appears to have allowed a pervasive background uplift vector to overcome a reduced subsidence vector.

Extensive alluvial fan and fan-delta developments are currently seen in the Corinth Basin (fig. 5.1) and other Aegean basins, downlapping onto the basinal sediment surface. Alluvial profiles correspond to a Holocene base-level, and yet most are presently inactive as depositional systems and many are being incised by streams. Sediment supply rates onto these fans are therefore inferred to have been higher earlier in the Holocene than they are now. Syn-depositional tectonic activity on respective bounding faults may have increased topographic gradients across these structures and so enhanced erosion rates and increased rates of sediment supply. However, the enhanced development of early Holocene fans occurs in basins as far apart as the Corinth, Lamia and Buyuk Menderes grabens (fig. 2.2). A synchronous short-lived pulse of extensional tectonism over such a wide area is geologically improbable. An alternative suggestion is that climatic conditions in the early Holocene enhanced rates of erosion and sediment supply, and produced the prevalence of mass and flow transport mechanisms seen in the fan deposits. Subsequent Mediterranean climatic conditions continue to be less erosive and sediment supply rates onto fan surfaces are therefore reduced. This model accords with early Holocene records of climatic variation which suggest higher rainfall rates occurred in the eastern Mediterranean and North Africa during the early Holocene (Street & Glove 1979). A programme of dating fan materials would be needed to quantitatively constrain sediment supply rates through the Holocene, but the point serves to illustrate the potential influence of climatic conditions on sediment supply rates and hence depositional facies geometries.

5.8 CONCLUSIONS

The recent stratigraphy of the southern Corinth Basin provides a dramatic demonstration of the significance of interacting extensional tectonism and base-level changes in affecting facies distribution patterns and geometries.

The palaeogeography of the Corinth Basin at the time of deposition of the latest Pleistocene marine sub-sequence may be summarised as a shoal and shelf area in the south with shallow warm seas in which oolites were produced and reworked under the influence of tidal currents. The southern part of the basin was bounded to the east by a basement structural high. A narrow structural trough at Isthmia probably connected with the Aegean Sea to the east and so funnelled tidal currents into and out of the Gulf of Corinth, so generating large-scale tidal bedforms. The distribution of these tidal facies was constrained by a normal fault-induced syn-sedimentary topography in the southern part of the basin. Earlier Neogene sediments in the north of the basin were at high structural levels and therefore underwent erosion, supplying multi-cycle sediment into the Corinth Basin to the south and west.

Following a relative fall in base-level, alluvial sedimentation in the southern Corinth Basin was controlled in terms of facies and facies geometries by syn-depositional tilt block faulting. At the same time the Saronic area underwent preferential rates of tectonic subsidence to the east such that the east to west depositional slope in the southern Corinth Basin was reversed. The Saronic Gulf is thus currently in a marine depositional environment, while the southern and central Corinth Basin has been uplifted and is now undergoing net erosion.

CHAPTER 6 DISCUSSION - FACIES PATTERN CONTROLS AND EVOLUTION

6.1 CORINTH BASIN EVOLUTION: INTERACTION OF MECHANISMS CONTROLLING FACIES DISTRIBUTION

Chapters 3-5 detail the sedimentary facies patterns evident at different stages within the syn-rift evolution of the Corinth Basin. Through this Pliocene-Recent period, the structural form of the basin has changed markedly. Structural displacement vectors across the basin have changed, as have sea-level and climatic conditions at certain times within that period. The product has been a varying interaction of controlling mechanisms which determine sedimentary facies distribution.

In the Lower Pliocene sequence (chapter 3) the weight of evidence suggests that normal faulting was the major variable determining facies patterns and their evolution. Basin margin fault activity controlled the gross subsidence rate and basinwide facies trends. Basinwide geometries were in turn modified by local intrabasinal faulting, at certain times (section 3.7.2). An overall relative base-level rise during the Lower Pliocene depositional history is reflected in the transgressive trend towards marine environments, with the youngest Upper Conglomerates recording widespread submergence of the basin floor. It may therefore be tempting to relate this overall transgression to the global sea-level transgressive phase which Vail et al (1977) propose during the Lower Pliocene. Whilst some component of transgression by eustatic sea-level rise has not been discounted, the strong evidence for syn-sedimentary tectonic subsidence does not require a second mechanism of relative sea-level rise to be inferred.

Of other factors influencing sedimentary facies distribution, climatic conditions were apparently relatively constant through the Lower Pliocene episode, as indicated by the stratigraphically widespread occurrence of lignites and humic soil developments. Sediment supply rates may, however, have been locally influenced by the variable resistance to erosion of basement lithologies. This observation is based on the qualitative correlation of the dominant progradation of the Multi-Coloured Series axial fluvio-deltaic system with its serpentinite composition and ophiolitic derivation (section 3.8).

The sedimentary record for the Late Pliocene to Early Pleistocene is discontinuous and disrupted by faulting in the Corinth Basin. Chronological data is absent from deposits post-dating the Mid-Pliocene volcanic suite and pre-dating sediments datable by U-series disequilibrium isotopic dating. Qualitative comments may be made however. A fluvial sequence lies above the intermediate lavas of the western end of the Charalampos fault block (grid ref. 3.80 22.20). North-easterly palaeoflows and basement limestone and red chert lithologies indicate a contemporaneous north-eastwards tilt to the basin in a sub-aerial setting. In contrast, a syn-depositional growth faulting infill is seen immediately south-west of the Charalampos fault block (fig. 3.3). This Late Pliocene and/or Early Pleistocene sequence commences with fluvial conglomerates which are unconformable on Mid-Pliocene volcanics but passes rapidly up into variously marine and ?brackish-lacustrine calcareous silts and sands, with conglomeratic wedges. During the Late Pliocene-Early Pleistocene interval intrabasinal normal faulting segregated the Corinth Basin fill into distinct fault blocks. These include the Charalampos and Asprakhomata-Kalamona fault blocks.

Bounding faults had no influence on and thus post-date the Lower Pliocene sequence. These northerly intrabasinal fault blocks formed structural highs and underwent erosion for at least part of the interval, prior to being alternately downlapped by fans and incised by rivers during the Quaternary, probably as a product of cyclical sea-level changes (enclosure 1). The lack of chronological evidence precludes further comment on the sequence of events or rates of tectonic deformation during the Late Pliocene-Early Pleistocene interval. However, it is pointed out that there is nil evidence for any tectonic compressive phase in the Early Pleistocene, as has been proposed by Mercier (1979, 1981) and co-workers. All observed structures are extensional.

Late Quaternary sedimentation in the Corinth Basin has been characterised by repeated transgressive-regressive geometries which reflect the background cyclical variation in sea-level across this time (e.g. Imbrie et al 1984). Figure 6.1 represents such transgressive-regressive wedge geometries in 2-dimensions, and mimics the modelled geometries described in chapter 4. The precise form of each wedge response to a eustatic cycle will depend on the concurrent history of tectonic displacement and deposition rate at any locality. Thus within a syn-rift basin of asymmetric form, the sedimentary product will vary from place to place within that basin, depending on the local tectonic and sediment supply conditions. For instance, while the tectonically uplifting Corinth Isthmus is characterised by a series of superimposed transgressive sub-sequences, the rapidly subsiding hangingwall to the active basin margin fault to the west of Corinth is characterised by fan delta deposits which are stacked internally (fig. 6.2). This internal stacking (also

Figure 6.1

Cartoon of transgressive-regressive geometries which may be produced by glacio-eustatic cycles on a subsiding coastal slope e.g. position B in figure 6.3

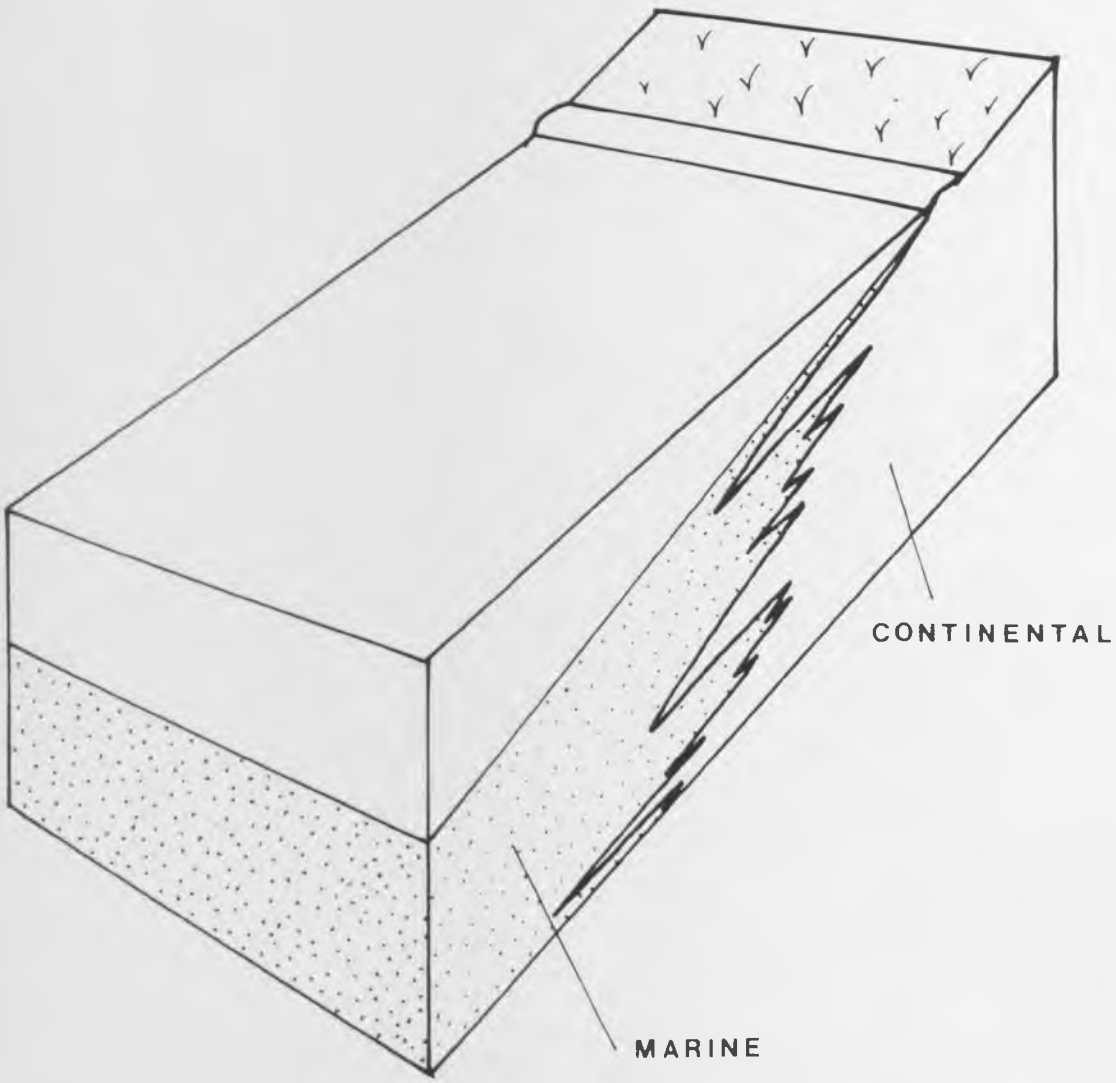
CONTINENTAL
MARINE

Figure 6.2

3.5 kHz seismic profile across the Gulf of Lechaios (see inset for location), from Perissoratis et al (1986). Stacked fan delta geometries are seen against the southern margin of the present marine basin.
x marks unconformity of Wurmian eustatic lowstand.

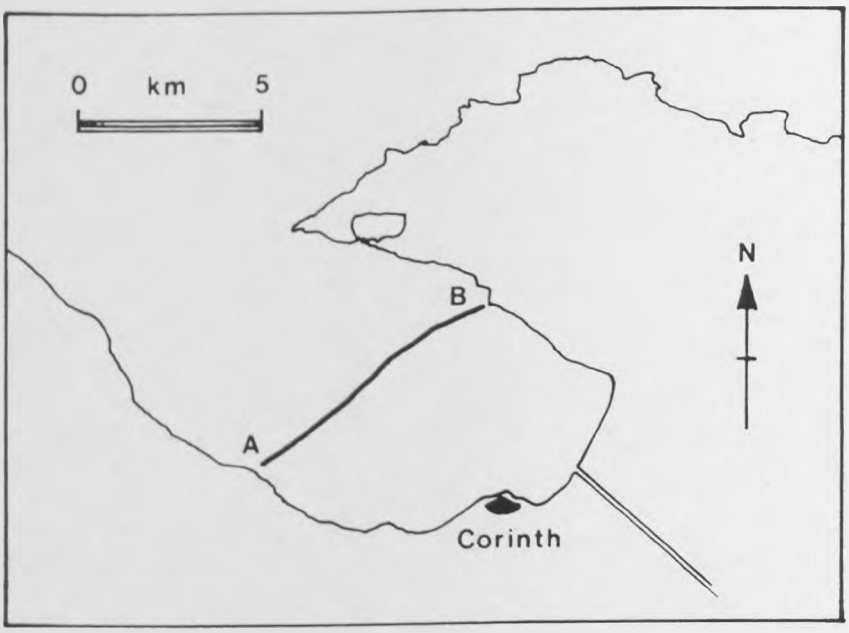
0 km 5
N
B
A
Corinth

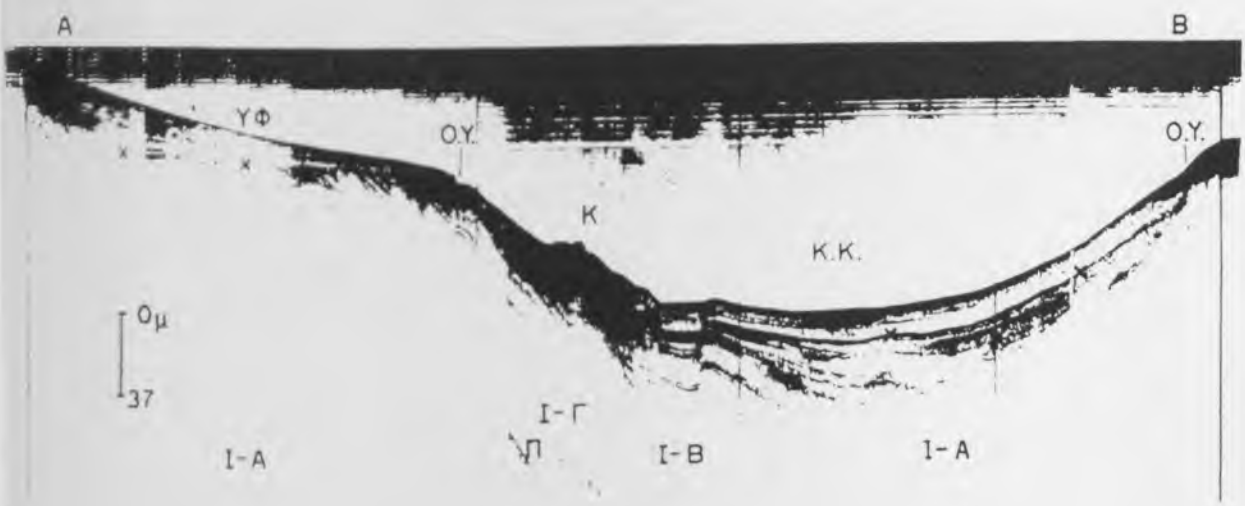
A
B
ΥΦ
O.Y.
O.Y.
K
K.K.
0μ
37
I-Γ
I-A
I-B
I-A

in Aksu et al 1987) records the rapid progradation of deltaics during sea-level lows followed by rapid aggradation and then progradation of deltaics at a higher level (generating the stacked geometry) during the next sea-level relative highstand.

The Corinth Basin is currently structurally separated from the Saronic Gulf and Aegean Sea to the east, other than for the canal connection which was completed in 1895. At the western end of the Gulf of Corinth, the straits linking into the Gulf of Patras are only about 50m in depth (Heezen et al 1966). If a similar structural condition existed through much of the Late Pleistocene, then during glacio-eustatic low stages, the Gulf of Corinth would have been disconnected from open marine conditions. The salinity of basin waters at such times would have been determined by climatic conditions, controlling rates of evaporation and freshwater supply into the basin. The variably brackish to marine character of Pleistocene basinal marls in the Corinth Basin may reflect this periodic isolation and reconnection of the Gulf of Corinth basin system with the Mediterranean marine environment. A programme of drilling through the Pleistocene Gulf of Corinth basinal sedimentary sequence would be needed to further constrain this history.

The diagrammatic representation of facies geometries in figure 6.1 is limited by effectively only being in two-dimensions. The transgressive wedge repeats, as seen in the Corinth canal, are a reasonable first approximation to a laterally-consistent beach-shoreface section, as discussed in section 4.4. However, marked variations in geometry will occur in response to the tectonic setting, as already described, but also by any variation in sedimentary facies themselves. The position of distributaries

along a coastline may be a product of the structural form of the basin margin, but will itself exert a second order control on facies geometries along the coastline. Compare the positions at A, B and C on a notional subsiding hangingwall in figure 6.3:

The position of a distributary stream crossing a basin footwall is initially determined by the en echelon fault segmentation of the basement margin. With a fall in sea-level to SL_1, pre-existing coastal deposits are incised by the distributary stream. At the same time the distributary (perhaps a fan delta) system at the mouth of the distributary stream migrates rapidly basinwards. The stream at this time will tend to have a braided form, being limited by the valley or canyon it has cut. With a rise in sea-level from SL_1 to SL_2, what is now a drowned valley or ria may be rapidly infilled by the aggradation and then progradation along its length of deltaic and then alluvial deposits. [Analogous incision and ria-infill episodes are seen in Late Quaternary deposits in the Gulf of Taranto, southern Italy (F. Massari, pers. comm.). Note that the low stream gradients which may be achieved after alluviation of the ria may tend to generate a meandering stream character (and architecture). Predicted facies geometries within the ria may be characterised as an unconformity transgressed by marine facies which then retreat ahead of a rapidly prograding fluvio-deltaic front. The offshore equivalents may under appropriate tectonic conditions be stacked fan delta geometries, as illustrated in figure 6.2.

At position B (fig. 6.3) a high rate of sediment supply is being maintained by degradation of the footwall scarp. If the rate of sediment supply is high enough, the subsiding hangingwall graben may continue to be alluviated even as sea-level falls. Marine deposits may transgress back up the hangingwall graben with a

Figure 6.3

Cartoon of notional subsiding basin hangingwall with 3 sedimentary environments which will show different sequence geometry responses to changing sea-level. Refer to text for explanation.

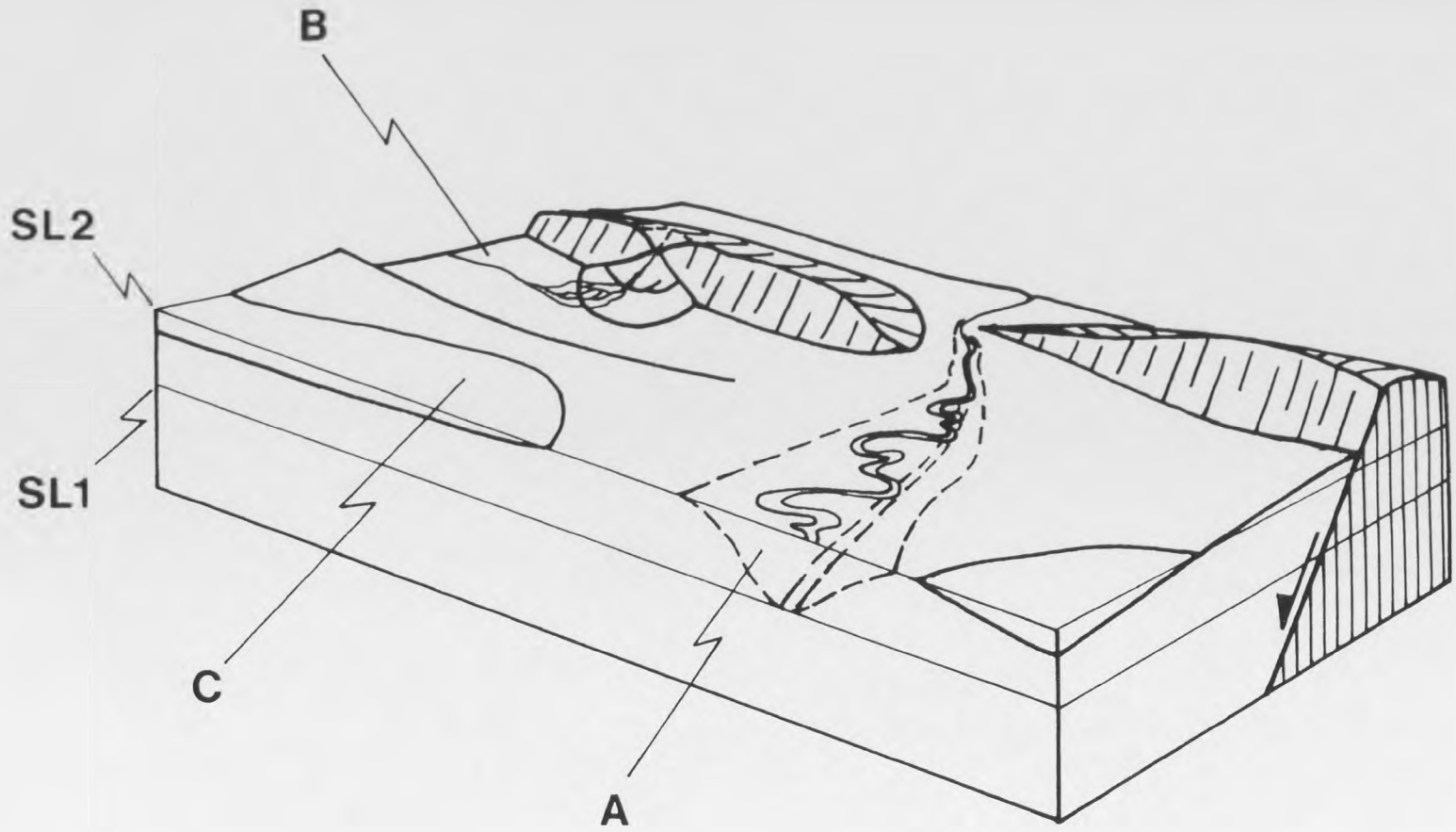
B
SL2
SL1
C
A

rise in sea-level from SL_1 to SL_2, but the hangingwall graben sequence will not contain any erosive discontinuities.

Position C in figure 6.3 represents a non-distributary coastal environment equivalent to that seen in the Corinth canal section. A low-relief erosional surface is likely to be the product of a fall in sea-level to SL_1 if the rate of sea-level fall exceeds any subsidence of the depositional surface. A transgressive beach-to-shoreface sub-sequence will be generated with rise in sea-level from SL_1 to SL_2.

Repeated, cyclical sea-level changes will generate complex sub-sequence architectures. Distributary systems may exhibit repeated incision and ria-fill geometries - this is postulated to be the situation in the Solomos River channel belt in the Corinth Basin (fig. 5.1). Figure 4.6 represents the type of profile that would be predicted for a cyclical sea-level variation history superimposed on a subsiding coast at position B (also fig. 6.1). The Corinth canal section with its repeated transgressive sub-sequence geometries illustrates the product of repeated sea-level cycles superimposed on an uplifting non-distributary beach/shoreface profile.

The structural and eustatic settings of positions A and C in figure 6.3 are identical. The sedimentary processes acting at each locality and the rates of sediment supply at each locality are however determined by their respective environments. So in this sense, the sedimentary facies themselves exert an influence on the resulting facies geometries. If the position of the distributary system changed through time, either as a response to structural events or by random channel avulsion processes (more likely in the eustatic high, meandering-style stages), then the

3-dimensional facies record would reflect this. A non-distributary facies sequence might be superceded by a distributary facies sequence, or vice versa, each reflecting the background eustatic conditions. A change in the character of structural deformation at any locality within the basin, a change in the style of eustatic variation through time, or a change in climate affecting sediment supply rates into the basin could all alter the 3-dimensional facies patterns through time.

6.2 PROBLEMS OF INTERPRETATION: MODERN AND ANCIENT

Several problems arise from the intrinsically variable sedimentation and structural histories of evolving syn-rift basins. These relate both to the interpretation of observed sedimentary facies, in outcrop or down-hole, and to the recognition of the mechanism or mechanisms which controlled facies distribution patterns at any time.

One problem which has been met during this study of Corinth Basin sediments is the difficulty of distinguishing between 1st and 2nd (or higher) cycle materials. Specifically, the distinction of primary from reworked faunas. The recognition of this complication in facies determination which will be widespread through both modern and ancient rift basins, should modify the degree of confidence attached to facies interpretations made on the basis of macro- or microfaunal content alone. The example of alluvial sediments in the Isthmia-Kehcriae area (section 5.6) containing a well-preserved and varied marine microfauna demonstrates the dangers. Had these alluvial deposits been encountered down-hole and ascribed a facies interpretation on the basis of drill chippings, they would almost certainly have been

described as marine deposits. The information that these deposits record the progressive rotation and erosion of the Isthmia-Kechriae domino tilt block train and a relative fall in base-level from a marine to an alluvial environment would have been lost. A similar position exists with regard to the environment of deposition of the "Corinth Marls", which contain both freshwater and marine microfaunal elements at different localities and stratigraphic levels. Do these record changes in base-level or record the spasmodic generation of intrabasinal structural highs supplying 2nd cycle sediment back into the basinal environment?

The situation is further complicated by the possibility of mixed freshwater/brackish/marine faunas being a primary assemblage, representing for instance flow stage fluctuation in fluvial-dominated deltaics and the resultant advance and retreat of the basinal saline wedge (see section 3.5.4). An awareness of surrounding facies associations and geometries is therefore a prerequisite to distinguishing primary from reworked assemblages.

The importance of process rates and the interaction of rates of tectonic displacement, sea-level change and sediment supply as influences on facies distribution have been emphasized. The difficulties of isolating these rates quantitatively has also been discussed. This problem is particularly acute within actively extending basins. Structural compartmentalisation of a basin may lead to quite different tectonic displacement histories in neighbouring parts of a basin (compare for instance the recent subsidence and uplift histories for the Saronic Gulf and Isthmus within the Corinth Basin; sections 5.6 and 5.7).

The lack of stratigraphic markers across rift basin basement

margins into basinal sediments remains a problem if trying to estimate fault displacement values, whether from outcrop or in seismic section. Only in rare special cases will volumetric calculations of sediment derived from basement footwalls, or fission track cooling (uplift) ages from basement footwall rocks allow some constraint of structural displacements.

The estimation of syn-depositional sea-levels prior to about 700 ka b.p. is not currently possible with any degree of confidence. The glacio-eustatic curve is not known accurately prior to that date and any isotopic (let alone biostratigraphic) dating of sediments will have error margins that may encompass a considerable range of sea-level values.

The problem of estimating process rates becomes more extreme with increasingly ancient geological examples. The entire Neogene history of the Aegean would fit within the error margins of isotopically dated materials from a Palaeozoic basin. Averaging process rates through time becomes meaningless because of the erratic nature of rift evolution. Qualitative comments may be made, however, with a target of constructing an "event stratigraphy" for any ancient basin example. The qualitative approach is exemplified by the description of the Lower Pliocene history of the Corinth Basin (chapter 3). The weight of evidence implies a dominant control by normal faulting on facies and their geometries. A second, more localised control on sediment supply rates along the axial distribution system apparently took the form of variations in the erodability of basement source lithologies.

By way of contrast, a repetitious transgressive-regressive or erosional-alluviation sedimentary history might imply some

influence by Milankovitch-type eustatic cyclicity. Known glacial episodes in the geological record such as the Carboniferous-Permian glacial phase must be prime candidates for such controls having been operative. At such time a background of highly variable sea-level should be the expected environment over which tectonic and other controls have been superimposed.

A basinwide event stratigraphy, in the seismic stratigraphic sense, may be built up to describe local and/or basinwide unconformities or transgressive-regressive cycles. Different relative base-level change records which developed simultaneously in different parts of a basin would tend to suggest laterally variable tectonic effects (or at least tectonic effects superimposed upon any background eustatic variation). But as illustrated in figure 6.3 the possibility of geometric variation being a product of respective sedimentary environments must be considered. Basinwide and more regional contemporaneous relative base-level changes would suggest eustatic effects (or more regional tectonism).

Once some qualitative model of active facies controls has been inferred from the event stratigraphy of a basin, the model may be tested. This may be done, as in chapter 4, by generating stratigraphic models constructed on the basis of inferred relative process rates. If such modelling reproduces observed facies geometries then at least one combination of controlling mechanisms will have been demonstrated to be a plausible scenario for the syn-depositional situation. Where one or more variables may be quantified, such as fault displacements from seismic or syn-depositional base-levels in Late Quaternary examples, these values may be used to constrain the unknown variables (as in

section 4.8.

Stochastic modelling or stratigraphic profile simulation provide a way forward in isolating possible controls on facies distribution patterns in ancient settings. Models may be set up and tested against observed patterns. Particular variables may then be altered within the models and the effects compared with the observed geological data. It remains vital that any such modelling is geologically reasonable, for example in terms of realistic rates of sediment supply or sea-level change, or in terms of tectonic fault behaviour.

6.3 FUTURE WORK

As discussed in the previous section, the development of quantitative stratigraphic modelling techniques should provide a useful tool in the analysis of sedimentary facies patterns within extensional (and other) basins. But in all cases, ancient and modern, some reference framework of empirical data is needed if models are to be tested.

In the case of the Neogene Corinth Basin, and other basins in the Aegean province, two principal problems exist in relation to the description and quantification of basin evolution: Firstly, there is as yet inadequate chronostratigraphic data to fully describe the structural evolution of the basin and to relate deposits to the sea-level curve (where known for the Late Quaternary). The second problem is that very little is known about the state of the continental crust at time of rift initiation. Central Greece still has a N-S core of Hellenide-overthickened crust up to 45km in thickness (Makris 1978). But it is not known, for instance, what thickness of crust existed

and therefore at what topographic level the Corinth asymmetric graben lay at the time the rift started to develop. Such information is necessary if any estimation of total subsidence and crustal attenuation values are to be achieved.

A further important subject in need of attention is the mechanism(s) by which intrabasinal and North Peloponnesian footwall uplift is taking place. Footwall uplift (sensu Jackson & McKenzie 1983), the isostatic response to a simple shear crustal geometry (Buck et al 1988, Dunbar & Sawyer 1988), isostatic and strain responses to changes in the geometry and movement of the underlying subducted slab (e.g. Spakman et al 1988) and possible lower crustal accretion of basaltic materials at the western end of the Aegean Arc are all potential mechanisms for inducing uplift. A programme of geophysical research will be required to constrain these possibilities.

More immediate advances will be made by gathering further isotopic and biostratigraphic (where possible) age data. This is particularly relevant to the Late Pleistocene-Holocene history of the basin, during which time the eustatic base-level may be reasonably constrained and tectonic displacements distinguished - to continue the work outlined in chapters 4 and 5. Shallow seismic surveys and boreholes would additionally constrain the sub-sequence response to interactions of tectonic and sea-level displacements. A drilling programme through Gulf of Corinth basin-floor deposits would be needed to fully constrain concurrent salinity variations within the basin and hence periods of structural isolation of the basin from open marine conditions through the Late Quaternary.

6.4 CONCLUSIONS

Sedimentary facies distribution patterns within the Corinth Basin, central Greece have been described. The variation of these patterns through the fourth dimension, time, has been discussed. This has enabled the history of normal fault activity through time to be constrained on the basis of observed facies patterns. Characteristic patterns of lateral distribution systems supplied from exposed fault scarps interacting with axial drainage systems occupying topographic lows sub-parallel to controlling faults are recorded across a range of basinwide and intrabasinal fault block scales.

Qualitative, and where possible quantitative, assessments have been carried out of the mechanisms which controlled sedimentary facies patterns. Three principal controls are usefully considered; rates of tectonic displacement, sea-level change and sediment supply. The high degree of variability of tectonic displacement and sediment supply rates in active rift basins has been demonstrated in both time and space.

Stratigraphic modelling is useful in illustrating the influence of variations in rates of the principal controls. Such models may be utilised to test the plausibility of inferred facies controlling mechanisms at any time against the observed geological record. There is scope for developing 3-dimensional stratigraphic models in a range of sedimentary environments. Even in their current primitive form though, such models provide test-frameworks through which an improved understanding of stratigraphic facies geometries may be attained.

REFERENCES

Aksu, A.E., Piper, D.J.W. & Konuk, T. 1987. Late Quaternary tectonic and sedimentary history of Outer Izmir and Candarli Bays, western Turkey. Marine Geology, 76, 89-104.

Alexander, J. 1986a. Sedimentary and tectonic controls of alluvial facies distribution: Middle Jurassic, Yorkshire and North Sea Basins and Holocene, SW Montana, USA. PhD thesis, Univ. of Leeds, pp. 261.

----- 1986b. Idealised flow models to predict alluvial sandstone body distribution in the Middle Jurassic Yorkshire Basin. Marine & Petroleum Geology, 3, 298-305.

----- & Leeder, M.R. 1987. Active tectonic control of alluvial architecture. p.243-252. In: Etheridge, F.G., Flores, R.M. & Harvey, M.D. (eds.), Fluvial Sedimentology. Spec. Publ. Soc. Econ. Palaeontol. Mineral. 39.

Allen, J.R.L. 1974. Studies in fluviatile sedimentation: Implications of pedogenic carbonate units, Lower Old Red Sandstone, Anglo-Welsh outcrop. Geological Journal, 9, 181-208.

----- 1978. Studies in fluviatile sedimentation: an exploratory quantitative model for the architecture of avulsion controlled alluvial suites. Sedimentary Geology, 21, 129-147.

----- 1980. Sand waves: A model of origin and internal structure. Sedimentary Geology, 26, 281-328.

Allen, P.A., Cabrera, L., Colombo, F. & Matter, A. 1983. Variations in fluvial style on the Eocene-Oligocene alluvial fan of the Scala Dei Group, SE Ebro Basin, Spain. Journal of the Geological Society, London, 140, 133-146.

Anderson, R.E., Zoback, M.L. & Thompson, G.A. 1983. Implications of selected subsurface data on the structural form and evolution of some basins in the northern Basin and Range province, Nevada and Utah. Bulletin of the Geological Society of America, 94, 1055-1072.

Anderton, R. 1985. Clastic facies models and facies analysis. In: Sedimentology: Recent Developments and Applied Aspects (eds. Brenchley, P.J. & Williams, B.P.J.). Geological Society of London Special Publication no. 18, 31-47.

Angelier, J. 1984. Tectonic analysis of fault slip data sets. Journal of Geophysical Research, 89, 5835-5848.

----- 1985. Extension and rifting: the Zeit region, Gulf of Suez. Journal of Structural Geology, 7, 605-612.

-----, Dumont, J.F., Karamandaresi, H., Poisson, A., Simsak, S. & Uysal, S. 1981. Analysis of fault mechanisms and expansion of southwestern Anatolia since the late Miocene. Tectonophysics, 75, T1-9.

Artemjev, M.E. & Artyushkov, E.V. 1971. Structure and isostacy of the Baikal Rift and the mechanism of rifting. Journal of

Geophysical Research, 76, 1197-1211.

Atkinson, T.C., Harman, R.S., Smart, P.L. & Waltham, A.C. 1978. Palaeoclimatic and geomorphic implications of 230Th/234U dates on speleothems from Britain. Nature, London, 272, 24-28.

B.P. (British Petroleum) 1971. The geological results of petroleum exploration in western Greece. Institute of Geology & Subsurface Research, publ. no. 10, Athens.

Baldwin, B. 1971. Ways of deciphering compacted sediments. Journal of Sedimentary Petrology, 41, 293-301.

Bally, A.W., Bernoulli, D., Davis, G.A. & Montadert, L. 1981. Listric normal faults. Oceanol. Acta, Proc. 26th Int. Geol. Cong., Geology of Continental Margins Symposium, Paris, Colloque C3, 87-101.

Barnett, J.A.M., Mortimer, J., Rippon, J.H., Walsh, J.J. & Watterson, J. 1987. Displacement geometry in the volume containing a single normal fault. Bulletin of the American Association of Petroleum Geologists, 71, 925-937.

Barr, D. 1987. Lithosphere stretching, detached normal faulting and footwall uplift. p.75-94. In: Coward, M.P., Dewey, J.F. & Hancock, P.L. (eds.), Continental Extensional Tectonics. Spec. Publ. Geol. Soc. London no. 28. pp.637.

Beard, J.H., Sangree, J.B. & Smith, L.A. 1982. Quaternary chronology, palaeoclimate, depositional sequences, and eustatic cycles. Bulletin of the American Association of Petroleum Geologists, 66, 158-169.

Becker-Platen, J.D. 1970. Lithostratigraphie Untersuchungen im Kanozoikum Sudwest-Anatoliens (Turkei). Beihefte zum Geologischen Jahrbuch, 97, pp.244. Hanover July 1970.

Bellon, H., Jarrige, J-J. & Sorel, D. 1979. Les activites magmatiques egeenes de l'Oligocene a nos jours et leurs cadres geodynamiques. Donnees nouvelles et synthese. Revue de Geologie Dynamique et de Geographie Physique, 21, 41-55.

Bender, M.L., Fairbanks, R.G., Taylor, F.W., Matthews, R.K., Goddard, J.G. & Broecker, W.S. 1979. Uranium-series dating of the Pleistocene reef tracts of Barbados, West Indies. Bulletin of the Geological Society of America, 90, 577-594.

Berggren, W.A. & Van Couvering, J.A. 1974. The Late Neogene: Biostratigraphy, geochronology and palaeoclimatology of the last 15 million years in marine and continental sequences. Palaeogeography, Palaeoclimatology, Palaeoecology, 16, 1-216.

Berner, R.A. & Raiswell, R. 1984. C/S method for distinguishing freshwater from marine sedimentary rocks. Geology, 12, 365-368.

Bessis, F. 1986. Some remarks on the study of subsidence of sedimentary basins. Application to the Gulf of Lions margin (western Mediterranean). Marine & Petroleum Geology, 3, 37-63.

Bingol, E. 1976. Evolution geotectonique de l'Anatolie de l'Ouest. Bulletin de Societe Geologie de France, 7e serie, XVIII,

431-450.

Blanc, J.J. 1958. Recherches geologiques et sedimentologique compagne 1955 en Mediterranee nord-orientale. Annls. Inst. Oceanogr., Monaco, 34, 158-211.

Bloom, a.l., Broecker, W.S, Chappell, J.M.A., Matthews, R.K. & Mesolella, K.J. 1974. Quaternary sea level fluctuations on a tectonic coast: New 230Th/234U dates from the Huon Peninsula, New Guinea. Quaternary Research, 4, 185-205.

Bornovas, J. & Rodiogianni-Tsiambaou, Th. 1983. Geological map of Greece, 1:500,000. Publ. Institute of Geology & Mineral Exploration, Athens.

Bosworth, W. 1985. Discussion on the structural evolution of extensional basin margins; reply by A.D. Gibbs. Journal of the Geological Society, London, 142, 939-942.

Bott, M.H.P. 1971. Evolution of young continental margins and formation of shelf basins. Tectonophysics, 11, 319-327.

----- 1976. Formation of sedimentary basins of graben type by extension of the continental crust. Tectonophysics, 36, 77-86.

Bousquet, B., Dufaure, J.J., Keraudren, B., Pechoux, P.Y., Philip, H. & Sauvage, J. 1976. Les correlations stratigraphiques entre les facies marins lacustres et continentaux du Pleistocene de Grece. Bull. Soc. geol. Fr., 18, 413-418.

Bridge, J.S. & Leeder, M.R. 1979. A simulation model of alluvial stratigraphy. Sedimentology, 26, 617-644.

Broecker, W.S., Andree, M., Klas, M., Bonani, G., Wolfi, W. & Oeschger, H. 1988. New evidence from the South China Sea for an abrupt termination of the last glacial period. Nature, London,, 333, 156-158.

Brooks, M. & Ferentinos, G. 1980. Structure and evolution of the Sporadhes Basin of the North Aegean trough, northern Aegean Sea. Tectonophysics, 68, 15-30.

----- & ----- 1984. Tectonics and sedimentation in the Gulf of Corinth and the Zakynthos and Kefallania channels, Western Greece. Tectonophysics, 101, 25-54.

----- & Kiriakidis, L. 1986. Subsidence of the North Aegean trough: an alternative view. Journal of the Geological Society, London, 143, 23-27.

----- & Williams, G.D. 1982. Extensional tectonics in Neogene and Quaternary sequences at the western margin of the Axios basin, northern Greece. Journal of the Geological Society, London, 139, 293-297.

Brun, J.-P. & Choukroune, P. 1983. Normal faulting, block tilting and decollement in a stretched crust. Tectonics, 2, 345-356.

Buck, W.R. 1986. Small-scale convection induced by passive rifting: The cause for uplift of rift shoulders. Earth & Planetary Science Letters, 77, 362-373.

-----, Matinez, F., Steckler, M.S. & Cochran, J.R. 1988. Thermal consequences of lithospheric extension: pure and simple. Tectonics, 7, 213-234.

Bucknam, R.C. & Anderson, R.E. 1979. Estimation of fault-scarp ages from a scarp-height-slope-angle relationship. Geology, 7, 11-14.

Bull, W.B. 1977. The alluvial fan environment. Prog. Phys. Geogr. 1(2), 222-270.

Cant, D.J. 1978. Development of a facies model for sandy braided river sedimentation: comparison of the South Saskatchewan River and the Battery Point Formation. p.627-639. In: Miall, A.D. (ed.), Fluvial Sedimentology. Mem. Can. Soc. Petrol. Geol. no. 5, pp. 859.

----- & Walker, R.G. 1976. Development of a braided-fluvial facies model for the Devonian Battery Point Sandstone, Quebec. Can. J. Earth Sci., 13, 102-119.

----- & ----- 1978. Fluvial processes and facies sequences in the sandy braided South Saskatchewan River, Canada. Sedimentology, 25, 625-648.

Carver, R.E. 1968. Differential compaction as a cause of regional contemporaneous faults. Bulletin of the American Association of Petroleum Geologists, 52, 414-419.

Channel, J.E.T., D'Argenio, B. & Horvath, F. 1979. Adria, the African promontory, in Mesozoic Mediterranean palaeogeography. Earth Science Reviews, 15, 213-292.

Chappell, J. 1974. Geology of coral terraces, Huon Peninsula, New Guinea: A study of Quaternary tectonic movements and sea-level changes. Bulletin of the Geological Society of America, 85, 553-570.

----- & Shackleton, N.J. 1986. Oxygen isotopes and sea level. Nature, London, 324, 137-140.

Cloos, E. 1968. Experimental analysis of Gulf Coast fracture patterns. Bulletin of the American Association of Petroleum Geologists, 52, 420-444.

Cochran, J.R. 1983. Effects of finite rifting times on the development of sedimentary basins. Earth & Planetary Science Letters, 66, 289-302.

Colella, A. & D'Alessandro, A. 1988. Sand waves, Echinocardium traces and their bathyal depositional setting (Monte Torre Palaeostrait, Plio-Pleistocene, southern Italy. Sedimentology, 35, 219-237.

Collier, R.E.Ll. 1987 (unpublished). Field Guide: The Neogene and Recent of the Gulf of Corinth, Greece. pp.25.

----- in press (a). Modelling the role of differential compaction and tectonics upon Westphalian facies architecture in the Northumberland Basin. In: Gutteridge, P., Arthurton, R.S. &

Nolan, S.C. (eds.), The Role of Tectonics in Devonian and Carboniferous Sedimentation in the British Isles. Publ. Yorkshire Geological Society.

----- in press (b). Tectonic evolution of the Northumberland Basin: The effects of renewed extension upon an inverted extensional basin. Submitted to the Journal of the Geological Society.

----- in press (c). Eustatic and tectonic controls upon the sedimentary history of the Quaternary of the Corinth Basin, Greece. Basin Research.

Crane, R.L. 1982. A computer model for the architecture of avulsion-controlled alluvial suites. PhD thesis, Univ. of Reading.

Davison, I. 1986. Listric normal fault profiles: calculation using bed-length balance and fault displacement. Journal of Structural Geology, 8, 209-210.

Deperet, C. 1913. Observations sur l'histoire geologique pliocene et quaternaire du golfe et de l'isthme de Corinthe. C.R.s.Ac.Sc., 156, 1048-1052.

Dewey, J.F. & Sengor, A.M.C. 1979. Aegean and surrounding regions: complex multiplate and continuum tectonics in a convergent zone. Bulletin of the Geological Society of America, 90, 84-92.

Doutsos, Th., Nikolaus, Kontopoulos & Ferentinos, G. 1985. Das westliche Ende des Korinth-Grabens. N.Jb.Geol.Palaont.Mh., H11, 652-666.

Duchaufour, P. 1977. Pedology. Publ. Allen & Unwin Ltd. pp. 448.

Dufaure, J.-J., Bousquet, B. & Pechoux, P.-Y. 1979. Contributions de la geomorphologie a la connaissance du Quaternaire continental grec, en relation avec les etudes de neotectonique. Revue de Geologie Dynamique et de Geographie Physique, 21, 29-40.

-----, Kadjar, M.H., Keraudren, B., Mercier, J.L., Sauvage, J. & Sebrier, M. 1975a. Les deformations plio-pleistocenes autour du golfe de Corinthe. C.R.Somm.Soc.geol.Fr., 18-20.

-----, Keraudern, B. & Sebrier, M. 1975b. Les terrases de Corinthie (Grece): Chronologie et deformations. C.R.Acad.Sc.Paris, 281, 1943-1945.

Dumont, J.-F., Letouzey, J. & Uysal, S. 1981. Sur l'importance des alternances de phases tectoniques compressives at distensives dans l'evolution des fosses intracontinentaux du sud-ouest de la Turquie. C.R.Acad.Sc.Paris, 292, Serie II, 1157-1160.

-----, Uysal, S., Simsek, S. & Karamanderesi, I.H. 1978. Formation of the grabens in southwestern Anatolia. Turk. Miner. Res. Explor. Bull., 92, 7-18.

Dunbar, J.A. & Sawyer, D.S. 1988. Continental rifting at pre-existing lithospheric weaknesses. Nature, London, 333, 450-452.

Elliott, T. 1974. Interdistributary bay sequences and their genesis. Sedimentology, 21, 611-622.

Emiliani, C. 1978. The cause of the ice ages. Earth & Planetary Science Letters, 37, 349-352.

Eyal, M., Eyal, Y., Bartov, Y. & Steinitz, G. 1981. Tectonic development of the western margin of the Gulf of Elat (Aqaba) rift. Tectonophysics, 80, 39-66.

Eyidogan, H. & Jackson, J.A. 1985. A seismological study of normal faulting in the Demirci, Alasehir and Gediz earthquakes of 1969-70 in western Turkey: implications for the nature and geometry of deformation in the continental crust. Geophysical Journal of the Royal Astronomical Society, 81, 569-607.

Ferentinos, G., Brooks, M. & Collins, M. 1981. Gravity-induced deformation on the north bank and floor of the Sporadhes Basin of the North Aegean Sea Trough. Marine Geology, 44, 289-302.

-----, ----- & Doutsos, T. 1985. Quaternary tectonics in the Gulf of Patras, western Greece. Journal of Structural Geology, 7, 713-717.

-----, Papatheodorou, G. & Collins, M.B., in press. Sediment transport processes on a submarine escarpment of an active asymmetric graben, Gulf of Corinth, Greece.

Fielding, C.R. 1984a. A coal depositional model for the Durham Coal Measures of NE England. Journal of the Geological Society, London, 141, 919-932.

----- 1984b. Upper delta plain lacustrine and fluviolacustrine facies from the Westphalian of the Durham coalfield, NE England. Sedimentology, 31, 547-567.

Flemming, N.C. 1968. Holocene earth movements and eustatic sea level change in the Peloponnese. Nature, London, 217, 1031-1032.

Freyberg, B.v. 1967. Die Neogen-Diskordanz in Central-Kythira. Praktika Akad. Athinon, 42, 361-381.

----- 1973. Geologie des Isthmus von Korinth. Erlanger Geologische Abhandlungen, 95, pp. 183. Publ. Junge & Sohn, Universitats-Buchdruckerei, Erlangen.

Fytikas, M., Giuliani, O., Innocenti, F., Marinelli, G. & Mazzuoli, R. 1976. Geochronological data on Recent magmatism of the Aegean Sea. Tectonophysics, 31, T29-T34.

-----, Innocenti, F., Manetti, P., Mazzuoli, R., Peccerillo, A. & Villari, L. 1984. Tertiary to Quaternary evolution of volcanism in the Aegean region, p. 687-699. In: Dixon, J.E. & Robertson, A.H.F. (eds.), Spec. Publ. Geol. Soc. London no.17, pp. 824.

Gaitanakis, P., Mettos, A. & Fytikas, M. 1985. Geological map, 1:50,000 Sofikon sheet. Publ. Institute of Geology & Mineral Exploration, Athens.

Garfunkel, Z. & Bartov, Y. 1977. The tectonics of Suez rift. Bull. geol. Surv. Israel, 71, 1-44.

Gawthorpe, R.L. 1986. Sedimentation during carbonate ramp-to-slope evolution in a tectonically active area: Bowland Basin (Dinantian), northern England. Sedimentology, 33, 185-206.

----- & Clemmey, H. 1985. Geometry of submarine slides in the Bowland Basin (Dinantian) and their relation to debris flows. Journal of the Geological Society, London, 142, 555-566.

Gibbs, A.D. 1983. Balanced cross-section construction from seismic sections in areas of extensional tectonics. Journal of Structural Geology, 5, 153-160.

----- 1984a. Structural evolution of extensional basin margins. Journal of the Geological Society, London, 141, 609-620.

----- 1984b. Clyde Field growth fault secondary detachment above basement faults in the North Sea. Bulletin of the American Association of Petroleum Geologists, 68, 1029-1039.

----- 1987. Development of extension and mixed mode sedimentary basins. p.19-33. In: Coward, M.P., Dewey, J.F. & Hancock, P.L. (eds.), Continental Extensional Tectonics. Spec. Publ. Geol. Soc. London no. 28. pp.637.

Gillet, S. 1963. Nouvelles donnees sur le gisement villafranchien de Nea-Corinthos. Praktika Akad. Athinon, 38, 400-419.

Graham, S.A. & Bachman, S.B. 1983. Structural controls on submarine-fan geometry and internal architecture: Upper La Jolla Fan System, offshore S. California. Bulletin of the American Association of Petroleum Geologists, 67, 83-96.

Gross, W.W. & Hillmeyer, F.L. 1982. Geometric analysis of upper-plate fault patterns in the Whipple-Buckskin detachment terrane, California and Arizona, p.256-265. In: Frost, E.G. & Martin, D.L. (eds.), Mesozoic-Cenozoic Tectonic Evolution of the Colorado River Region, California, Arizona and Nevada. Cordilleran Publishers, San Diego.

Haldorsen, H.H. & Lake, L.W. 1984. A new approach to shale management in field-scale models. Soc. Petrol. Eng. J., 447-457.

Hamblin, W.K. 1965. Origin of 'reverse drag' on the down-thrown side of normal faults. Bulletin of the Geological Society of America, 76, 1145-1163.

Hancock, P.L. & Barka, A.A. 1987. Kinematic indicators on active normal faults in western Turkey. Journal of Structural Geology, 9, 573-584.

Hanks, T.C., Bucknam, R.C., Lajoie, K.R. & Wallace, R.E. 1984. Modification of wave-cut and faulting-controlled landforms. Journal of Geophysical Research, 89, 5771-5790.

Hardenbol, J., Vail, P.R. & Ferrer, J. 1981. Interpreting palaeoenvironments, subsidence history and sea level changes of passive margins from seismic and biostratigraphy. Oceanologica Acta, Proc. 26th Int. Geol. Cong., Geology of Continental Margins Symposium, Paris, Colloque C3, 33-44.

Harland, W.B., Cox, A.V., Llewellyn, P.G., Pickton, C.A.G., Smith, A.G. & Walters, R. 1982. A Geologic Time Scale. Publ. Cambridge University Press, pp. 131.

Hays, J.D., Imbrie, J. & Shackleton, N.J. 1976. Variations in the Earth's orbit: pacemaker of the ice ages. Science, 194, 1121-1132.

-----, Saito, T., Opdyke, N.D. & Buckle, L.H. 1969. Pliocene-Pleistocene sediments of the equatorial Pacific, their paleomagnetic, biostratigraphic and climatic record. Bulletin of the Geological Society of America, 80, 1481-1514.

Heezen, B.C., Ewing, M. & Johnson, J.L. 1966. The Gulf of Corinth floor. Deep-Sea Research, 13, 381-411.

Herforth, A., Schroder, B. & Theodoropoulos, D. 1971. Zur jungpleistozanen und holozanen Kustenmorphologie zwischen Korinth und Sud-Attika. Bull. Geol. Soc. Greece, 8, 194-198.

Hooke, R. Le B. 1972. Geomorphic evidence for Late-Wisconsin and Holocene tectonic deformation, Death Valley, California. Bulletin of the Geological Society of America, 83, 2073-2098.

Horvath, F., Berckhemer, H. & Stegena, L. 1981. Models of Meditteranean back-arc basin formation. Philosophical Transactions of the Royal Society, London, A300, 383-402.

Hossack, J.R. 1984. The geometry of listric growth faults in the Devonian basins of Sunnfjord, W Norway. Journal of the Geological Society, London, 141, 629-638.

Hubbard, R.J., Pape, J. & Roberts, D.G. 1985. Depositional sequence mapping as a technique to establish tectonic and stratigraphic framework and evaluate hydrocarbon potential on a passive continental margin, 79-91. In: Berg, O.R. & Woolverton, D.G. (eds.), Seismic Stratigraphy II: An Integrated Approach to Hydrocarbon Exploration. Publ. AAPG, pp. 276.

Imbrie, J. 1985. A theoretical framework for the Pleistocene ice ages. Journal of the Geological Society, London, 142, 417-432.

-----, van Dork, J. & Kipp, N.G. 1973. Paleoclimatic investigation of a late Pleistocene Caribbean deep-sea core: comparison of isotopic and faunal methods. Quaternary Research, 3, 10-38.

-----, Hays, J.D., Martinson, D.G., McIntyre, A., Mix, A.C., Morley, J.J., Pisias, N.G., Prell, W.L. & Shackleton, N.J. 1984. The orbital theory of Pleistocene climate: support from a revised chronology of the marine d18O record. p. 269-305. In: Berger, A.L., Imbrie, J., Hays, J., Kukla, G. & Saltzman, B. (eds.), Milankovitch and Climate, Part 1. Publ. D.Reidel, Dordrecht.

Ivanovich, M. & Harmon, R.S. (eds.) 1982. Uranium Series Disequilibrium: Applications to Environmental Problems. Publ. Clarendon Press, pp.571.

Jackson, J.A. 1987. Active normal faulting and crustal extension. p. 3-17. In: Coward, M.P., Dewey, J.F. & Hancock, P.L. (eds.), Continental Extension Tectonics. Spec. Publ. Geol. Soc. London

no. 28, pp.637.

-----, Gagnepain, J., Houseman, G., King, G.C.P., Papadimitriou, P., Soufleris, C. & Virieux, J. 1982a. Seismicity, normal faulting and the geomorphological development of the Gulf of Corinth (Greece): the Corinth earthquakes of February and March 1981. Earth & Planetary Science Letters, 57, 377-397.

-----, King, G. & Vita-Finzi, C. 1982b. The neotectonics of the Aegean: an alternative view. Earth & Planetary Science Letters, 61, 303-318.

----- & McKenzie, D. 1983. The geometrical evolution of normal fault systems. Journal of Structural Geology, 5, 471-482.

----- & ----- 1984. Rotational mechanisms of active deformation in Greece and Iran. p. 743-754. In: Dixon, J.E. & Robertson, A.H.F. (eds.), The Geological Evolution of the Eastern Meditteranean. Spec. Publ. Geol. Soc. London no. 17, pp.824.

-----, White, N.J., Garfunkel, Z. & Anderson, H. 1988. Relations between normal-fault geometry, tilting and vertical motions in extensional terranes: an example from the southern Gulf of Suez. Journal of Structural Geology, 10, 155-170.

Jarvis, G.T. & McKenzie, D.P. 1980. Sedimentary basin formation with finite extension rates. Earth & Planetary Science Letters, 48, 42-52.

Jongsma, D. 1974. Heat flow in the Aegean Sea. Geophysical Journal of the Royal Astronomical Society, 37, 337-346.

Jopling, A.V. 1965. Hydraulic factors and the shape of laminae. Journal of Sedimentary Petrology, 35, 777-791.

Keen, C.E. 1985. The dynamics of rifting: Deformation of the lithosphere by active and passive driving mechanisms. Geophysical Journal of the Royal Astronomical Society, 80, 95-120.

Keller, E.A. & Rockwell, T.K. 1984. Tectonic geomorphology, Quaternary chronology and palaeoseismicity. In: Costa, J.E. & Fleisher, P.J. (eds.), Developments and Applications of Geomorphology.

Keraudren, B. 1979. Le Plio-Pleistocene marin et oligohalin en Grece: stratigaphie et paleogeographie. Revue de Geologie Dynamique et de Geographie Physique, 21, 17-28.

----- & Sorel, D. 1987. The terraces of Corinth (Greece) - a detailed record of eustatic sea-level variations during the last 500,000 years. Marine Geology, 77, 99-107.

Kissel, C., Jamet, M. & Laj, C. 1984. Palaeomagnetic evidence of Miocene and Pliocene rotational deformations of the Aegean Area. p.669-699. In: Dixon, J.E. & Robertson, A.H.F. (eds.), The Geological Evolution of the Eastern Mediterranean. Spec. Publ. Geol.Soc. London no. 17. pp.824.

Kitto, H.D.F 1951. The Greeks. Publ. Penguin (1986 reprint). pp.256.

Koide, M. & Goldberg, E.D. 1965. U234/U238 in sea water. p.173-177. In: Sears, M. (ed.), Progress in Oceanography, vol. 3. Publ. Pergamon Press.

Kollman, H.A. 1973. Pliocane Brack- und Susswasserfossilien vom Isthmus von Korinth. p.171-173. Erlanger Geologische Abhandlungen, 95, pp.183. Publ. Junge & Sohn, Universitats-Buchdruckerei, Erlangen.

Kulen, M. (director) 1975. Lower Buyuk Menderes Basin - Hydrogeological Investigation Report. Republic of Turkey Ministry of Energy and Natural Resources, General Directorate of State Hydraulic Works, Ankara, pp.72.

Le Pichon, X. & Angelier, J. 1979. The Hellenic arc and trench system: a key to the neotectonic evolution of the eastern Mediterranean area. Tectonophysics, 60, 1-42.

----- & ----- 1981. The Aegean Sea. Philosophical Transactions of the Royal Society, London, A300, 357-372.

-----, Lyberis, N. & Alvarez, F. 1987. Discussion on the subsidence of the North Aegean trough: an alternative view; reply by Brooks, M & Kirikidis, L. Journal of the Geological Society, London, 144, 349-351.

----- & Sibouet, J. 1981. Passive margins: A model of formation. Journal of Geophysical Research, 86, 3708-3720.

Leeder, M.R. 1978. A quantitative stratigraphic model for alluvium with special reference to channel deposit density and interconnectedness. p.587-596. In: Miall, A.D. (ed.), Fluvial Sedimentology. Can. Soc. Petrol. Geol. Memoir 5.

----- 1982. Upper Palaeozoic basins of the British Isles - Caledonide inheritance versus Hercynian plate margin processes. Journal of the Geological Society, London, 139, 479-491.

----- 1983. Lithospheric stretching and North Sea Jurassic clastic sourcelands. Nature, London, 305, 510-513.

----- 1987. Sediment deformation structures and the palaeotectonic analysis of extensional sedimentary basins. In: Jones, M. & Preston, R.M.F. (eds.), Deformation of Sediments and Sedimentary Rocks. Spec. Publ. Geol. Soc. London no. 29.

----- & Alexander, J. 1987. The origin and tectonic significance of asymmetrical meander belts. Sedimentology, 34, 217-226.

----- & Gawthorpe, R.L. 1987. Sedimentary models for extensional tilt block/half graben basins. p. 139-152. In: Coward, M.P., Dewey, J.F. & Hancock, P.L. (eds.), Continental Extensional Tectonics. Spec. Publ. Geol. Soc. London no. 28.

-----, Ord, D.M. & Collier, R. 1988. Development of alluvial fans and fan-deltas in neotectonic extensional settings: implications for the interpretation of basin fills. p. 187-199. In: Nemec, W. & Steel, R.J. (eds.), Fan Deltas: Sedimentology and Tectonic Settings. Publ. Blackie & Son.

Lister, G.S., Banga, G. & Feenstra, A. 1984. Metamorphic core

complexes of Cordilleran type in the Cyclades, Aegean Sea, Greece. Geology, 12, 221-225.

Lockwood, J.G. 1985. World Climatic Systems. Publ. Edward Arnold, pp. 292.

Makris, J. 1976. Geophysical studies and interpretation for the Aegean Area. In: Closs, H. et al (eds.), Mobil Earth: International Geodynamics Project; Final Report of the Federal Republic of Germany. Dt. Forschungsgemeinschaft. Boppard, Boldt, 1980.

----- 1978. Some geophysical considerations on the geodynamic situation in Greece. Tectonophysics, 46, 251-268.

----- 1985. Geophysics and geodynamic implications for the evolution of the Hellenides. p. 231-248. In: Stanley, D.J. & Wezel, F.-C. (eds.), Geological Evolution of the Meditteranean Basin. Publ. Springer-Verlag, pp. 589.

Makropoulos, K.C. & Burton, P.W. 1985a. Seismic hazard in Greece. I. Magnitude recurrence. Tectonophysics, 117, 205-257.

----- & ----- 1985b. Seismic hazard in Greece. II. Ground acceleration. Tectonophysics, 117, 259-294.

Mansinha, L. & Smylie, D.E. 1971. The displacement fields of inclined faults. Bulletin of the Seismological Society of America, 61, 1433-1440.

Mariolakis, I. & Stiros, S.C. 1987. Quaternary deformation of the Isthmus and Gulf of Corinthos (Greece). Geology, 15, 225-228.

Martinsson, A. 1970. Toponomy of trace fossils. In: Crimes, T.P. & Harper, J.C. (eds.), Trace Fossils. Geological Journal Special Issue 3, 323-330.

Mercier, J.L. 1979. Signification neotectonique de l'Arc Egeen. Un revue des idees. Revue de Geologie Dynamique et de Geographie Physique, 21, 5-15.

----- 1981. Extensional-compressional tectonics associated with the Aegean Arc: comparison with the Andean Cordillera of south Peru - north Bolivia. Philosophical Transactions of the Royal Society, London, A300, 337-355.

----- 1983. Some remarks concerning the paper "The neotectonics of the Aegean: an alternaive view" by J.A. Jackson, G. King & C. Vita-Finzi. Earth & Planetary Science Letters, 66, 321-325.

-----, Carey, E., Philip, H. & Sorel, D. 1976. La neotectonique plio-quaternaire de l'arc Egeen externe et de la Mer Egee et ses relations avec la seismicite. Bull. Soc. geol. Fr., 7e serie, XVIII, 355-372.

-----, Carey-Gailhardis, E., Monyaris, N., Simeakis, K., Roundoyannis, T. & Anghelidhis, C. 1983. Structural analysis of Recent and active faults and regional state of stress in the epicentral area of the 1978 Thessaloniki earthquakes (Northern Greece). Tectonics, 2, 577-600.

-----, Delibassis, N., Gauthier, A., Jarrige, J.J., Lemeille, F., Philip, H., Sebrier, M. & Sorel, D. 1979a. La neotectoniue de l'arc Egeen. Revue de Geologie Dunamique et de Geographie Physique, 21, 67-92.

-----, Mouyaris, N., Simeakis, C., Roundoyannis, T. & Anghelidhis, C. 1979b. Intra-plate deformation: a quantitative study of the faults activated by the 1978 Thessaloniki earthquakes. Nature, London, 278, 45-48.

-----, Sorel, D. & Simeakis, K. 1987. Changes in the state of stress in the overriding plate of a subduction zone: the Aegean Arc from the Pliocene to the present. Annales Tectonicae, 1, 20-39.

Meulenkamp, J.E. 1985. Aspects of the Late Cenozoic evolution of the Aegean region. p.307-321. In: Stanley, D.J. & Wezel, F.C. (eds.), Geological Evolution of the Mediterranean Basin. Publ. Springer-Verlag, pp.589.

Miall, A.D. 1973. Markov chain analysis applied to an ancient alluvial plain succession. Sedimentology, 20, 347-364.

---- 1977. A review of the braided river depositional environment. Earth Science Reviews, 13, 1-62.

----- 1978. Lithofacies types and vertical profile models in braided river deposits: A summary. p. 597-604. In: Miall, A.D. (ed.), Fluvial Sedimentology. Mem. Can. Soc. Petrol. Geol. 5, pp. 859.

----- 1981. Alluvial sedimentary basins: tectonic setting and basin architecture. p. 1-33. In: Miall, A.D. (ed.), Sedimentation and Tectonics in Alluvial Basins. Geol. Assoc. of Canada Spec. Paper no. 23.

----- 1984. Principles of Sedimentary Basin Analysis. Publ. Springer-Verlag, pp. 490.

Middleton, G.V. 1978. Facies. p.323-325. In: Fairbridge, R.W. & Bourgeois, J. (eds.). Encyclopedia of Sedimentology. Publ. Stroudsburg, Pa., Dowden, Hutchinson & Ross.

Moore, R.C. (chief editor). Treatise on Invertebrate Palaeontology. Publ. Geological Society of America & University of Kansas.

Morley Davies, A. 1975 (2nd edition). Tertiary Faunas. Publ. Allen & Unwin, 2 vols.

Morton, W.H. & Black, R. 1975. Crustal attenuation in Afar. p.55-65. In: Pilger, A. & Rosler, A. (eds.), Afar Depression of Ethiopia. Inter-Union Commission on Geodynamics, Sci. Rep. no. 14. E. Schweizerbart'sche Verlagsbuchhandlung, Stuttgart.

Myrianthis, M.L. 1984. Graben formation and associated seismicity in the Gulf of Korinth (Central Greece). p. 701-707. In: Dixon, J.E. & Robertson, A.H.F. (eds.), The Geological Evolution of the Eastern Medtitteranean. Spec. Publ. Geol. Soc. London no. 17, pp. 824.

McKenzie, D.P. 1978a. Some remarks on the development of sedimentary basins. Earth & Planetary Science Letters, 40, 25-32.

----- 1978b. Active tectonics of the Alpine-Himalayan belt: the Aegean Sea and surrounding regions. Geophysical Journal of the Royal Astronomical Society, 55, 217-254.

----- & Jackson, J. 1986. A block model of distributed deformation by faulting. Journal of the Geological Society, London, 143, 349-353.

McPherson, J.G. Shanmugam, G. & Moiola, R.J. 1987. Fan-deltas and braid deltas: Varieties of coarse-grained deltas. Bulletin of the Geological Society of America, 99, 331-340.

Nash, D.B. 1984. Morphologic dating of fluvial terrace scarps and fault scarps near West Yellowstone, Montana. Bulletin of the Geological Society of America, 95, 1413-1424.

Okaya, D.A. & Thompson, G.A. 1985. Geometry of Cenozoic extensional faulting: Dixie Valley, Nevada. Tectonics, 4, 107-125.

Ord, D.M. 1988. Sedimenation, tectonics and diagenesis in the Dinantian of the Solway Basin. PhD thesis, Univ. of Leeds, pp. 440.

-----, Clemmey, H. & Leeder, M.R. 1988. Interaction between faulting and sedimentation during Dinantian extension of the Solway basin, SW Scotland. Journal of the Geological Society, London, 145, 249-259.

Pamir, H.N. 1974. Explanatory text of the geological map of Turkey, Denizli sheet, 1:500,000. Ankara, pp. 83.

Papanikolaou, D.J. 1984. The three metamorphic belts of the Hellenides: a review and a kinematic interpretation. p.551-561. In: Dixon, J.E. & Robertson, A.H.F. (eds.), The Geological Evolution of the Eastern Mediterranean. Spec. Publ. Geol. Soc. London no. 17, pp.824.

Pavlides, S.B. & Kilias, A.A. 1987. Neotectonic and active faults along the Serbomacedonian zone (SE Chalkidiki, northern Greece). Annales Tectonicae, 1, 97-104.

Pe-Piper, G. & Piper, D.J.W. 1984. Tectonic setting of the Mesozoic Pindos basin of the Peloponnese. p. 563-567. In: Dixon, J.E. & Robertson, A.H.F. (eds.), The Geological Evolution of the Eastern Meditteranean. Spec. Publ. Geol. Soc. London no. 17, pp. 824.

Perissoratis, C., Mitropoulos, D. & Angelopoulos, I. 1984. The role of earthquakes in inducing sediment mass movements in the eastern Korinthiakos Gulf. An example from the February 24 - March 4, 1981 activity. Marine Geology, 55, 35-45.

-----, ----- & ----- 1986. Marine geological research at the eastern Corinthiakos Gulf. p. 381-401. Geological & Geophysical Research, Special Issue, I.G.M.E. Athens.

Pickett, J.W., Thompson, C.H., Kelley, R.A. & Roman, D. 1985.

Evidence of high sea level during isotope stage 5c in Queensland, Australia. Quaternary Research, 24, 103-114.

Piper, D.J.W. & Panagos, A.G. 1981. Growth patterns of Acheloos and Evinos deltas, western Greece. Sedimentary Geology, 28, 111-132.

Pitman III, W.C. 1978. Relationship between eustacy and stratigraphic sequences of passive margins. Bulletin of the Geological Society of America, 89, 1389-1403.

Proffett, J.M.Jr. 1977. Cenozoic geology of the Yerrington district, Nevada, and implications for the nature and origin of Basin and Range faulting. Bulletin of the Geological Society of America, 88, 247-266.

Psilovikos, A. & Syrides, G. 1984. Neogene and Quaternary palaeoenvirnoments in the northern Aegean area. Ann. Geol. Pays Hellen., 32, 105-114.

Radtke, U., Grun, R. & Schwarz, H.P. 1988. Electron spin resonance dating of the Pleistocene coral reef tracts of Barbados. Quaternary Research, 29, 197-215.

Reading, H.G. (editor) 1986. Sedimentary Environments and Facies, 2nd edition. Publ. Blackwell Scientific Publishing.

Ricci Luchi, F. 1975. Depositional cycles in two turbidite formations of northern Apennines (Italy). Journal of Sedimentary Petrology, 45, 3-43.

Richards, G.W. 1982. Intertidal molluscs as sea-level indicators: A comparative study of modern and fossil Mediterranean assemblages. PhD thesis, University College, London.

----- 1985. Fossil Mediterranean molluscs as sea-level indicators. Geological Magazine, 122, 373-381.

Richter, D., Mariolakis, I. & Risch, H. 1978. The main flysch stages of the Hellenides. p.434-438. In: Closs, H., Roeder, D. & Schmidt, K. (eds.), Alps, Appenines, Hellenides. Publ. Schweizerbart'sche Verlagsbuchhandlung, Stuttgart, pp.620.

Ricou, L.E., Marcoux, J. & Whitechurch, H. 1984. The Mesozoic organization of the Taurides: one or several ocean basins? p.349-360. In: Dixon, J.E. & Robertson, A.H.F. (eds.), The Geological Evolution of the Eastern Mediterranean. Spec. Publ. Geol. Soc. London no. 17, pp.824.

Robertson, A.H.F. & Dixon, J.E. 1984. Introduction: aspects of the geological evolution of the Eastern Mediterranean. p.1-74. In: Dixon, J.E. & Robertson, A.H.F. (eds.), The Geological Evolution of the Eastern Mediterranean. Spec. Publ. Geol. Soc. London no. 17, pp.824.

Rotstein, Y. 1985. Tectonics of the Aegean block: rotation, side arc collision and crustal extension. Tectonophysics, 117, 117-137.

Royden, L. & Keen, C.E. 1980. Rifting process and thermal evolution of the continental margin of eastern Canada determined

from subsidence curves. Earth & Planetary Science Letters, 51, 343-361.

Russell, R.J. 1954. Alluvial morphology of Anatolian rivers. Assoc. Am. Geog. Ann., 44, 363-391.

Salger, M. 1973. Untersuchungen zur Mineralogie der Buntem Serie des Pliocan vom Isthmus von Korinth. p.175-177. Erlanger Geologische Abhandlungen, 95, pp.183. Publ. Junge & Sohn, Universitats-Buchdruckerei, Erlangen.

Savage, J.C. & Hastie, L.M. 1966. Surface deformation associated with dip-slip faulting. Journal of Geophysical Research, 71, 4897-4904.

Schroder, B. 1975. Bemerkungen zu marinen Terrassen des Quartars im NE-Peloponnes/Griechenland. Comments on Quaternary marine terraces in the NE Peloponnesos/Greece. N. Jb. Palaont. Abh., 149, 148-161.

Schwartz, D.P. & Coppersmith, K.J. 1984. Fault behaviour and characteristic earthquakes: examples from the Wasatch and San Andreas fault zones. Journal of Geophysical Research, 89, 5681-5698.

Schwarz, H. & Gascoyne, M. 1984. Uranium-series dating of Quaternary deposits. p. 33-51. In: Mahaney, W.C. (ed.), Quaternary Dating Methods. Publ. Elsevier, pp. 431.

Sclater, J.G. & Christie, P.A.F. 1980. Continental stretching: An explanation of the post-mid-Cretaceous subsidence of the Central North Sea Basin. Journal of Geophysical Research, 85, 3711-3739.

Scott, W.E., Pierce, K.L. & Hait, M.H.Jr. 1985. Quaternary tectonic setting of the 1983 Borah Peak earthquake, central Idaho. Bulletin of the Seismological Society of America, 75, 1053-1066.

Sebrier, M. 1977. Tectonique recente d'une transversale a L'Arc Egeen: Le Golfe de Corinthe et ses regions peripheriques. Thesis, Univ. Paris XI.

Seilacher, A. 1967. Bathymetry of trace fossils. Marine Geology, 5, 413-428.

Sellwood, B.W. & Netherwood, R.E. 1984. Facies evolution in the Gulf of Suez area: sedimentation history as an indicator of rift initiation and development. Modern Geology, 9, 43-69.

Sengor, A.M.C. 1987. Cross-faults and differential stretching of hangingwalls in regions of low-angle normal faulting: examples from western Turkey. p. 575-589. In: Coward, M.P., Dewey, J.F. & Hancock, P.L. (eds.), Continental Extensional Tectonics. Spec. Publ. Geol. Soc. London no. 28.

-----, Satir, M. & Akkok, R. 1984a. Timing of tectonic events in the Menderes Massif, western Turkey: implications for tectonic evolution and evidence for pan-African basement in Turkey. Tectonics, 3, 693-707.

----- & Yilmaz, Y. 1981. Tethyan evolution of Turkey: a plate

tectonic approach. Tectonophysics, 75, 181-241.

-----, ----- & Sungurlu, O. 1984b. Tectonics of the Mediterranean Cimmerides: nature and evolution of the western termination of Palaeo-Tethys. p.77-112. In: Dixon, J.E. & Robertson, A.H.F. (eds.), The Geological Evolution of the Eastern Mediterranean. Spec. Publ. Geol. Soc. London no. 17, pp.824.

Shackleton, N.J. 1987. Oxygen isotopes, ice volume and sea level. Quaternary Science Reviews, 6, 183-190.

-----& Opdyke, N.D. 1973. Oxygen isotope and palaeomagnetic stratigraphy of equatorial Pacific core V28-238: Oxygen isotope temperatures and ice volumes on a 10^5 year and 10^6 year scale. Quaternary Research, 3, 39-55.

Smith, A.G. & Spray, J.G. 1984. A half-ridge transform model for the Hellenic-Dinaric ophiolites. p.629-644. In: Dixon, J.E. & Robertson, A.H.F. (eds.), The Geological Evolution of the Eastern Mediterranean. Spec. Publ. Geol. Soc. London no. 17, p.824.

-----, Woodcock, N.H. & Naylor, M.A. 1979. The structural evolution of a Mesozoic continental margin, Othris mountains, Greece. Journal of the Geological Society, London, 136, 589-603.

Smith, R.B. & Bruhn, R.L. 1984. Intraplate extensional tectonics of the eastern Basin-Range: interfaces on structural style from seismic reflection data, regional tectonics and thermal-mechanical models of brittle-ductile deformation. Journal of Geophysical Research, 89, 5733-5762.

Smythe, D.K., Dobinson, A., McQuillin, R., Brewer, J.A., Matthews, D.H., Blundell, D.J. & Kelk, B. 1982. Deep structure of the Scotiish Caledonides revealed by the MOIST reflection profile. Nature, London, 299, 338-340.

Soufleris, C. & Stewart, G.S. 1981. A source study of the Thessaloniki (northern Greece) 1978 earthquake sequence. Geophysical Journal of the Royal Astronomical Society, 67, 343-358.

-----, Jackson, J.A., King, G.C.P., Spencer, C.P. & Scholz, C.H. 1982. The 1978 earthquake sequence near Thessaloniki (northern Greece). Geophysical Journal of the Royal Astronomical Society, 68, 429-458.

Spakman, W. Wortel, M.J.R. & Vlaar, N.J. 1988. The Hellenic subduction zone: a tomographic image and its geodynamic implications. Geophysical Research Letters, 15, 60-63.

Spray, J.G., Bebien, J., Rex, D.C. & Roddick, J.C. 1984. Age constraints on the igneous and metamorphic evolution of the Hellenic-Dinaric ophiolites. p.619-628. In: Dixon, J.E. & Robertson, A.H.F. (eds.), The Geological Evolution of the Eastern Mediterranean. Spec. Publ. Geol. Soc. London no. 17, pp.824.

Steckler, M.S. & Watts, A.B. 1978. Subsidence of the Atlantic-type continental margin off New York. Earth & Planetary Science Letters, 41, 1-13.

----- & ----- 1980. The Gulf of Lion: subsidence of a young

continental margin. Nature, London, 287, 425-429.

Stein, R.S. & Barrientos, S. 1985. Planar high-angle faulting in the Basin and Range: Geodetic analysis of the 1983 Borah Peak, Idaho, earthquake. Journal of Geophysical Research, 90, 11355-11366.

Stewart, I. & Hancock, P.L., in press. Degradation of active fault scarps in the Aegean region: implications for the early stages of basin evolution. Basin Research.

Stiros, S.C. 1986. Model for the N. Peloponnesian (C. Greece) uplift. 7th International Symposium on Recent Crustal Movements of the Earth. Tallinn, USSR, 8-13 Sept. 1986.

Street, F.A. & Grove, A.T. 1979. Global maps of lake-level fluctuations since 30,000 yr B.P. Quaternary Research, 12, 83-118.

Surlyk, F. 1978. Submarine fan sedimentation along fault scarps on tilted fault blocks (Jurassic-Cretaceous boundary, East Greenland). Gronlands Geologiske Undersogelse, bull. no. 128.

Theodoropoulos, D. 1968. Stratigraphie und Tektonik des Isthmus von Megara (Griechenland). Erlanger Geologische Abhandlungen, 73, pp.23. Publ. Junge & Sohn, Universitats-Buchdruckerei, Erlangen.

Tselentis, G.A. & Makropoulos, K. 1986. Rates of crustal deformation in the Gulf of Corinth (central Greece) as determined from seismicity. Tectonophysics, 124, 55-66.

Umemoto, S. 1965. U234/U238 in sea water from the Kurashio region. Journal of Geophysical Research, 70, 5326-5327.

Underhill, J.R. 1988. Triassic evaporites and Plio-Quaternary diapirism in western Greece. Journal of the Geological Society, London, 145, 269-282.

Vail, P.R., Mitchum, R.M.Jr. & Thompson III, S. 1977. Part three: Relative changes of sea level from coastal onlap. p. 63-82. Part four: Global cycles of relative change of sea level. p. 83-97. In: Payton, C.E. (ed.), Seismic Stratigraphy - Applications to Hydrocarbon Exploration. Publ. A.A.P.G., Memoir 26, pp. 516.

van Harten, D. 1986. Use of ostracods to recognize downslope contamination in palaeobathymetry and a preliminary reappraisal of the palaeodepth of the Prasas Marls (Pliocene), Crete, Greece. Geology, 14, 856-859.

Varnavas, S., Ferentinos, G. & Collins, M. 1986. Dispersion of bauxitic red mud in the Gulf of Corinth, Greece. Marine Geology, 70, 211-222.

Vita-Finzi, C. & King, G.C.P. 1985. The seismicity, geomorphology and structural evolution of the Corinth area of Greece. Philosophical Transactions of the Royal Society, London, A314, 379-407.

Walker, R.G. (editor) 1984. Facies Models. 2nd edition. Geoscience Canada Reprint Series 1, pp.317.

Wallace, R.E. 1977. Profiles and ages of young fault scarps, north-central Nevada. Bulletin of the Geological Society of America, 88, 1267-1281.

----- 1980. Degradation of the Hebgen Lake fault scarps of 1959. Geology, 8, 225-229.

Watterson, J. 1986. Fault dimensions, displacements and growth. Pure & Applied Geophysics, 124, 365-373.

Weller, J.M. 1959. Compaction of sediments. Bulletin of the American Association of Petroleum Geologists, 43, 273-310.

Wernicke, B. 1981. Low-angle normal faults in the Basin and Range Province: nappe tectonics in an extending orogen. Nature, London, 291, 645-648.

----- 1985. Uniform-sense normal simple shear of the continental lithosphere. Canadian Journal of Earth Sciences, 22, 108-125.

----- & Burchfiel, B.C. 1982. Modes of extensional tectonics. Journal of Structural Geology, 4, 105-115.

Westcott, W.A. & Ethridge, F.G. 1980. Fan-delta sedimentology and tectonic setting - Yallahs fan delta, southeast Jamaica. Bulletin of the American Association of Petroleum Geologists, 64, 374-399.

----- & ----- 1983. Eocene fan delta-submarine fan deposition in the Wagwater Trough, east-central Jamaica. Sedimentology, 30, 235-247.

Wheeler, J. 1987. Variable-heave models of deformation above listric normal faults: the importance of area conservation. Journal of Structural Geology, 9, 1047-1049.

White, N.J., Jackson, J.A. & McKenzie, D. 1986. The relationship between the geometry of normal faults and that of the sedimentary layers in their hanging walls. Journal of Structural Geology, 8, 897-909.

----- & McKenzie, D. 1988. Formation of the "steer's head" geometry of sedimentary basins by differential stretching of the crust and mantle. Geology, 16, 250-253.

Williams, G. & Vann, I. 1987. The geometry of listric normal faults and deformation in their hangingwalls. Journal of Structural Geology, 9, 789-795.

Wilson, J.L. 1975. Carbonate Facies in Geologic History. Publ. Springer-Verlag, New York, pp.471.

Wood, R. & Barton, P. 1983. Crustal thinning and subsidence in the North Sea. Nature, London, 302, 134-136.

Wright, L.D. & Coleman, J.M. 1974. Mississippi River mouth processes: effluent dynamics and morphologic development. Journal of Geology, 82, 751-778.

APPENDIX 1

PALAEOENVIRONMENTAL INTERPRETATION OF NEOGENE OUTCROP SAMPLES FROM THE GULF OF CORINTH, GREECE

by J. ATHERSUCH July 1987

BP Research Centre, Sunbury-on-Thames

This appendix reproduces selected results from the above report on fifty-three outcrop samples collected in 1986 from the Gulf of Corinth extensional basin system (BP internal ref. STR/64/87).

Athersuch notes that whilst the samples are all known to be of Miocene to Recent age, it has not been possible to use the recovered microfaunas to refine these dates further. Additionally, the mixed marine/non-marine assemblages yielded by some samples is recognised as being due to either a) syn-depositional mixing, as in an estuary, or b) subsequent reworking.

For each sample initial field comments of this author (Collier) are followed by the microfaunal observations and environmental interpretations of Athersuch. Age brackets are determined by stratigraphic relations with isotopically dated materials. Original field sample numbers identify the following samples from the Corinth Basin.

LOWER PLIOCENE

16.7.3

Calcareous silts with Viviparus sp. - freshwater (?) lacustrine.

Microfossils: This sample is dominated by abundant Cythenissa sp. (of various instars), with abundant indeterminate cyprids, common Cyprideis, and small cyprids. This assemblage indicates a largely freshwater lacustrine environment.

4.6.1

Alluvial overbank silts with plant fragments.

Microfossils: Fragments of tuberculate ostracods, probably referable to Cyprideis tentatively indicate a non-marine depositional setting.

5.6.1, 6.6.4

Calcareous silts-fine sands, planar and trough-bedded, with siliceous nodule horizons. Probably freshwater.

Microfossils: The microfauna of 5.6.1 is dominated by abundant gastropod opercula and two species of Cyprideis; Amplocypris is common and a single charophyte oogonium was found. A

freshwater, lacustrine setting is suggested. The presence of Hemicyprideis, Candona and gastropod opercula in sample 8.8.4 is also indicative of freshwater lacustrine environments.

7.6.2

White calcareous silts with dwarf gastropod casts - freshwater/brackish/lagoonal?

Microfossils: The microfauna in this sample is dominated by ?Tyrrenocythere sp. with accompanying rare occurrences of ?Aurila, Cyprideis, cyprids, ?Herpetocypris reptans and gastropod opercula. This is a mixed brackish to freshwater assemblage.

8.8.2

Green medium sands, with Viviparus sp. and freshwater mollusc fragments, of suspected distal deltaics transported into brackish shelf (estuarine) environment.

Microfossils: A fragment of Cyprideis and a gastropd (?Viviparus) are indicative of fresh to brackish water environments.

16.7.2, 8.8.6

Multi-Coloured Series sands of braided fluvial system.

Microfossils: Sample 16.7.2 yields abundant Cyprideis sp. and rare Aurila sp. and a gastropod opercula. A brackish environment is indicated. Sample 8.8.6 has common marine ostracods referrable to Hemicythere and Aurila together with rare cyprids, Cyprideis and gastropod opercula. A marine to brackish environment is indicated.

LATE PLEISTOCENE

10.5.1

Dark grey clays.

Microfossils: Abundant Uvigerina peregrina, Nonion sp., common echinoid spines and Valvulineria cf. bradyana, and rare Cassidulinia carinata, indeterminate planktonic forams and a single specimen of the ostracod Echinocythereis indicate marine shelf sedimentation.

10.5.3

Calcareous fine silts with thin-shelled bioclastics.

Microfossils: This sample is dominated by several undetermined species of gastropod and bivalves (mostly fragments). The foraminifera Uvigerina peregrina and Ammonia sp. are common. Cibicides sp. and Cassidulina carinata are also present (rare)

together with rare specimens of the ostracods Cyprideis (tuberculate), Urocythereis britannica, Aurila, Callistocythere crispata, Carinocythereis, Loxoconcha sp., L. ovata, L. alata and Xestoleberis. A single charophyte oogonium was recovered, and echinoid spines were common. This is a predominantly marine shelf assemblage, although the presence of a charophyte and Cyprideis does suggest freshwater influence.

13.9.1

Marl/limstone with dwarf fauna.

Microfossils: Charophyte oogonia and gastropod opercula are common in this sample, accompanied by rare ostracods, including ?Cyprideis, ?Cytherissa, Loxoconcha and a small cyprid. A non-marine lacustrine or lagoonal setting is implied.

21.9.3

Calcareous fine sands/silts, packstone-wackestone with dwarf gastropods and bivalves.

Microfossils: The ostracod genus Xestoleberis, represented by two species, is abundant in this sample and accompanied by common Callistocythere spp., including C. crispata. Bivalves, gastropods, echinoid spines and the foraminifer ?Anomalina sp. are rare. The ostracod fauna in particular indicate a shallow marine (inner sublittoral) environment.

21.9.8

White-grey shelly fine sands (calcareous) with varied shallow marine fauna (Ostrea, Pecten, Cerithids etc.).

Microfossils: Common miliolids, Elphidium, Discorbis, Asterigerina and other, undetermined foraminifera indicate a marine environment. In addition, a large number of ostracod species, mainly represented by one or two specimens each further indicate shallow sub-littoral environments; taxa include Urocythereis britannica, Sagmatocythene napoliana, Loxoconcha alata, L. adriatica, L. cf. stellata, Callistocythere ?badia, C. crispata, Heterocythereis sp., Xestoleberis cf. communis and Hemicythere sp. Gastropods are abundant and echinoid spines common; the latter confirm deposition under normal salinities.

10.5.7, 11.5.3, 21.9.4

Laminated calcareous silts (11.5.3 is v. poorly-sorted calcareous silt - v. coarse sand) with dwarf fauna.
Marine/brackish/lagoonal?

Microfossils: Sample 10.5.7 is dominated by undetermined bivalves and gastropods. Common Cyprideis sp. indicate fresh to brackish environments, whereas rare Elphidium cf. complanata suggest marine influence. Sample 11.5.3 is characterised by undetermined gastropods and common, large Elphidium sp. The

rest of the fauna comprises rare Ammonia beccarii (var papillosa and tepida), miliolids, Lagena, echinoid spines and bivalves. The ostracod Xestoleberis is also present. A shallow marine environment is indicated. Sample 21.9.4 yields common bivalve fragments alone.

17.9.1

Marine fossiliferous green sands of marine incursion into structural graben.

Microfossils: This sample yields a marine fauna of abundant gastropods, common bivalves, Elphidium and Ammonia spp. with rare fish teeth.

30.4.4, 23.5.1, 24.5.1

Calcareous fine-medium sands. Marine, with Natica sp.

Microfossils: Foraminifera, including Cibicides in sample 23.5.1, indicate a marine depositional setting.

30.4.1

Alluvial calcareous fine-medium sands (with Viviparus sp.), but reworked from syn-depositionally exposed marine sands of 30.4.4 (hence marine bioclastics found).

Microfossils: The presence of rare Elphidium sp. and also rare possible Xestoleberis sp. confirms a marine origin of the microfauna.

30.4.2, 30.4.3

Alluvial loams/calcareous soils with rootlets. Alluvial fines interdigitated with sands of 30.4.1.

Microfossils: The foraminifera Elphidium sp., Ammonia beccarii, Cibicides sp. and Asterigerina sp. in sample 30.4.2 suggest a shallow marine environment. 30.4.3 yields similar but less diverse assemblages. The additional presence in 30.4.2 of the ostracod Cyprideis suggests fresh or brackish water influence.

ANO ALMIRI - KATAMALION TILT BLOCKS; AGE UNKOWN

26.4.1, 26.4.2, 26.4.3

Respectively white, brown and olive calcareous fine silts/clays, probably lacustrine.

Microfossils: Sample 26.4.1 yielded rare charophyte oogonia and Cyprideis, indicative of fresh to brackish lacustrine environments. Sample 26.4.2 was barren and sample 26.4.3 yielded only a fragment of ?Cytherissa sp., possibly indicating freshwater depositon.

APPENDIX 2

The following x-ray diffraction traces record the mineralogical content of scleractinian corals sampled for U-series disequilibrium dating (refer to chapter 4).

Records are shown for the following samples:
87.7.8.1
87.26.8.1b
87.29.8.1

Predicted peaks for relevant minerals occur at the following 2-theta angles:

26.25	aragonite
26.70	quartz
27.25	aragonite
29.50	calcite
33.20	aragonite
36.15	aragonite
37.30	aragonite
37.85	aragonite
38.45	aragonite

All three samples show good aragonite peaks. Recrystallization of original aragonite structure to calcite and detrital calcite is not thought to be significant. This is supported by scanning electron micrograph records (section 4.6.2).

****

Wed,30 Sep 1987.14:42:33
TIME SECS=1017.10

Sample name 7.8.1

2-theta	d-space	R.I.
26.250	3.395	100
27.250	3.272	70
29.650	3.013	14
33.200	2.698	47
36.150	2.485	51
37.300	2.411	29
37.900	2.374	40
38.500	2.338	44

SAMPLE 7.8.1 scan factor 4

Scan begins at 25 deg. and ends at 40 deg.

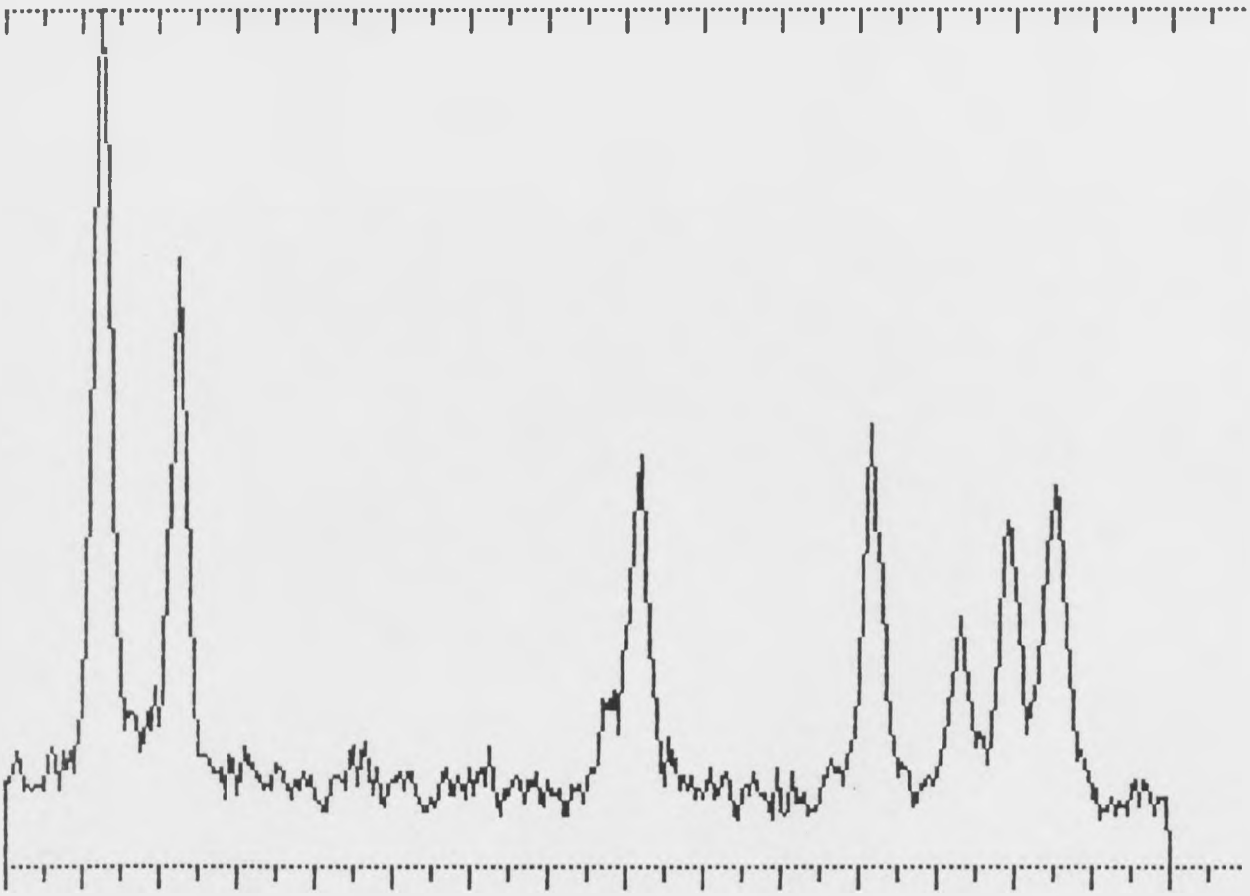

Wed,30 Sep 1987.13:52:22
TIME SECS=1017.07

Sample name 26.8.1

2-theta	d-space	R.I.
25.150	3.541	45
26.250	3.395	100
26.800	3.326	46
27.200	3.278	76
29.450	3.033	40
30.250	2.954	41
33.000	2.714	48
36.100	2.488	48
37.250	2.414	37
37.950	2.371	36

SAMPLE 26.8.1 scan factor 4

Scan begins at 25 deg. and ends at 40 deg.

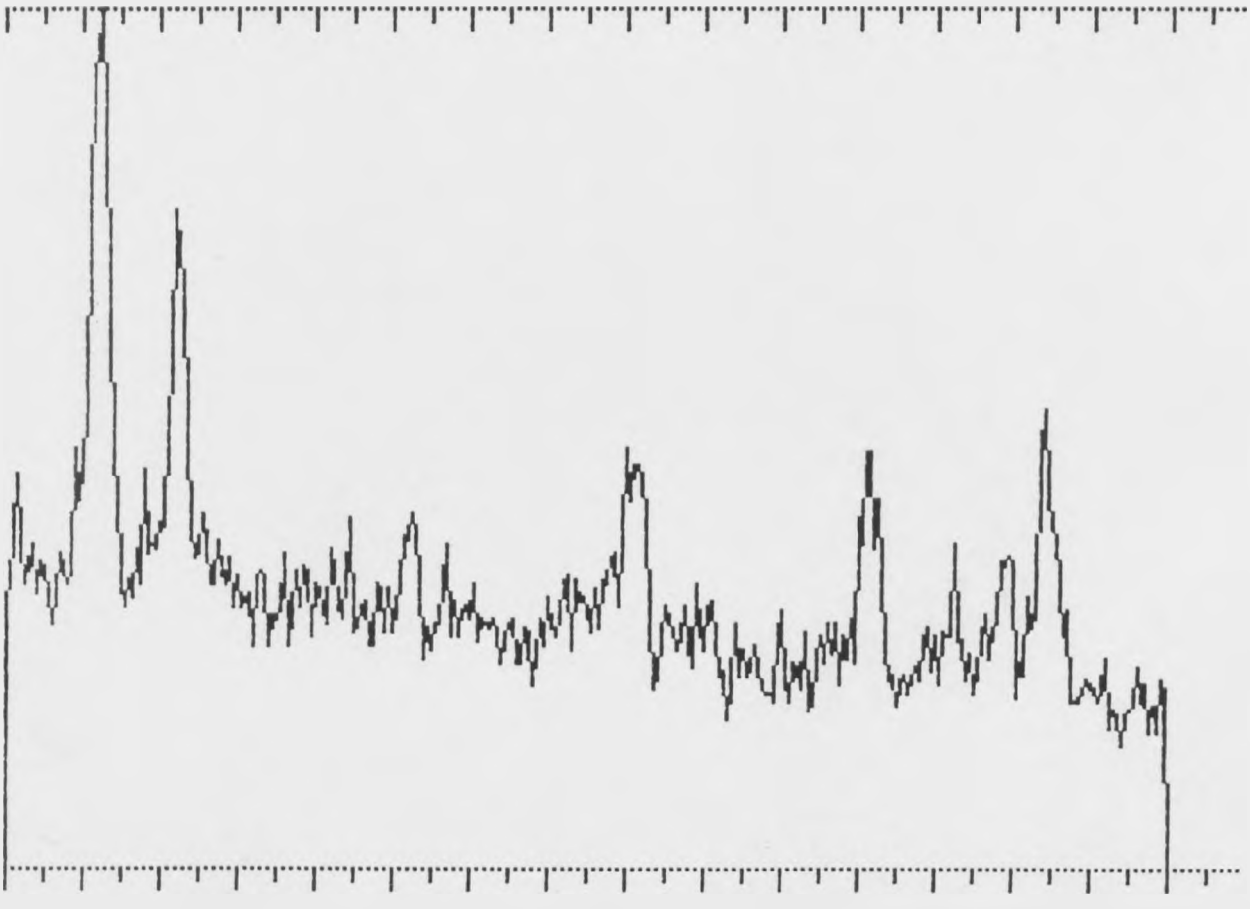

Wed.30 Sep 1987.13:13:26
TIME SECS=1017.10

Sample name 29.8.1

2-theta	d-space	R.I.
26.200	3.401	100
27.250	3.272	59
29.500	3.028	22
32.700	2.738	21
33.100	2.706	48
36.100	2.488	48
37.250	2.414	29
37.850	2.377	38
38.450	2.341	38

SAMPLE 29.8.1 scan factor 4

Scan begins at 25 deg. and ends at 40 deg.

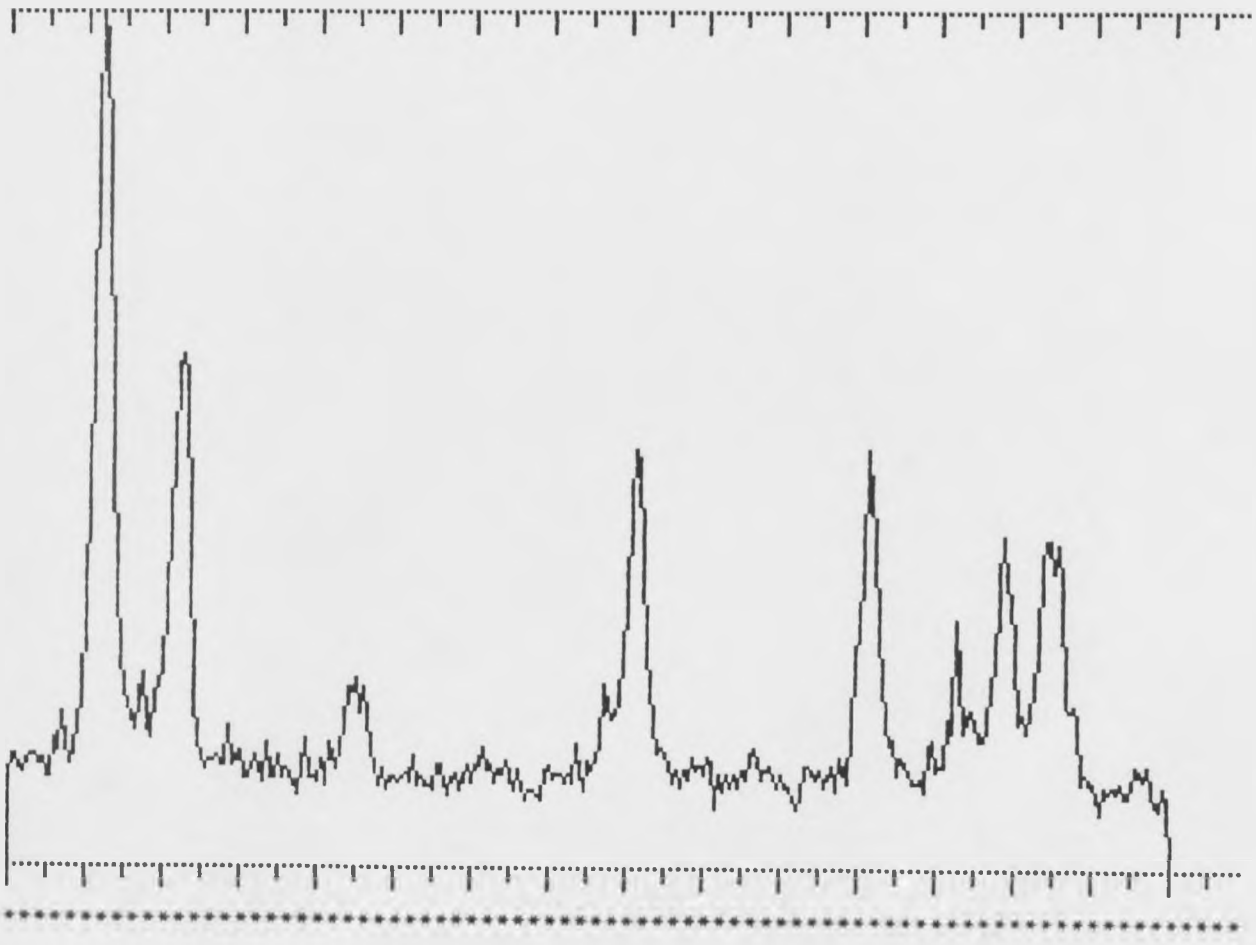

ENCLOSURE 2

GRAPHIC LOG SYMBOLS

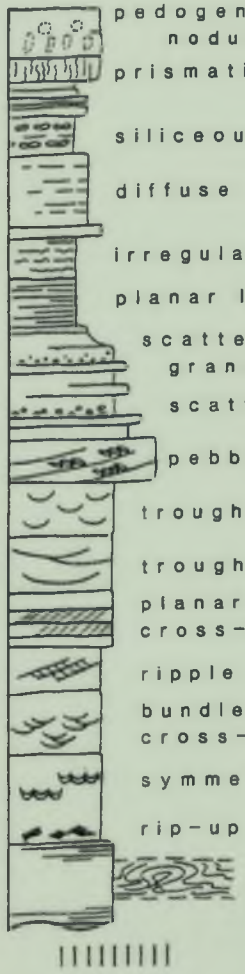

pedogenic carbonate nodules

prismatic structure

siliceous nodules

diffuse bedding

irregular laminations

planar laminations

scattered sand/ granule grains

scattered pebbles

pebble imbrication

trough cross-beds

trough scours

planar cross-stratification

ripple cosets

bundled trough cross-beds

symmetric ripples

rip-up clasts

syn-sedimentary contortions

|||||||||

Grain sizes: clay | f. silt | c. silt | f. sand | m. sand | c. sand | granule | pebble | cobble

|| -sparse

|| || vertical burrows

|| || || -intense

= = horizontal burrows

branched burrows

rootlets

plant fragments

freshwater bivalve

fresh/brackish gastropod (fragment)

Cardium

oyster

marine bivalve

marine gastropod

serpulid

coral (scleractinian)

foraminifera

4 5 6 7 8

23 22 21 20 19

Kalamaki

±Ag.Ch.

N

0 km 1

SARONIC GULF

Fan level 1, Holocene

Fan level 2

Fan level 3

?Upper Pliocene – Pleistocene

Mid Pliocene andesites

Lower Pliocene: Upper Conglomerates

Multi-Coloured Series Sands

Multi-Coloured Series "Marls"

Agios Charalampos Conglomerates

Asprakhomata-Kalamona Formation

Pre-Neogene ophiolite

Palaeoflow vector means:

n 1-5 (non-directional)

n 6-20 (directional)

n greater than 20

n (total) 440

Normal fault

Contours in metres

Greek national 1:50,000 grid

ENCLOSURE 1

LOWER PLIOCENE OUTCROP

CORINTH BASIN